HUNGARIAN UNIVERSITY OF AGRICULTURE
AND LIFE SCIENCES

Modelling and optimization of large-scale grid-connected photovoltaic systems with enabling technologies

PhD Dissertation

by

Teklebrhan Tuemzghi Negash

Gödöllő
2025

Doctoral school and program denomination:

Doctoral School of Engineering Sciences

Doctoral Program of Mechanical Engineering

Science: Engineering

Head of School: Prof. Dr. László Bozó, MHAS
Institute of Environmental Sciences
Hungarian University of Agriculture and Life Science, Budapest, Hungary

Program leader: Prof. Dr. Gábor Kalácska, DSc
Institute of Technology
Hungarian University of Agriculture and Life Science, Gödöllő, Hungary

Supervisor: Prof. Dr. István Farkas, DSc
Institute of Technology
Hungarian University of Agriculture and Life Science, Gödöllő, Hungary

Co-Supervisor: Dr. István Seres, PhD
Institute of Mathematics and Basic Sciences
Hungarian University of Agriculture and Life Science, Gödöllő, Hungary

…… ……

Affirmation of supervisor(s) Affirmation of head of doctoral program

CONTENTS

NOMENCLATURE AND ABBREVIATION

a-Si	Amorphous silicon module
AC	Alternating current (A)
BES	Battery energy storage (MWh)
CC	Correlation coefficient (-1,1)
CdS	Cadmium sulfide
CdTe	Cadmium telluride
$Ch_{\text{lose\_S}}$	Charging loss (MW)
CIGS	Copper-indium-gallium-selenide solar cells
DC	Direct current (A)
$Disch_{\text{lose\_S}}$	Discharging loss (MW)
E_p	Hourly curtailed power with diurnal storage (MW)
GaAs	Gallium arsenide
Li-ion	Lithium-ion battery
MAE	Mean Absolute error (kW)
MBE	Mean bias error (kW)
MSE	Root mean squared error (kW)
N	Number of hours in a normal year (8760)
n	Total number of observations
P	Penetration (% of annual demand)
$P'_{sat,i}$	Rescaled satellite-derived PV power (kW)
P_{cos}	Hourly consumed RE (MW)
P_{dem}	Demand (MWh)
P_{dpf}	Final hourly unmet demand (MW)
P_{nd}	No-dump power generation (MWp)
P_{excess}	Excess generation (MW)
P_{gen}	Generated Power (MW)
P_{inj}	Direct injected power (MW)
P_{limit}	Injection limit (MW)
P_{mean}	Mean value (kW)
$P_{meas,i}$	Measured value (kW)
$P_{pred,i}$	Predicted value (kW)
$P_{PV,cur}$	Curtail PV power
P_{room}	Hourly remaining capacity (MW)
P_{room_S}	Hourly remaining capacity-seasonal storage (MW)
$P_{sat,i}$	Satellite-derived PV power (kW)
P_{std}	Standard power curve (MW)
P_{used}	Power integrated to the local network (MW)
P_u	Hourly unmet power with diurnal storage (MW)
P_{wind}	Wind generation (MW)
pc-Si	Poly-crystalline module
P_{mix}	Mismatch between generation and demand (net-load) (MW)
p_{pv}	Photovoltaic generation (MW)

r	PV ratio (0 -1)
R^2	Coefficient of determination (0 -1)
S	Stored energy (MWh)
S_h	Seasonal storage stored energy (MWh)
S_{maxh}	Maximum capacity of seasonal storage (10-average daily demand)
S_{max}	Maximum energy capacity of diurnal storage (0.8 average daily demand)
SU	Storage utilization (fraction of max storage capacity)
SUI	System-use index
T	Time (1 - 8760)
TRE	Total renewable energy generation Rayleigh number (-)
V	wind speed (m/s)
V_Dev	Voltage deviation
X_{max}	Maximum of the observed data
X_{min}	Minimum of the observed data
X_n	Min-max scaler (0 – 1)
z	Z-score transformation
z_0	Roughness length(m)
Δt	Change in time (hr)
Δt_{full}	Minimum time required to charge or discharge the storage (hrs)
Δt_{full_disch}	Minimum time required to charge the seasonal storage (72 hrs)
Δt_{full_ch}	Minimum time required to discharge the seasonal storage (96 hrs)
τ	The Kendall correlation coefficient (-1,1)

Greek symbols

ρ	Air density (kg/m^3)
$\alpha(r)$	Unifying factor
β	Over generation factor (2 – 6 P_{nd})
η_{ch}	Charging efficiency (%)
η_{dis}	Discharging efficiency (%)
$\eta_{\mathrm{ch\_s}}$	Electrolyser efficiency (%)
$\eta_{\mathrm{dis\_s}}$	Fuel cell efficiency (%)
μ_{sat}	Mean of satellite-derived power (kW))
σ_{sat}	Standard deviation of satellite-derived power (kW)
μ_{meas}	Mean of measured PV power (kW)
σ_{meas}	Standard deviation of measured PV power (kW)

Subscripts

ch	Charging
dis	Discharging
$meas$	Measured value
$pred$	Predicted value
sat	Satellite value

Abbreviations

CNN	Convolutional neural network
DRF	Deep Reinforcement learning
GRU	Gated recurrent network
GWA	Global wind atlas
IRENA	International Renewable Energy Agency
LSTM	Long and short-term memory
MPPT	Maximum power point tracking
PPO	Proximal Policy Optimization
PV	Photovoltaics
PVGIS	Photovoltaic Geographic Information System
RE	Renewable Energy
RF	Reinforcement Learning
VRE	Variable Renewable Energy
SARIMAX	Seasonal AutoRegressive Integrated Moving Average with eXogenous regressors
TCN	Temporal convolutional network
THD	Total Harmonic Distortion
ThdI	Current total harmonic distortion
ThdV	Voltage total harmonic distortion
VRE	Variable Renewable Energy
XGBoost	Extreme gradient boosting

1. INTRODUCTION, OBJECTIVES

This chapter outlines the significance of the research topic and presents the study's objectives.

1.1. Introduction

Global electricity demand is growing rapidly, driven by population growth, industrial expansion, and the surging energy needs of data centers (IEA, 2025). In response, a global shift toward renewable energy (RE) has become a top priority globally. In 2023, renewable capacity expanded by 570 GW, a 50% increase from 2022, with a major growth coming from solar PV (IEA, 2024). Furthermore, forecasts show that utility-scale PV installations will account for approximately 66.7% of the global energy mix by 2050. Similarly, the adoption and utilization of residential PV are skyrocketing, as buildings, once primary energy consumers, have become energy producers (Silva and Hendrick, 2017a). Declining costs of home batteries and PV components are driving consumers to generate their own power locally, reducing their grid reliance (Teklebrhan et al., 2025). However, extensive deployment of these resources challenges the grid, as large-scale integration requires complex system adaptations. Key issues include intermittency, matching, forecast uncertainty, adequacy, and grid stability (Solomon, 2019). To overcome these challenges, various solutions have been proposed in the literature, including energy storage (Denholm and Mai, 2019) resource complementarity, curtailment, resource diversity and advanced forecasting (Limouni et al., 2023), (Perez et al., 2019), (Simoes et al., 2017).

In the context of large-scale PV integration, it is crucial to evaluate the combined impact of multiple enabling tools, including the PV-wind mix, storage capacity and duration, curtailment strategies, and balancing requirements. Considering these factors together provides a more comprehensive understanding of system design and operation, as focusing on PV alone fails to capture the full complexity and interdependencies inherent in modern power system dynamics. A well-balanced PV-wind mix can increase RE penetration while reducing storage and curtailment compared to standalone PV systems. Integrating large-scale PV requires diverse energy storage solutions, which are essential for enhancing grid flexibility, increasing renewable penetration, and accelerating the transition to 100% RE (Bullich-Massagué et al., 2020). Energy storage technologies can be classified as long-term storage, such as hydrogen, which can be utilized for extended durations ranging from weeks up to months (Breunig et al., 2024), and short-term storage, such as lithium-ion batteries, which are more suitable for daily cycling or even sub-daily (hourly) balancing needs (Javed et al., 2019). Other enabling tools, such as curtailment (intentional dumping of RE output), offer technical advantages by lowering storage and balancing capacity requirements. Studies show that adopting curtailment policies can enhance the cost-effectiveness and feasibility of integrating high shares of RE into the grid (Perez et al., 2019). Curtailing a portion of Variable Renewable Energy (VRE) generation can enhance the balance between supply and demand, thereby reducing storage requirements and enabling higher renewable penetration (Solomon et al., 2019). This illustrates part of the required paradigm shift in operating the future renewable-dominated grids as compared to the current traditional practices (Teklebrhan et al., 2023).

In the context of RE integration, identifying the potential optimized solutions aligned with a specific country or regional scale is essential for advancing the transition toward RE-dominated power systems (Oyewo et al., 2021). However, there are critical challenges that require close examination. First, the inherent variability of renewable resources complicates the development of clear system design principles for achieving 100% RE systems. Traditional approaches–such as screening curves and load duration curves–are increasingly inadequate in a landscape dominated by large-scale PV and wind, and diverse storage technologies (Jean-

Michel, 2021). Second, the development of future energy markets that prioritize efficiency and societal welfare requires a clear understanding of evolving system needs and analytical tools capable of visualizing system boundaries over time (Jean-Michel, 2021). Notably, scenarios that appear techno-economically viable may still result in reduced net energy output, underscoring the risks associated with multidimensional pricing structures and operational uncertainties (Solomon et al., 2024). These considerations, coupled with location-specific climatological conditions, underscore the necessity of a comprehensive understanding of the interplay among various physical parameters to determine sustainable design options and their complementary operational requirements. In addition, the adoption of advanced, innovative technologies and AI-based tools for power generation forecasting (Limouni et al., 2023) and grid management and optimization is crucial for enabling the large-scale integration of renewable energy sources (Cardo-Miota et al., 2025).

1.2. Objectives

Understanding how penetration, storage capacity and duration, curtailment, PV-wind mix, and balancing requirements interact provides key insights for managing the transition to a renewable-dominated grid and anticipating its operational requirements. However, empirical data showing the interaction between these parameters with sufficient detail does not exist. The majority of the current energy transition studies are primarily driven by least-cost optimization (techno-economic) models, often overlooking these critical technical factors in favour of extensive economic data. This work, therefore, aims to develop a flexible modelling framework that assesses interactions among key system design parameters and supports optimized PV integration while leveraging the benefits of residential PV and advanced PV generation forecasting and optimization.

The primary objectives of this research are to:

- Maximize the share of PV in the electricity grid with high reliability and operational efficiency, contributing to a sustainable energy system;
- Investigate the complex interaction among the various system design parameters, such as PV-wind mix, storage capacity and duration, curtailment strategies, and balancing requirements, and their impact on system design and performance;
- Formulate a relationship among the major design parameters and system efficiency, supported by robust empirical data, to develop practical guidelines for achieving high levels of renewable integration.
- Enhance the contribution of residential PV on the power mix by exploring the impact of feed-in constraints on promoting higher local consumption of residential PV in low-voltage local networks;
- Leverage machine learning-based PV generation forecasting to enhance real-time operational management and optimization of PV systems, mitigating uncertainties and limitations inherent in the design phase of PV integration.

By addressing these objectives, this study aims to deepen the understanding of the design and operational strategies of future renewable-dominated grids through the application of a clear and transparent model that accounts for varying system parameters. Ultimately, it contributes to the broader effort to unify related studies under a more coherent theoretical foundation.

2. LITERATURE REVIEW

This chapter offers a comprehensive overview of large-scale renewable energy (RE) integration and its related technical requirements. It discusses fundamental concepts of various components, focusing on PV, and other technologies that enable large-scale PV integration, including wind, storage, curtailment, forecasting, and balancing requirements. This chapter digests the literature that defines the interactions among the system design parameters required for large-scale PV integration. It also discusses recent methodologies, approaches, and models for large-scale RE integration and identifies the existing gaps that motivate this study.

2.1. Photovoltaics Technology

Photovoltaic is a combination of two words: *photo*, which refers to light, and *volta*, derived from the name of an Italian physicist, Alessandro Volta, the unit of voltage (Quaschning, 2016). Photovoltaic energy directly converts sunlight into electricity through the photoelectric effect. When photons of solar irradiance strike a free electron in the p-n junction of a semiconductor device, they excite the free electrons, generating an electric current (Miles et al., 2005).

2.1.1. PV principle, operation, and characterization

Photovoltaic cells or solar cells are the building block of the photovoltaic system that converts the energy of photons into electricity (DC current) through the photovoltaic effect (Shubbak, 2019). Their working principle is based solely on the behavioural architecture of semiconductor materials. When two semiconductor regions with different charge concentrations are combined, an effect is created that results in special charge mobility along the edges of the semiconductor devices. When these two (positively charged plates called p-type and the negatively charged zone called n-type) semiconductor devices are placed together a charge transfer effect is produced, which ultimately leads to the production of an electric field (Luceño-Sánchez et al., 2019). The phenomenon of the photoelectric effect had been known for nearly a century, the milestone widely recognized as the beginning of the modern era of PV power generation was the production of around 6% efficient crystalline silicon solar cell in 1954 (Ali et al., 2025). From that time, the efficiency of silicon cells has been increasing continuously, with lab efficiency currently exceeding 20%. Although a significant leap has been recorded in PV efficiency enhancement, several research studies are ongoing to enhance efficiency further and decrease the overall cost of PV-generated electricity (NREL, 2025).

As shown in Fig. 2.1 silicon cells are made up of two layers, p-junctions (layers of holes) and n-junctions (layers of electrons). Due to the unique properties of the semiconductor material, only a small amount of energy is required to excite an electron from the valence band to the conduction band, creating a free-moving electron and enabling electric current flow (Abdelhady et al., 2017).

During the 1960s, photovoltaic cells were produced manually, which made them very costly and limited their use to space applications. By the late 1980s, mass production methods were introduced, significantly lowering costs and broadening their applications to include standalone and remote devices, as well as grid-connected systems. Since the first discovery of solar PV in 1839, advancements have been made in manufacturing costs, efficiency, and capacity. Furthermore, the technology has been experiencing significant growth and innovations in various technical fields, including materials, chemistry, physics, electronics, and mechanics.

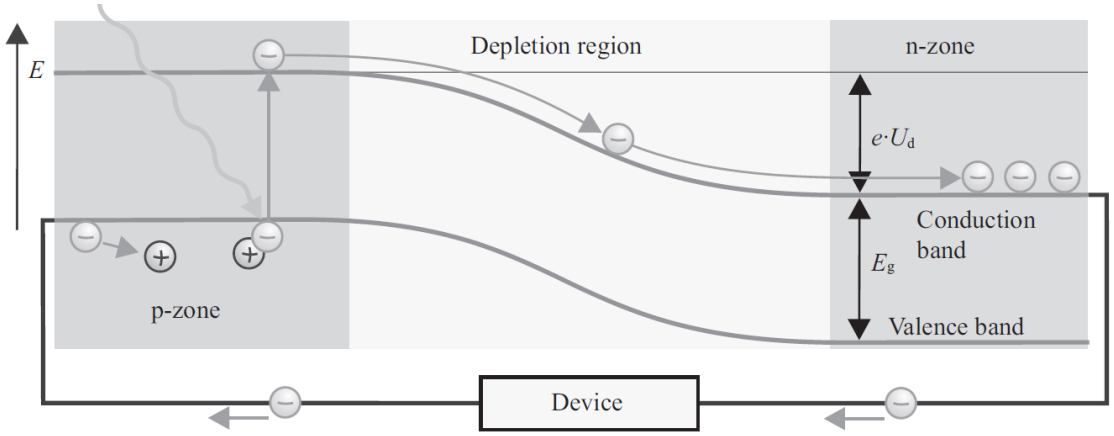

Fig. 2.1. Energy band model showing how solar cell works (Quaschning, 2016)

There are different solar PV technologies, such as thin film, amorphous silicon (a-Si), cadmium telluride (CdTe), poly-crystalline (pc-Si) modules, and perovskite. The efficiency, temperature coefficients, and spectral response of these technologies vary widely due to the intrinsic structure (Cañete et al., 2014). Moreover, the technological maturity and market penetration of these technologies vary widely. Modules such as conventional mono-si and poly-si are at their higher technological maturity, and the dominant technology of solar PV compared to thin film technologies (Schmela et al., 2022)

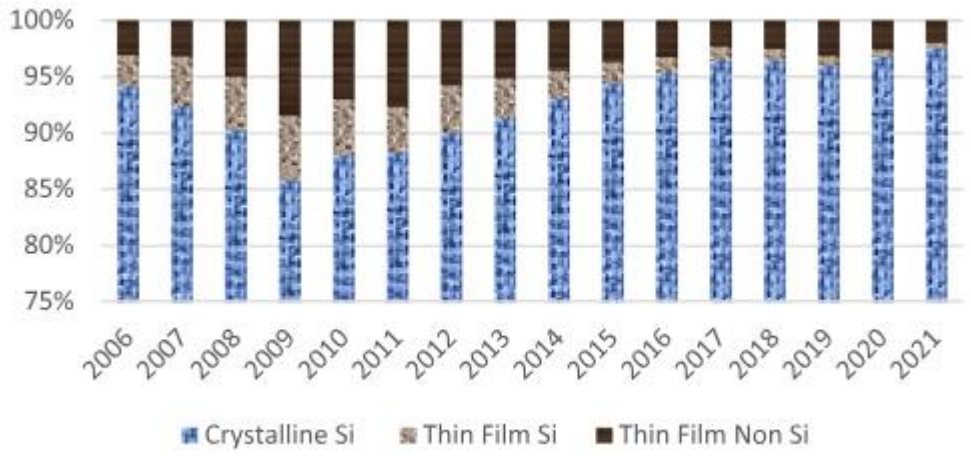

Fig. 2.2. Share of different solar PV technologies in manufacturing capacity (Schmela et al., 2022)

According to their development stages, solar photovoltaics can also be categorized into different parts:

- The first generation includes crystalline silicon technologies, such as monocrystalline, polycrystalline, and gallium arsenide (GaAs).
- The second generation includes technologies tied to amorphous silicon (a-Si), microcrystalline silicon, cadmium telluride/cadmium sulfide (CdTe/CdS), thin-film technologies, and copper-indium-gallium-selenide (CIGS) solar cells.
- The third generation encompasses technologies utilizing new compounds, including nanocrystalline films, active quantum dots, organic (polymer-based) solar cells, and tandem or stacked multilayers made from inorganic materials like GaAs/GaInP. It also includes dye-sensitized solar cells, among others.

- The fourth generation comprises innovative inorganic nanostructures like metal nanotubes and metal oxides, commonly referred to as ‘inorganic.

The different PV generation technologies and their respective commercial and lab efficiencies are given in Fig. 2.3.

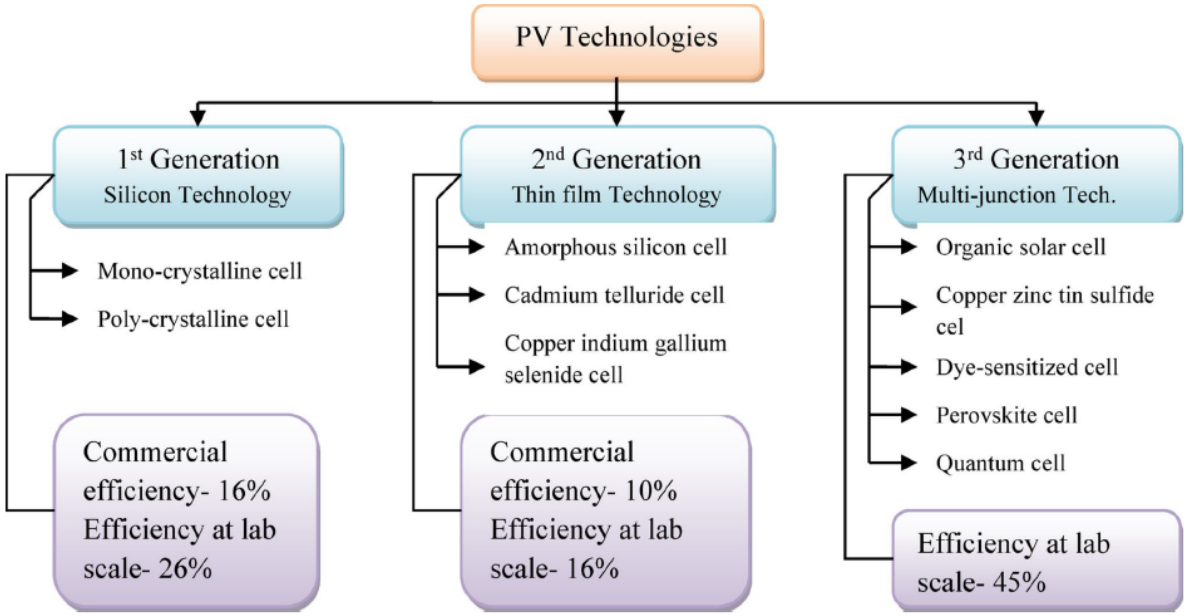

Fig. 2.3. Solar PV generations and their efficiency (Dhankar et al., 2025)

First-generation PV cells are the most efficient and mature technology with efficiency ranging from 15-22%; however, their large-scale deployment is hindered due to their higher cost. In response to the high cost of the first generation, research is being initiated to address this in the second generation (Nayak et al., 2019). Although the second generation shows material effectiveness, they still have concerns about toxicity, instability, and low efficiency, and their large-scale deployment has not been realized. The third generation that covers a wide range of design variations has several advantages, such as working in dim light and being cheaper to manufacture as they can be manufactured from inexpensive materials, but they are still prone to the environment as technologies such as perovskites are sensitive to humidity and heat. The need for more efficient, eco-friendly, and stable solar cells necessitates the latest research in fourth-generation solar cells. This generation combines all the benefits of previous generations and features a cost-effective, flexible structure with stable nanomaterials. It also introduces various advanced materials, including 2D solar cells, and holds great promise for future PV advancements. (Rehman et al., 2023) .

Atsu et al., (2021) conducted a performance evaluation of different grid-connected PV technologies, namely, pc-Si) and a-Si modules. The authors use different performance indicators to assess and compare the performance of the different PV technologies installed at the lab of the Hungarian University of Agriculture and Life Sciences. They found that Hungary has relatively high solar energy potential compared to other neighbouring European countries, but it has not yet been fully exploited.

2.1.2. Modelling of solar cells

A solar cell can be defined as an electrical circuit that contains a p-n junction (acting as a diode), a resistor, and the main component, called the photocurrent generator. A circuit that contains such a component is referred to as a single diode solar cell model (Vinod et al., 2018).

A PV model is a mathematical expression that enables us to assess the electrical behavior and performance of PV panels under varying operating conditions, as the output power of PV is influenced by environmental factors such as incident radiation, temperature, irradiance, and material properties (Olayiwola et al., 2024). An effectively designed PV cell model can assist in:

- Understand the electrical characteristics of a PV cell
- Improve the overall performance and efficiency of the PV system
- Enhance the control system by assisting in optimization of the maximum power point tracking system (MPPT)

Modelling the electrical behaviour of PV cells is typically categorized into three main types: circuit models, analytical models, and empirical models. Accurate modelling of solar cells is essential for the design and optimization of PV systems. The best model should accurately determine the electrical behaviour of the PV cell with simplicity. However, there is always a trade-off between accuracy and complexity. The circuit model – shown in Fig. 2.4 – is the most widely used approach for representing the electrical behaviour of PV cells. However, due to the nonlinear nature of the current-voltage (I-V) characteristics, parameter estimation remains a challenging task in achieving efficient solar system design (Jordehi, 2016). In the figure, Iph, I_D, and Ip represent the photocurrent, diode current, and parallel current, respectively. Whereas R_s and R_P are the series and parallel resistances.

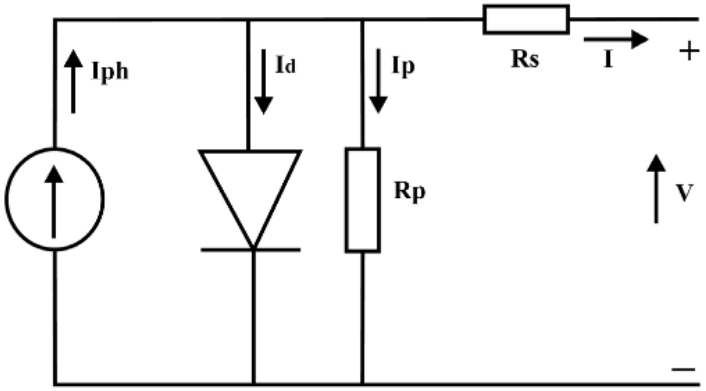

Fig. 2.4. Single diode equivalent circuit of the real model of solar cell (Quaschning, 2016)

Traditional modelling approaches, such as the analytical methods, face challenges in accurately determining the various parameters due to the non-linear and complex, multimodal features of the models.

Zheng et al. (2022) utilize a powerful tool, an advanced optimization modelling tool, called the Peafowl Optimization Algorithm from the recently developed meta-heuristic algorithm for solar cell parameter identification. The authors validated the proposed approach using two types of PV cell models, the double diode model and the triple diode model. The results showed that the Peafowl optimization Algorithm can determine and identify unknown solar cell parameters accurately compared to other algorithms at a higher convergence speed.

Precise modelling of PV cells is crucial for enhancing the performance of photovoltaic systems, as it enables the accurate identification of key parameters. Cutting-edge optimization methods, such as the Peafowl Optimization Algorithm, have significantly improved the accuracy and speed of parameter estimation, thereby enhancing the reliability of PV modelling. As research progresses, the integration of artificial intelligence, hybrid optimization techniques, and data-

driven models is expected to further enhance predictive accuracy, adaptability, and computational efficiency.

Looking forward, enhanced PV modelling will facilitate the seamless integration of large-scale renewable energy. It will boost system reliability, minimize inefficiencies, and optimize storage while interacting with the grid. This is especially crucial for maintaining stable operations when renewable energy penetration is high. A well-designed PV system model serves as the foundation for both standalone and grid-connected applications.

The modular feature of photovoltaics offers a wide range of applications, from small milliwatt devices, such as watches, to large gigawatt utility power plants (Quaschning, 2016). This scalability enables PV systems to be implemented in various forms, including standalone units that supply energy in isolated locations and grid-connected setups that enhance grid stability, facilitating the transition toward sustainable energy. A grid-connected PV system can be either a utility-scale PV installation or a residential PV system. The following section examines these configurations, with a focus on the grid-connected PV system.

2.1.3. Stand-alone photovoltaic

Photovoltaic technologies that operate independently of the grid are called stand-alone systems. These systems comprise a photovoltaic generator, batteries for storage, AC and DC loads, and various power conditioning components, as shown in Fig. 2.5. A photovoltaic generator is composed of multiple arrays connected in a systematic manner to meet the load requirements. Each array contains several modules connected in series and parallel configurations. The storage system stores electricity when production exceeds the load and releases it when production is low or insufficient. Stand-alone systems can supply power to both AC loads, such as heaters and motors, as well as DC loads, such as lighting. The power conditioning system, including charge controllers, DC to AC inverters, and blocking diodes, provides the necessary protection and interface among the components of the PV system (Hansen et al., 2000).

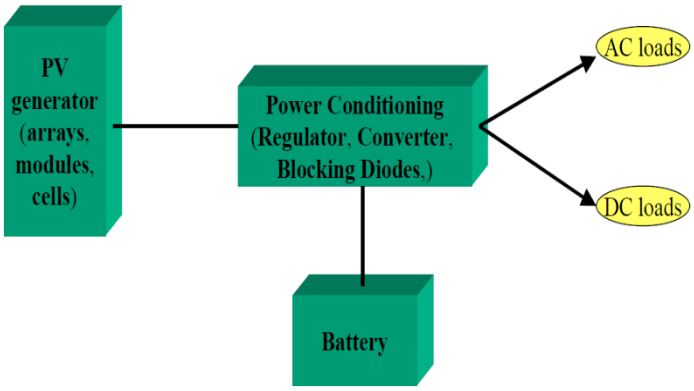

Fig. 2.5. Stand-alone PV system components (Hansen et al., 2000)

2.1.4. Grid-connected photovoltaic system

The integration of renewable energy into the utility network is showing substantial interest by utilities and governments for its numerous advantages. Among various renewable energy sources, the integration of solar PV into transmission and distribution networks remains a key focus, with significant future growth potential. Compared to standalone systems, grid-connected PV systems offer several advantages, including higher energy harvesting efficiency and better utilization of generated power. Notably, grid-connected PV installations account for

more than 99% of the total installed capacity worldwide. In the case of residential grid-connected PV, the need for energy storage is reduced or eliminated, depending on the design and grid standards of the specific region. Consequently, all or part of the generated electricity is injected into the grid without requiring excessive storage, particularly during periods of surplus generation around noon (Kouro et al., 2015). Additionally, these systems support the grid by supplying power to local consumers and feeding excess electricity into the grid during peak solar hours, thereby reducing transmission and distribution losses (Obi and Bass, 2016).

However, the seamless integration of PV systems into the utility grid needs to satisfy a set of technical guidelines and standards from both the PV system side and the utility side. Strict implementation of these technical guidelines and standards is compulsory for safe and efficient integration of PV to the utility grid. The rapid increase of PV installation has also called for evolutionary conversion technologies. The development of converter along with the other semiconductor interfaces brings several advantages in grid-connected PV systems such as ease of integration, efficiency enhancement, and reduction in cost. The technology of PV inverter/converter is evolving rapidly and reaches at a level of efficiency of about 98%. Moreover, modern PV converters are extremely reliable, efficient and compact (Kouro et al., 2015). Inverters are devices that convert the DC power output of PV arrays to AC power that can be used in ordinary power systems and are compatible with the grid standard frequency.

The power output of PV plants fluctuates over time due to the stochastic nature of solar radiation. Therefore, any drop in power generation from a solar plant must be compensated for by increased generation from another plant to meet customer demand. This presents a significant challenge for power operators, particularly when the penetration of PV increases, as sufficient reserves with rapid ramping capabilities must always be available to dampen sudden fluctuations. A proper understanding of the temporal and spatial characteristics of PV power output can partially solve this (Femin et al., 2016).

Fig. 2.6 shows the components of the conventional grid-connected PV system. As shown in the figure, the DC current generated in the PV array is transformed and transferred via various interfacing devices to the grid. Optional components, such as a DC/DC converter, boost the voltage to a certain level if required and decouple the PV from the grid-connected inverter. The low-frequency transformer is an optional device that is integrated into the system depending on the system topology and regulation. Other elements such as grid connection filter and grid monitoring unit are also incorporated to the system to provide safety features such as synchronization and anti-islanding detection (Kouro et al., 2015).

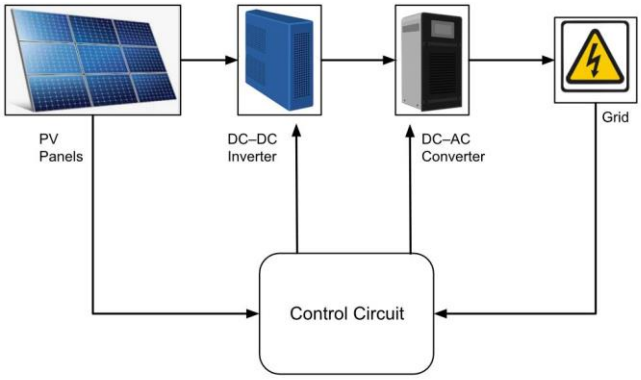

Fig. 2.6. Schematic representation of a grid-connected PV system (Soham et.al., 2017)

In contrast to small, distributed PV generators, large-scale grid-connected PV systems necessitate careful configuration and design to maximize energy extraction. The output current and voltage of PV modules are significantly lower than the grid's voltage and current. Therefore, modules are connected in series and parallel to enhance voltage and current, respectively. Additionally, the quantity and placement of converters introduce various configuration options. The configuration of the grid-connected PV system is shown in Fig. 2.7.

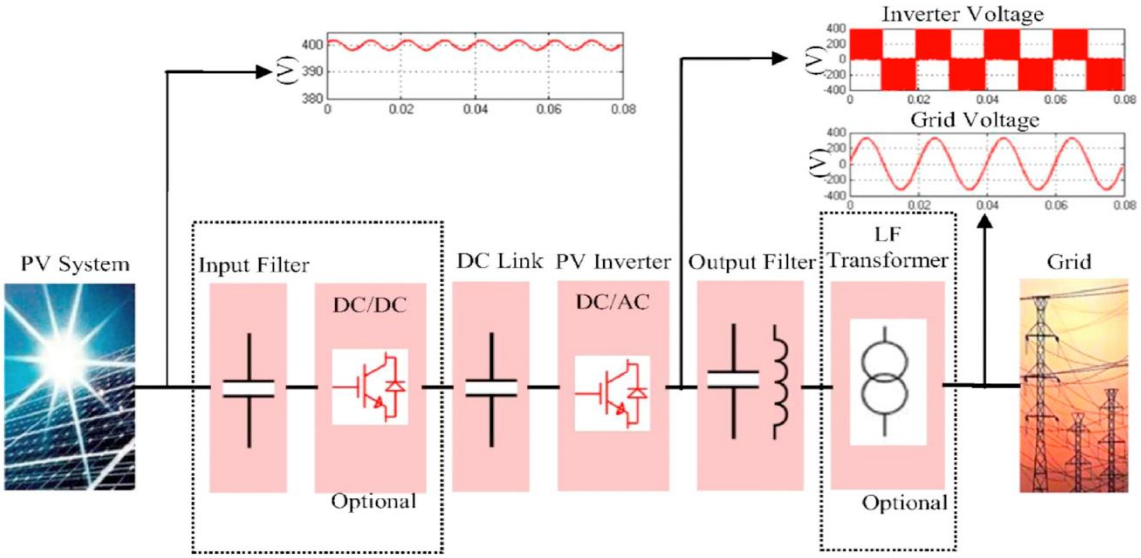

Fig. 2.7. Inclusive representation of a grid-connected PV system (Zeb et al., 2018)

In a centralized configuration system depicted in Fig. 2.8a, modules connect in both series and parallel to supply power to the commutated inverter. In the string topology represented in Fig. 2.8b, each string channels power to the grid via an inverter. Likewise, the multi-string setup, shown in Fig. 2.8c, includes a DC-DC converter for each string, designed for maximum power point tracking. Ultimately, the strings transmit their power output through a DC link to an inverter. A more reliable and efficient system emerges when multiple low-power parallel inverters are used instead of a single centralized inverter. The fourth generation, illustrated in Fig. 2.8d, offers several advantages such as improved expandability and simplified installation, utilizing a complex power electronic interface for each module (Mirhassani et al., 2015).

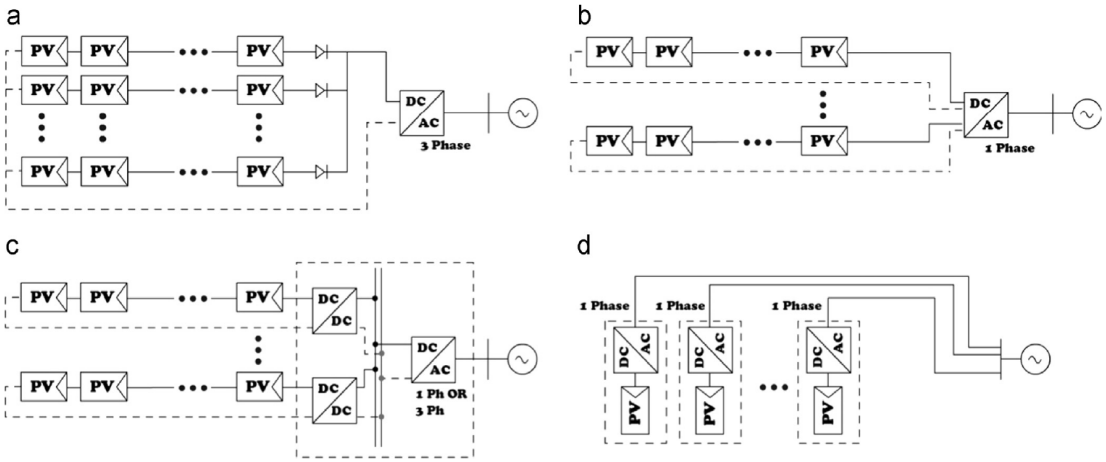

Fig. 2.8. Different topologies for a grid-connected PV system: a) Centralized approach, b) String approach, c) Multi-string approach, d) AC-module approach (Mirhassani et al., 2015)

2.1.5. Grid-connected residential photovoltaic system

Residential PV has become a crucial aspect of distributed generation, transforming buildings from mere electricity consumers into significant contributors due to their increasing implementation (de Oliveira e Silva and Hendrick, 2017a). This trend has considerable potential to lower the carbon footprint of residential buildings (Chandel et al., 2024). Additionally, the falling prices of residential PV systems and home battery storage encourage consumers to produce energy locally, thereby diminishing their reliance on the grid (Procopiou et al., 2019). Nevertheless, the rise in PV energy from homes might surpass local demand. Such uncontrolled integration of PV systems can disrupt load patterns, potentially threaten grid stability (Ruf, 2018a), violate dispatch margins, and elevate the overall operational costs of the power system (Dierckxsens et al., 2015; Kenneth and Folly, 2014). Utilizing AI technologies like machine learning, blockchain, and the Internet of Things (IoT) (Tajjour and Singh Chandel, 2023), alongside grid management strategies, such as feed-in limits, can effectively manage unpredictable renewable energy generation.

Numerous studies indicate that a considerable portion of a household's electricity demand can be satisfied by combining PV with battery storage at the residential level (Camilo et al., 2017; Gudmunds et al., 2020; Li et al., 2018). In an effort to attain self-sufficiency in household energy consumption through affordable methods, several nations have enacted support policies and incentives to promote the installation of residential PV-battery storage systems (Held et al., 2020; Zeh and Witzmann, 2014). However, there is a lack of research explicitly examining developing countries, such as Eritrea, which has a less stable energy system.

In Ruf. (2018b) a comprehensive grid planning strategy in Germany is discussed, along with its implications for inducing technical constraints. Germany is the leading nation in renewable energy utilization and adoption in Europe, credited to its cutting-edge research and development initiatives. The authors indicate that the current grid planning strategy is not encouraging large-scale PV integration at all levels, particularly in the low-voltage work, as such feed-in from PV at the low-voltage network was not considered during the design stage of the existing grid. However, new technologies can increase the hosting capacity of the low-voltage distribution network.

Another study that deals with the Belgian electricity grid evaluates different combinations of residential PV, storage, and fixed wind capacity with the sole aim of increasing the direct consumption of PV and wind generation in the electricity grid (Meuris et al., 2019). The model utilizes hourly historical data to simulate the case study, selecting the scenario that maximizes the directly injected generation from PV and wind sources. Increasing PV and wind requires some curtailment of generated electricity, and adding a battery at this stage increases the overall effectiveness of the system. However, they identified an upper limit above which any additional battery storage does not return benefits to the system. They also found that minimum curtailment, along with optimal storage, could be cost-effective in the future grid dominated by renewables. Another study, conducted by Teklebrhan et al. (2025), examined the effect of the feed-in limit in low-voltage networks using historical data from Eritrea. The study indicates that residential PV can contribute up to 32% of total demand when combined with a battery and an optimal feed-in limit. They developed a transparent and easy-to-follow algorithm to determine injection limits, battery sizing, and PV configuration, maximizing the total injected PV and wind power into the low-voltage network. Feed-in limits between 0.4 and 0.5 kW/kWp, combined with home battery storage of less than 2 kWh/kWp, yield the most favourable

outcomes. A schematic illustration of a grid-connected residential PV system with an energy storage device is given in Fig. 2.9.

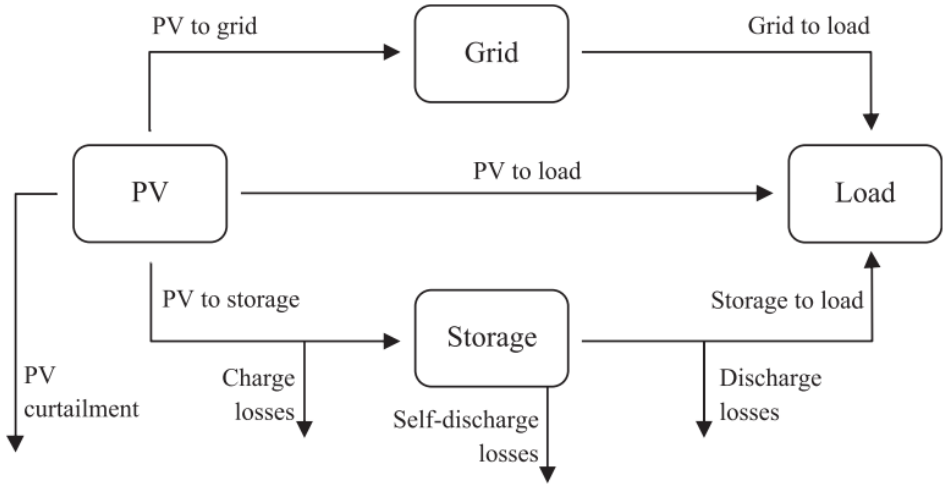

Fig. 2.9. Illustrate diagram how the Residential PV works (Silva and Hendrick, 2017)

2.1.6. Grid inverter technologies

The grid-inverter is the essential element of a distributed generation system; it serves as a crucial interface for distributed renewable energy resources. A PV inverter's primary function is to maximize energy capture from the solar PV system through Maximum Power Point Tracking (MPPT) technology and effectively convert it into a utility-compatible power source. It ensures efficient power conversion from DC to AC, aligns with the grid frequency, and facilitates the smooth integration of solar electricity into the desired distribution or transmission network. Furthermore, contemporary inverters enhance system reliability, improve power quality, and contribute to grid stability by regulating voltage fluctuations and reactive power. Grid-connected inverters can be classified into four categories based on their configuration (Kabalcı, 2020; Zeb et al., 2018):

a. Central inverters
b. String inverters
c. Multi-string inverters and
d. AC Module inverters or microinverters

Each configuration has its own advantages and drawbacks. The topography of each category is shown in Fig. 2. 10.

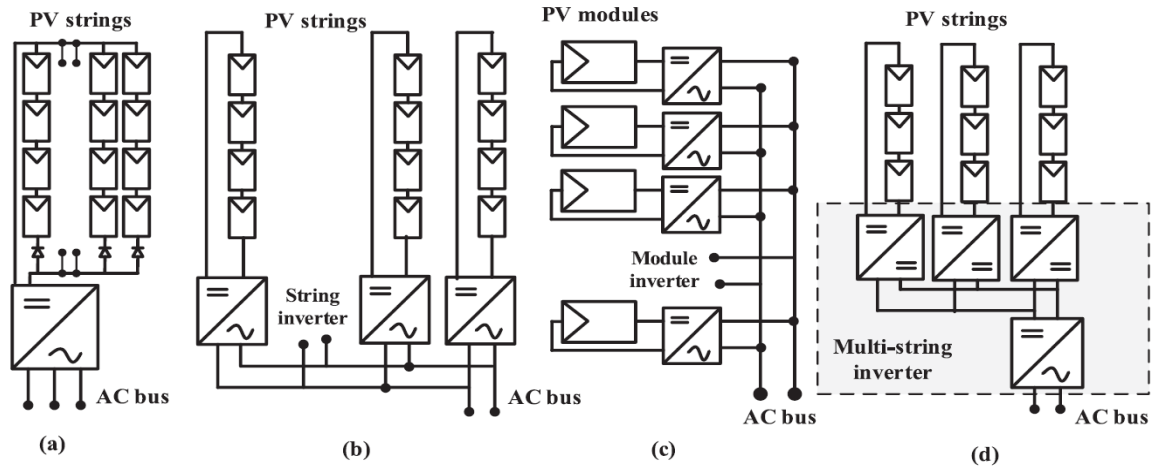

Fig. 2. 10. Configuration of grid-connected PV inverters (Zeb et al., 2018)

Inverters are responsible for detecting islanding and protecting human life and equipment from damage by disconnecting the PV system in a very short time. Islanding is the condition when the inverter continues to supply power to the grid when the utility side is stopped or disconnected due to different reasons, such as maintenance, damage, or accident (Kjaer et al., 2005). Such a situation is critical since utility operators may engage in different activities, assuming the grid is safe (not operating), but due to the grid-tied PV system, the grid can be energized, posing dangers to personnel working on the feeders. For this reason, inverters are equipped with anti-islanding protection features to quickly stop feeding power to the utility when the utility is disconnected.

2.1.7. Power quality issues in distributed generation

Renewable energy-based distributed generation systems are reaching a record high level of integration in the distribution network for their remarkable environmental, technical, and economic advantages. The main contributor of distributed generation is residential PV, as buildings once primarily electricity consumers are now contributing significantly to generation via residential PV installation (Silva and Hendrick, 2017a). In this context, the power system behaves differently as it changes from unidirectional, in conversational systems, to bidirectional power flow with distributed generation units. When the penetration level of solar PV in the distribution network increases, it creates several challenges in the distribution network, including reverse power flow, increased power losses, voltage unbalance, transformer and cable rating, and malfunction of on-load tap chargers (OLTC), and this ultimately affects the control, operation, and security of the traditional distribution feeders. The most critical power quality issues related to grid-connected PV systems are power fluctuation, voltage deviation, flicker, and harmonics (Hossain et al., 2018).

2.2. Enabling technologies supporting large-scale photovoltaic integration

Integrating large-scale renewable energy sources has proven to have numerous environmental and economic benefits. Specifically, integrating large-scale PV as the fastest-growing technology with a remarkable increase in capacity presents both opportunities and challenges (Mansouri et al., 2019). Extensive PV integration provides several benefits in addition to covering a significant share of demand. They help decrease emissions, promote energy independence, provide a cleaner energy mix, and improve grid stability. Additionally, these plants provide ancillary services, such as frequency control. Nonetheless, integrating large-scale PV presents various challenges, including system complexity, generation

unpredictability, technical constraints, voltage regulation issues, the need for coordination with traditional power plants, and the implementation of sophisticated control strategies to comply with grid code requirements, particularly during periods of peak generation (Rakhshani et al., 2019). The literature proposes various enabling tools that maximize their reliable and efficient integration.

Solomon et al. (2019) discussed several supply-side enabling technologies, including resource complementarities, energy storage, transmission interconnection, improved forecasting, and curtailment that facilitate large-scale PV integration. Utilizing these enabling technologies can facilitate large-scale PV integration by addressing challenges like variability, uncertainty, and system adequacy. However, a solid theoretical framework is necessary for designing a secure system, as the significance of one technology may differ based on PV share (penetration) and the role of other enabling technologies. Enabling technologies, such as demand response, can help adjust consumption in relation to PV generation by shifting loads to different times, thereby enhancing grid stability. In Zubi et al. (2025), the importance of energy storage solutions in managing variability and uncertainty, as well as balancing supply and demand, is presented and discussed, along with their impact on grid operation and economic viability.

A time series simulation was conducted on the Texas grid to examine the impact of variable generation, with varying ratios of PV, concentrating solar power, and wind designed to provide approximately 80% of the total demand (Denholm, 2011). The author examined various enabling technologies, including energy storage, conventional generator flexibility, demand response, and load shifting. Different combinations of these enabling technologies create a better energy mix at a specific level of renewable penetration by minimizing surplus curtailed solar and wind energy.

The renowned renewable energy report from IRENA indicates that the innovation landscape for integrating large-scale renewable energy necessitates synergies among various enabling technologies to achieve a viable solution (IRENA, 2019). The report classified the solution for the significant uptake of solar and wind energy into four major categories: innovation, enabling technologies, market design, business model, and system operation. The most significant enabling technologies that facilitate large-scale PV integration have been identified, including electric vehicles, smart charging, utility-scale batteries, Internet of Things, behind-the-meter batteries, artificial intelligence, big data, and blockchain.

Mansouri et al. (2020) investigate the importance of enabling technologies in facilitating the integration of large-scale photovoltaic (PV) systems into the power grid. The technologies investigated include energy storage, active power curtailment, advanced inverters, and innovative grid technologies that help mitigate power quality issues such as harmonics, voltage fluctuation and imbalance. Several challenges created by PV integration are resolved using these supporting technologies, including power quality, system stability, and reliability. The study identifies the primary issues arising from the large-scale integration of PV in the public network. It quantifies the impact of various enabling technologies on large-scale PV integration.

In Denholm and Margolis (2007a) a detailed analysis of technologies that enable the integration of 50% of PV power into the utility grid was conducted by simulating hourly solar insolation and load data to address the limitations of conventional generators on PV integration. Various enabling techniques, such as increased flexibility, energy storage, and load shifting, were

explored to reduce the curtailed PV that occurs at high penetration levels. Increasing system flexibility by lowering the system minimum can facilitate greater absorption of PV, while shifting loads to times of higher PV generation can enhance the usability of the generated PV power.

Solar PV is among the most promising variable renewable energy sources, anticipated to make a significant contribution to the power mix. However, its increased deployment is accompanied by numerous challenges. In Mateo et al. (2017), technical solutions that can overcome the barriers that hinder the integration of large-scale PV into the electricity network were proposed. The solutions are grouped into three big categories: distribution system operator solutions, prosumer solutions, and interactive solutions. Among the various proposed solutions, PV curtailment enhanced PV hosting capacity and eliminated unnecessary PV-driven network investments.

Although the aforementioned studies differ in the scenarios considered and the geographical locations analysed, they all share the common goal of identifying the optimal combination of enabling technologies to support large-scale PV integration. This thesis identifies four key enabling technologies that support higher PV penetration: resource complementarity, energy storage, curtailment strategies, and advanced forecasting. Each of these plays a crucial role in facilitating the integration of large-scale PV. These technologies will be reviewed in detail in the following sections.

2.2.1. Complementarity of solar PV with wind

Renewable energy resources such as solar and wind are naturally intermittent and unpredictable. Large-scale integration of these resources could result in various technical challenges, as the existing grid is not designed for variable supply but for variable load demand. Specifically, the integration of variable renewables in weak grids without a proper or sufficient storage system could severely affect the reliability of the power system. The variability and intermittency of renewables can be partially solved by mixing two renewables into an optimum combination, improving overall system reliability and adequacy (Badwawi et al., 2016).

The concept of complementarity in renewables basically refers to how different renewables, such as solar and wind (variable renewables) or hydropower and geothermal (non-variable renewables), complement each other's variability in time (diurnal or seasonal), or space (geographically diverse resources), or both in time and space. Fig. 2.11 shows the seasonal variability of solar, wind, and electricity demand.

Jurasz et al. (2020) grouped complementarity into three main categories:

1) Spatial complementarity: In this category, one or more renewable energy resources can complement each other in a certain region. For example, a resource deficit in region A can be complemented by a resource of its kind in region B. By doing so, we can improve the smoothing level of distributed resources.
2) Temporal complementarity: In this category, two or more VRE resources complement each other in the time domain. For example, at the seasonal level, limited solar energy during the winter is complemented by stronger wind generation in the same season, while in summer, higher solar output can offset lower wind availability. A comparable analogy exists for daily changes in solar and wind energy production; diminished or absent solar output at night can be offset by robust wind generation during the night.

3) Spatio-temporal complementarity: Refers to the ability of different renewable energy sources to compensate for each other's variability across time and space. When single or multiple VRE resources are investigated for complementarity simultaneously in time and space domains.

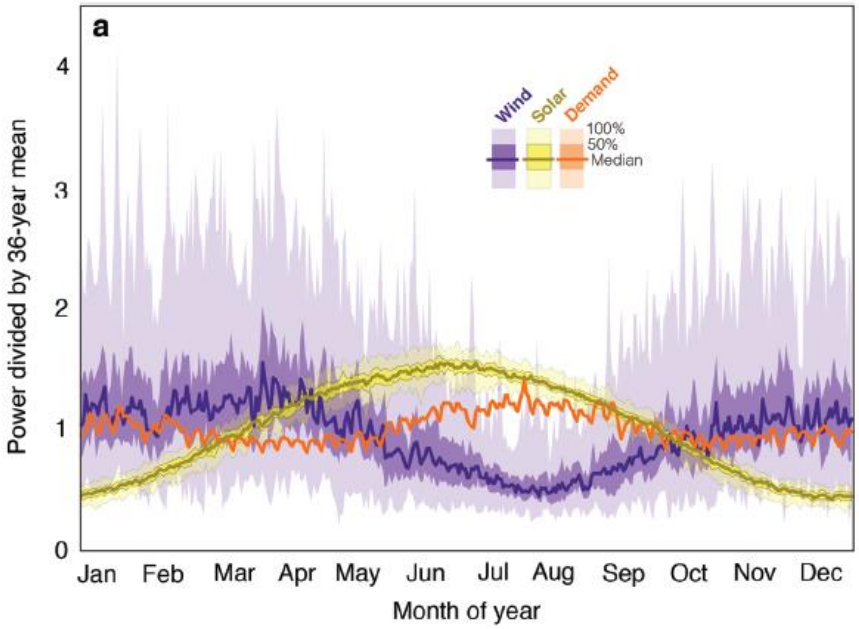

Fig. 2.11. Time-based variation in solar, wind, and electricity demand (Shaner et al., 2018)

Resource complementarity is defined as the ability of a mix of renewable generation resources, spread across space and time, to enhance electricity supply conditions. Thanks to the better alignment of output with demand profiles, this improvement occurs with fewer operational challenges and a reduced reliance on enabling technologies. Resource complementarity offers significant benefits to the power grid by smoothing generation profiles, particularly wind-PV complementarity, providing multi-dimensional benefits such as increasing penetration, reducing curtailment, improving energy storage requirements, and improving overall system reliability. Compared to stand-alone PV or wind, complementarity significantly increases grid penetration without energy storage; however, as capacity increases, the benefit of complementarity on increasing the grid penetration decreases due to the mismatch between generation and demand (Solomon et al., 2020).

Different metrics and indices, such as the correlation coefficient (CC) and standard deviation, are used to assess the local complementarity of renewable resources at various time scales (Miglietta et al., 2017). Other studies, such as in Naeem et al. (2019) utilize generation profiles to maximize the economic benefits by exploiting the PV and wind complementarity across different time steps.

The study indicated that anticorrelated PV and wind sites present the best-case scenario for meeting demand without storage and curtailment. In this context, a negative correlation (CC=-1) is ideal for smoothing generation profiles and enhancing the penetration of PV and wind without requiring additional enabling technologies.

Although several studies have been conducted to analyse the benefits of PV and wind complementarity, most focus on examining correlations and other statistical indicators of renewable resources over time and/or space. Studies based on data collected from actual utility plants are rare. Such studies could provide valuable insights into how a future grid dominated by renewables might be sustained. However, because of the current low share of renewables,

comprehensive information cannot be obtained to address the challenges that may arise for future grids due to the integration of large-scale renewables. Some studies use actual generation profiles from utilities to examine the complementarity benefits in the power system. In Couto and Estanqueiro, (2021) correlation and energy metrics are used to assess the hourly and daily complementarity potential of actual wind parks with solar PV plants in Portugal. They found a high correlation between PV and wind, allowing the integration of a higher share of variable renewables at reduced excess generation. Fig. 2.12 shows the concept of complementarity using a sine signal.

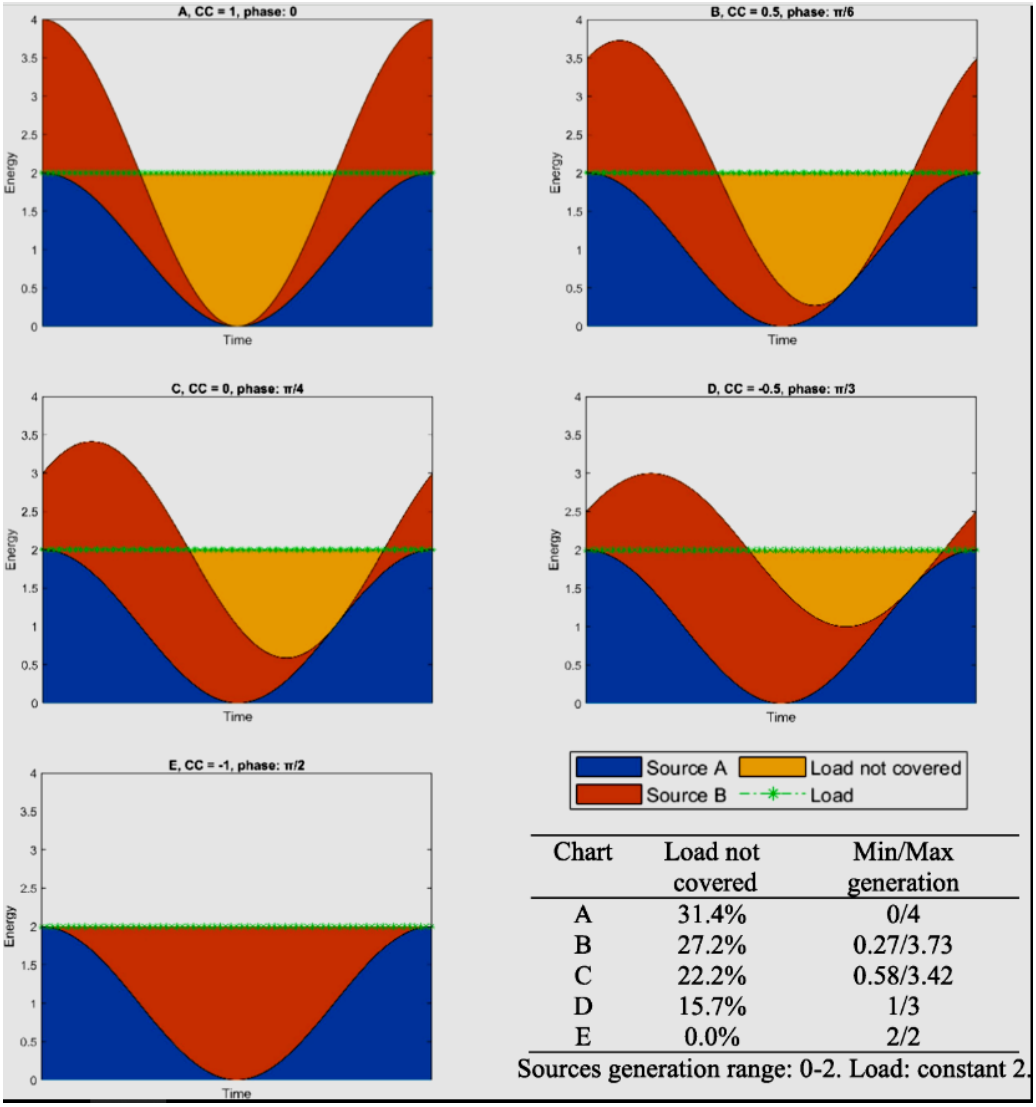

Chart	Load not covered	Min/Max generation
A	31.4%	0/4
B	27.2%	0.27/3.73
C	22.2%	0.58/3.42
D	15.7%	1/3
E	0.0%	2/2

Sources generation range: 0-2. Load: constant 2.

Fig. 2.12. The complementary concept is explained by means of a sine signal. CC – coefficient of correlation (Jurasz et al., 2020)

Transitioning to clean energy requires integrating large-scale VRE resources, such as PV and wind, which in turn raises several uncertainties in grid reliability and operational requirements. The current grid has strict standards, such as planning supply that meets peak load with an additional 15% reserve margins (Cauley and Cook, 2011). However, unlike the existing grid, which has uncertainty only from the demand side, the future grid dominated by renewables will pose uncertainty challenges from both the supply and demand sides. Thus, a future grid will behave differently, as it will require significant energy curtailment accompanied by subtly used large conventional balancing capacity and large storage facilities. Though hybrid systems are believed to relieve such grid stress to some extent, demand response is also thought to help

maintain such a new grid infrastructure by leveraging loads with generation. A study by Solomon et al. (2016) conducted a deeper and comprehensive analysis to understand the characteristics of a high-renewable California electricity grid by closely examining the year-round generation and demand profiles and dispatch patterns. The authors explore the supply-side reliability issues and the impact of complementarity on system design and operation. They reported that PV-wind complementarity offers several benefits, such as increased penetration and reliability. Further, they noted that at a particular curtailment level of 20%, their optimal mix enables higher penetration at reduced storage and balancing capacity requirements.

While these studies may vary in scope, geography, metrics, methodologies, and the variables used, their ultimate goal is to quantify the ideal combination of renewable sources and the accompanying enabling technologies. Most of these studies demonstrate that PV-wind complementarity is the most promising approach to achieving a future grid with a high share of renewables, as it offers several benefits to this grid. Comparison between studies is still not possible as these studies consider different scenarios, resource potential, and locations. However, they may share common performance indicators and system parameters such as penetration (% annual demand met by renewables), resource mix, storage size, and curtailment.

To wrap up, the benefits of resource complementarity (in our context PV-wind) to the grid can be generalized into three main categories: improving reliability, reducing balancing requirement and storage capacity, and improving grid penetration.

2.2.2. Electrical Energy Storage

The existing power system would undergo a transformative paradigm shift if energy storage operations reached a high efficiency level with better economic viability. Intermittent renewables, such as PV and wind, could be widely deployed to transition the energy mix to a eco-friendlier and more sustainable model. Technologically mature and efficient energy storage could improve the stability and reliability of a power system. The most important feature of energy storage is that it can be used both during deficit and excess generation. When intermittent renewables generate excess power, energy storage can shift the high generation to off-peak hours or deficit times. This allows the system to run more efficiently in balanced mode without disturbance. Moreover, energy storage can encourage distributed generation by enabling the use of residential PV and wind systems. Energy storage offers several benefits to the power system such as operational flexibility and intermittency mitigation (Rahman et al., 2020).

Energy storage is a device that converts energy from one form to another, depending on the purpose, in our context, to electricity, after being kept for some specific duration. Energy storage can be characterized by its response time, storage duration, and function. However, it can also be more effectively classified into mechanical, electrochemical, electrical, and chemical categories, based on the type of energy stored (Rahman et al., 2020). Based on how energy is converted back, storage devices can also be divided into power-to-power, power-to-thermal, power-to-liquid, and power-to-gas. If excess renewable electricity is stored in electrical energy storage and converted back to electricity, it is called a power-to-power system. This system is the most promising energy storage system and is widely used for several applications. Its advantages include, but are not limited to, time-shifting power dispatch, smoothing mismatch, consequently allowing a higher level of RE integration, encouraging distributed generation, decreasing curtailment, enhancing electricity value chain, increasing overall system efficiency, and maintaining system frequency and voltage fluctuation that ultimately improves grid reliability and security (Gallo et al., 2016).

Fig. 2.13 depicts the finer classification of the various categories of energy storage systems. These technologies are at different levels of technological maturity and market penetration. Recently, energy storage systems have evolved rapidly with swift technological advancement and cost decline. Electro-chemical batteries such as Vanadium-redox, lithium ion (Li-ion), sodium-sulfur and lead-acid batteries are extensively used in different applications, with Li-ion having emerged as a transformative breakthrough in storage applications. With advances in technology and cost reductions, large-scale grid-integrated battery storage systems have become increasingly necessary in modern power systems (Rahman et al., 2020). Specifically, ambitious renewable integration targets, increasing electronic energy conversion devices (allowing bidirectional flow), and Electric Vehicles make such diversity and increasing use of battery services imperative for the next-generation power system. However, optimal technical and economic operation and performance will remain a primary concern in the future (Zhao et al., 2023).

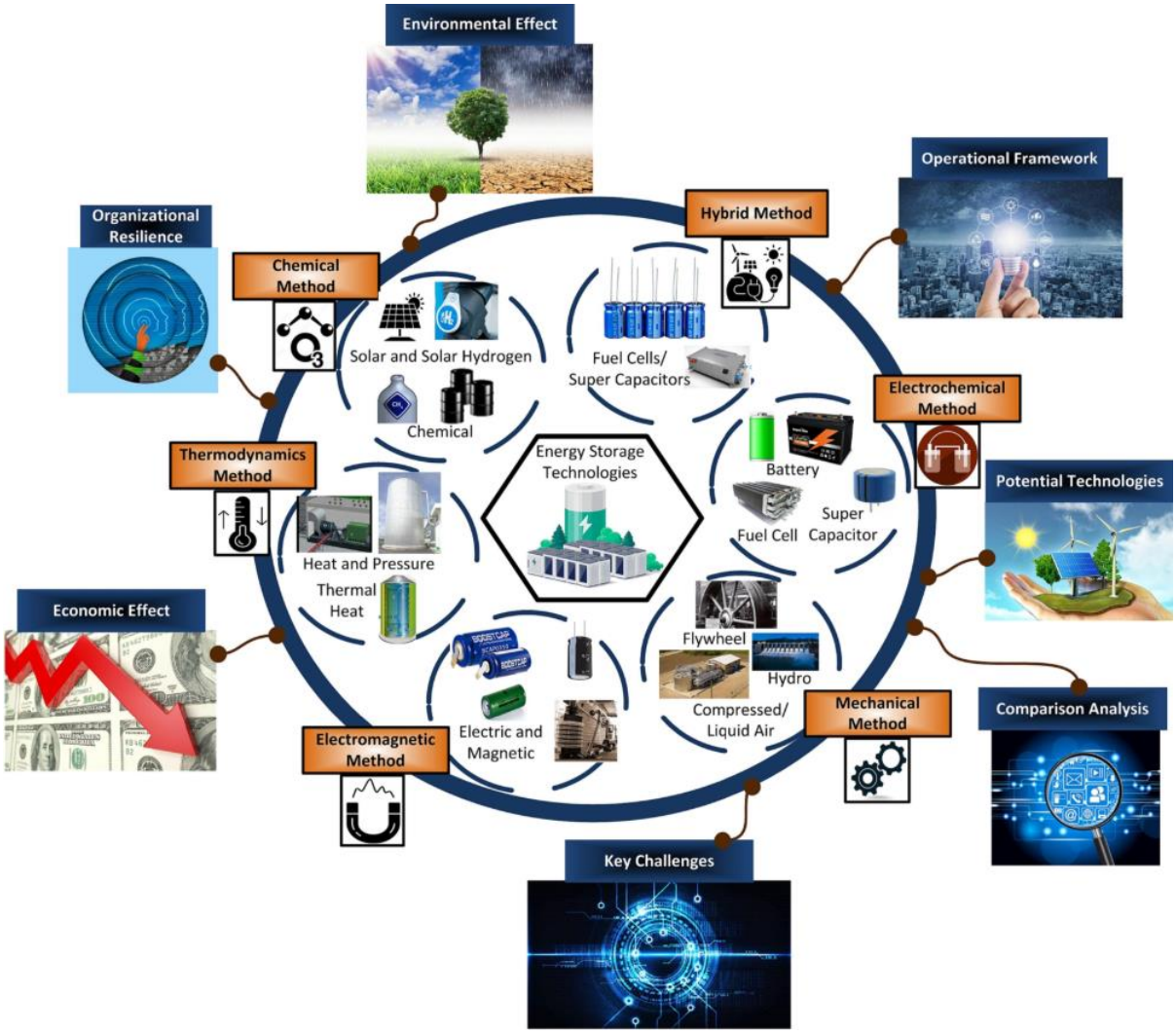

Fig. 2.13. Different types of Energy Storage technologies and their interaction (Amir et al., 2023)

The literature discusses various aspects of the grid-connected storage system, including performance evaluation, techno-economic assessment, and technological advancements. In Noyanbayev et al. (2018) a simulation model was developed to investigate the efficiency performance of a system installed at the University of Manchester. They identified the optimum operation mode by accounting for the state of charge and the rate of battery storage charging

and discharging. They reported that the developed simulation model was well aligned with hardware performance, with a difference of approximately 2%. Another study was performed on modelling, simulation, and performance evaluation of grid-integrated PV with battery storage. They introduced a control method to manage and enhance the battery storage's state of charge, charging, and discharging, providing a benefit for regulating DC bus voltage (Daud et al., 2012).

Engineering design must ensure technical feasibility and economic viability of options. Studies show that PV plus storage offers a significant economic advantage by utilizing energy that would otherwise be wasted. As study by Denholm et al. (2017) conducted a case study in southern California, using their engineered metric called Benefit/cost ratio. They evaluated the trade-off of using PV plus storage with the shared inverter. At a low PV penetration of 6%, they found that the Benefit/cost ratio for PV without storage is higher than that of PV with storage. However, the trend changes as the PV penetration increases. The results suggest that decreasing PV values can be offset by incorporating storage, facilitating cost-effective large-scale PV integration.

When the VRE penetration level is low, integration, operation, and performance improvement are manageable; however, as penetration increases, unforeseen issues arise due to the mismatch between generation and demand. Diurnal and seasonal weather variability strongly affect storage operation and overall system performance. A study by Twitchell et al. (2023) evaluates the depth and breadth of future decarbonized grid energy mismatches and identifies that two types of long-term energy storage are required for a fully decarbonized grid: 20-hour storage for diurnal cycles and longer-lasting weeks or months for seasonal mismatches.

Other studies examined various energy storage technologies suitable for solar and wind hybrid systems, each designed with unique characteristics that optimize them for specific time scales and applications. These technologies comprise batteries (Javed et al., 2019), hydrogen storage (Gabrielli et al., 2020), pumped hydro storage (Guezgouz et al., 2019), compressed air energy storage (CAES) (Torreglosa et al., 2015), and hybrid storage systems, such as battery-hydrogen (Li et al., 2023).

Energy storage technologies are deployed at various levels of renewable penetration to mitigate diurnal and seasonal weather-induced generation fluctuations. Therefore, integrating both diurnal and seasonal storage is essential for addressing the weather-driven variability of daily and seasonal cycles in a renewable-dominated grid.

Fig. 2.14 shows the energy and power components of the major energy storage technologies widely deployed at scale.

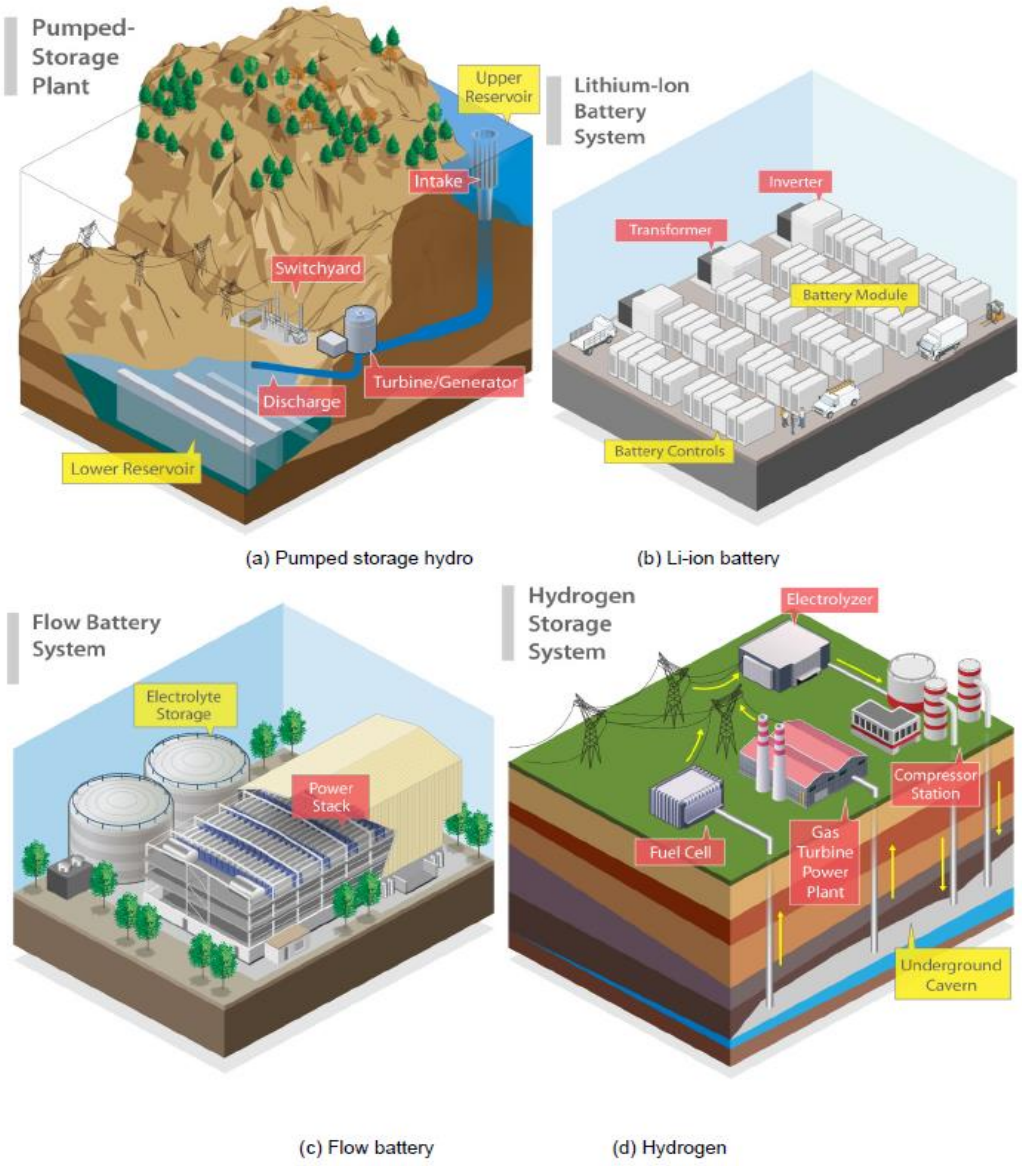

Fig. 2.14. Different energy storage technologies show both energy and power components (Denholm et al., 2021)

2.2.2.1. Diurnal storage for daily cycles

Renewable energy deployment has been shown to be beneficial in creating a carbon-free and eco-friendly energy system. However, their introduction necessitates additional weather-derived informed decision-making to ensure a secure and reliable power system (Bloomfield et al., 2018). A thorough understanding of the meteorological drivers that cause the fluctuation in renewable generation is imperative. Moreover, understanding these variables' cyclic pattern and time step or frequency of occurrence is crucial in designing a secure system, as local weather patterns could affect the short-term (diurnal) or long-term (seasonal) system performance (Bloomfield et al., 2022).

Solar and wind energy show variations over different timescales, from minutes to seasons, influenced by elements like atmospheric conditions, Earth's rotation, orbital position, and axial tilt. The daily cycle of solar radiation leads to considerable fluctuations in PV generation, peaking between noon and 3 pm, then declining until it approaches zero in the late evening. Similarly, wind patterns exhibit a distinct diurnal variation, influenced by surface temperature

caused by solar radiation. Wind speeds generally reach their peak in the afternoon after the maximum surface heating and dip to their lowest in the early morning, about 12 hours earlier (Mulder, 2014). Such diurnal variation leads to generation fluctuation, consequently affecting the matching ability of renewable generation and load.

The net load, which results from subtracting variable renewable generation from total load, needs to be balanced throughout the year using a dispatchable power supply unit. This can include non-variable renewables like hydropower or geothermal, or energy storage solutions (Graabak and Korpås, 2016).

The choice of a storage technology is influenced by factors such as storage capacity, response time, cost-effectiveness, energy losses, and its effectiveness for short-term or long-term energy shifting. For short-term (intraday) energy storage batteries, such as Li-ion and flow batteries, are ideal due to their high, rapid response, round-trip efficiency, and relatively low energy loss. They effectively handle daily intermittency in PV and wind-generated electricity by storing excess electricity produced during peak generation hours and supplying it at a generation deficit. Due to their special features in modularity and scalability, they can be used in both large-scale grid-connected systems and in small-scale distributed generation (which may be stand-alone or grid-connected) applications. However, the limited storage duration and associated high capital expenditure make them unsuitable for long-term seasonal energy storage (Denholm et al., 2023).

The literature presents a range of storage solutions, along with detailed evaluations of their performance and techno-economic viability (Child and Breyer, 2016; Cole and Frazier, 2023; Denholm et al., 2022), In a study conducted for Texas grid, Denholm and Mai. (2019) analysed storage duration required to integrate large-scale renewable energy to the grid with reasonable curtailment. The study revealed that the addition of a storage capacity of about 8.5 GW with a four-hour duration could drastically reduce curtailment from 11-16% (without storage) to 8-10%. The technical feasibility and the cost become challenging when RE penetration exceeds 80-90% as shown in Fig. 2.15.

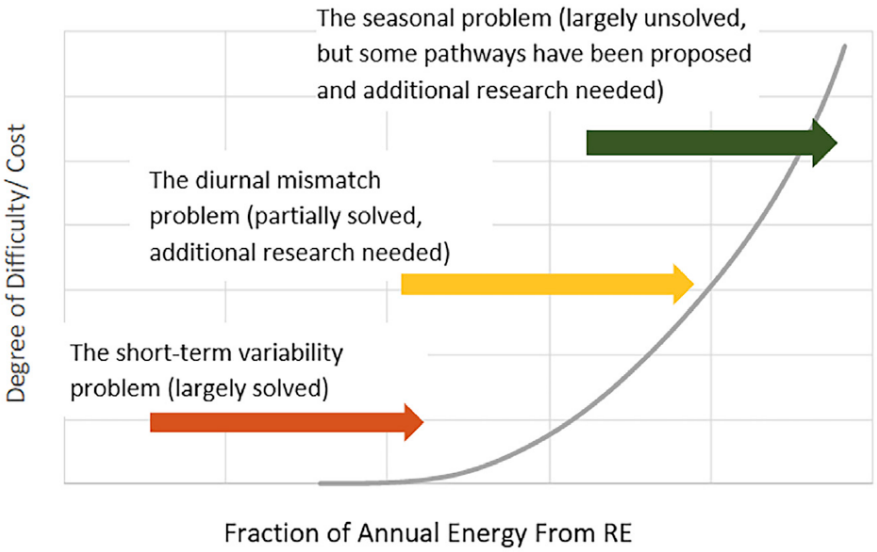

Fig. 2.15. The increasing difficulty and cost of RE deployment with balance challenges (Denholm et al., 2021a)

Recently, there has been a growing interest in utilizing energy storage systems with a capacity lasting more than four hours, owing to their crucial role in integrating large-scale renewables and transitioning to a decarbonized grid. A diurnal storage range of 6-10 hours has shown

economic opportunities for hundreds of Gigawatts of storage, even with existing policies for reducing carbon emissions. The potential and role of diurnal storage in decarbonizing and integrating large-scale renewable energy are tremendous. Studies in the US grid show that the capability of diurnal storage (4-hour storage) to meet peak demand in summer can be enhanced by deploying large-scale solar generation (Denholm et al., 2023).

However, the role of diurnal storage is reduced as the penetration of renewables increases. After a certain penetration threshold, any addition of diurnal storage offers negligible benefits in increasing penetration, as clearly elaborated in (Solomon et al., 2017). Therefore, long-term storage that offsets the seasonal mismatch is required at high levels of renewable penetration.

2.2.2.2. Long-term seasonal mismatches

Understanding storage behaviour at different time scales and penetration levels gives a strong foundation for modelling and designing a reliable power system dominated by renewables. Short-term energy storage technologies, as discussed above, are suitable for satisfying the daily generation fluctuations. However, solar and wind exhibit seasonal fluctuations driven by different factors such as the axial tilt and orbital position. The amount of solar radiation reaching the Earth's surface varies considerably depending on the season and the latitude of the specific location (Quaschning, 2016). The seasonal variation in solar radiation is more pronounced at higher latitudes, where a difference of about a factor of 6 in solar insolation between summer and winter is observed. In contrast, the difference in insolation at lower latitudes, such as the Western Sahara, shows less seasonal variation, with the difference between summer and winter varying by a factor of about 1.5. This suggests that PV generation output can vary by a factor of approximately 1.5 to 6, depending on the geographical location of the plant, although this range may be slightly influenced by power conversion efficiency and other system-specific factors. Likewise, wind speed shows seasonal fluctuations, generally peaking in winter compared to summer. This seasonal variation can be as much as twofold in numerous areas, with winter wind speeds nearly double those during summer. This difference is crucial for assessing the seasonal potential of wind energy and for the strategic planning of renewable energy systems (Mulder, 2014). Such fluctuations present a significant technical challenge for a renewable-dominated grid in ensuring a reliable supply to meet demand, where a greater flexibility in system design and operation is required. Identifying the necessary storage solution that fulfils the requirements is highly effective for balancing supply and demand, as it offers operational reserves (Zakeri and Syri, 2015).

Diurnal storage, such as Li-ion batteries, has been proven to increase the share of renewables significantly; however, their role and significance decrease as renewable penetration increases, typically above 80%. In contrast, seasonal storage technologies such as hydrogen storage and pumped hydro storage (PHS) offer a better fit for long-term energy storage. With an efficiency of 70-85% and a long lifespan, PHS is the most mature and widely used long-term storage technology (Dujardin et al., 2017a). Recently, hydrogen storage has emerged as the most flexible and scalable storage solution, promising a bright future for balancing seasonal fluctuations caused by weather variability. Hydrogen storage utilizes an electrolyser in combination with a fuel cell or gas turbine. Excess renewable energy is stored as hydrogen produced through electrolysis, and this stored hydrogen is converted back into electricity via a fuel cell or gas turbine when there is a need for generation deficit (Ourya et al., 2023). For long-term applications, hydrogen storage provides significant advantages, including high energy density and the ability to store energy with minimal losses (Breunig et al., 2024). Additional advantages, such as application in transportation and aviation, make it a cost-

effective solution (Denholm et al., 2022). Its lower round-trip efficiency makes it better suited for seasonal applications instead of frequent (daily) charging and discharging. Fig. 2.16 shows the seasonal challenge for a very high RE penetration (nearly 100% RE) for the ERCOT grid.

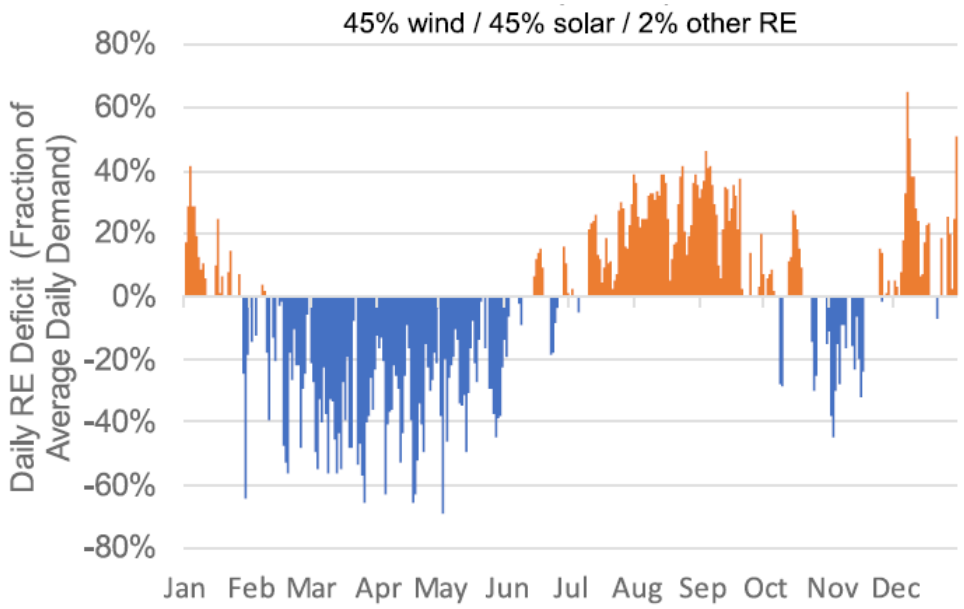

Fig. 2.16. Seasonal challenge for a nearly 100% renewable energy system in the ERCOT grid (Mai et al., 2022)

Other studies also explore the benefits of hybrid storage, including short-term battery storage combined with long-term hydrogen storage. This combination provides unique advantages by leveraging the strengths of both short-term and long-term storage. In these configurations, batteries are used to balance short-term fluctuations, typically lasting 4 to 8 hours, while hydrogen addresses the long-term seasonal mismatch of over 12 hours. This combined strategy boosts system reliability, reduces curtailment, and maximizes the utilization of renewable resources (Guerra et al., 2020a; Qiu et al., 2024).

Several studies agree on the necessity of various flexibility options, including seasonal and diurnal storage, balancing capacity, and curtailment, to achieve a high renewable penetration, typically exceeding 80% (Guerra et al., 2020a). Denholm et al. (2022) demonstrated that a penetration of approximately 90% can be achieved by deploying wind, PV, diurnal storage, advanced transmission, and other technologies currently used extensively at scale at minimal incremental cost. However, satisfying the remaining 10% of the demand remains uncertain as the technologies that lead to complete decarbonization, such as low-carbon fuels and hydrogen, are still not yet utilized at scale. Mai et al. (2022) proposed multiple solutions to tackle the difficulties in meeting the last 10% of demand while ensuring 100% renewable energy integration. Some of the suggested pathways are uncertain as they depend on various emerging technologies that are in their initial phase of development. Various types of seasonal storage are among the proposed solutions that have the potential to satisfy the last 10% of the demand. Seasonal storage can mitigate the seasonal mismatch that occurs in peak summer and winter, as deploying short-term diurnal storage and installing additional VRE capacity at this stage might provide minimal benefits to the system (Denholm et al., 2021a).

Therefore, efforts to achieve a high penetration level require deploying various technologies currently utilized at scale, such as PV, wind, and diurnal storage, to attain approximately 90%

of the penetration. However, the remaining 10% of the demand can be satisfied by seasonal storage, such as hydrogen storage, and other non-variable dispatchable renewable resources, such as geothermal and hydropower.

2.2.3. Renewable curtailment

In recent decades, the integration of renewable energy resources, especially PV and wind, has substantially increased, driven by policy incentives and cost reductions. However, their increased penetration raises concerns about their integration into the power system due to a mismatch between generation, demand, and transmission or operational constraints. Such circumstances require power operators to act to maintain system operation in a safer mode by utilizing various techniques. One such technique involves accepting a limited portion of renewable generation while dumping the excess, which is curtailment. Curtailment can be taken for different reasons, such as transmission congestion, lack of transmission, constraints to local networks, and balancing challenges (Gu and Xie, 2014). Although the definition of curtailment may vary, in this context, it refers to producing a limited portion of the available potential of PV and wind power at a specific time. Curtailment due to over-generation during periods of low demand can happen when must-run plants produce more power than the load and desired exports (Golden and Paulos, 2015). Curtailment in wind power plants can be associated with two main circumstances: transmission and system balancing issues, as wind energy is more available during the night when loads are at their minimum. Similarly, for solar generation, curtailment occurs in the distribution network when there is more energy at the feeders than is consumed, which can cause reverse flow (Bird et al., 2016). If protective mechanisms and other safeguards are not designed in advance, reverse flow can cause serious problems to connected devices. In Henriot. (2015) The advantages of economic/optimum curtailment in VRE were discussed. The study highlighted that in a power system with a large share of VRE and inflexible thermal generators, curtailment of intermittent renewables could lead to system efficiency gains. The penetration of intermittent renewables increases with modest curtailment; however, the gain in penetration beyond 20% of renewable curtailment is minimal (Negash et al., 2023).

The interaction between storage, penetration, and curtailment is complex, therefore, understanding how these parameters interact is essential for identifying safer design options and their operational requirements. Specifically, when designing a power system with a significant share of intermittent renewables, a clear understanding of the interaction between renewable penetration, energy storage requirements, curtailment, PV-wind mix ratio, and balancing capacity requirements has paramount importance in foreseeing its operational requirements (Negash et al., 2023). Several studies have examined the relationship between these parameters to some extent, (Ardenas et al., 2021; Denholm and Margolis, 2007b; Perez et al., 2019). Remarkably, the authors in (Frew et al., 2021; Kroposki et al., 2017; Perez et al., 2019) challenge the common sense that curtailment is a waste of energy by clearly demonstrating its economic and technical advantages. These studies demonstrate the benefits of curtailment and indicate its trajectory toward becoming the new normal in future grids.

While the literature provides numerous studies on energy transition pathways, most of these studies emphasize economic aspects by utilizing techno-economic models (Bogdanov et al., 2021; Cole et al., 2021; Denholm et al., 2022; Guerra et al., 2020; Jacobson et al., 2019; Teske, 2022). Because the studies primarily focus on economic aspects, the physical interaction

among these parameters and their impact are inadequately explored. However, some studies, such as those in Israel (Solomon et al., 2019), North America (Guerra et al., 2021) and Europe (Gils et al., 2017), have attempted to formulate and reveal the link between these system parameters. Due to the difference in their approach and the difference in scenarios and details explored, a comparison between these studies is challenging. However, when comparable methodologies are applied, consistent trends emerge in how physical parameters interact, though location-specific climatological and demand-related factors still introduce differences. This highlights the need for more studies that generate comparable data through improved methodologies and standardized parameters, thereby supporting a unified framework that captures location-independent parameter interactions while also clarifying the influence of location-specific system differences.

This underscores the need for approaches that not only capture the complex interactions among key system design parameters but also translate these interactions into quantifiable relationships that can inform system efficiency and practical integration strategies. By developing such a framework, it becomes possible to interpret how curtailment, storage, and penetration collectively influence performance across different scenarios, providing a bridge between generalizable trends and location-specific characteristics. For example, in Solomon et al. (2019), when only solar PV is deployed, a conventional generator capacity of about 0.5% is required at a 20% curtailment level. In contrast, Gils et al. (2017) show that the system requires conventional generation equivalent to approximately 1% and 8% of demand at a 30% curtailment level even while benefiting from PV-wind complementarity. Both studies underline the necessity of seasonal storage after penetration of renewables exceeds 80%. In all these papers, the three system parameters- curtailment, storage, and penetration- increase simultaneously.

The common argument of the aforementioned studies is to show the need for an optimal economic curtailment as a means of flexibility in integrating large-scale intermittent renewables. This could potentially lead to a paradigm shift in how future grids operate in renewable-dominated systems. Despite significant research progress in energy transition concepts (100% renewable grids), empirical data demonstrating the complex interactions between key design parameters–curtailment, storage, penetration, and the PV-wind mix–remains lacking, a gap that this thesis aims to address.

2.2.4. Balancing capacity requirement

Both solar PV and wind are implemented across various system scales due to their scalability. Therefore, the increasing share of their integration into the power system necessitates re-evaluating the existing power infrastructure to accommodate the new requirements posed by the recently added intermittent renewables. Due to the intermittency and variability of solar PV and wind power, balancing supply and demand is the most challenging task (Eltawil and Zhao, 2010). With the increasing share of intermittent renewables, the risk of structural imbalances in the power system intensifies. The widespread adoption of decentralized sources, such as residential PV systems and prosumer participation, further exacerbates this challenge. Consequently, maintaining key operational parameters of the electricity system within defined limits becomes essential for stable and reliable grid performance. The two widely adopted mechanisms for this purpose are curtailment (Gils et al., 2017) and storage (Budischak et al., 2013). The current policy utilizes curtailment as a tool to prevent surplus and balances or back-

up facilities (which can include non-variable renewables or fast-ramping generators, dispatchable units) during deficits. This strategy supports the existing grid in achieving the higher renewable penetration. However, a future renewable-dominated grid requires further policy improvements beyond these limited enablers. The deployment of various storage technologies has demonstrated their critical role in facilitating the energy transition by helping to balance supply and demand. However, the potential of electrical energy storage to perform this function has an upper limit, beyond which additional solutions are necessary to address the remaining imbalances (Hirth and Ziegenhagen, 2015). In this context, balancing generators (conventional power plants) are required to serve as backup when deployed RE storage fails to balance supply and demand (Solomon, et al., 2012).

Conventional balancing generators must sustain frequent on-off cycles throughout the year. They should possess fast ramping capabilities and a quick start, which are suitable for providing peak loads whenever they are called up (Solomon et al., 2012). Energy dumping, specifically up to 20%, significantly improves system performance by increasing storage utilization, increasing penetration, and reducing the balancing requirements. Heuberger & Mac Dowell. (2018) examine system reliability and operability during the transition to 100% renewable energy, highlighting real-world challenges that may emerge in the process of rapid decarbonization. For example, at about 30% curtailment, the system requires conventional power plants to cover between 1% and 8% of the demand (Gils et al., 2017).

Understanding the complex interactions among various system design parameters, such as balancing capacity, storage, curtailment, and the PV-wind mix, and their impacts is essential for designing systems that can effectively address the weather-driven uncertainties.

2.2.5. PV generation forecasting

Several factors, such as resource potential (Quaschning, 2016), cost reduction (Kavlak et al., 2018), efficiency enhancement, and improvements in manufacturing motivates the adoption of solar PV more than any other renewable option. However, its dynamic, intermittent, and variable nature is a bottleneck for large-scale deployment aimed at transitioning to decarbonized grids (Hansen et al., 2019). The increased deployment of electronic devices in response to the large-scale deployment of renewables brings a new challenge to the existing grid, which is designed without accounting for such features. Advanced forecasting is among the several solutions proposed to address such challenges. Such strategies allow for balancing and managing the supply and demand, ultimately enhancing grid stability, optimizing storage dispatch, reducing backup capacity, and increasing overall system performance (Voyant et al., 2017).

The indeterministic nature of solar and wind generation, along with the underlying factors affecting their output, makes accurate forecasting challenging. While solar PV and wind energy present significant forecasting challenges, solar forecasting is particularly complex due to its dependence on various weather variables such as cloud cover, rainfall, and temperature (Abdel-Nasser and Mahmoud, 2019). These parameters vary widely across all time scales, from seconds to seasons, and forecasting should also address such time scales to provide a practical solution for grid operational management.

Depending on the time horizon, forecasting of PV generation can be grouped into four broad categories: ultra-short-term, short-term, medium-term, and long-term horizon predictions, (Limouni et al., 2022). Predicting solar PV on different time scales addresses various challenges encountered at the system management level. For example, intra-hour forecasting

can help mitigate power fluctuations and rapid changes (flicker and power ramps), enabling power operators to manage real-time dispatch and marketing operations more effectively. While intraday and day-ahead forecasting, which is mid-term forecasting, can improve transmission scheduling and optimize balancing reserves (Pierro et al., 2017). Predictions that address long-term horizons are important for long-term policy planning and decision-making, transmission expansion, distribution expansion, and infrastructure development (Limouni et al., 2022).

Based on the modelling approach, PV forecasting can also be divided into physical, statistical, and artificial intelligence (AI) (Antonanzas et al., 2016). Physical forecasting techniques utilize weather variables to build models that predict future PV generation based on physical properties (Ye et al., 2022). The simplest method for physical forecasting involves creating a model that transforms solar irradiance into PV power output (Huang et al., 2010). The most widely recognized physical model, the Numerical Weather Prediction (NWP) model, employs various thermodynamic and other differential equations to characterize the physical state and dynamics of the atmosphere (Limouni et al., 2022).

In contrast, statistical forecasting methods do not require detailed knowledge of the complex physical processes involved in photoelectric conversion within PV systems. Instead, they rely on large volumes of historical data to establish functional relationships between inputs and outputs through techniques like curve fitting and parameter estimation. The most common models include regression analysis and autoregressive moving average (ARIMA). Formulating a model that generalizes across various regions is relatively simple in this approach. Nevertheless, it requires a considerable amount of historical data from weather prediction models and significant computational power, especially for short-term forecasts (Dai et al., 2023). In (Li et al., 2016). a different approach to day-ahead PV power forecasting was introduced, utilizing a nonlinear regression technique called Multivariate Adaptive Regression Splines (MARS). The study found MARS to be more straightforward and deliver more reliable results compared to other nonlinear models like k-nearest neighbors (KNN) and Artificial Neural Networks (ANN). Fig. 2.17 illustrates the various stages of a machine learning-based forecasting model.

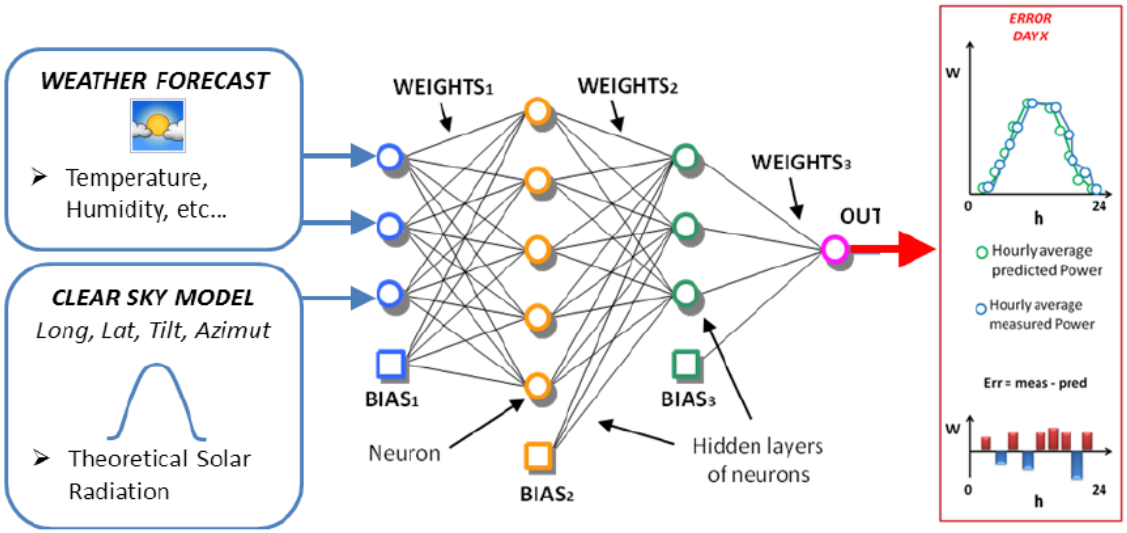

Fig. 2.17. General layout of forecasting model (Dolara et al., 2018)

Recently, sophisticated forecasting methods utilizing Artificial Intelligence (AI) have become increasingly popular because of their remarkable capacity to learn patterns from intricate, non-linear inputs-patterns that traditional modelling techniques often struggle to capture (Inman et

al., 2013). AI-based forecasting has a broader impact on various sectors, and solar PV forecasting is no different. The rapidly growing interest in the field reflects promising results and is expected to enhance the share of PV in the energy mix. Several researchers are using the most notable methods, such as Artificial Neural Network (ANN), Long-Short-Term Memory (LSTM), Support Vector Machines (SVM), and other hybrid models to predict solar PV generation on different time scales (Limouni et al., 2023). These models can be implemented using straightforward approaches, such as Artificial Neural Networks (ANN), to achieve reasonable accuracy in PV generation forecasting, as demonstrated in (Mellit et al., 2014) for a 1 MW grid-connected plant in southern Italy. In that study, solar irradiance and module temperature were used as input parameters, classified into three distinct daily conditions to improve forecasting accuracy. Other studies, such as those conducted in (Abdel-Nasser and Mahmoud, 2019), propose a more complicated hybrid model to forecast PV output in Aswan and Cairo, Egypt. The LSTM's unique memory unit capability in extracting temporal patterns was used to reduce the prediction error. Limouni et al. (2023) introduced an innovative hybrid forecasting method that combines Long Short-Term Memory (LSTM) with Temporal Convolutional Networks (TCN) to forecast photovoltaic (PV) power generation. This method utilizes publicly available historical data from Alice Springs, Australia. The model takes advantage of LSTM's strength in capturing temporal dependencies within the input data while integrating TCN to effectively correlate input features with output results. The authors assessed the hybrid model's performance against standalone LSTM and TCN models across various seasons and daytime conditions, including cloudy, clear, and intermittent scenarios. The findings indicated that the hybrid model consistently surpassed both individual models regarding standard error metrics.

LSTM is widely used for PV generation forecasting over different time frames, thanks to its effective management of complex sequences and errors through its memory structure (Hochreiter and Schmidhuber, 1997). Recently, there has been a growing emphasis on integrating LSTM with other models, such as GRU, which provide complementary advantages to improve forecasting accuracy and computational efficiency by addressing the shortcomings of individual models (Negash et al., 2025). This hybrid strategy leverages LSTM's capabilities in recognizing temporal patterns and controlling errors. Models such as reinforcement learning (RL) are used for grid management and optimization of storage charge and discharge(Cardo-Miota et al., 2025).

However, a significant challenge with AI forecasting methods is the necessity for substantial amounts of high-quality historical data. This section addresses this challenge by establishing an empirical relationship between satellite and real data measurements.

2.3. Modelling large–scale renewable integration

The concept of achieving a 100% renewable electricity system has recently evolved from an idealistic vision into a serious topic of scientific inquiry in the research community (Palmintier and Webster, 2016). Extensive assessments have been carried out at the continental scale, including North America (Becker et al., 2014), Europe (Heide et al., 2011, 2010), and Australia (Elliston et al., 2016). Additionally, numerous national-level analyses have been performed for countries such as Sweden (Zhong et al., 2021), Switzerland (Dujardin et al., 2017b), UK (Ardenas et al., 2021), US (Denholm et al., 2022), South Africa (Oyewo et al., 2019), and China (Ren et al., 2022).

Energy modelling or planning to achieve 100% clean energy considers various resource potential to reach an optimal resource mix that balances supply and demand. The most commonly deployed renewables are solar and wind, along with other enabling technologies (Denholm et al., 2022). Different approaches, such as simulation, optimization, and commercial and open energy modelling tools, combine various renewables to quantitatively meet demand. The advantages and disadvantages, as well as the suitability of each model for generation expansion planning, were outlined in (Fattahi et al., 2020).

Renewable energy integration requires several approaches to analyse the technical requirements and their impact on the energy system. Although different methods are employed, computer tools remain the most commonly used for modelling energy systems. Notable examples include EnergyPLAN, NEMS, MARKAL, MESSAGE, TIMES, and RETScreen, which are among the most popular computer tools (Connolly et al., 2010). These low-carbon energy system models aim to provide policymakers with actionable insights as they make long-term energy transition decisions.

Although numerous energy system models have been developed, they often lack consistency in reaching similar conclusions. For instance, as noted in (Fattahi et al., 2020) regarding the goal of achieving 100% renewable electricity in the EU by 2050, studies vary significantly in their estimates of the additional annual costs required for a carbon-free energy system. Some even conclude that achieving 100% renewable power is unfeasible. These discrepancies likely stem from differences in underlying assumptions, the selection of parameters, the level of technological detail, and the degree of system flexibility considered in each model.

Therefore, developing an energy transition model at the national level is strongly recommended. Such an approach offers several advantages, including access to high-resolution data, the use of context-specific and logical assumptions, and the creation of an open and transparent framework that ensures reproducibility and clarity of results. In this context, the present study aims to develop an innovative modelling approach, using Eritrea as a case study centred on solar PV and wind technologies, integrated with essential enabling technologies.

Although the data used in this study is specific to Eritrea, the developed methodology is generic and can be quantitatively applied on a global scale.

2.4. Summary of literature review

The current literature review provides a comprehensive assessment of the technical feasibility of large-scale PV grid integration, along with the supporting technologies that facilitate this process. To analyse the existing knowledge advancements and highlight the opportunities and challenges of large-scale integration, the review investigates state-of-the-art research articles, review papers, and International Energy Agency reports. The main research activities and directions in this topic can be categorized into the following points:

- It reviews the fundamentals of PV technology and its evolution in terms of materials and performance, providing a detailed analysis of its modelling approaches and technical characterization. Furthermore, it highlights how advancements in PV cell materials and performance will play a critical role in enabling the stability, efficiency, and scalability of future renewable-dominated power grids.
- It provides a comprehensive examination of various PV system types, including standalone, grid-connected, and residential systems, critically analysing their

configurations, development trajectories, and technological progress and control strategies. The discussion also underscores the pivotal role each system plays in shaping the next-generation energy landscape and accelerating the decarbonization of power grids.

- It reviews the most up–to–date research on energy transition concepts, encompassing methodologies such as modelling, optimization, and simulation. The studies are critically categorized to identify patterns and formulate emerging relationships, aiming to lay the groundwork for unified theories that can guide the development of future high-renewable energy grids.
- It critically reviews the various enabling technologies utilized to support large-scale PV integration, examining their individual roles, complex interdependencies, and overall impact on system stability, flexibility, and performance. The review highlights how these technologies, such as storage, curtailment, balancing needs, and AI based forecasting and optimisation, collectively facilitate high-penetration PV systems' reliable and efficient operation.

After a comprehensive analysis of the broadly categorized research topics and more detailed aspects within each category related to this thesis's objectives, the following gaps were identified.

- Most existing approaches depend on complex optimization algorithms or proprietary commercial tools that lack public accessibility, limiting transparency and reproducibility of their findings. Furthermore, a key challenge in achieving 100% renewable energy penetration lies in the uncertainty surrounding the identification of an optimal (least-cost) technology mix, an issue that remains insufficiently addressed in current literature. Moreover, due to the inherent variability of renewable resources and system configurations, clear design principles for achieving full (100%) RE integration are still lacking.
- Most energy transition models – models that allow large-scale RE integration – rely heavily on techno-economic models, which typically yield a limited set of optimal solutions aligned with predefined economic objectives. However, the physical interactions among key design parameters, such as PV-wind mix, curtailment, storage requirements, renewable penetration, and balancing needs, are often overshadowed by dominant economic datasets. Thus, the need to design a modelling approach that captures the complex interactions among the critical system design parameters, such as curtailment, storage, penetration, and generation mix, is clearly identified.
- The review highlights a critical gap in establishing a unified theoretical framework for future renewable-dominated grids, particularly one supported by data-driven empirical evidence that explores the complex interaction among key system design parameters.
- While the literature provides numerous studies on energy transition pathways, due to the differences in their approach and the differences in scenarios and details explored, a comparison between these studies is challenging. However, when comparable methodologies are applied, consistent trends emerge in how physical parameters interact, though location-specific climatological and demand-related factors still introduce differences. This highlights the need for more studies that generate comparable data through improved methodologies and standardized parameters,

thereby supporting a unified framework that captures location-independent parameter interactions while also clarifying the influence of location-specific system differences.

- Though residential PV integration represents a paradigm shift, with its contribution expected to increase as conventional grids evolve to support local consumption. The typical method used in residential PV integration is based on a customer-led control strategy–charging home batteries during PV surplus and discharging them during supply deficits. However, this approach presents challenges for LV networks: limited night-time demand prevents full battery discharge, reducing available capacity for the next day's PV surplus and causing early saturation before peak generation. This undermines the batteries' role in mitigating reverse power flow. Despite increasing adoption, there is still a lack of data-driven insights on how to optimize residential PV integration without compromising LV network power quality.
- The literature clearly articulates the significance of AI-based PV generation forecasting and system optimization on maximizing PV integration; it also highlights a critical challenge for extensive historical measurement data to ensure accurate predictions. However, there is no significant progress in data pre-processing techniques to bridge the gap.

By addressing these gaps and limitations, this study seeks to develop a distinctive approach that establishes a functional relationship between key design parameters, facilitating the integration of large-scale PV in the power system.

3. MATERIALS AND METHODS

This chapter provides a comprehensive explanation of the materials, techniques, and equipment utilized. It presents a detailed account of both the numerical and empirical formulations underlying the novel methodology and indicators introduced. Additionally, the scientific methods employed for data collection and pre-processing are thoroughly described, ensuring alignment with the thesis's overall objectives. The methods section is divided into three major sections – large-scale PV integration, Residential PV, and PV forecasting – while providing all necessary methodological approaches, such as experimental data collection and geographical descriptions of study sites for each section.

3.1. PV integration modelling

In this section, all possible ways to maximize the integration of large–scale PV into the utility grid will be explored.

3.1.1. Site description and data collection approach

The study is conducted in Eritrea, North East Africa, located in the arid and semi-arid regions of the Sahel region in Africa. Eritrea is a small country with one time zone, located on the western side of the Red Sea at a latitude between 12 ° 22′ and 18° 02′ N and a longitude between 36° 26′ and 43° 13′ E (Ghebrezgabher et al., 2016). Its strategic location features a lengthy coastline of more than 1,200 kilometres along the Red Sea, stretching from the northern border with Sudan to the southern border with Djibouti. The country's topographical orientation is broadly divided into three regions: the central highlands, the eastern coastal areas, and the Western lowlands.

Eritrea possesses rich renewable energy resources, particularly in solar and wind, with considerable technical potential (Negash et al., 2020) as shown in Fig. 3.1. In the southern coastal regions, wind speeds can reach up to 9.5 m/s at a 10-meter height, while additional promising wind sites exist in the central highlands (Rosen et al., 1999). Solar energy availability is also high, with irradiance levels ranging from 5.28 to 6.55 kWh/m²/day (Kbret, 2006). By harnessing the complementary nature of these resources, Eritrea can address its energy demands with reduced reliance on extensive storage and balancing infrastructure.

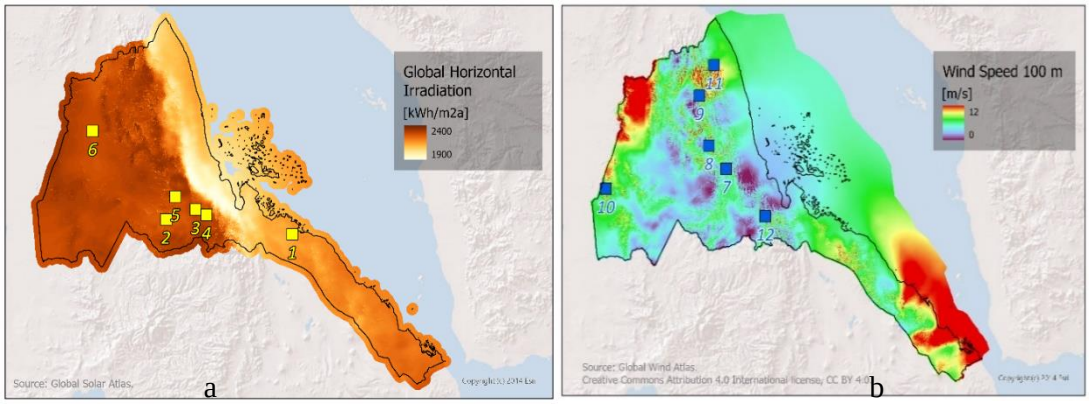

Fig. 3.1. Geographical location of studied sites and spatial distribution: a) daily solar radiation, b) wind speed resources in Eritrea

Data for this study were sourced from multiple databases. Historical solar irradiation and wind speed data for 25 sites were obtained from Eritrea's Ministry of Energy and Mines but were not used for modelling due to outdated measurements, technical gaps, and limited national coverage. Instead, these data served as a benchmark to evaluate online datasets. A comprehensive analysis was conducted to identify the most reliable databases that accurately represent ground measurement data. The Photovoltaic Geographical Information System (PVGIS) and the Global Wind Atlas (GWA) were selected as the most reliable sources to represent actual conditions.

Potential sites for solar and wind energy were then chosen after a thorough analysis of their complementarity and resource potential using PVGIS and GWA. Demonstrating self-balancing through a suitable mix of geographically diverse VRE sources and various enabling tools will create a vital foundation for designing a renewable-dominated grid. Tables 1 and 2 provide the geographical information for the chosen sites.

Table 1. Solar sites (actual sites may be located near the listed towns and cities)

Site	Map No.	Geographical location	Altitude (m)	Annual AC electricity kWh/kWp
Araeta	1	14.69N, 40.64E	23	1687
Areza	2	14.92N, 38.57E	1949	1752
Dekemhare	3	15.07N, 39.05E	2015	1800
Digsa	4	14.99N, 39.23E	2143	1770
Himbrti	5	15.27N, 38.72E	2161	1769
Kerkebet	6	16.28N, 37.36E	384	1801

Table 2. Wind sites (actual sites may be located near the listed towns and cities)

Site	Map No.	Geographical location	Altitude (m)	Roughness length (z_o)	Average wind speed (10 m)	Full load hours
AdiTekelezan	7	15.68N, 38.75E	2539	0.05	6	3106
Gizgiza	8	16.04N, 38.45E	1180	0.3	6.3	3626
Nakfa	9	16.81N,38.29E	1724	0.3	6.2	3607
Teseney	10	15.37N, 36.68E	950	0.1	9	4787
Qarora	11	17.28N, 38.54E	413	0.005	5	3575
Qohaito	12	14.94N, 39.42E	2671	0.2	6.4	3188

3.1.2. Solar PV and wind generation modelling

The year–long hourly time series data for solar PV generation profiles and wind speed utilized in this study were obtained from the open-source database PVGIS, which offers comprehensive global information on solar radiation and other weather parameters. From the various options provided on the platform, a non-tracking, freestanding crystalline silicon PV system with optimized slope and azimuth angles and an overall system loss of approximately 14% in the AC power generation was selected (Huld et al., 2012).

Based on the pattern and magnitude of the measured data, estimating the wind speed for each site is done in two steps. The wind speed obtained from PVGIS showed a similar pattern to the measured data, whereas the magnitude resembles the GWA data. Therefore, the hourly wind

speed from PVGIS was scaled using the mean wind speed from GWA (Davis et al., 2023). The scaled wind speed (v_{th}) was then extrapolated to the 80 m turbine hub height using the log-law equation as follows:

$$v_{\text{th}} = v_r \frac{ln(z/z_o)}{\ln(z_r/z_o)}, \tag{3.1}$$

where: v_r is the wind speed at the reference height z_r and z_o is the roughness length.

In estimating wind power, roughness length (commonly represented as z_o) is an essential parameter that describes how surface features, such as vegetation, buildings, and terrain, affect wind flow near the ground. In this work z_o was estimated through a combination of on-site visual inspection and GWA to characterize barriers. However, for the sites that are not easily accessible, GWA was the only tool used to estimate the roughness value.

Air density plays a crucial role in wind power generation, with higher density enabling more air mass to flow through the turbine, thus boosting energy output. As air density reduces with altitude, turbines situated at higher elevations may generate less power than those positioned lower, even in similar wind conditions. A density correction was implemented to account for these discrepancies, as there is a significant elevation difference between the selected sites.

The local density (ρ) of each site depends on temperature and altitude, and is given by:

$$\rho = 3.4837 \frac{101.29 - z \cdot 0.011837 + z^2 \cdot 4.793 \cdot 10^{-7}}{T}, \tag{3.2}$$

where: T is temperature in kelvin, and
z is altitude above sea level in meters.

The manufacturer-provided standard power curve $P_{\text{std}}(v)$, applicable at standard air density, was adjusted by scaling the input wind speed based on the following formula:

$$P_{v_{\text{th}}}(t) = P_{\text{std}}\left(v_{\text{th}} \left(\frac{\rho}{\rho_0}\right)^{1/3}\right), \tag{3.3}$$

where: ρ_o=1.225 kg/m^3 is the standard air density.

The wind generation capacity is evenly distributed between the six locations, with the total generation normalized to a peak capacity of 1 MW. Similarly, the solar PV generation, distributed equally across six sites, is normalized to a peak capacity of 1 MW, while the annual load normalizes the load profile.

The load data for Eritrea used in this study were collected from three sources. One year of hourly electricity consumption data was obtained from the Ministry of Energy and Mines, Eritrea, but it was unsuitable for detailed analysis and used only as a benchmark. The main limitations are its age (2004) and the lack of evidence that it represents actual demand without load shedding. In the presence of load shedding, the data may reflect generator capacity rather than true consumption patterns. Next, two additional options were explored. The second option involved identifying publicly available load data for developed countries, for which Greece and Denmark were chosen to represent the consumption patterns of Eritrea's highlands and lowlands, respectively. As a third option, a relevant hourly time series data from Ethiopia, a neighbouring country with similar climatic and cultural characteristics to Eritrea, was obtained for the full year. After comparing the three profiles, the Ethiopian dataset was chosen for the analysis, as it best captured Eritrea's seasonal variability and consumption patterns.

The load time series from Ethiopia is then scaled to a near-future scenario in Eritrea, where per

capita power consumption is projected to reach 2000 kWh, resulting in a total demand of about 16 TWh.

3.1.3. Assessing complementarity

Initially, solar PV and wind generation profiles were collected for several sites across the country. Criteria were set to identify the potential sites to be included in the modelling. The criteria considered were the potential of complementarity between spatially distributed sites (PV with wind or wind with wind), proximity to load centres, and cross-border energy exchange potential, a key for enhancing system flexibility and resilience.

The Kendall correlation coefficient (τ), the one adopted in this study is considered the most suitable statistical measure to assess resource complementarity among RE sources (Ren et al., 2019).

Let's say $(P_s(t1), P_w(t1))$, and $(P_s(t2), P_w(t2))$ are two pairs of independent generation profiles of solar PV $P_s(t)$ and wind power $P_w(t)$. The Kendall correlation coefficient is computed according to

$$\tau = P\{(P_w(t1) - P_w(t2)) - (P_s(t1) - P_s(t2)) > 0\} - \{\{(P_w(t1) - P_w(t2)) - (P_s(t1) - P_s(t2)) < 0\}\} \quad (3.4)$$

where: $\{P\}$ is a probability of the occurrence of an event,

$\{(P_w(t1) - P_w(t2)) - (P_s(t1) - P_s(t2)) > 0\}$ is concordance, and

$\{(P_w(t1) - P_w(t2)) - (P_s(t1) - P_s(t2)) < 0\}$ is discordance

The values of τ varies between 1 and -1. When the value τ is positive, solar PV and wind generation profiles exhibit similar temporal patterns. In this condition, PV and wind do not complement each other. However, if the value τ is negative, PV and wind power generation are predominantly opposite temporally, allowing them to complement each other at times. The MATLAB function *corr* is used to compute the correlation coefficient.

3.1.4. Mathematical modelling of PV-Wind mix and energy balance

In this thesis, a novel and transparent simulation model is developed, specifically designed to account for several interacting parameters in a MATLAB computing environment on a high-performance PC equipped with a Core i7 processor and 32 GB of RAM. The modelling requires high-resolution datasets with a minimum of hourly generation profiles. Thus, all inputs, both generation profiles (PV and wind) and the load profile, are provided at a 1-hour resolution for the whole year. Using the hourly generation profiles and load data, a forward-running simulation was carried out to evaluate how different combinations of solar PV and wind generation could meet the hourly load demand.

The following assumptions were adopted in conducting the energy transition modelling, which evaluates the technical feasibility of achieving 100% renewable energy (RE) penetration:

- No transmission constraints: Following the "copper plate" assumption, all solar PV and wind generation sites are assumed to be connected to the main grid without any transmission or distribution constraints.

- Fully flexible balancing capacity: All conventional generators used for balancing supply-demand are assumed to be fully flexible, with fast ramping capabilities.
- Worst-case scenario focus: The analysis focuses solely on supply-side options, without incorporating demand-side management measures, which could otherwise enhance system performance.

Based on these assumptions and by exploring various critical scenarios and sensitivities, this modelling identifies multiple pathways and options to achieve a user-specified penetration level by quantitatively adjusting the PV/wind mix while balancing storage needs and managing curtailment levels. However, the main target is to identify the pathway with the optimum combination of the different parameters to achieve 100% RE penetration with a high share of PV, compatible with my stated objective of maximizing the share of PV in the electricity grid.

The modelling adopts a hierarchical approach, progressing from broader system-level analyses to more detailed evaluations.

- By iteratively mixing various PV and wind generation ratios, it creates a search space. This approach aids in identifying the ideal ratios of solar PV and wind power that minimize the gap between generation and demand.
- Assessing different technical scenarios to facilitate the integration of large-scale RE. These scenarios primarily concentrate on analysing the resource mix required to fulfil electricity demand, along with the corresponding design requirements, which include a storage model, curtailment, and balancing capacity aspects.

The generation mix at each hour of the year that quantitatively combines different mixes of solar PV and wind power (in MW) is calculated according to:

$$P_{\text{rew}}(t) = p\,\alpha(r)\,(r\,p_{\text{PV}}(t) + (1-r)\,p_{\text{wind}}(t)), \tag{3.5}$$

where: t - is a time step,

$p_{\text{PV}}(t)$ - is PV generation at hour t relative to its peak capacity (MW/MWp),

$p_{\text{wind}}(t)$ - is the wind turbine generation at time t relative to its peak capacity (MW/MWp),

r - is the PV ratio ranges from 0 to 1 in increments of 0.1, whereas
$r = 0$ corresponds to 100% wind (hereafter called wind-only scenario)
$r = 1$ corresponds to 100% solar (hereafter called solar-only scenario)
$r = 0.5$ correspond to 50 PV and 50 wind (hereafter called 50-50 PV-wind scenario),

p - is the minimum of the no-dump capacity (P_{nd}) (in MWp). It is the maximal power generated by renewables without necessitating power dumping. In other words, the generated power is fully integrated into the grid without any curtailment or storage requirement.

$\alpha(r)$ – is a factor that is determined from a requirement that:

$$\sum_t \alpha(r)(r\,p_{\text{PV}}(t) + (1-r)\,p_{\text{wind}}(t)) = \text{const}\ , \tag{3.6}$$

and that $\alpha(0.5) = 1$. By this construction, a variation of the PV ratios (r) leaves the annually generated electric energy from renewables unchanged. This is reasonable, since a comparison of different mixes is only relevant when the annual generation is the same for the mixes.

The two equations below determine the no-dump capacity (in MWp):

$$P_{ND} = \frac{P_{\text{load}}(t)}{(r\, p_{\text{PV}}(t) + (1-r)\, p_{\text{wind}}(t))}, \tag{3.7}$$

P_{ND} is a matrix of 8760 ×11. Then the minimum no-dump capacity (P_{nd}) is consequently determined according to

$$P_{nd} = min\begin{bmatrix} P_{i,j}^{ND} & P_{i,j+1}^{ND} & \cdots & P_{i,11}^{ND} \\ P_{i+1,j}^{ND} & P_{i+1,j+1}^{ND} & \cdots & P_{i+1,11}^{ND} \\ \vdots & \vdots & \cdots & \vdots \\ P_{8760,j}^{ND} & P_{8760,j+1}^{ND} & \cdots & P_{8760,11}^{ND} \end{bmatrix} \tag{3.8}$$

where $P_{\text{load}}(t)$ is the hourly load demand, and the minimum is taken first with respect to t, then to r. This ensures that the generation $P_{\text{rew}}(t)$ is always lower than the consumption $P_{\text{load}}(t)$.

The net load (P_{mix}), the mismatch between renewable generation and load can be computed as:

$$P_{\text{mix}}(t) = \beta\, P_{\text{nd}}\, \alpha(r) \left(r\, p_{\text{PV}}(t) + (1-r)\, p_{\text{wind}}(t)\right) - P_{\text{load}}(t), \tag{3.9}$$

where β is a multiplier that enables oversizing the generation. Each multiplier β represents a renewable-to-load energy ratio, calculated by dividing the total renewable generation by the total load. The model generates various mismatch values (P_{mix}): positive when renewable generation exceeds the load, zero when generation exactly matches the load, and negative when generation falls short. This is achieved by iteratively oversizing the generation capacity-up to 8 times the minimum no-dump capacity-while allowing unrestricted energy dumping.

A range of individual generation profiles is developed by varying the share of PV (r) from 0 to 1 in steps of 0.1, while adjusting the wind share to 1-r, to maintain a constant total renewable capacity. Each PV-wind combination was evaluated against hourly electricity demand over the course of a year to assess compatibility and derive the corresponding net load profile (P_{mix}). This net load profile was then used to inform the design and dispatch strategy for the proposed energy storage system. The aim is to examine the resource and technical limitations of achieving a high-renewable electricity system.

3.1.5. Storage modelling

When the mismatch is positive ($P_{mix} > 0$), it indicates that the renewable energy generation exceeds the electricity demand at that hour. In this case, the surplus energy is first stored in the storage system, taking into account a charging efficiency (η_{ch}). If the storage system reaches its maximum capacity, any additional surplus energy that cannot be stored is curtailed, meaning it is intentionally discarded to maintain system balance. Conversely, when the mismatch is negative ($P_{mix} < 0$), the renewable generation is insufficient to meet the electricity demand. In such instances, the model attempts to supply the deficit by discharging energy from the storage system, considering a discharging efficiency (η_{dis}). If the available stored energy is inadequate to fully cover the shortfall, it is assumed that the remaining unmet demand is supplied by a balancing capacity reserve (such as back-up from dispatchable generators). The

energy losses associated with storage, such as self-discharge and inefficiencies during charging and discharging, are equally incorporated into the model by embedding them into the charging (η_{ch}) and discharging (η_{dis}) efficiencies.

3.1.5.1. Diurnal storage modelling

In this study, diurnal storage is modelled using a battery with a round-trip efficiency of 90%, meaning that the combined charging and discharging processes retain 90% of the stored energy. To represent this, the model assumes equal charging and discharging efficiencies, with each efficiency set to the square root of the round-trip efficiency ($\eta_{ch} = \eta_{dis} = \sqrt{0.9}$) (Zucker and Hinchliffe, 2014). While there are different storage technologies, each offers distinct advantages and limitations, Li-ion batteries are particularly favoured in this analysis due to their high scalability, allowing them to be easily adjusted to meet a wide range of storage capacity needs. Furthermore, batteries can help reduce transmission and distribution losses because they can be strategically deployed close to major load centres, thereby minimizing the distance electricity must travel and enhancing overall system efficiency.

This study focuses on Li-ion as short-term storage. As a mature and widely adopted technology (Technology Readiness Level 8-9), Li-ion technology offers high energy and power density, making it ideal for both transportation and stationary uses. Competing technologies include Lead-acid batteries, known for low cost and moderate efficiency; flow batteries, valued for long service life, low self-discharge and fast response; and emerging options like Sodium Sulphide (NaS), which offer high specific energy for specific applications (Kebede et al., 2022). However, these alternatives struggle to match Li-ion's dominance, driven by ongoing cost reductions and scalability. In fact, the successor to short-duration Li-ion storage may simply be longer-duration Li-ion systems. Emerging technologies face significant challenges in competing with Li-ion's established market presence. Rapid growth in electric vehicle adoption continues to accelerate innovation and cost declines, which will likely benefit stationary applications as well. For newer technologies to achieve cost parity, large-scale deployment is essential (Denholm et al., 2023).

The storage model can be represented by

$$S(t) = \begin{cases} S(t-\Delta t) + \min\left(\eta_{\text{ch}}\, P_{\text{mix}}(t), P_{\text{room\_d}}(\text{t})\right)\Delta t, & \text{if } P_{\text{mix}} \geq 0 \\ S(t-\Delta t) + \min\left(\frac{P_{\text{mix}}(t)}{\eta_{\text{dis}}}, P_{\text{room\_d}}(\text{t})\right)\Delta t\,, & \text{if } P_{\text{mix}} < 0 \end{cases} \qquad (3.10)$$

$$\forall \text{t} \in |1, N|$$

$$S(0) = 0$$

where: $S(t)$ – is the stored energy (MWh) at time $t, \Delta\, t = 1$ h is the time step,

N – is the number of hours in a normal year, 8760, and

$P_{\text{room\_d}}\Delta t$ – is the hourly remaining capacity of storage during charging and discharging (MWh), and

$$P_{\text{room\_d}}(t) = \begin{cases} \min\left(S_{\max} - S(t-1),\ \frac{S_{\max}}{\Delta t_{\text{full}}}\right), & \text{if } P_{\text{mix}} \geq 0 \\ -\min\left(S(t-1), \frac{S_{\max}}{\Delta t_{\text{full}}}\right), & \text{if } P_{\text{mix}} < 0 \end{cases} \qquad (3.11)$$

where: $S_{\max}$ – represents the maximum energy capacity of the storage system, and varies from 0.01 to 0.8 times the average daily demand, and

Δt_{full}– denotes the minimum time needed to charge or discharge the storage fully. This is equivalent to the energy-to-power ratio, or inversely, the maximum C-rate.

The storage model relies on the storage system's energy and power capacity. In this study, the storage's charging and discharging capabilities are constrained by its minimum charging time up to the full state, set at Δt_{full}. The value of Δt_{full} was changing between 1h, 2h, 4h, 6h, 8 h and 10h, according to the scenario. But we use Δt_{full} value of 6 hours (h) as a focus of my reporting due to reasons to be clarified in the result, and literature data that considers 6h storage is most effective in resolving the timing mismatch between midday solar PV generation and peak electricity demand in the evening, thereby enhancing system adequacy and flexibility (Denholm et al., 2022). Perhaps such predetermined constraints are expected to impose some limitations on the flexibility of the model's performance. The storage model, however, was devised to conduct simulations by iteratively adjusting the storage capacity from its minimum to a maximum of 0.8 times the average daily demand.

3.1.5.2. Seasonal storage modelling

The effectiveness of diurnal storage decreases as the penetration increases. Typically, penetration levels above 80-90% the role of diurnal storage diminishes as longer duration mismatch requires another application other than diurnal storage. Seasonal storage (hydrogen) is introduced to complement the limitations and drawbacks of diurnal storage. Hydrogen storage is considered due to its suitability for seasonal energy shifting, high energy density, and ability to complement large-scale PV generation. Although its technology readiness level (TRL) ranges from 3–7 depending on the application, mature components such as electrolysers and fuel cells are increasingly demonstrated at pilot and commercial scales, making it a viable option for modelling long-term storage scenarios (Sebastian et al., 2023).

First, the behaviour of the excess generation after diurnal storage is studied.

The excess power (E_{p}) at any time t, after the diurnal storage has reached full capacity can be calculated as follows:

$$E_{\text{p}}(t) = P_{\text{mix}}(t) - \min\left(P_{\text{mix}}(t),\ \frac{P_{\text{room\_d}}(t)}{\eta_{\text{ch}}}\right), \tag{3.12}$$

The deficit power P_u (unmet demand) after deploying diurnal storage is ($P_{\text{mix}} < 0$)

$$P_u(t) = -P_{\text{mix}}(t) - \min(-P_{\text{mix}}(t)\,, -\eta_{\text{dis}} P_{\text{room\_d}}(t)), \tag{3.13}$$

Seasonal storage is introduced only when the following two conditions are met after the deployment of diurnal storage.

i. when the renewable energy penetration surpasses 80% and
ii. Excess generation or curtailment (E_p) is greater or equal to 5%.

Above this threshold, further increases in penetration would require a disproportionately large expansion of diurnal storage, which would minimize its overall effectiveness, which calls for seasonal applications. Below these thresholds, seasonal storage is not required, as diurnal storage alone effectively manages the system with high storage utilization.

Seasonal storage S_h at each hour of the year is computed according to

$$S_h(t) = \begin{cases} S_h(t-\Delta t) + \min\left(\eta_{\text{ch\_s}}\, E_{\text{p}}(t), P_{\text{room\_s}}(\text{t})\right)\Delta t, & \text{if } P_{\text{mix}} \geq 0 \\ S_h(t-\Delta t) - \min\left(\frac{P_{\text{u}}(t)}{\eta_{\text{dis\_s}}}, -P_{\text{room\_s}}(\text{t})\right)\Delta t\,, & \text{if } P_{\text{mix}} < 0 \end{cases} \quad (3.14)$$

where: S_{maxh} – is the maximum capacity of the hydrogen storage (seasonal storage),

$\eta_{\text{ch\_s}}$ – is the electrolyser efficiency,

$\eta_{\text{dis\_s}}$ – is fuel cell efficiency, and

$P_{\text{room\_s}}$ – is the available capacity at each hour and is computed according to:

$$P_{\text{room\_s}}(t) = \begin{cases} \min\left(S_{\text{maxh}} - S_h(t-1),\ \frac{S_{\text{maxh}}}{\Delta t_{\text{full\_ch}}}\right), & \text{if } P_{\text{mix}} \geq 0 \\ -\min\left(S_h(t-1), \frac{S_{\text{maxh}}}{\Delta t_{\text{full\_disch}}}\right), & \text{if } P_{\text{mix}} < 0 \end{cases} \quad (3.15)$$

where: $\Delta t_{\text{full\_ch}}$ – denotes the charging hours for the electrolyser

$\Delta t_{\text{full\_disch}}$ - denotes the discharging hours of the fuel cell, respectively.

The curtailed power after both storage technologies are deployed (P_{dpf}) at time t is computed according:

$$P_{\text{dpf}}(t) = E_{\text{p}}(t) - \min\left(E_{\text{p}}(t),\ \frac{P_{\text{room\_s}}(t)}{\eta_{\text{ch\_s}}}\right), \quad \text{if } P_{\text{mix}} \geq 0 \quad (3.16)$$

The unmet demand (P_{uf})

The charging ($Ch_{\text{lose\_S}}$) and discharging($Disch_{\text{lose\_S}}$) loss is computed according to

$$Ch_{\text{lose\_S}}(t) = \left(1 - \eta_{\text{ch\_s}}\right) \min\left(E_{\text{p}}(t),\ \frac{P_{\text{room\_s}}(t)}{\eta_{\text{ch\_s}}}\right), \quad (3.17)$$

The unmet demand (P_{uf})

$$P_{\text{uf}}(t) = P_u(t) - \min(P_{\text{u}}(t)\,, -\eta_{\text{dis\_s}} P_{\text{room\_s}}(t)), \quad \text{if } P_{\text{mix}} < 0 \quad (3.18)$$

$$Disch_{\text{lose\_S}}(t) = \left(\frac{1}{\eta_{\text{dis\_s}}} - 1\right)\left(\min\left(\frac{P_{\text{u}}(t)}{\eta_{\text{dis\_s}}}, P_{\text{room\_s}}(\text{t})\right)\right) \quad (3.19)$$

Table 3 presents the detailed specification and the parameters used in each storage technology.

Table 3. Technical properties of storage technologies

Storage application	Storage technology	Storage (average daily demand*)	Charging/ discharging hours (hrs)	Roundtrip efficiency (%)	Lifetime (calendar years)	Source
Short-term (Diurnal storage)	Li-ion	0.16	6	90	15	(Zucker and Hinchliffe, 2014)
Long-term (Seasonal storage)	Hydrogen	10	72/96	40	18	(Guerra et al., 2020b)

*1 average daily demand is equivalent to 43.8 GWh

3.1.6. System performance indicators

This study explores the interrelated dynamics of future renewable energy systems by assessing various system parameters, including renewable penetration, curtailment, PV-wind mix and balancing capacity requirements by linking with newly introduced system used index (a proxy of system efficiency). Through this analysis, the study offers valuable insights into how varying energy mixes influence overall system performance, operational resilience, and the integration of variable renewable resources. By quantifying the complex interaction between the various design parameters, the study addresses the main objective of the thesis.

Renewable penetration (P) represents the net fraction of total electricity demand met by solar PV and wind, accounting for storage losses and curtailed energy.

$$\mathrm{P} = \frac{\sum P_{\mathrm{con}}\,\Delta t}{\sum P_{\mathrm{load}}\,\Delta t}, \tag{3.20}$$

where: $P_{\mathrm{con}}(t)$ – is the total consumed RE that is supplied to the grid after removing the losses and dumped part:

$$P_{con}(\mathrm{t}) = P_{\mathrm{rew}}(\mathrm{t}) - (P_{\mathrm{dpf}}(t) + Ch_{\mathrm{lose\_S}}(t) + Disch_{\mathrm{lose\_S}}(t)), \tag{3.21}$$

This parameter includes both energy losses resulting from storage inefficiencies and power that is directly wasted due to excess generation.

The unmet demand (P_{um}) can be computed:

$$P_{\mathrm{um}}(t) = -P_{\mathrm{mix}}(t) - \min(-P_{\mathrm{mix}}(t)\,, -\eta_{\mathrm{dis}}P_{\mathrm{room}}(t)), \tag{3.22}$$

The balancing capacity is then computed as the maximum of the unmet demand divided by peak load. The model is designed to allocate the hourly balancing capacity required to meet the year-round hourly power deficit. Quantifying the requirement for balancing capacity holds immense importance in the design of such a system. While storage technologies provide balancing in both negative and positive power mismatches, balancing generators are utilized only in the case of negative power mismatches.

This study presents a novel multi-functional approach to optimize the use of RE across various mixing ratios. It is designed with an innovative framework aimed at achieving a more thorough understanding of interactions among these factors. New metrics, such as storage utilization and the system use index (a proxy for system efficiency), are introduced to assess the impact of different tools. Storage utilization (SU) is defined as the ratio of annual energy delivered by storage to the total storage capacity. SU can be interpreted as a number of full battery cycles per year.

$$SU = \frac{-\sum(S(t) - S(t-\Delta t))}{S_{max}}, \qquad \text{if} \quad S(t) < S(t-\Delta t) \tag{3.23}$$

System-use index (SUI) is computed as:

$$\mathrm{SUI} = \mathrm{SU} \times k \times m \times u \tag{3.24}$$

where: $k, m\ and\ u$ – are calculated by dividing annual energy discharge by the total consumed RE, average charging power by power capacity (PC), and total consumed RE by total RE generation, respectively:

$$k = \frac{-\sum(S(t) - S(t-\Delta t)}{\sum P_{useful}}, \qquad \text{if} \quad (S(t) < S(t-\Delta t) \tag{3.25}$$

$$m = \frac{\sum S(t) - (S(t-\Delta t)}{PC}, \qquad \text{if } (S(t) > S(t-\Delta t) \tag{3.26}$$

where: $PC = {S_{\max}}/{\Delta t_{\text{full}}}$

$$u = \frac{\sum P_{useful}}{\sum P_{rew}}. \tag{3.27}$$

The proposed approach enables me to create a novel and improved 3D visualization of the intricate relationships among these various interactive factors, providing a more comprehensive understanding of their interactions. The created index gives an arbitrary index that can compare the system performance in relation to used storage characteristics, curtailment and storage energy delivery.

This study examines the impact of complementarity on system performance by creating various solar and wind mixes, from which PV ratios of 0%, 50%, and 100% of the total renewable generation, representing wind-only, 50-50 wind-solar, and solar-only scenarios, respectively, were selected to represent the extreme and median conditions of their complementarity

Technoeconomic analysis

In this study preliminary economic analysis based on unit cost analysis is conducted to validate the techno-economic suitability of the proposed approach. The economic requirements of three conditions were investigated: first, satisfying demand with over generation and curtailment without storage, second, satisfying demand with storage and over generation/curtailment, and third, the optimal mix scenario. Based on recent literature data (Bloomberg, 2023), the difference in lifetimes between the batteries and the PV–wind systems was accounted by assuming the battery lifetime to be roughly half that of the PV and wind plants. Over the 30-year project horizon, this results in one full battery replacement. This approach allows the preliminary unit-cost estimates to incorporate the effect of replacement cycles and provide indicative cost values for the configurations. Although a fully annualized cost (i.e., spreading the total cost evenly over each year of operation) was not calculated, the inclusion of replacement cycles ensures that our cost estimates are more realistic than using a single installation cost for each technology (PV, wind, and storage). The main objective of the economic analysis is to demonstrate the general applicability and techno-economic viability of the proposed approach. Some assumptions, such as land availability under government ownership (as in Eritrea), were made. The study primarily focuses on exploring the complex technical interactions among design parameters, forming a foundation for future comprehensive modeling that will integrate detailed economic, transmission, and policy constraints.

3.2. Residential PV integration

Large-scale PV integration requires coordinated efforts across utility-scale PV plants and distributed residential PV systems. Residential PV has become a vital part of distributed generation, as buildings, which were once mainly consumers of electricity, now also generate significant power due to the adoption of rooftop PV systems.

The data sets employed in the study are detailed in Table 1. The simulation begins by selecting 100 MWp of residential PV and 120 MWp of wind that can be integrated to the grid without storage or curtailment requirements, with the ultimate goal of maximizing the direct use of the generated electricity.

3.2.1. PV feed-in limit

PV injection is managed by installing inverters with capacities smaller than the PV peak output. Fig. 3.2 shows the simplified algorithm employed, which applies feed-in limit after a certain PV injection level to avoid grid congestion during high PV generation. When PV output is below this limit, all generated electricity is fed into the distribution network for local use. If PV output exceeds the limit, the surplus is stored in a battery, and any excess beyond the battery's capacity is curtailed.

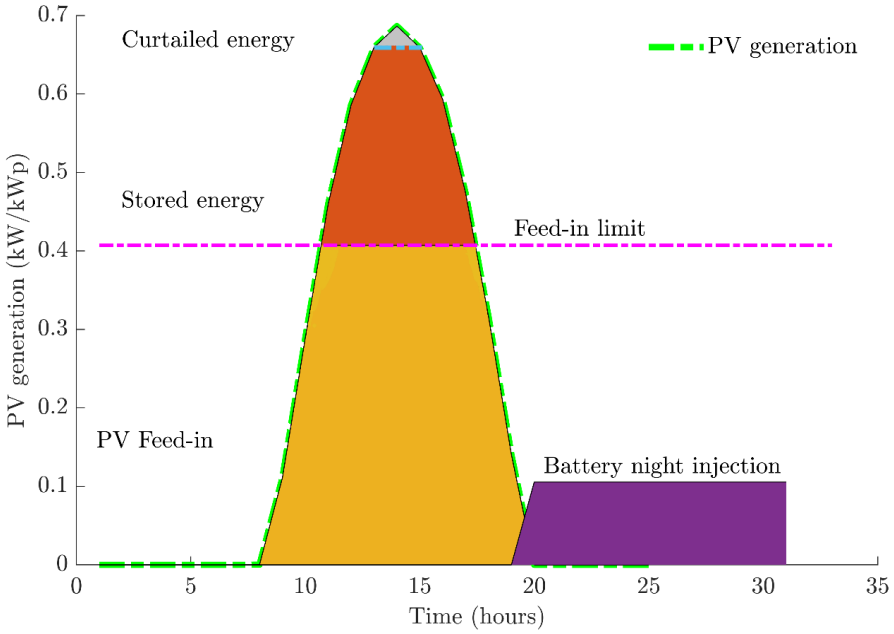

Fig. 3.2. An illustrative diagram showing the PV-battery dispatch strategy in the proposed method, with a feed-in limit applied (for June 1st)

3.2.2. PV-battery dispatch strategy

In the simulation, a fixed battery capacity (kWh) is installed behind the meter for each installed PV unit (kWp). Placing the battery behind the meter provides two main benefits:

1) it avoids the need for a separate DC/AC inverter and
2) reduces network congestion by storing energy on the consumer side.

In practice, residential loads are also behind the meter, and the difference between local PV generation and local demand is typically subject to the feed-in limit. However, we only have aggregated load data and lack information on individual residential loads, which can also differ greatly from one house to another. Moreover, during peak PV production periods, residential load tends to be low, so analysing the scenario shown in Fig. 3.3 is justified.

The battery storage is charged when PV generation is above the predetermined feed-in limit. The storage is then discharged to the LV network during night hours equally at constant rate and a fresh storage is ready every morning. This strategy solves the limitations discussed in (Procopiou et al., 2019; Ruf, 2018) which are based on customer-let control strategy, that is charging home batteries during PV surplus periods and discharging them during supply deficits. These limitations arise because home batteries cannot fully discharge overnight due to lower night-time residential demand. Consequently, there is less storage available to store

surplus PV generation for the next day and reach their full state of charge early, before high PV generation occurs, when batteries are most needed to reduce reverse power flow.

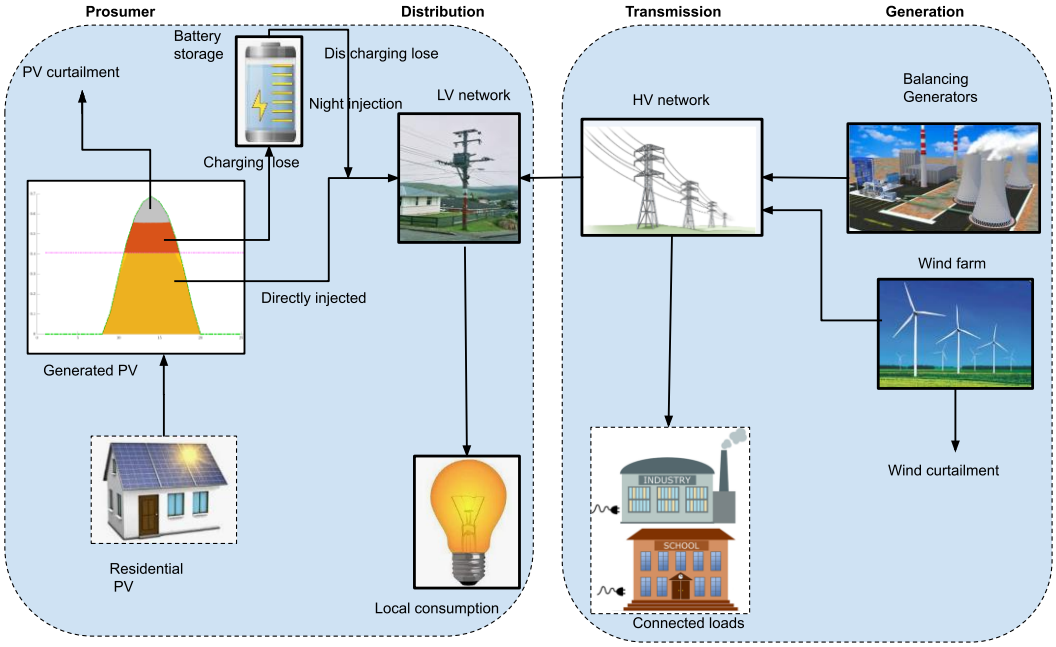

Fig. 3.3. Simplified schematic illustration detailing the employed energy flow mechanism

In accordance with thesis objective of enhancing residential PV in the power mix, the following dispatch algorithms are computed at each time step, at the distribution side of the network.

The power that is directly fed (P_{inj}) to the grid at a time, t is:

$$P_{\text{inj}}(t) = \min\left(P_{\text{gen}}(t), P_{\text{limit}}\right), \tag{3.28}$$

where: P_{gen} – is the generated PV power at time t and

P_{limit} – is the injection limit.

Based on the generated PV (P_{gen}) the battery energy storage (BES) is charged at that particular hour until it reaches its maximum capacity. Here, the battery round-trip efficiency is assumed to be 90% (Zucker and Hinchliffe, 2014b), with equal charging and discharging efficiencies ($\eta_{\text{ch}} = \eta_{\text{dis}} = \sqrt{0.9}$).

$$\text{BES}(t) = \text{BES}(t-1) + \min\left(\eta_{\text{ch}}\left(P_{\text{excess}}(t), P_{\text{room}}(\text{t})\right)\right)\Delta t \; - P_{\text{bat,inj}}(t), \tag{3.29}$$

where: P_{excess} – is the excess generation above the feed-in limit

$$P_{\text{excess}}(t) = P_{\text{gen}}(t) - P_{\text{limit}}\,, \tag{3.30}$$

and

$$P_{\text{room}}(t) = \frac{(\text{BES}_{\text{max}} - \text{BES}(t-1))}{\Delta t} \tag{3.31}$$

Δt – is time step of the simulation,

$P_{\text{bat,inj}}$– denotes the constant night-time battery discharge (battery injection to the grid) from 18:00 to 7:00, calculated by dividing the total daily stored energy by total night-time hours, accounting for η_{dis}, and

BES_{max} – is battery rated capacity.

Consequently, curtailed part of the PV becomes

$$P_{PV,cur}(t) = P_{excess}(t) - {P_{room}(t)}/{\eta_{ch}} \quad (3.32)$$

After integrating and managing the PV generation in distribution side of the network wind energy is added in the HV side of the network. The total renewable energy generation (TRE) in the power system is then determined by:

$$TRE(t) = P_{inj}(t) + P_{bat,inj}(t) + P_{wind}(t) \quad (3.33)$$

Finally, the energy balance between generation and demand (P_{dem}) is checked at each time step (hour). When TRE exceeds demand at that specific hour the excess energy is curtailed from wind generation

$$P_{wind,cur}(t) = TRE(t) - P_{dem}(t), \quad \text{if} \quad TRE(t) > P_{dem}(t) \quad (3.34)$$

and if TRE is less than demand the deficit is met by balancing gen sets (P_{BC}).

$$P_{BC}(t) = P_{con}(t) - TRE(t), \quad \text{if} \quad TRE(t) < P_{dem}(t) \quad (3.35)$$

The system performance is then accessed using two distinct performance indicators called penetration (Pen) and curtailment:

$$Pen = \frac{\sum_i P_{used}(t_i)}{\sum_i P_{dem}(t_i)} \quad (3.36)$$

where:

$$P_{used}(t) = P_{dem}(t) - P_{BC} \quad (3.37)$$

The total curtailed energy is then computed by

$$\frac{\sum_i P_{PV,cur}(t_i) + P_{wind,cur}(t_i)}{\sum_i TRE(t_i)}, \quad (3.38)$$

3.2.3. Experimental setup for power quality analysis

The experiment was conducted at the Hungarian University of Agriculture and Life Sciences, Szent István Campus (coordinates 47°35′40.7″N and 19°21′42.3″E), at the grid-connected PV system located in front of the Aula building. Measurements were taken at the point of common coupling, where the transparent glass modules of the monocrystalline Si connected to the grid through the SolarEdge inverter. Connectors were installed to safely facilitate measurements using a standard power quality analyser, the Wally 'A' Power Quality Analyzer. The PV system, with a total capacity of 3.3 kW, is installed at an inclination of 40° and an azimuth of 10°, west to south. The specification of the PV system and inverter is given in Appendix A7. Fig. 3.4 and Fig. 3.5 show the complete set of measurement setups. The power quality measurement analyser records various power quality parameters, including current and voltage total harmonic distortion (ThdI and ThdV), interharmonic distortion, voltage deviation, and voltage unbalance, and special events for voltage and current. Measurements were taken at various time scales from milliseconds to hours.

Fig. 3.4. A 3.3 kW transparent glass PV module at the entrance of the Aula building

Measurements were conducted on October 12 and 13, 2025, under partly sunny conditions. These dates were deliberately selected to assess the impact of varying weather conditions on power quality. On October 12, data collection occurred between 10:30 a.m. and 5:40 p.m., while on October 13, measurements were taken from 7:30 a.m. to 5:15 p.m.

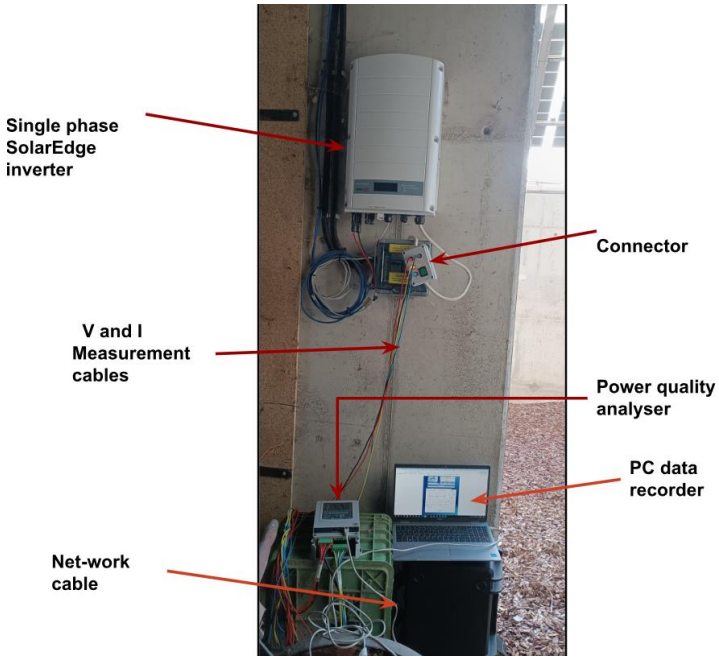

Fig. 3.5. Power quality analyser measurement setup

3.3. PV power generation forecasting

Designing a power system with a high share of renewables is inherently challenging due to the variability and uncertainty of weather conditions. System design typically relies on historical weather data, which can differ significantly across timescales, ranging from minutes to seasons and even across years. As a result, systems optimized on past data may underperform under actual operating conditions. To mitigate this, system design based on historical data should be complemented by real-time control and forecasting strategies. However, accurate forecasting remains difficult due to the stochastic nature of key influencing factors. Weather variables such as cloud cover, temperature, and rainfall have complex, non-linear impacts on PV output,

complicating the prediction process. Fig. 3.6 provides the general schematic diagram of the methodological approach followed in this section.

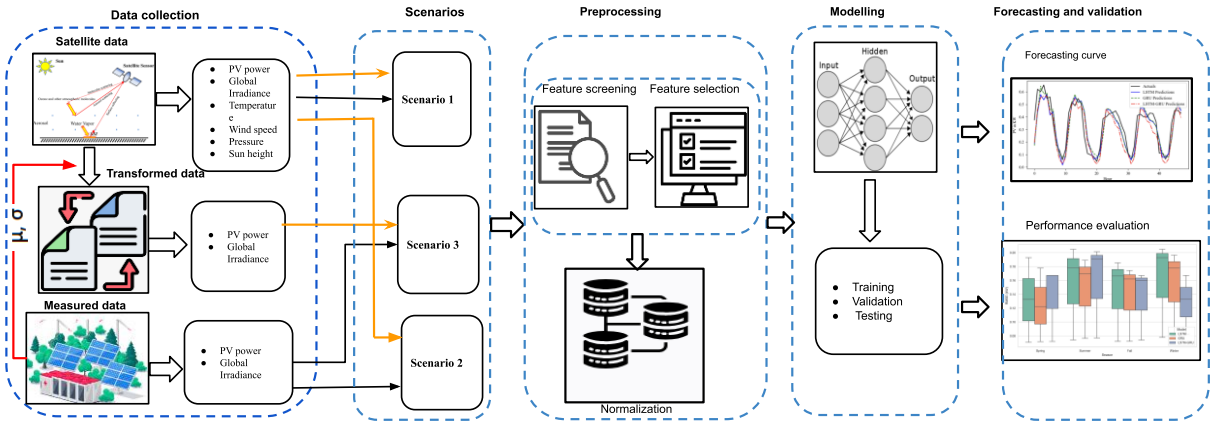

Fig. 3.6. Graphical abstract of the proposed methodological approach followed

3.3.1. Data collection and reprocessing techniques

Full-year measured data were collected from the Areza site (see Table 1 for details), complemented by satellite-based PVGIS data, which are readily available online. Areza is a site where a 1.25 MWp PV plant is installed. The PV-based microgrid is powered by 1.25 MWp of PV, battery storage, and diesel generators with a sophisticated SCADA-based control system. The microgrid generates sufficient power to serve the local rural villagers' energy needs. The study utilizes 17 years of hourly weather data from the PVGIS data assimilation platform, along with one year of measured data from the actual plant, to develop a forecasting model for predicting hours ahead of PV power generation. The PVGIS dataset offers extensive data with multiple features, including historical PV generation, reflected irradiance, direct irradiance, diffuse irradiance, temperature, wind speed, and sun angle. However, the measured data is limited to one year and consists of only two features (historical PV generation, global solar irradiation), which restricts the forecasting to the available features in the measured data. Two engineered features were introduced to help the models capture seasonal and time-related patterns: the sine and cosine transformations of the timestamp.

Model accuracy largely depends on the quality of training and testing data. Outliers and missing values, often resulting from measurement errors or equipment failures, can significantly degrade forecasting accuracy. To address this, all outliers and missing values were removed. A key challenge was data sparsity, especially in solar generation data, where over 50% of values are null due to diurnal cycles. These night-time nulls distort training, so only daytime data was used. Additionally, since features had different units and magnitudes, normalization was essential to avoid bias. All features were scaled to X_n in range of 0 to 1 using the MinMax Scaler, computed as:

$$X_n = \frac{X - X_{min}}{X_{max} - X_{min}} \tag{3.39}$$

where:

X – the observed value

X_{min} – the minimum of the data

X_{max} – is the max of the data

3.3.2. Model development

This study explores several deep learning models for accurate PV power forecasting, including LSTM, GRU, and a hybrid LSTM-GRU network as base models. LSTM and GRU are widely used in time-series forecasting due to their ability to retain temporal patterns and model sequential dependencies. The LSTM-GRU hybrid enhances performance on complex time series by combining the strengths of both architectures. The forecasting accuracy of these base models is then evaluated against traditional approaches like Extreme Gradient Boosting (XGBoost) and SARIMAX, as well as advanced models such as CNN, TCN, and transformers.

LSTM networks are particularly well-suited for time-series analysis, as they can effectively model the intricate dependencies between successive data points and depth-related variations. This capability makes them ideal for capturing complex temporal patterns in solar irradiance data. The model structure, key equations, and operational principles are given in (Limouni et al., 2023). GRU is a streamlined version of LSTM with fewer gates and parameters. Despite its simpler structure, it effectively captures temporal dependencies, making it well-suited for time-series tasks like PV forecasting. The model architecture and its working principle, along with the model equations, are given in (Elmousaid et al., 2024).

Then, a hybrid LSTM-GRU model is developed that combines the advantages of both architectures to effectively learn complex temporal patterns. The model begins with three LSTM layers (256, 128, 64 units) for extracting high-level features, followed by reshaping. It then uses three GRU layers (64, 32, 16 units) to further refine the temporal information, and concludes with a Dense layer with linear activation for both uni-step and multi-step forecasting.

The base case model is then evaluated against different widely used solar PV forecasting models, such as XGBoost and SARIAMX, due to their ability to handle missing data and non-linear relationships efficiently, and advanced forecasting architectures such as convolutional neural networks (CNNs) and informer-based architectures which have significantly advanced time series forecasting tasks, including solar PV power prediction. Detailed descriptions of the model architectures and formulations can be found in (Krizhevsky et al., 2017) for CNNs, (Bai et al., 2018) for Temporal Convolutional Networks (TCNs), and (Zhou et al., 2021) for informers. Hybrid models such as CNN-LSTM, CNN-GRU, and TCN-LSTM are constructed to benefit from their combined features.

3.3.3. Modified Z-score transformation

The Z-score transformation is widely applied across disciplines such as medicine (Andrade, 2021), (Wang et al., 2024), signal processing (Yaro et al., 2023), and time series analysis – especially in solar radiation studies (Chauhan, 2017) – due to its ability to highlight patterns and detect outliers without biasing results toward features with larger magnitudes. Forecasting models require a large quantity of data to predict the target variable accurately. However, in our case, the scarcity of high-quality and sufficiently extensive actual PV generation data limits prediction accuracy. Data shortages, inconsistencies, and incompleteness are among the main barriers to achieving high prediction accuracy. To address this, data-driven models were trained using 17 years of satellite data to predict actual PV generation, with one year of test data from the actual PV site. Since, the distribution of the two data sets were not uniform, a modified Z-score transformation was applied to mitigate the distribution-related errors. The modified version of the Z-score transformation aligns satellite-derived solar data with ground-based

measurements by linking the mean and standard deviation of both datasets. To address the issue of negative values at low generation levels, the entire data set was shifted by a small positive constant. This modified approach is designed to reduce distribution-related error.

For each value in satellite-derived data, we find the standard normal form using the Z-score transformation (z).

$$z = \frac{P_{sat,i} - \mu_{sat}}{\sigma_{sat}} \tag{3.40}$$

The rescaled value ($P'_{sat,i}$) is computed to match the distribution of the measured data using:

$$P'_{sat,i} = z * \sigma_{meas} + \mu_{meas} \tag{3.41}$$

where:

$P_{sat,i}$ – satellite-derived hourly PV generation

μ_{sat} – mean of the satellite-derived data,

σ_{sat} – standard deviation of the satellite-derived data,

μ_{meas} – mean of the measured data,

σ_{meas} – standard deviation of the measured data.

3.3.4. Evaluation of model performance

In this study, the forecasting model's accuracy was evaluated using four distinct metrics: Root Mean Squared Error (RMSE), Mean Absolute Error (MAE), Mean Bias Error (MBE), and R-squared (R^2) score, as given below. These metrics are widely utilized in PV forecasting studies to capture different dimensions of model accuracy and reliability.

The equations for these metrics are given as follows:

$$RMSE = \sqrt{\frac{1}{n}\sum_{i=1}^{n}\left(P_{pred,i} - P_{meas,i}\right)^2} \tag{3.42}$$

$$MAE = \frac{1}{n}\sum_{i=1}^{n}\left|P_{pred,i} - P_{meas,i}\right| \tag{3.43}$$

$$MBE = \frac{1}{n}\sum_{i=1}^{n}\left(P_{pred,i} - P_{meas,i}\right) \tag{3.44}$$

$$R^2 = 1 - \frac{\sum_{i=1}^{n}\left(P_{pred,i} - P_{meas,i}\right)^2}{\sum_{i=1}^{n}\left(P_{pred,i} - P_{mean}\right)^2} \tag{3.45}$$

where:

$P_{pred,i}$ is the predicted value at time I,

$P_{meas,i}$ is the measured value at time I,

n is the total number of observations, and

P_{mean} is the mean of the measured data.

The forecasting model was optimized using the Adam algorithm with a learning rate of 0.0005. A window size of 12 proved most effective during training trials, and the model was trained for 150 epochs to ensure comprehensive learning and convergence. Table 4 summarizes the performance of the different forecasting scenarios developed, along with the different input and output parameters utilized in each scenario.

Table 4. The different scenarios analysed and the corresponding meteorological variables used

Scenario	Reason/ Advantage (+) and disadvantage (-)	Training data Input +output	Test data Input +output
Scenario 1 (Based on satellite-derived data)	(+) Availability of sufficient publicly accessible satellite-derived meteorological data to train models (+) offer long-term coverage (+) Help define the hyperparameter baseline (-) fail to capture microclimatic effects such as local shading, soiling, or aerosol	Satellite-derived PV generation, Satellite-derived meteorological data, season, and periodic encoding + satellite-derived PV generation	Satellite-derived PV generation, Satellite-derived meteorological data, season and periodic encoding + satellite-derived PV generation,
Scenario 2 (Satellite-derived data + actual data) without data transformation	(+) Leverage the advantages of more reliable actual PV generation and publicly available satellite-derived meteorological and PV generation data (-) Ground-based meteorological and PV generation data are limited in duration and coverage (-) data distribution mismatch	Satellite-derived PV generation, satellite-derived direct irradiance data, periodic encoding + Satellite-derived PV generation	Actual PV generation, actual solar irradiance, periodic encoding + actual PV generation
Scenario 3 (Satellite-derived data + transformed actual data)	(+) Leverage the advantages of more reliable actual PV generation and publicly available satellite-derived meteorological and PV generation data by developing an empirical relationship	Transformed satellite-derived PV generation and direct solar irradiation, periodic encoding + actual PV generation	Actual PV generation, actual solar irradiance, periodic encoding + actual PV generation

3.3.5. Reinforcement Learning

Reinforcement Learning (RL) is a rapidly evolving area of machine learning that provides a solid framework for addressing dynamic optimization and control challenges. Unlike conventional supervised learning, which depends on labelled datasets to guide decisions, RL allows autonomous agents to learn the best strategies through direct interaction with their environment. This process involves a feedback loop: the agent chooses actions, observes the resulting state changes, and receives numerical rewards that encourage good behaviours and discourage poor ones. Over time, this fosters adaptive learning, enabling RL agents to operate effectively in complex, uncertain systems and improve their performance through experience (Cardo-Miota et al., 2025).

In this research, RL is used to optimize battery dispatch in PV integration. The agent learns to manage energy flows-charging, discharging, and curtailment-based on hourly PV and wind generation and load demand. The problem is modelled as a Markov Decision Process (MDP), where the agent observes the current battery state, renewable supply, and load, then selects a continuous action representing the dispatch decision. The environment updates the battery state and calculates the reward, reflecting the balance between served load, curtailment, and energy losses.

The goal of the RL agent is to maximize the total reward over time, which aligns with increasing energy delivery efficiency while reducing curtailment and unmet demand. This approach enables the agent to develop a control policy that adapts to changing supply and demand, thereby enhancing system reliability and increasing the penetration of renewable energy. This well-established RL algorithm was customized, as shown in Fig. 3.7, to meet the specific design requirements of the new methodological approach presented in Section 3.1, and then applied to validate it.

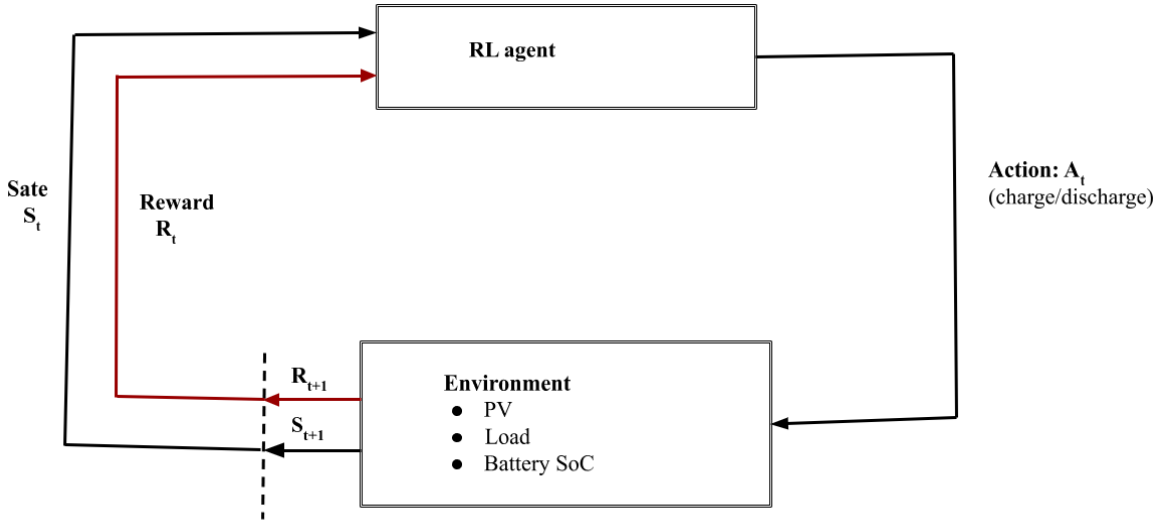

Fig. 3.7. Reinforcement learning system optimization algorithm

4. RESULTS AND DISCUSSION

This chapter presents the detailed results of the newly developed methodological framework for integrating large-scale PV, which aligns with the thesis objective. It highlights the insights gained through the application of the novel algorithm and the new performance indices introduced in the study, emphasizing their role in revealing the complex interdependencies among key system parameters. Particular attention is also given to the contribution of residential PV systems in enhancing large-scale PV integration, supported by results generated from a dedicated algorithm designed for this purpose. Furthermore, the chapter examines the significance of PV power forecasting and optimization. Each section offers findings that directly or indirectly contributes to increasing the penetration of PV in modern power systems. Finally, the chapter concludes with a summary of the key scientific findings from this thesis.

4.1. Large-scale PV integration

This section examines the impact of the various enabling technologies on system performance by creating various solar and wind mix, from which PV ratio of 0%, 50%, and 100% of the total renewable generation, representing wind-only, 50-50 PV-wind, and solar-only scenarios, respectively, were selected to represent the extreme and median conditions of their complementarity.

4.1.1. Generation and load variability

Solar energy in Eritrea demonstrates consistent availability throughout the year, making it a highly reliable resource for power generation, as depicted in Fig. 4.1. In contrast, wind energy exhibits strong seasonal variation due to the influence of two dominant monsoon winds: the Northeast Monsoon (November–March), which affects the southern coastal regions, and the Southwest Monsoon (May–September), impacting the entire length of the Red Sea (Rosen et al., 1999). The spatial and temporal complementarity between solar and wind resources presents a strategic opportunity for hybrid renewable systems. Deploying wind farms across geographically diverse locations-such as the central highlands and northern coastline-can complement each other, thereby smoothing overall power generation. Moreover, integrating wind with PV significantly reduces the dependence on large-scale energy storage. A detailed analysis of the data reveals that the correlation between solar PV and wind increases (becomes more negative) as the temporal resolution shifts from hourly to daily, further supporting their complementary relationship in hybrid system design.

Fig. 4.1 illustrates the daily averages and full data distribution (with the shaded region representing the minimum to maximum range) for solar PV, wind (as normalized to peak hourly values), and electricity demand (normalized to total demand). At the daily time scale, wind generation exhibits significant variability, peaking in June at a level approximately 6.5 times higher than its minimum in November. However, the aggregated wind output never drops to zero due to the combined contribution of multiple geographically dispersed wind sites. In contrast, solar generation in Eritrea displays a relatively steady daily pattern with minor seasonal fluctuations. The central highlands, in particular, maintain stable solar potential year-round, with only a modest dip in output during the rainy months of July and August. Electricity demand, meanwhile, exhibits less variability and remains more stable compared to both solar and wind generation.

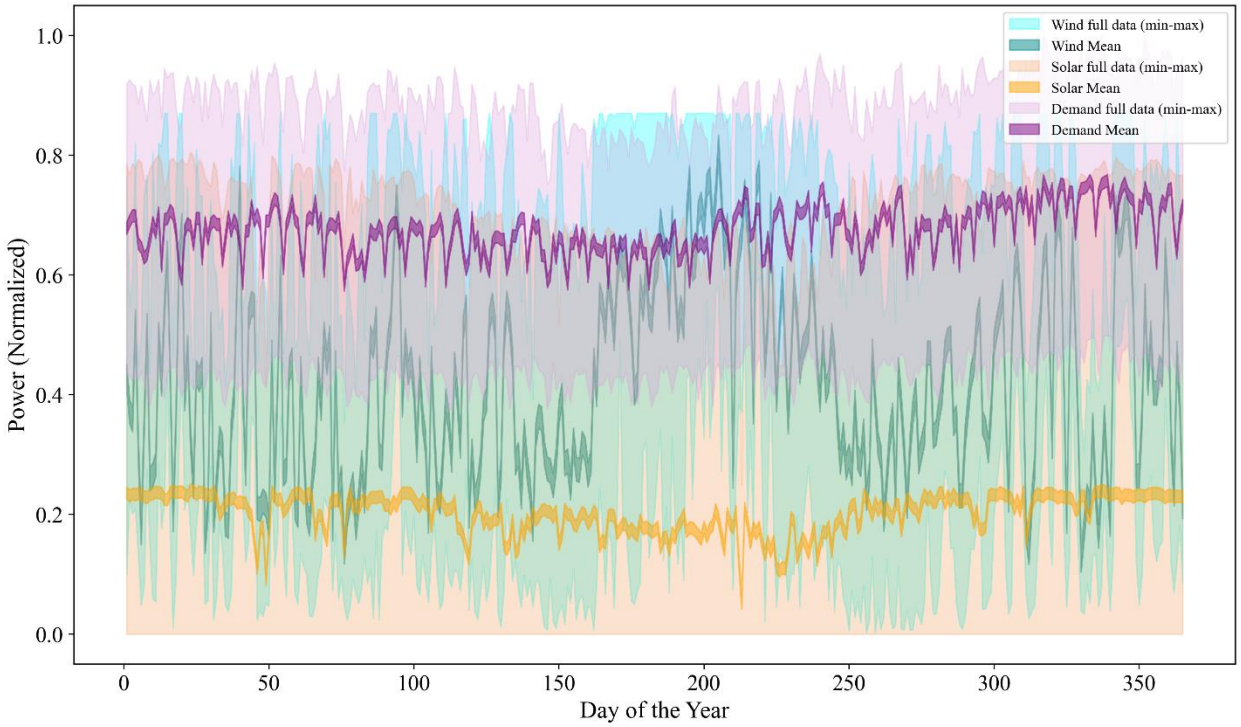

Fig. 4.1. Aggregated national generation profiles of solar PV, wind, and load

The diurnal profile of solar PV generation, depicted in Fig. 4.2, aligns closely with the natural daylight cycle. In contrast, wind generation demonstrates the most significant variability over the course of the day when compared to both solar PV output and electricity demand. While the daily demand pattern is smoother than the fluctuations in solar PV and wind (represented by the light coral shading in Fig. 4.2), it still exhibits a broadly similar trend with solar PV and wind generation. Demand steadily increases from early morning to midday, experiences a slight dip in the afternoon, and then peaks around 7 p.m., a period when wind output remains relatively strong. This pattern indicates that residential consumption is the primary contributor to overall electricity demand. Notably, the figure demonstrates that solar PV generation, wind power, and demand generally exhibit similar diurnal trends. Such synchronicity is advantageous, as it underscores the potential of renewable resources to substitute fuel-based power generation. However, uncertainties associated with the use of proxy datasets cannot be fully avoided. According to Negash et al. (2021), actual measured wind speeds are higher than those provided by the GWA dataset, with the discrepancy being more pronounced over rough surface topographies. Consequently, the results reported in this study can be considered conservative, as measured values would yield higher estimates than GWA-based data. Similarly, measured and PVGIS-derived solar radiation profiles show consistent patterns and magnitudes (Ghebrezgabher et al., 2016). Likewise, although the use of Ethiopian data is justified by its close similarity to Eritrea in terms of climate, cultural practices, and seasonal weather and consumption patterns, some degree of uncertainty may still arise from regional and contextual disparities.

Evaluating a range of scenarios and technology combinations could help identify practical solutions to meet electricity needs. However, given the mismatch between renewable output and demand, significant solar PV and wind capacity must be installed, often leading to some level of surplus generation.

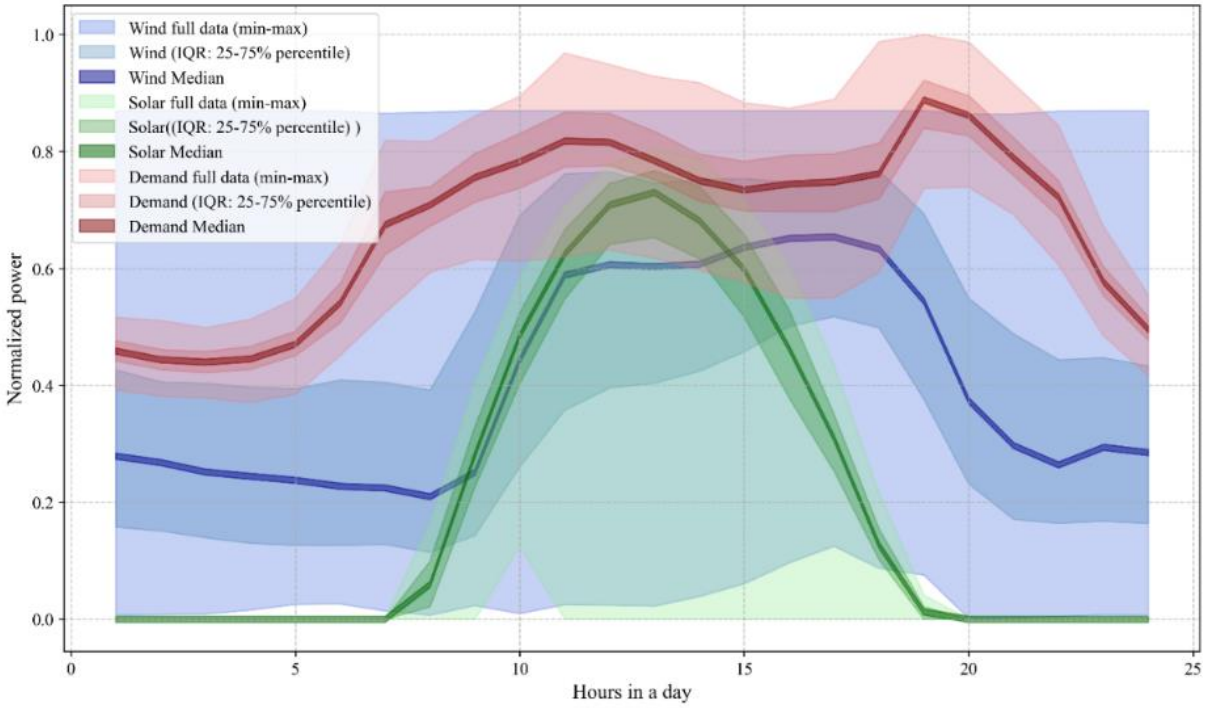

Fig. 4.2. Diurnal variability of aggregated generation (PV and wind) and demand

The figure displays the full data distribution (min-max), InterQuartileRank (25^{th} to 75^{th} percentile of the data), and median values (wind and PV normalized to peak generation and demand normalized to annual values).

Understanding the mismatch between VRE generation and demand across different time scales is a fundamental requirement for designing and sizing energy storage solutions. Several studies have used net load to model storage requirements, highlighting its role in balancing grid operations (Ardenas et al., 2021; Dujardin et al., 2017a; Heide et al., 2011b). In a similar approach, the analysis begins with understanding the mismatch between different PV-wind mixes and demand. This analysis provides insights into net load variability and structural patterns under different mixing ratios. Fig. 4.3a illustrates how mismatch power varies with changes in the PV fraction when RE-to-load ratio of 1 is applied. The vertical axis represents the frequency, indicating the number of hours within each 100 MW mismatch interval. The frequency of positive mismatch (VRE greater than load) increases with decreasing PV fraction. However, the magnitude of the mismatch capacity decreases with the decreasing PV fraction. In contrast, both the magnitude and frequency of the negative mismatch (VRE less than load) increase with increasing PV fraction. The optimal system should have a maximum frequency at a minimum mismatch capacity (MW); however, as shown in Figure 4.3a, the optimal mismatch has a lower frequency as depicted by the valley between the two peaks, particularly at solar-dominated mixes.

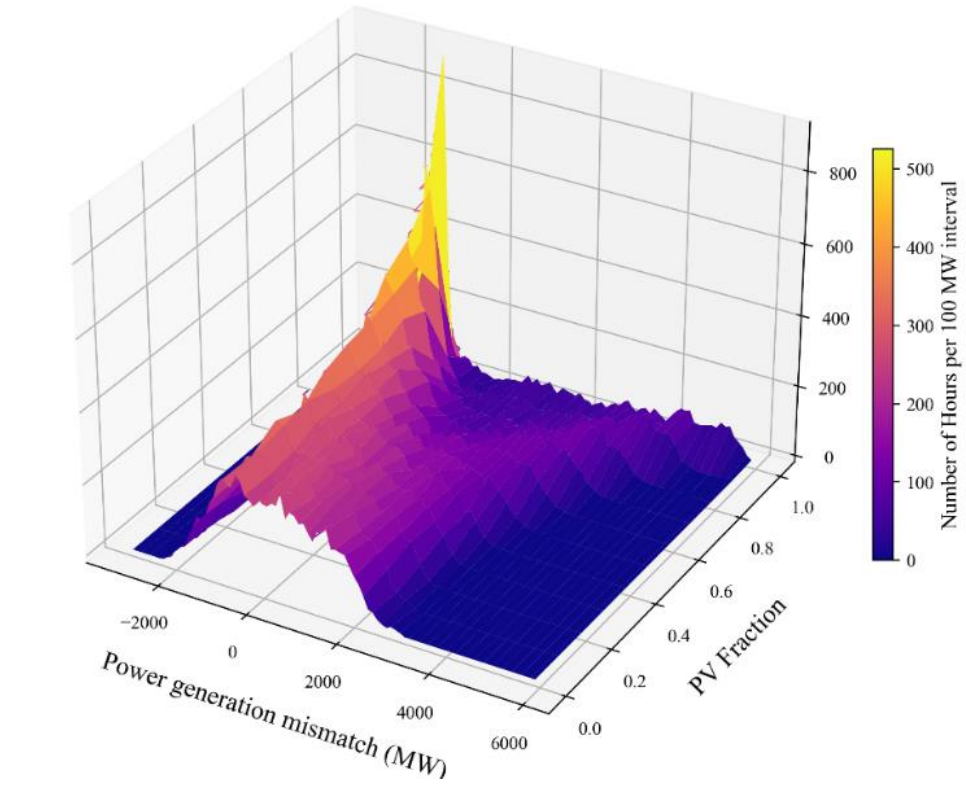

(a)

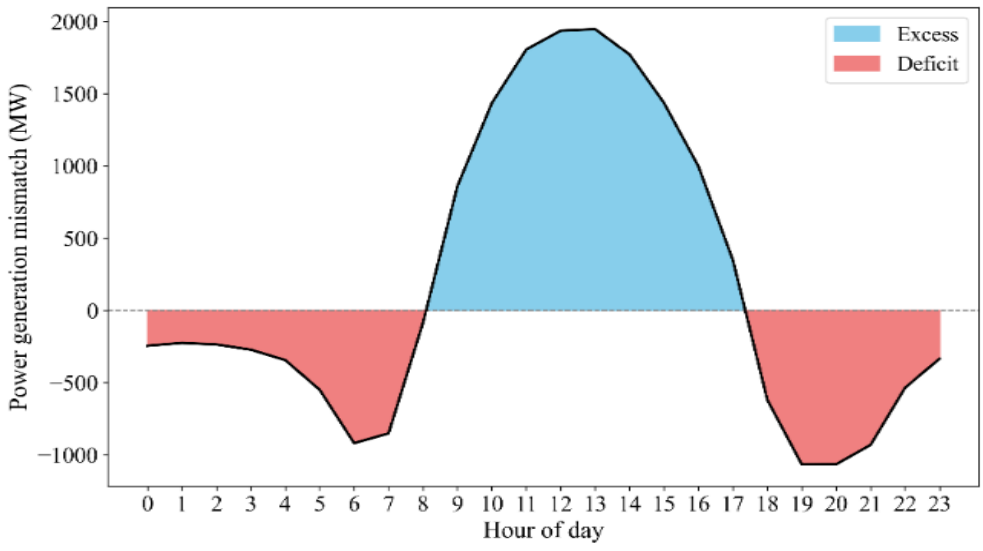

(b)

Fig. 4.3. Variable generation mismatch as a function: a) PV fraction and frequency, b) diurnal-hourly average values

Fig. 4.3a does not give the complete picture of the netload variability in terms of time scale; therefore, understanding the time series and its time distribution in diurnal and seasonal scales is crucial for balancing supply and demand. Fig. 4.3b illustrates the diurnal variability of the net load (mismatch) for the 50-50 PV-wind scenario. As shown in Fig. 4.3a, the mismatch is positive during the daytime, specifically from 8:00 AM to 7:00 PM, due to the diurnal cycle of

solar generation. Although the RE-to-load ratio is 1, there is an hourly mismatch between generation and demand. Furthermore, there is a complete absence of solar PV at night, resulting in a negative mismatch. Solar-dominated mixes experience higher positive mismatch during the daytime and face shortages at night. In contrast, the mismatch in wind-only and wind-dominated mixes is lower and randomly distributed throughout the daytime. Such a daily mismatch can be addressed using short-term battery storage, which can store and deliver energy at high density for a few hours. Even though the daily mismatch is resolved, a seasonal variability issue may remain unaddressed. With the same RE-to-load ratio 1, overgeneration occurs during the summer, characterized by spikes in net load in June and July (Fig. A6). Conversely, significant generation deficits are observed throughout much of the spring. In the remaining seasons, however, variability tends to fluctuate on a monthly basis rather than across entire seasons. Therefore, understanding these variabilities is crucial for designing a system that addresses all the uncertainties of a VRE-dominated grid. Our approach utilizes various enabling tools, including diurnal storage, seasonal storage, curtailment, and balancing generators, to balance year-round hourly supply and demand. The following section explores how different PV-wind mixes align with electricity demand and their influence on achieving high levels of VRE penetration.

Table 5 outlines the key components of selected renewable energy scenarios designed to study system design issues and associated performance. Though results for a number of storage hours are produced, due to the similarity of the results and the performance superiority observed at 6h, the discussion is made mainly using 6h of storage.

Table 5. Description of the different scenarios analysed

Scenarios Names	Solar share (%)	Wind share (%)	Hours of storage	Storage technology
Solar only	100	0	1,2,4,6,8,10	Li-ion battery
50-50 scenario	50	50	1,2,4,6,8,10	Li-ion battery
Wind only	0	100	1,2,4,6,8,10	Li-ion battery

4.1.2. Renewable use without storage

Fig. 4.4a illustrates the required no-dump capacity across the full range of PV-wind mix ratios under a strict no-curtailment condition. As shown, the lowest no-dump capacity occurs in the wind-only scenario (100% wind), while the highest is observed in the 100% PV ratio (solar-only scenario). This variation is primarily driven by differences in resource profiles, total energy output, and their alignment with electricity demand. The associated no-dump penetration results, presented in Fig.4.4b, highlight that penetration levels depend on both the resource quality and capacity. Wind energy, characterized by more evenly distributed generation over time and a higher full load hour, achieves greater penetration than solar, even with a smaller capacity. As the share of solar energy increases, the complementarity between solar and wind energy also increases, consequently enhancing their matching with demand and overall penetration, which peaks at around a 30% PV mix. Beyond this point, penetration begins to decline due to the increasing lesser time distribution of solar generation. Overall, these findings suggest that maximizing renewable energy use with minimal curtailment and storage is feasible when complementarity between sources is optimized. However, accurately quantifying the extent of this benefit remains difficult due to the interplay of multiple influencing factors. The data so far reveals three key insights:

1) a significant increase in RE penetration is only possible when supported by curtailment and storage strategies, as seen in other studies (Solomon et al., 2010).
2) resource complementarity can mitigate reliance on both tools, aligning with findings in (Heide et al., 2011a, 2010); and
3) Eritrea's strong renewable resource potential may offer a more favourable outcome compared to regions with similar conditions (Shaner et al., 2018; Solomon et al., 2016). To better understand the role of curtailment and other enabling tools, I examine the scenario of higher penetration using curtailment as the sole mechanism.

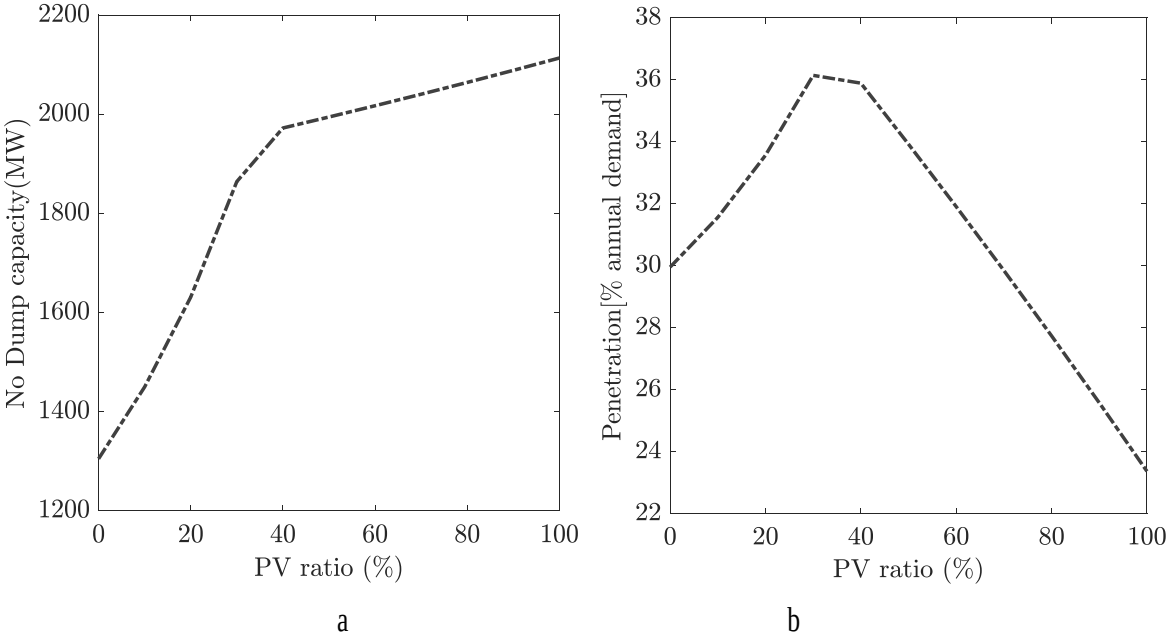

Fig. 4.4. No dump: a) capacity, b) penetration as function of PV ratio

Note that all discussions, including figures in the following sections, refer to scenarios where penetration exceeds no-dump capacity, requiring either curtailment, storage, or a combination of both. Fig. 4.5 shows the penetration and curtailment for different PV-wind mix when no storage is employed. As can be seen from the figure, for all PV ratios increase in system size leads to a simultaneous increase of VRE penetration and curtailment. But the magnitude of the impact depends on the mix. Wind dominated mix have achieved higher penetration for all RE to load ratios and thus experienced lower curtailment. However, as the PV ratio increases the corresponding VRE penetration gradually decreases and the curtailment starts to dominate, showing that role of curtailment is dependent on the PV-wind mix. The change in the observed penetration and curtailment remains insignificant when PV ratio was lower than 40% share, the amount above which pronounced difference emerges as the ratio increases to 100%. For example, at (RE to load ratio value of 1.1) a penetration of 79% and 47% is achieved for wind and solar only scenarios, respectively, where the corresponding curtailment were 28% and 58%, respectively. The maximum penetration, even though the gain over the wind only scenario was small, is reached at around 20 to 25 % of PV ratio when the curtailment remains less than 30%. The above result clearly shows the impact of time-distribution of the solar PV and wind output in matching the local electricity demand. Wind only and wind dominated scenarios enjoys high use of RE at lower curtailment for almost all cases of system size increase. However, pushing to higher penetration will need massive curtailment even for the wind dominated system, indicating the need for storage under all PV-wind mix condition. For example, a penetration of 90% can be achieved by dumping around 50% of the generation at

high RE to load ratio of about 1.87. Note that previous studies show that neither massive nor low curtailment leads to technoeconomic benefit (Perez et al., 2019) , thus the best solution is to understand the interlink between various factors to estimate the acceptable range during system design.

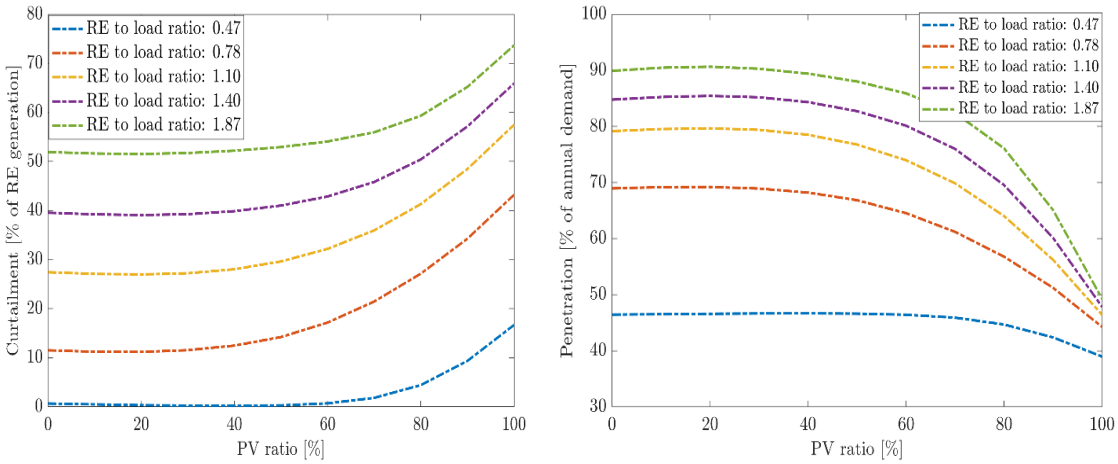

Fig. 4.5. Renewable energy a) penetration and b) curtailment as function PV ratio

Fig. 4.6a illustrates the relationship between penetration, curtailment, and resource mix in no storage condition. As depicted in the figure, there is a rapid increase in penetration with a slight initial curtailment rise, which gradually slows as curtailment increases. As depicted in Fig.4.6b, the impact of curtailment on penetration is significantly affected by the resource mix. In wind-dominated mix with a small solar share of about 0.2, the highest penetration is achieved. However, in a solar-dominated mix, particularly in a solar-only scenario, the increase in penetration with curtailment is negligible. This is because the diurnal (day – night) cycle of solar generation limits the matching capability more severely and thus requires energy storage for the dark hours of the day as a result the penetration is seen to be much lower than the wind dominated mix. The above discussion shows that maximizing renewable use requires an optimal use of various enabling tools, a subject to be explored later with more details.

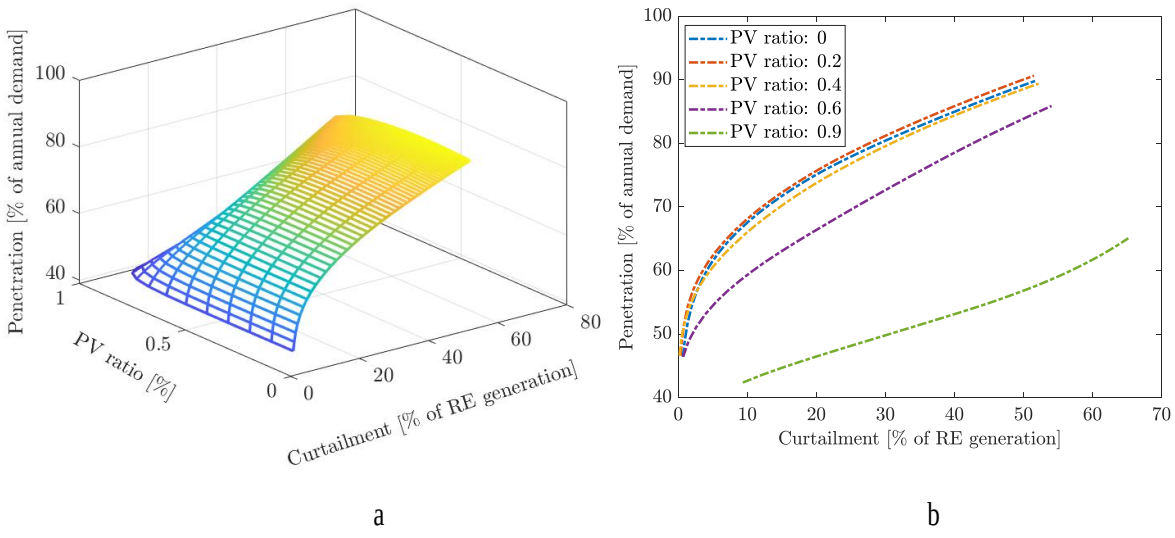

Fig. 4.6. Renewable energy: a) penetration and curtailment as function of PV ratio, b) curtailment versus penetration

4.1.3. Renewable use with energy storage application

Let's examine the impact of different storage technologies and types on increasing renewable penetration.

4.1.3.1. Diurnal storage application

Let us examine what happen when some storage size is applied as RE system size increases same way as for Fig. 4.5. Fig. 4.7. shows how the penetration and curtailment varies with varying PV–wind mixes at fixed storage capacity of 0.41 average daily demand – equivalent to 18 GWh which is small storage capacity when compared to Eritrea's average daily demand of 43.8 GWh. It is worth noting that even the largest storage that we considered in this study remains smaller than the average daily demand. At smaller system size, the storage removes curtailment (compared to the corresponding no storage condition of Fig. 4.5) observed at higher PV share in order to increase penetration. Consequently, the change in penetration and curtailment become relatively negligible, regardless of the wind-solar mix. In response to modest increase in RE system size (RE to load ratio of 0.47 to 0.78), low solar share scenarios already result insignificant curtailment difference while penetration shows some favor for wind-solar mix, particularly for solar dominated mix. Interestingly, the trend showed a marked difference as RE to load ratio increases to 1.1 (at storage 0.41 average daily demand) where we already observe approximately 96% penetration for only 9% curtailment at 80% PV mix. In Fig.4.5, a 90% penetration is achieved by building a significantly larger system size (with an RE-to-load ratio of 1.87) and curtailing more than 50% of the energy in wind-dominated mixes. However, with the addition of storage at the same RE to load ratio of 1.87, 100% renewable energy penetration is attained for certain solar mixes (ranging from 20% to 80% solar share). This is because the storage partially reduces curtailment, leading to increased penetration compared to scenarios without storage. The data corresponding to RE to load ratio of 1.4 shows that 100% RE could be achieved without increasing the system to an RE to load ratio of 1.87. My extensive data shows that, for other storage size, 100% RE could be achieved at even lower curtailment than observed in this case. Theoretically, with unlimited ideal energy storage, variable electricity demand could be met with complete reliability using only wind and solar power, without the need for excess generation capacity.

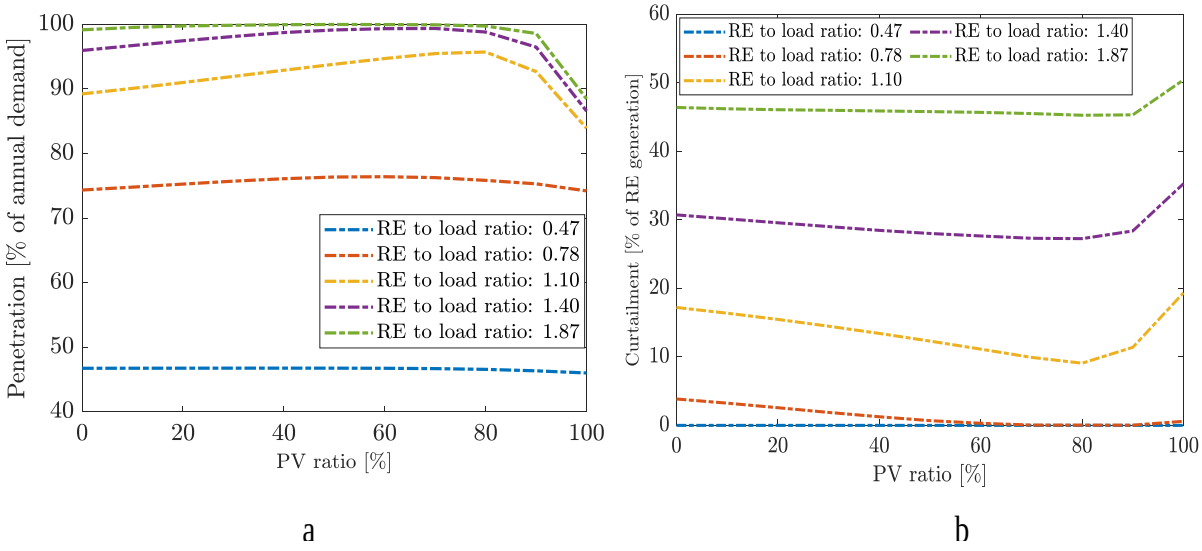

Fig. 4.7. Renewable energy: a) Penetration, b) Curtailment as a function PV ratio, with 0.41 of average daily demand

The above result shows that while wind appears to achieve higher penetration as curtailment increases due to time distribution of its generation, solar penetration improves significantly with addition of small storage due to the day-and-night cycle of solar generation profile. The mixture of the two combines these characteristics to achieve higher penetration at lower loss and storage capacity need. However, the overarching question is how one can design and build a more effective system in a system that bears much complexity as any choice may involve disregarding some technical benefit that cannot be seen in economic based decision making.

Fig. 4.8 presents the dependence of VRE penetration on curtailment for the storage size applied in Fig. 4.7. Penetration increases with a slight rise in curtailment, but the rate of penetration growth diminishes as curtailment continues to increase, depending on the resource mix. This demonstrates that controlled curtailment can be beneficial for optimizing system performance. In the following subtopic, we will examine other scenarios to understand the broader perspective.

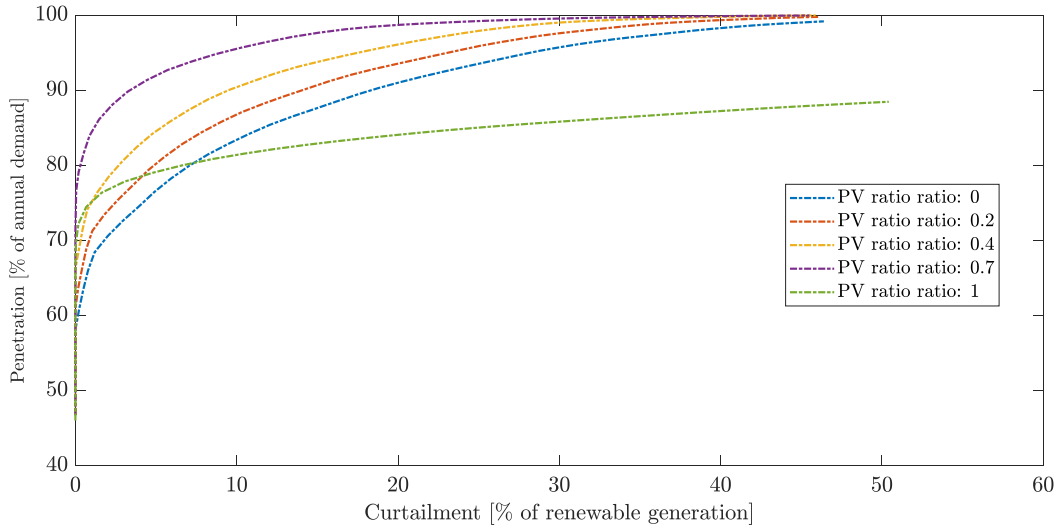

Fig. 4.8. Penetration as a function of curtailment for varying PV ratios at storage capacity of 0.41 of average daily demand

The interaction between VRE penetration, storage capacity, and curtailment related to wind-only, 50-50 wind-solar mix, and solar-only scenarios is given in Fig. 4.9, Fig. 4.10 and Fig. 4.11, respectively.

As shown in Fig. 4.9 penetration increases with increase in storage size. At fixed storage size, increase in renewable generation increases penetration and curtailment simultaneously. The increase in penetration is much faster when renewable generation is low and slowly level off with further increase in renewable generation. By comparison, the increase in VRE penetration for wind dominated scenarios are mainly driven by the effect of curtailment than storage capacity. There exists a trade-off relationship between storage capacity and curtailment, whereby a decrease in storage capacity results in an increase in curtailment and vice versa. The increase in penetration is driven by both storage and curtailment, with curtailment having a more significant impact in this particular scenario.

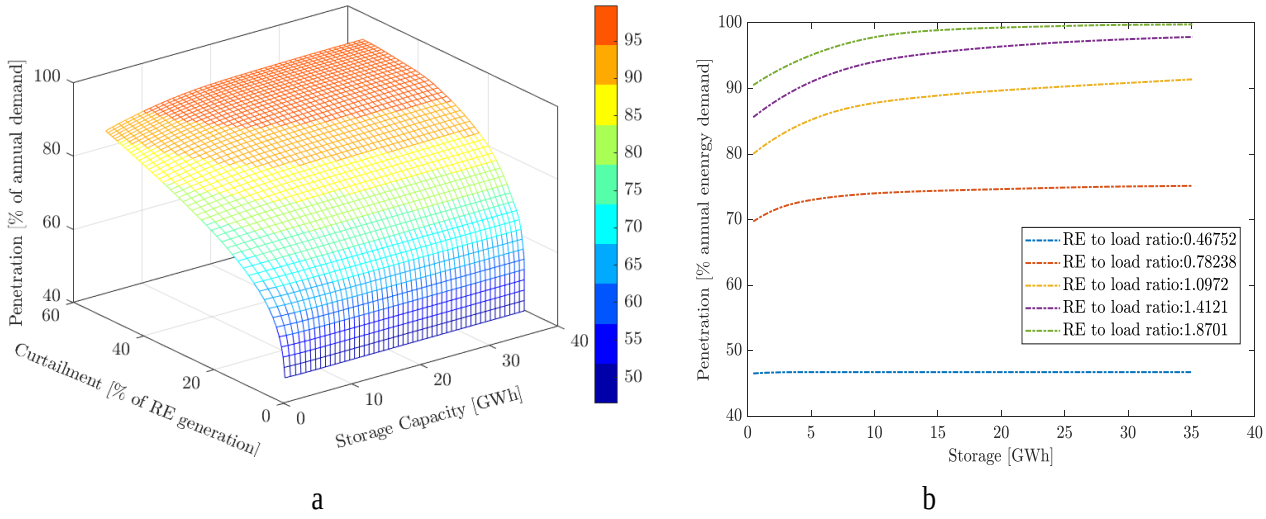

a b

Fig. 4.9. Wind-only scenario with 6 hours storage, interaction between: a) Penetration, curtailment, and storage capacity, b) Storage capacity and penetration

At low generation level (RE to load ratio 0.48 to 0.78) the penetration remains almost constant regardless of the storage size. This is because mismatch between wind generation and load can be accommodated even with the smallest storage capacity allocated and further increase in storage have no benefit to the system. At such low generation level storage has little impact on the system performance. But as the generation increases beyond RE to load ratio of 0.78 penetration increases and curtailment decreases with increase in storage capacity. In the absence of storage (as depicted in Fig. 4.6), the trend differs, as every increase in penetration is coupled with a corresponding rise in curtailment. The impact of curtailment is more significant in a wind-only scenario when compared to the effects of storage. As depicted in the Figure 4.9b, penetration exhibits a noticeable increase within the first few GWh of capacity. However, this increase gradually tapers off, with only marginal gains observed when exceeds approximately 10-15 GWh and beyond this point, further increase in storage capacity do not yield significant benefits to the system.

Fig. 4.10a shows the penetration and curtailment as function of storage capacity for the 50%-50% PV-wind scenario. This Scenario behaves similar to the wind only scenario as in both scenarios; penetration increases with storage capacity and curtailment. However, the impact of storage has some differences mostly at small storage capacity. Comparing Fig.4 9b and 4.10b, at low storage capacity the wind-only scenario outperforms in achieving higher penetration. This can be attributed to the nature of wind generation, which is less dependent on storage due to its inherent randomness; instead, it is primarily affected by curtailment. From this trend, it is evident that a configuration featuring a small storage capacity and significant curtailment provides more benefits to the system compared to constructing a large storage facility at a lower curtailment rate, in wind only scenario. In contrast, the 50-50 scenario depends significantly on storage due to the 50% solar share, which is influenced by the day-night cycle of solar radiation, necessitating storage solutions. The increase in penetration in the 50-50 PV-wind scenario is therefore, the combined effect of both storage capacity and curtailment. However, increasing curtailment beyond 20% offers negligible benefits to the system. At this level, penetration levels off for all cases as curtailment increases. The 50-50 PV-wind scenario demonstrates a significant improvement in achieving higher penetration when employing both enabling tools.

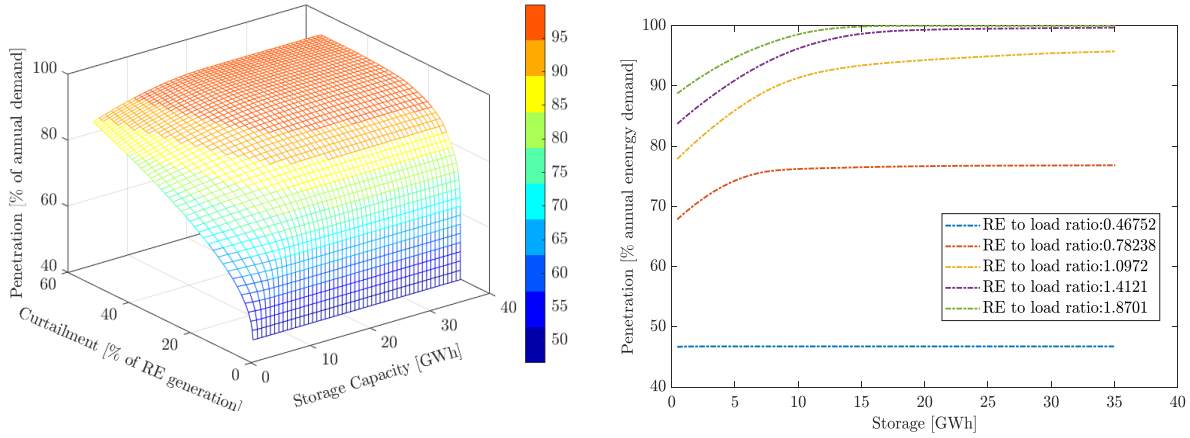

a b

Fig. 4.10. 50-50 PV-wind scenario with 6 hours storage, interaction between: a) Penetration, curtailment, and storage capacity, b) Storage capacity and penetration

The solar-only scenario shown in Fig. 4.11 shows a different pattern from the previous two scenarios. Regardless of the generation capacity (RE-to-load ratio), the penetration remains low at lower storage capacities, with significant curtailment (Fig.4.11a). This relates to the natural cycle of solar generation, which requires adequate storage solutions to address the diurnal mismatch. However, when small storage is added, a significant increase in penetration is observed, reaching its peak of 100% at considerably large storage sizes and generation capacities (Fig.4.11b). Nevertheless, it is possible to attain a solar penetration of 90% with a 20% curtailment, with a storage capacity of less than average daily demand. Achieving this penetration level would necessitate a substantially higher curtailment in a wind-only scenario.

The study's design highlights the complex relationships among various factors, offering multiple options for selecting combinations of storage and curtailment to achieve a specific penetration level that aligns with individual objectives and policy priorities. The most effective approach involves determining the ideal size for both storage and curtailment, finding a balance that maximizes penetration while ensuring both technical and economic feasibility.

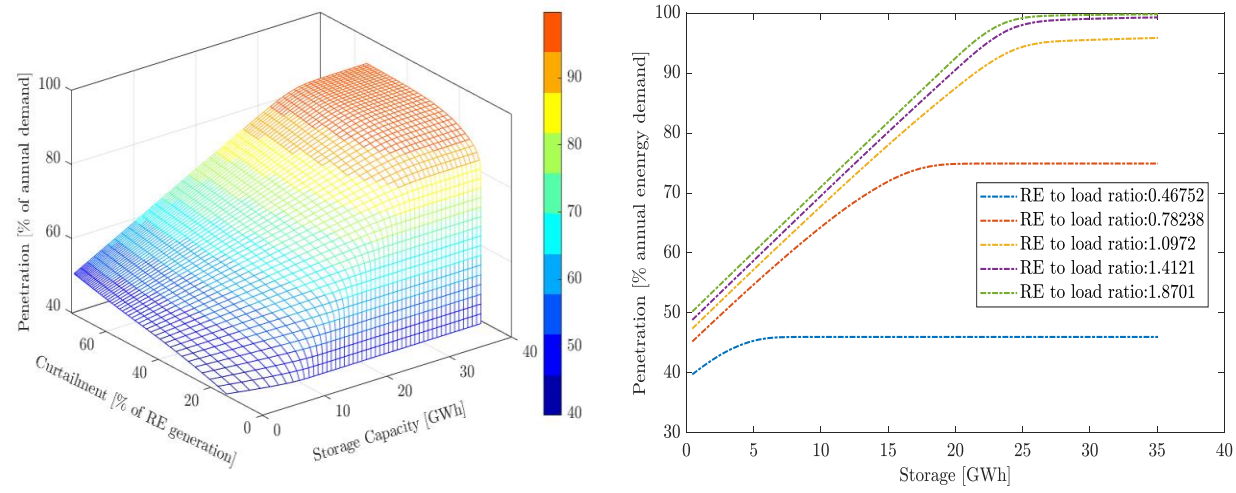

a b

Fig. 4.11 Solar-only scenario with 6 hours storage, interaction between, a) Penetration, curtailment, and storage capacity, b) Storage capacity and penetration

The design employed in this study builds a complex relationship between various factors that offers multiple options for choosing combinations of storage and curtailment to achieve a specific penetration (including 100%), tailored to individual priorities and policy preferences. The optimal approach, however, lies in determining the approximate optimal size for both variables, striking a balance that maximizes penetration while ensuring technical and economic feasibility.

Based on the aforementioned scenarios, it is evident that curtailment plays a beneficial role in enhancing grid penetration by maximizing the utilization of storage. Attaining a penetration target without any curtailment necessitates an oversized storage capacity alongside a large-scale renewable generation, resulting in low storage utilization. However, moderate and carefully managed curtailment, which is expected to become a new normal in future grids, can effectively increase renewable penetration while reducing the required storage size by maximizing its utilization. This finding aligns with previous research findings reported in (Solomon et al., 2014), though they use a different approach and cover different geographic locations represented by the corresponding resource and demand profiles.

The overall observation from Figs. 4 9, 4.10, and 4.11 revealed that, at a given generation capacity, penetration rises as storage capacity increases, leading to a reduction in dumped power. However, the impact of these factors differs across scenarios, the effect of curtailment is more dominant in wind only scenario, whereas in a solar-only scenario, the impact of storage surpasses that of curtailment. For the 50-50 PV-wind scenario however, penetration is the result of considerable effect of both storage and curtailment. The 50-50 PV-wind scenario demonstrates superior performance, allowing us to easily achieve a 90% penetration target of renewables with reasonable storage capacity and curtailment. This highlights how solar-wind complementarity can smooth out generation profiles while simultaneously increasing penetration. Across all scenarios, the increase in penetration exhibits a rapid rise for smaller storage capacities, but it gradually levels off after reaching a threshold value. Therefore, increasing storage capacity beyond this value offers a negligible benefit in achieving higher penetration. The specific threshold value depends on the generation size and storage capacity, but in all scenarios, penetration levels off at less than 0.8 times the average daily demand (equivalent to 35 GWh), indicating that further increases in storage provide no additional advantages to the system. However, the observed decrease in storage needs does not mean storage is not necessary at all. However, it shows the change in the manner of storage application and the suitable technology type. Before it levels off, diurnal application suitable storages are required, but after that, the system increasingly requires seasonal services, which use seasonal storage. This issue was discussed in (Denholm et al., 2022; Solomon et al., 2019) for U.S. and Israel, respectively. The study on Israel is based on a systematic analysis of several scenarios focused on solar energy, whereas the U.S. study seeks to quantify these requirements without detailed techno-economic considerations to assess the geophysical constraints of solar and wind generation in meeting demand. In contrast, my study explored a broader range of scenarios – including varying PV-wind mixes, storage capacities, and curtailment levels – to confirm that these effects are not case-dependent.

Fig. 4.12 illustrates the storage requirements necessary to achieve a penetration target of 90% for different RE-to-load ratios as a function of PV ratio. In the figure, only RE-to-load ratios of 1.10 and above are displayed, as these represent cases, where reaching 90% penetration is feasible. It can be noted that when the RE-to-load ratio is below 1.1, there is insufficient energy to reach 90% penetration.

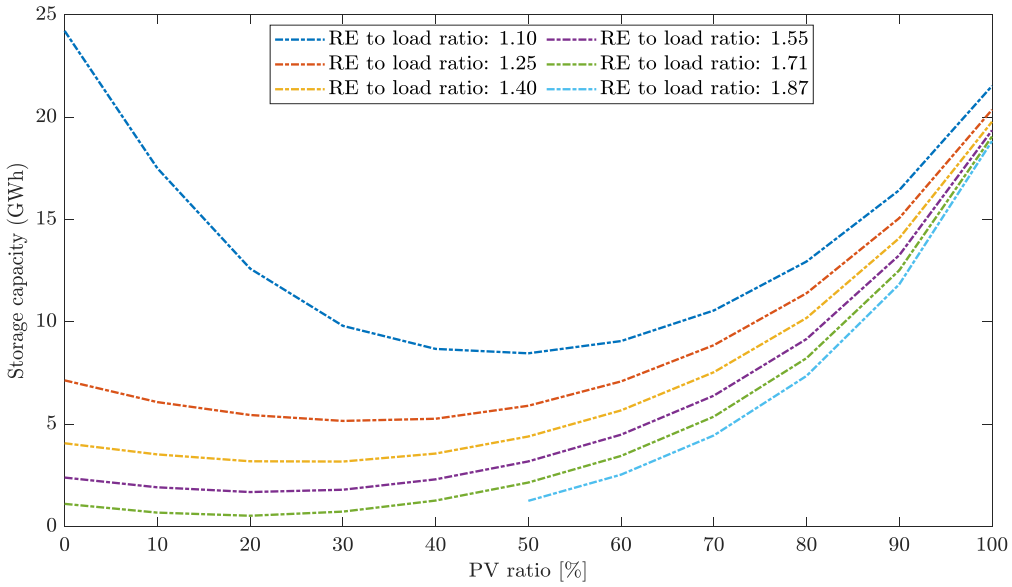

Fig. 4.12. Storage required to reach a penetration target of 90% using 6 hours of storage

The required storage capacity varies depending on the PV-wind ratio within these scenarios. The wind-only scenario requires less storage capacity when compared to the solar-only scenario, except in the case of RE-to-load ratio of 1.10. This discrepancy arises because the wind-only scenario is predominantly influenced by the generation size and curtailment rather than the storage size. At this specific RE-to-load ratio, the marginal increase in penetration from excess generation is minimal due to the system's limited capacity, making it challenging to achieve 90% penetration with minimal storage. Due to lower effectiveness in the use of storage, the wind-only scenario also needs higher storage capacity to reach 90% penetration at a RE-to-ratio of 1.1. However, as depicted in the figure (Fig. 4.12), at higher RE to load ratio, the wind-only scenario can achieve a 90% penetration target with significantly lower storage capacity because the time distribution of wind enables higher demand matching than solar only scenario. This is a further elaboration on how emphasizing either one of the tools (i.e., storage or curtailment) diminishes the importance of the other for the case of wind. Though the mechanism is not as strong, note that the storage needs decrease with more curtailment even for a solar-dominated system.

It is important to note that the solar-dominated scenario relies heavily on storage, with even a slight increase in storage capacity resulting in a significant enhancement in penetration. The reason behind the lower storage requirement for the RE to load ratio of 1.10 is attributed to the role of storage in solar energy. In the solar-only scenario, storage capacity plays a critical role, surpassing the influence of curtailment and generation size. That is why the storage requirement remains relatively similar regardless of the generation size, as depicted in Fig.4.12. The minimum storage required to reach the penetration target varies across each RE to load ratio and falls within the range of 20-30% PV ratio, except for the RE to load ratios of 1.10 and 1.87. At 1.87 RE to load ratio, the wind-dominated mix (up to 40% PV ratio) can attain the penetration target without requiring any storage. However, as the PV ratio increases, the storage requirement experiences a sharp rise and ultimately converges to a similar storage value for all other RE-to-load ratios. This provides further evidence on how the resource mix impacts the role of storage and curtailment. Thus, setting the optimal mix of various enabling tools will be crucial to achieving both financial and technical optimality in the future system.

As previously discussed, the increase in penetration is limited by the available storage capacity. Beyond a certain point, the rate of increase slows and eventually plateaus. At this stage,

implementing seasonal storage capable of holding energy for several days becomes essential to mitigate seasonal fluctuations. This will be discussed later; however, using only diurnal storage a penetration levels of up to 80-90% can be achieved in Eritrea by addressing the daily mismatch. When penetration exceeds this range, depending on PV-wind mix, multiday and seasonal mismatches pose challenges that diurnal storage alone cannot overcome, making seasonal storage necessary to meet demand. For example, in this study, achieving 96% VRE penetration with diurnal storage (e.g., at a 1.1 RE-to-load ratio in the 50-50 scenario) would require approximately 75% of the allocated storage capacity to contribute for the last 6% of the demand. Similarly, Fig.4.13 shows that a substantial portion of capacity is required to satisfy only a small fraction of the total demand. For instance, satisfying the last 10% of the demand in the 50-50 scenario requires nearly 46% of the deployed capacity. The situation is worst in the solar-only scenarios as every increase in penetration is accompanied by a large capacity requirement, specifically when exceeding 80% penetration. In both cases, satisfying the final 10% demand requires significantly increased installed capacity and storage. This is not feasible from a practical perspective, so alternative technologies that can function as seasonal storage should be considered at such high penetration levels (see below).

Compared to previous studies, the present work employs a unique and transparent simulation model, providing an alternative perspective with a more comprehensive analysis. It explores various interacting factors, including the PV-wind mix, curtailment, storage, and balancing needs, offering deeper insights into the complexities of renewable energy integration. The study presents a broader scenario-based approach to confirm that the phenomenon occurs under all conditions of the VRE mix. More importantly, the agreement with other studies' findinds produced using different datasets and models studying other locations (Denholm et al., 2022; Guerra et al., 2021) actually presents evidence that a common physical mechanism drives the interaction between VRE resources and their matching to electricity demand. Thus, developing a common theoretical framework to guide the designing and operation of the future system could enhance our ability to tackle the associated challenges better than the present approaches. But such an effort requires more studies of this kind.

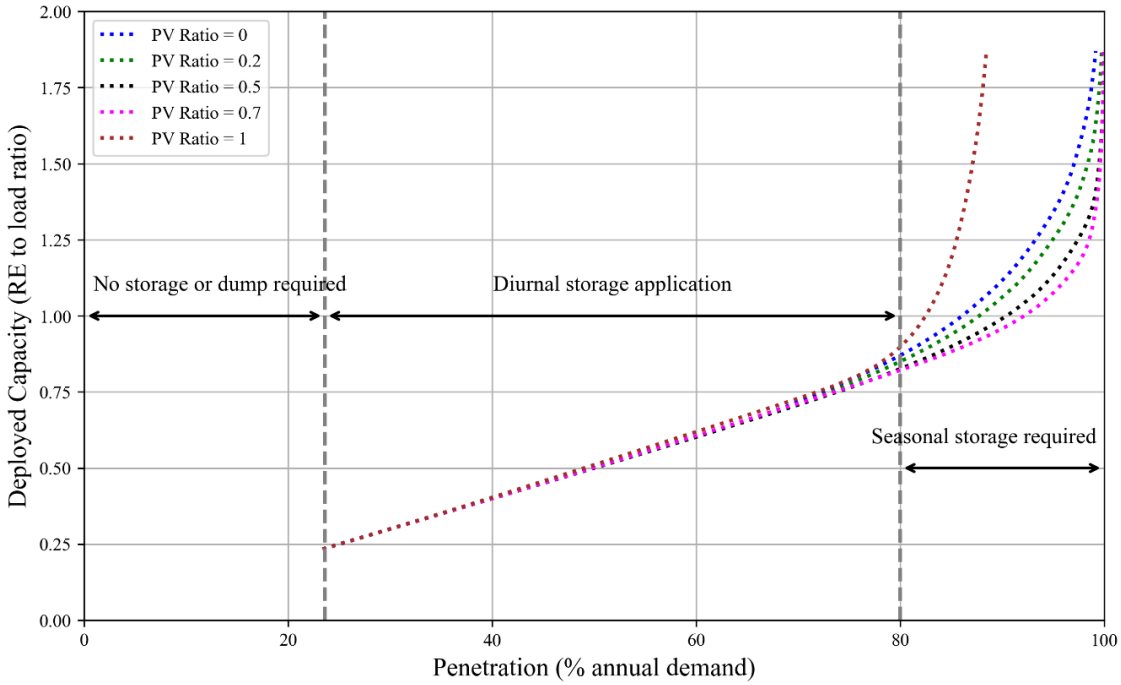

Fig. 4.13. Illustration of renewable energy requirements at different stages of renewable penetration

Fig. 4.13 illustrates the behaviour of penetration with increasing renewable energy deployment at a constant diurnal storage capacity of 0.41 times the average daily demand.

Now, let us return to studying the interaction between the different parameters when the hours of storage change from 6 to 1, 2, 4, 8, and 10. The pattern observed for these hours of storage closely resembles the relationship between penetration, curtailment and storage capacity presented in Figs 4.9a, 4.10a and 4.11a for wind only, 50-50 PV-wind and solar only scenarios, respectively. Regardless of the storage design and its effectiveness, the simultaneous increase of the three is a general trend. For example, the interaction between the three parameters for 2h and 6h of storage corresponding to a 50-50 wind-solar mix shows a similar trend (see Appendix, A6). However, the close resemblance does not mean all options are equally effective. This will be clarified in the next section by applying an appropriate tool devised to enable comparison of system performance for each combination of parameters.

Economic analysis of the proposed approach

A simplified, unit-cost economic analysis is presented to offer useful insights into the financial performance of the various system configurations discussed above.

Even though the focus of this study is not to perform a detailed economic analysis, one may question whether the demonstrated technical feasibility is linked to some economic viability. Here, a simplified unit cost-based economic analysis is presented to offer valuable insights into the financial performance of the various system configurations discussed so far. For this, we use the specific example of 18 GWh storage mentioned above. Based on current market trends (Table 6), achieving 100% penetration in the case of Eritrea through overbuilding and curtailment (PV and wind) as shown in Fig. 4.5, requires about 14.32 billion USD, accounting for the large RE generation requirement at a higher penetration level. In contrast, adding 18 GWh (0.41 average daily demand) of battery storage to the system (Fig. 4.7) reduces the overall cost to approximately 13.41 billion USD, while also accounting for battery replacements over the 30-year lifetime of PV and wind plants. However, balancing both enabling technologies, storage, and curtailment at the optimum mix (80% PV and 20% wind) offers a better benefit to the system in gaining techno-economic benefits and costs around 12.96 billion USD to reach 100% RE penetration. The cost reduction from USD 14.31 billion to USD 12.96 billion is mainly driven by several key system factors. Lower curtailment and/or overgeneration, combined with storage and the corresponding renewable-to-load ratio, as well as an optimized PV – wind mix those better matches varying demand conditions, are the primary contributors to reducing the overall system cost. Although a more detailed analysis is required to examine the technoeconomic benefits of the different configurations, unit cost analysis of the results highlights the importance of balancing the various enabling technologies in RE-dominated grids. This preliminary analysis shows that the optimized results are not only technically sound but also economically viable.

Table 6. Techno-economic data of different technologies used

Data	Technology			Source
	PV system	Wind system	Storage (Li-ion battery)	
Cost (2023)	758	1160	139	(Bloomberg, 2023; Fernández, 2023; IRENA, 2023)
unit	$/kWp	$/kWp	$/kWh	
Life (calendar years)	30	30	15	(Aghaei et al., 2022; Zucker and Hinchliffe, 2014)

4.1.3.2. Storage utilization and system-use index

Fig. 4.14a shows storage utilization as a function of storage capacity and corresponding curtailment for a wind-only scenario. The figure shows that storage utilization is significantly high at low storage capacity, particularly for some suitable curtailment ranges. However, the utilization index decreases as the storage capacity increases. This observation suggests that deploying large storage for diurnal applications with wind energy may not be advisable due to the risk of underutilization, as seasonal storage may be a more suitable option for such conditions.

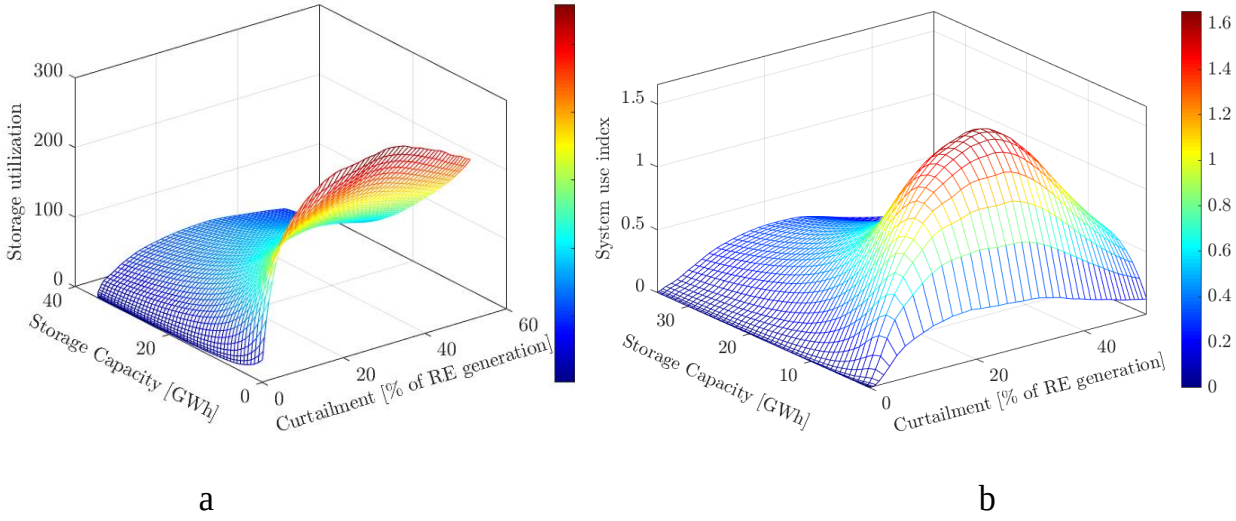

a b

Fig. 4.14. System performance indicators: a) Storage utilisation, b) System-use index for wind-only scenario at 6 hours of storage

The higher storage utilization index observed at lower storage capacities can be linked to the storage's frequent daily charging and discharging cycles. However, it should be noted that achieving a high utilization index does not necessarily translate into maximum system benefit, as the storage capacity is small and its contribution to overall energy coverage is limited. Thus, storage utilization has limitations in fully conveying the complete picture of its system benefits, which depend on various other factors. To address these limitations, we introduced a new index called the system-use index (SUI). This index provides a more comprehensive evaluation of system performance by linking storage utilization and RE consumption and generation with other factors, such as storage charging/discharging, and energy and power capacity. Unlike storage utilization, which primarily measures the extent of storage use, the system-use index offers deeper insights into how effectively storage is integrated within the broader energy system and its role in enhancing the system’s ability to manage variability and optimize resource deployment.

Fig.4.14b illustrates the system-use index for the wind-only scenario. The figure presents various combinations of storage and curtailment, along with their corresponding system-use index values. As depicted in the figure, the system-use index initially increases with both storage and curtailment until it reaches its peak value, and then it starts to decline. The storage and curtailment combination that leads to the top plateau region of the system-use index represents the optimal values that effectively maximize the overall system performance. Due to the ability of the system to also play some role of seasonal storage at such a high penetration, focus on the top peak point may be less relevant than the overall plateau region. Thus, depending on the generation size, several storage and curtailment combinations can benefit the system. For example, the maximum system-use index value (selected for ease of identification)

occurs at 7.5 GWh storage capacity and 27% curtailment at RE-to-load ratio of 1.4. Referring back to Fig.4.9a, this storage and curtailment combination enables achieving a penetration of 90%. However, this combination is associated with excessive dumping of renewable energy generation. The storage utilization achieved in this scenario is somewhat reasonable but still falls short of the optimal value. Fortunately, one can opt for optimal storage and curtailment, considering their unique goals and policy priorities while maintaining a reasonable system-use index.

Fig. 4.15a illustrates the storage utilization for the 50-50 wind-solar scenario. Like in the wind-only scenario, the highest storage utilization index is observed at relatively lower storage capacity values. However, the storage utilization is significantly higher than that of the wind-only scenario.

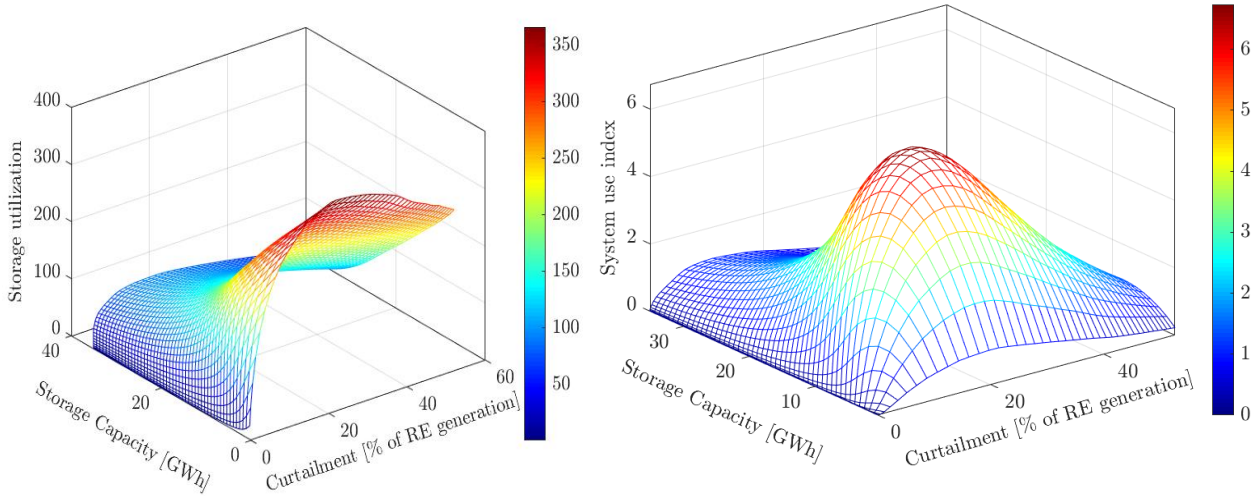

a b

Fig. 4.15. System performance indicators: a) Storage utilisation, b) System-use index for 50-50 wind-solar scenario at 6 hours of storage

The storage utilization gradually decreases as the storage capacity increases. At a given smaller storage value, the utilization index rises from zero to maximum as the generation size and curtailment increase. As depicted in the figure (Fig. 4.15a), a small curtailment rise significantly increases storage utilization index. However, with a further increase in curtailment, the storage utilization index increment slows down.

Fig. 4.15b presents the system-use index for the 50-50 wind-solar scenario. This scenario's SUI is significantly higher than the wind-only scenario. The SUI shows an increasing trend as both storage capacity and curtailment increase until it reaches its peak value (typically forms a hill with several comparable peak values), after which it starts to decline. The maximum SUI value occurs at 8.9 GWh and 16% of storage capacity and curtailment, respectively. Referring to Fig. 4.10a, this combination results in a penetration of 90% of renewables. In this scenario, storage utilization has seen a remarkable increase compared to the wind-only scenario. The maximum SUI is also achieved at a lower generation capacity (RE-to-load ratio of 1.10) compared to the wind-only scenario of 1.40. It is worth noting how complementarity enhances system performance by increasing storage utilization. Overall, it is worth noting that the graph in these figures builds a hill with a plateau top, showing several combinations with almost equal system benefits as shown in the contour plot Fig. 4.16.

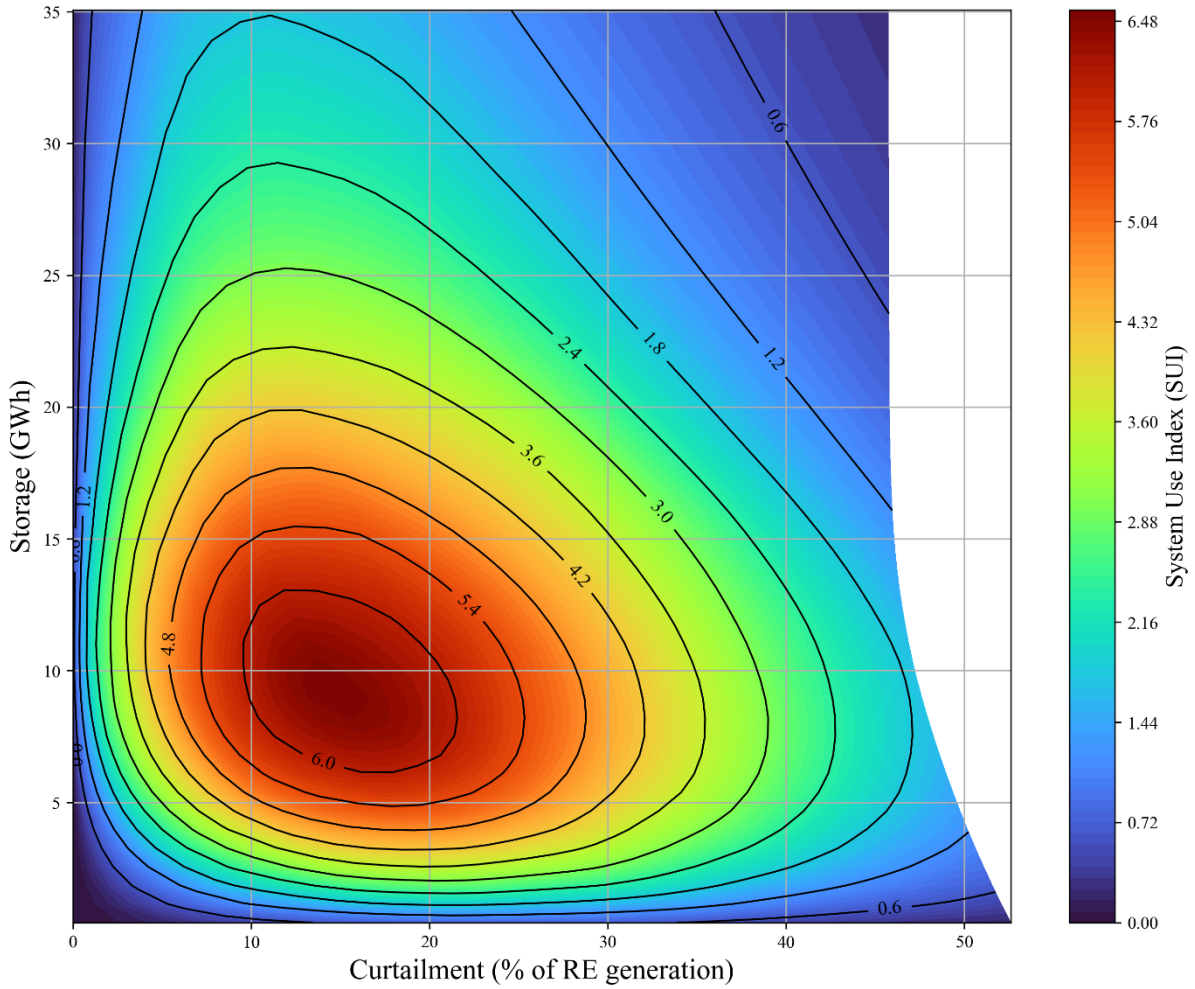

Fig. 4.16. Contour plot of the System Use Index (SUI) across a range of storage capacities and curtailment levels for 50-50 PV–wind Scenario

Based on these results, we can conclude that well-utilized storage capacity of approximately 0.2 of average daily demand, coupled with a reasonable curtailment of 16%, can effectively achieve a penetration target of 90%.

Fig. 4.17a illustrates storage utilization for solar-only scenarios where both storage utilization and curtailment increase with renewable generation at a fixed storage capacity, indicating that curtailment plays a crucial role in enhancing storage utilization.

The solar-only scenario exhibits highly efficient storage utilization, as the figure depicts. This efficiency can be attributed to the predictable day-night cycle of solar radiation, which provides a consistent pattern for charging and discharging the storage on a daily basis. As shown in Fig. 4.17a at very small storage sizes, the storage utilization is maximum because the storage fully charges and discharges almost every day, but the utilization decreases with an increase in storage size. Compared with the previous two scenarios, the solar-only scenario demonstrates a significantly higher energy contribution from storage. As illustrated in Fig. 4.17b, the SUI increases as curtailment and storage increase. However, once a peak point is reached, the SUI starts to decline with further increase in storage. This decline occurs because the storage becomes oversized, resulting in distorted daily charging and discharging patterns, and the storage remains full for several days.

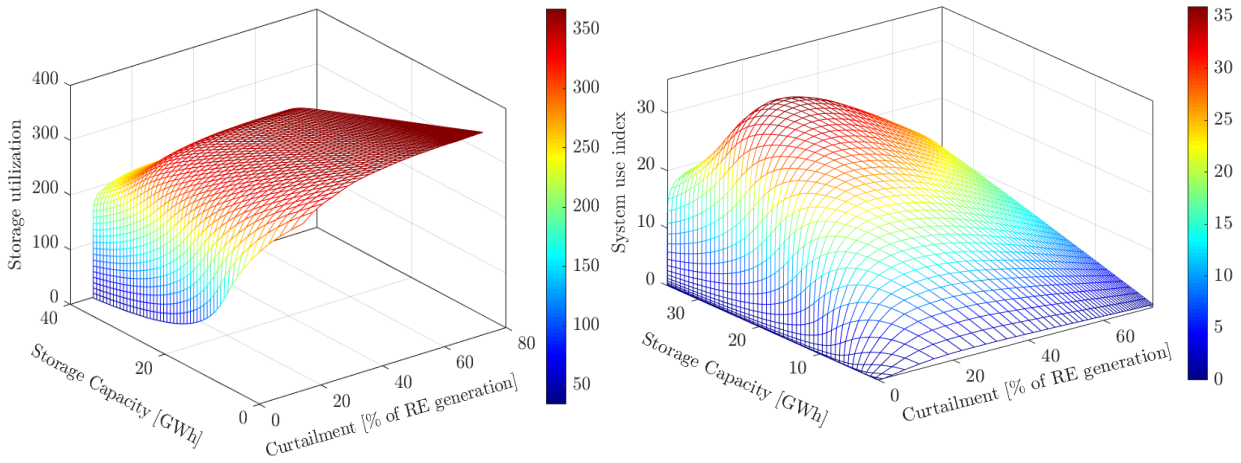

a b

Fig. 4.17. System performance indicators: a) Storage utilisation, b) System-use index for solar-only scenario at 6 hours of storage

Nevertheless, as depicted in the figure (Fig. 4. 17), a combination of reasonable curtailment and storage size can significantly benefit the system with a sufficiently high SUI. In this specific scenario, multiple combinations of storage and curtailment positioned on the plateau of the system-use index graph show a high storage utilization value. For instance, at 22 GWh and 13% curtailment, very high storage utilization can be attained while achieving a 90% renewable penetration. It is important to note that the solar-only scenario necessitates a larger storage capacity than the other two scenarios to achieve the same penetration level.

The above result discusses the case 6 hour of storage, the data for other hours present an interesting case regarding the effect of the energy-to-power ratio (storage duration) on system performance. The observed SUI value increases (discussed in reference to the peak plateau region of each plot) when we increase hours of storage from 1h to 6h showing that hours of storage value impacts system role of the storage. Beyond 6h, SUI gradually decreases. The small decrease may be because the high storage hours (like 10 h) allow the system some seasonal role in combination with curtailment. Fig. 4.18 presents SUI values for 2h, 6h and 10h storage for 50-50 PV-wind scenario. It is clear that SUI is an arbitrary index, but it carries an irreplaceable role in raising our understanding of the future system. In short, the relationship between these parameters, namely curtailment, penetration, wind-solar mix, storage capacity, and hours of storage, and its link to SUI indicates that an optimal range of these parameters that ensures an optimal system efficiency exists, which directly addresses the core objective of the thesis. This forms a multidimensional constraint that is difficult to implement in any technoeconomic modelling tool. This may explain why some techno-economically optimal scenario results were found to have low net energy production capability (Solomon et al., 2024).

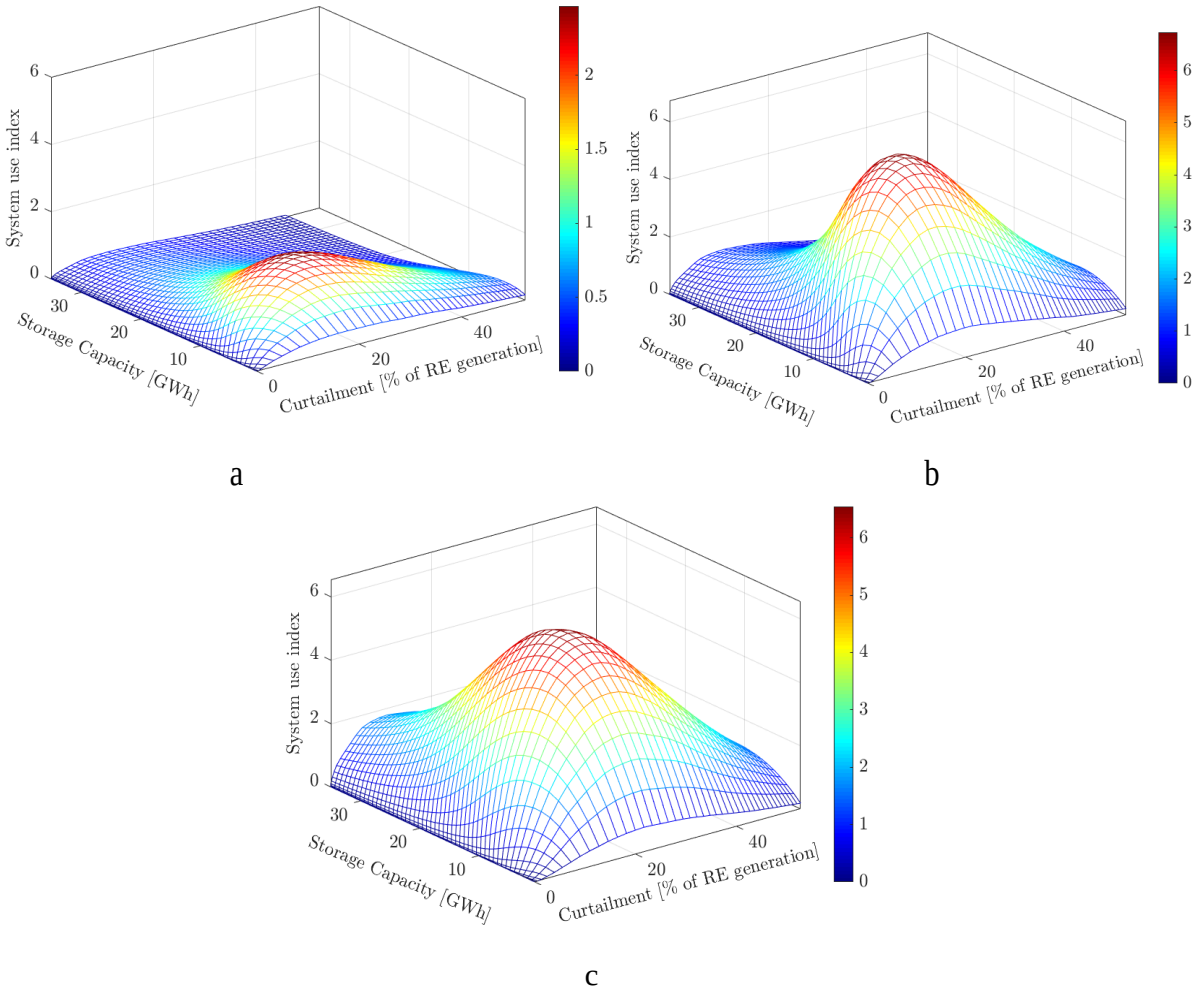

Fig. 4.18. System–use index for different storage durations: a) 2 hours, b) 6 hours, c) 10 hours

The overall results indicate that simulating large quantities of data across various scenarios enables me to identify the optimal combination of storage size, RE capacity, and curtailment tailored to a specific resource mix and diversity. The interesting lesson of this study is that the optimality of future systems can be compromised if careful designing is not followed during system development. The possibility of overcoming the impact of poor system design by achieving optimal system operation can even be limited in some cases of system designs, exposing the industry to losses. In other words, this study excels by showing that, despite numerous system design and modelling options, considering certain physical requirements such as system-use index (proxy of system efficiency) sets the boundary conditions from which economic models should choose. However, enforcing such requirements in the present modelling is not possible because such constraints are naturally multidimensional.

Fig. 4.19 illustrates the impact of diurnal storage on penetration and storage utilization for a system with a RE-to-load ratio of 1 across three scenarios. In all cases, penetration increases sharply at lower storage levels. However, it gradually slows and stabilizes beyond a certain threshold, typically 7.5 GWh for wind only, 10 GWh for 50-50 PV-wind, and 25 GWh for solar-only scenarios. Beyond this point, additional storage yields minimal gains, as small increases in penetration demand disproportionately require large diurnal storage. The rate at

which penetration increases with storage varies significantly across the scenarios. Adding storage initially cuts curtailment, but further capacity has little effect, as storage often stays full, causing excess generation to be curtailed and reducing overall utilization.

In the solar-only scenario, the diurnal cycle restricts penetration, necessitating significant storage to match supply with demand. Conversely, the wind-only case requires only a small storage capacity of 7 GWh (0.16 of average demand) to address the temporal mismatch, thanks to the smoother output from various locations. In the 50-50 PV-wind mix, penetration is realized through a combination of storage and curtailment. This finding is consistent with a study conducted on larger geographical scales in the U.S. (Shaner et al., 2018), where reanalysis datasets (MERRA-2) with a RE-to-load ratio of 1 were applied. The penetration achieved without storage, 48% and 78% for solar and wind-only scenarios, respectively, aligns with our findings.

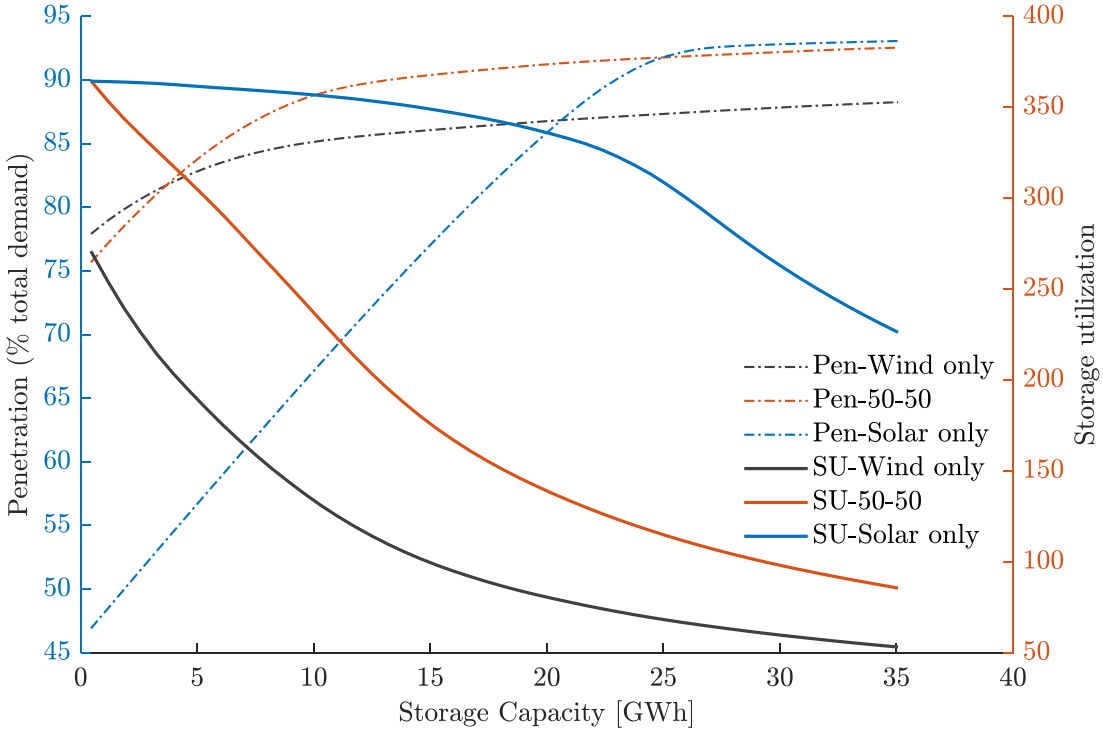

Fig. 4.19. Impact of storage on penetration and storage utilization across different scenarios for a system with a RE-to-load ratio of 1.0

While the rate varies across scenarios, the initial few GWh of storage capacity leads to a rapid increase in penetration, which then slows with further expansion. For instance, as shown in Fig. 4.19, in the 50-50 PV-wind scenario with a RE-to-load ratio of 1.0, approximately 33% of the installed 35 GWh storage capacity is effectively utilized to achieve 90% penetration. However, adding storage beyond this has minimal impact, contributing only a marginal increase in penetration. The wind-only scenario shares characteristics similar to the 50-50 PV-wind scenario. The solar-only scenario, however, exhibits a distinct pattern; it utilizes about 71% of the installed storage effectively with a storage utilization index exceeding 300 cycles per year.

The parameters discussed so far, storage, penetration, curtailment, and storage utilization, interact in complex ways and offer valuable insights into system performance. However, these metrics alone may not reflect the full system dynamics. For example, a high storage utilization

index might indicate frequent cycling, but if the storage size is small, its actual contribution to improving system outcomes, such as boosting renewable penetration, can be minimal. Thus, high utilization does not always translate to greater system benefit.

The SUI shown in Fig. 4.15b provides an in-depth system performance assessment by connecting storage utilization and RE consumption with other factors. SUI increases with storage and curtailment, reaching a peak before declining as both parameters continue to rise, clearly identifying the near-optimal system parameters that enhance overall system performance. In the 50-50 PV-wind scenario, the highest SUI, representing the most efficient utilization of storage and curtailment trade-offs, is achieved at a storage of 8.9 GWh (0.2 average demand) and a curtailment of 16%. Notably, this aligns well with the observed suitable range in Fig. 4.19, reinforcing the validity of the SUI as a meaningful metric. While it is not inherently guaranteed that the maximum SUI corresponds to an optimal system configuration, its alignment with Fig. 4.19 suggests that it effectively identifies near-optimal operating conditions. This connection strengthens the argument that the SUI is a reliable indicator for balancing storage capacity and curtailment in large-scale renewable integration, depending on priorities set, whether curtailment or storage is emphasized to achieve specific penetration targets. The near-optimal system parameters required to achieve 90% renewable penetration were derived from the newly introduced approaches, as summarized in Table 7. The peak demand is 2.7 GW.

Table 7. Optimal parameters that maximize system benefits at 90% RE penetration level

Scenario	Penetration (% annual demand)	RE generation (GW)	Storage (GWh)	Balancing capacity (GW)	Curtailment (% RE generation)	PV (GW)	Wind (GW)
Solar only	90	9.9	22	2.46	13	9.9	0
50 - 50 wind-solar	90	6.5	8.9	2.16	16	3.25	3.25
Wind only	90	6.1	7.5	2.19	27	0	6.1

In the final remarks, when only diurnal storage is deployed, based on my newly developed methodological approach, it is evident that a well-balanced system design can be attained by integrating various system parameters, as outlined in Table 7. For instance, in the case of a 50-50 system configuration with an 8.9 GWh storage capacity, the system needs to generate 6500 MW to achieve a penetration target of 90%. This allocation necessitates 3250 MW for wind energy, which translates to approximately 950 wind turbines, and another 3250 MW for solar photovoltaic (PV) energy, requiring approximately 81 km² of land. Conversely, when we distribute this PV generation across 1 million households, constituting residential PV systems, each home would receive an allocation of 3.25 kW of PV capacity, which is a reasonable amount for individual households. Likewise, a storage capacity of 8.9 GWh for 1 million households implies 8.9 kWh battery per household, a practical and reasonable house battery size.

When focusing on PV, the results highlight promising opportunities for both utility-scale solar farms and distributed residential PV+ battery systems. Meeting 45% of the demand (45% PV penetration), which is half of the total 90% target shown in Table 7 above, would require approximately 81 km² of land for utility-scale deployment. This could be expensive and compete with other valuable land uses, such as agriculture or economic activities. This challenge underscores the importance of exploring residential PV as an alternative pathway.

Distributing the required capacity across households not only reduces land-use pressure but also enhances energy self-sufficiency at the community level. Accordingly, Section 4.2 investigates strategies to maximize the share of residential PV in achieving the overall renewable energy penetration target.

4.1.3.3. Seasonal storage application for seasonal mismatch

Revisiting Fig. 4.13, renewable energy utilization changes significantly with increasing penetration levels. At lower penetration levels, renewables primarily displace conventional generators with minimal or without storage or grid readjustments. The figure illustrates how renewable energy requirements vary across different penetration levels for various PV-wind mixes. It highlights key characteristics of these variables beyond the no-dump capacity, the threshold beyond which the system necessitates storage, curtailment, or both. While this no-dump capacity varies depending on the PV-wind mix, the minimum penetration achievable without storage or curtailment is approximately 23.6%, a condition observed in the solar-only scenario where Fig.4.13 begins. Any increase in renewable generation beyond this level requires storage/curtailment or both to manage fluctuations, enabling penetration up to 80%. Beyond 80% penetration, renewable deployment rises sharply, even with only a slight increase in penetration. While the RE requirement for a given penetration target varies across PV-wind mixes, this variation remains relatively minor until 80% penetration. However, beyond this point, the differences in RE requirements become more significant.

Up to 80% RE penetration, diurnal storage plays a key role in balancing short-term fluctuations. However, meeting the last 20% of the demand presents a unique challenge. Fig.4.13 illustrates this challenge; RE deployment surges dramatically in this range, with a substantial increase in capacity required for even a small rise in penetration. This large generation/capacity requirement is attributed mainly to seasonal and peak demand imbalances, meaning that much of the additional renewable capacity remains underutilized for most of the year and is only effective during specific seasons of peak demand or low RE generation periods, or a combination of both. This challenge becomes even more demanding when attempting to meet the demand with PV, as it requires an impractically large generation capacity and extensive storage. The marginal returns from such capacity expansion are minimal. As shown in Fig. 4.13, complementarity helps mitigate the steep rise in capacity additions required for higher penetration levels. However, regardless of the PV-wind mix, meeting the final 20% of the demand necessitates a substantial increase in capacity and/or significant storage deployment, as also illustrated in Fig. 4.19.

Diurnal storage manages short-term fluctuations and facilitates a high renewable penetration of 80–90%, but its limitations become evident beyond this range. The ability of diurnal storage to handle daily fluctuations depends on the mix ratio and other factors. Still, longer-duration mismatches spanning multiple days to weeks necessitate the deployment of seasonal storage. Numerous studies indicate that achieving very high VRE penetration requires longer-duration storage beyond diurnal storage (Frazier et al., 2021; Shaner et al., 2018; Solomon et al., 2019). Though not yet widely deployed, seasonal storage solutions such as hydrogen and other fuels are recognized as key technologies that could help future grids achieve nearly 100% renewable penetration. Implementing seasonal storage enhances power system stability by reducing seasonal intermittency and significantly lowering curtailment, thereby maximizing renewable energy utilization.

Various conditions were examined for different configurations by adjusting the energy and power capacity of the diurnal storage to assess the impact of seasonal storage. Near-optimal parameters obtained from Figs. 4.19 and 4.15b were the upper limit for diurnal storage, after

which seasonal storage was introduced. Fig. 4.20 illustrates the penetration levels achieved when seasonal storage, along with diurnal storage with a 6-hour duration, is applied across the three scenarios analysed at a RE-to-load ratio of 1.3. Diurnal storage is used for lower penetration levels (< 80%). In comparison, seasonal storage is utilized at higher penetration levels, reaching approximately 100% and 98% at 180 GWh (equivalent to 4 average daily demand) for the 50-50 and wind-only scenarios, respectively. In contrast, the solar-only scenario requires a larger storage capacity to achieve the same penetration level. In this scenario, increasing diurnal storage from 0.16 to 0.5 average daily demand (Fig. 4.20b) enables 100% penetration at significantly reduced seasonal storage, unlike Fig. 4.20a, where 100% penetration is not achieved even at the maximum seasonal storage size. This pattern is also demonstrated in Fig. 4.19, where efficient storage utilization is observed across a wide range of diurnal storage capacities. Regardless of the PV-wind mix, seasonal storage plays a crucial role in enabling higher renewable penetration by mitigating seasonal mismatches.

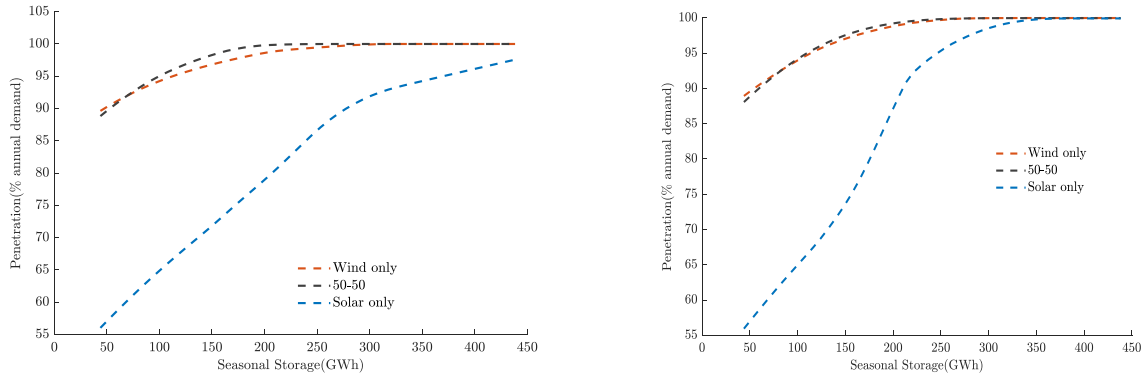

Fig. 4.20. RE penetration using seasonal storage combined with diurnal storage of capacities: a) 0.16, b) 0.5 times the average daily demand

Since seasonal storage is mainly used during periods of low generation, peak demand, or both, its utilization is expected to be limited to a few days each year. However, analysing the SU and SUI, the new indices introduced in this study (refer to section 4.1.3.2) offer valuable insights into how effectively the allocated storage is used, ensuring it is not underutilized.

Fig. 4.21 presents how the storage is utilized in the 50-50 scenario, demonstrating various combinations of storage and curtailment that maximize its utilization. For instance, achieving 100% renewable penetration requires 180 GWh of hydrogen storage, with storage utilization of 20 full days with minimal curtailment of approximately 7%. However, as storage capacity decreases, utilization improves. While storage utilization provides critical insights into how deployed storage is utilized, it does not capture the complete system dynamics, as it is limited to storage parameters without integrating broader system variables. To address this limitation, the SUI discussed in Section 4.1.3.2 and illustrated in Fig. 4.22 offers a more comprehensive measure by integrating all key design parameters, such as annual discharge, energy to pawer ratio, total storage capacity, and net renewable energy generation and consumption, into a single metric that captures system dynamics and performance within the context of broader energy infrastructure considerations.

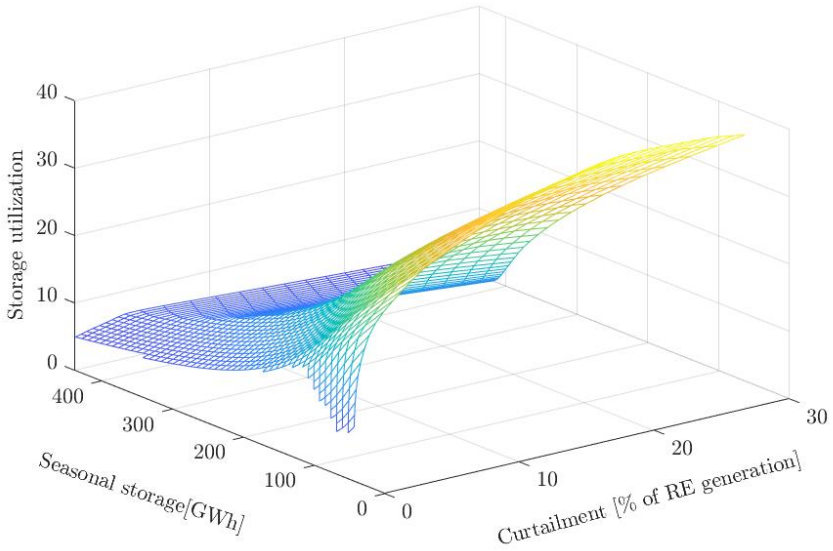

Fig. 4.21. Seasonal storage utilization for 50-50 scenario, diurnal storage 0.16 average daily demand with 6 hours duration

As shown in Fig. 4.22, SUI initially increases with storage and curtailment but declines beyond a certain threshold. The optimal combination lies within the plateau, where various storage and curtailment pairs contribute to an efficient balance. For example, in the 50-50 PV-wind scenario, a storage capacity of 67% GWh, combined with a curtailment level of 10%, falls within this plateau and enables a renewable penetration of approximately 95%. In the wind-only scenario, a similar storage capacity with slightly higher curtailment achieves around 94% penetration. The results indicate that the optimal SUI varies slightly between scenarios: the wind-only scenario benefits more from curtailment, whereas the 50-50 PV-wind scenario favours increased storage, as the 50% solar share benefits more from energy retention.

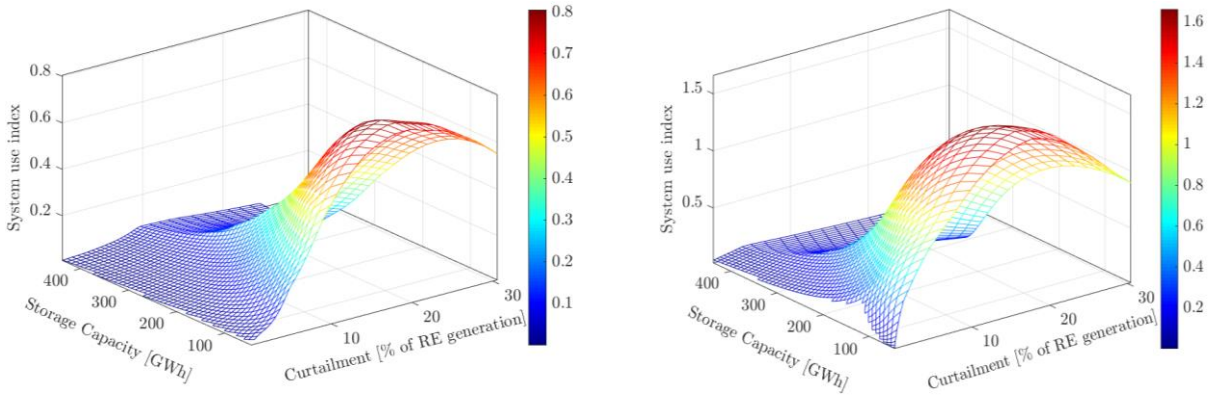

a b

Fig. 4.22. System use index: a) wind only, b) 50-50 scenario

SUI behaves differently in the solar-only scenario (Fig.4.23). Unlike the wind-only and 50-50 scenarios, the index in the solar-only case continues to increase with both storage and curtailment. The (near) optimal balance is reached at approximately 200 GWh of storage with 15% curtailment. Regardless of the generation mix, increasing seasonal storage beyond 250 GWh yields minimal additional benefits. Similarly, curtailment is advantageous at lower storage sizes, but its benefits decrease beyond a certain threshold, which varies depending on storage size.

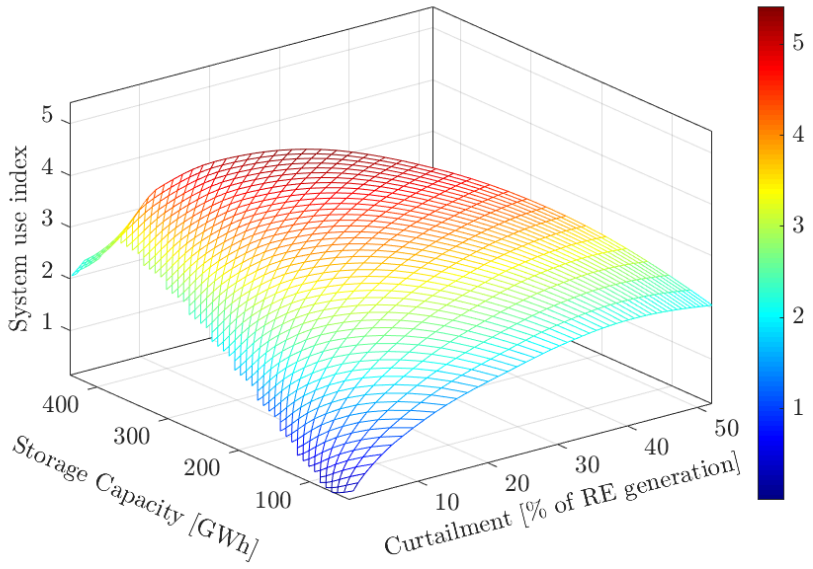

Fig. 4.23. System-use index for solar-only scenario

The impact of diurnal storage on seasonal storage requirements is then examined by changing the hours of diurnal storage to 1 hour. Short storage hours are well-suited for short-term, high-intensity power delivery with short but high renewable generation peaks. With a 1-hour duration, penetration slightly improves but demands more seasonal storage and balancing capacity. The near-optimal system parameters identified using the SUI and the maximum penetration achieved are presented in Table 8. The abbreviations for penetration (Pen), Curtailment (Cur), and Seasonal Storage (S.S.) are used only in this table to include them efficiently.

Table 8. Near-optimum system parameters for the three scenarios

Scenario	Diurnal storage 1hr duration				Diurnal storage 6 hr duration			
	Pen (%)	Cur (%)	S.S (av. daily demand)	Max. Pen (%)	Pen (%)	Cur (%)	S.S. (av. daily demand	Max. Pen
Solar only	83	13.6	4.9	99	80	14.5	4.7	99
50-50	93	11.3	2.3	100	92.5	13	2.2	100
Wind only	92.2	17	2.1	100	91	18	1.9	100

In the solar-only scenario, diurnal storage of 0.16 average daily demand with 1-hour duration reaches 63% penetration with significant curtailment. This configuration requires a slightly larger seasonal storage capacity of approximately 10 average daily demand to raise the penetration to 98%. In contrast, for the same diurnal storage, the 50-50 PV-wind scenario achieves 80% penetration with negligible curtailment, requiring considerably lower seasonal storage (5 average daily demand) to achieve a 100% RE penetration. A moderate increase in diurnal storage to 0.5 average daily demand with a 6-hour duration requires lower seasonal storage to reach near-optimal level. A trade-off relationship exists between increasing the diurnal storage and the seasonal storage requirement.

4.1.4. Dispatchable balancing requirements

In the preceding discussions, we demonstrated that all levels of renewables can be matched with PV–wind mix at reasonable diurnal and seasonal storage and curtailment levels.

Integrating such a large scale of renewables necessitates a form of conventional balancing capacity to address shortfalls in both renewables and storage to ensure a reliable supply of demand. Quantifying the required magnitude of this capacity mandates a comprehensive study of year-round hourly generation and demand profiles. Such analysis is crucial to determine the need for a conventional generator capable of balancing even in worst-case scenarios such as periods of high demand and low renewable output.

Fig. 4.24 illustrates the interplay between curtailment and balancing capacity requirements for different diurnal storage sizes in wind-only, 50-50 PV-wind, and solar-only scenarios, respectively. The unit of storage used in the figure is a fraction of the average daily demand. With varying degrees, the balancing requirement is observed to decrease as curtailment increases across all scenarios. Furthermore, the reduction in balancing requirement becomes more significant with an increase in storage capacities. Therefore, controlled curtailment has a significant advantage for system performance improvement by increasing penetration and decreasing conventional back-up requirements.

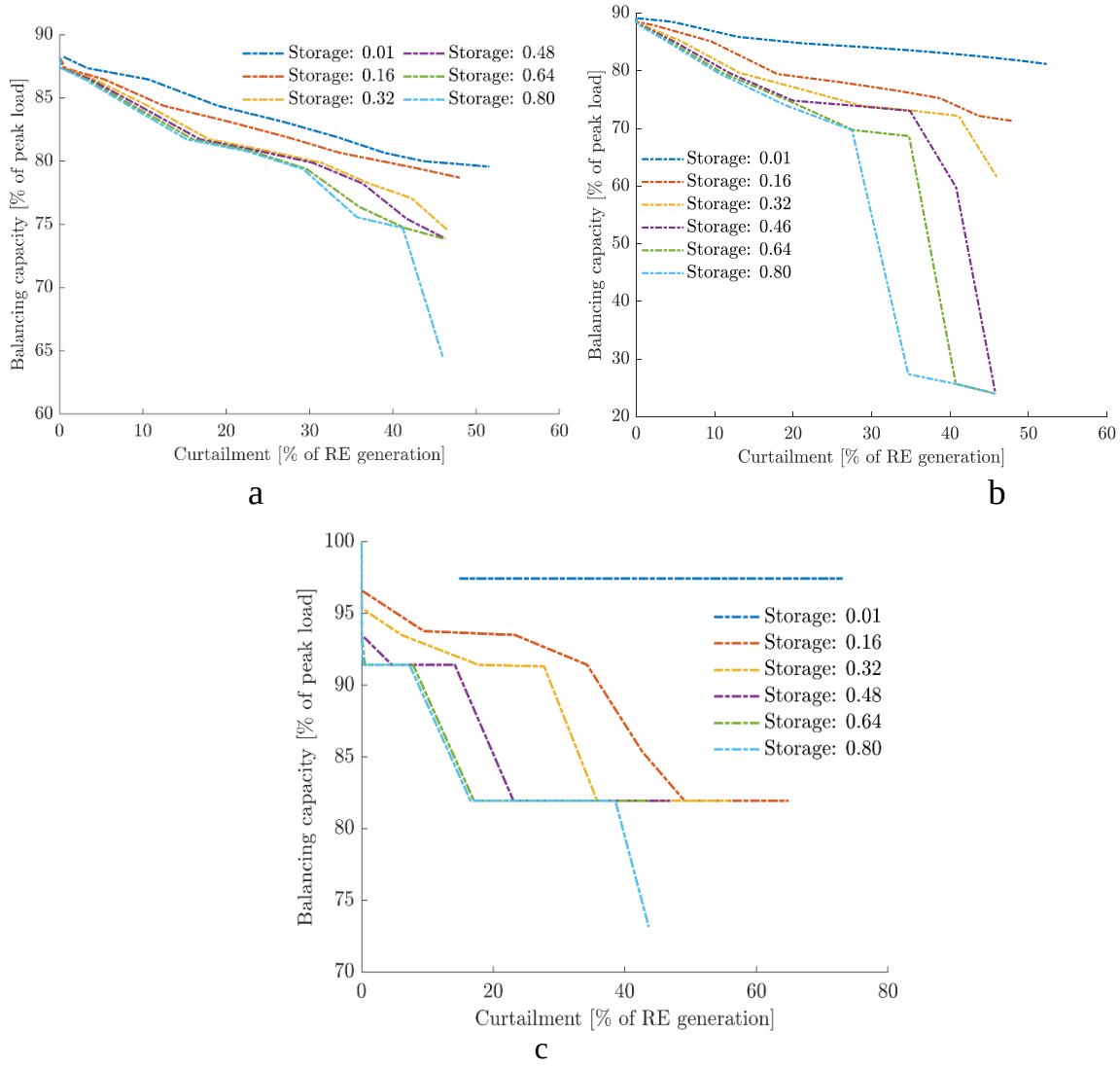

Fig. 4.24. The interaction between balancing capacity and curtailment: a) Wind-only scenario, b) 50-50 wind-solar scenario, (c) Solar-only scenario

Comparing the three scenarios, the 50-50 PV–wind scenario performs better in reducing balancing requirements by leveraging the advantage of resource complementarity. However, at very low curtailment levels, the wind-only scenario requires less balancing capacity compared to the other two scenarios. The reduction in balancing requirements occurs more rapidly in the 50-50 PV-wind scenario, while the solar-only scenario exhibits the highest balancing demand. This is due to the diurnal cycle of solar generation and the lack of storage dispatch optimization.

As illustrated in the Fig. 24, the balancing requirement exhibits a high magnitude, representing the maximum theoretical capacity needed. This is attributed to the fact that the model did not adhere to any storage dispatch strategy. The employed storage model in this study does not follow a structured dispatch strategy; rather, instead it is based on a use-as-available approach, which results in higher balancing needs when facing challenging weather conditions. This is particularly evident when consecutive cloudy days collide with a lack of wind. However, a flexible storage dispatch strategy is expected to reduce the need for higher balancing capacity substantially.

Fig. 4.25 shows the contribution of all system input variables, including balancing (back-up) generators and curtailed energy, over the first week of January (50-50 PV–wind scenario, with a 1.1 RE-to-load ratio and storage capacity equal to 0.41 times the average daily demand).

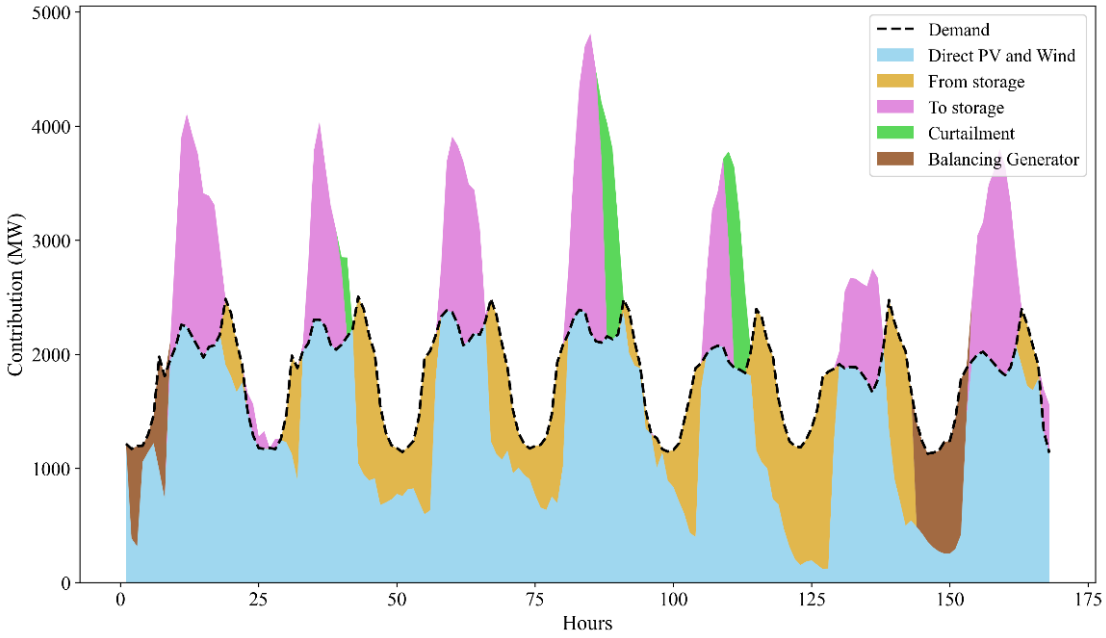

Fig. 4.25. Contribution of all deployed technologies in meeting the demand

Balancing generators account for a significant portion of the system's capacity yet contribute only a small fraction to the demand, as illustrated in Fig. 4.25. Consequently, their capacity factors are low, leading to higher costs than the system’s average cost, as these generators must recover their expenses with limited generation. Therefore, generators in this role should have lower capital costs, regardless of operating expenses, to enhance their economic viability for such tasks. Depending on the amount of penetration and system mix, overcoming such challenges are possible by coupling its dispatch with flexible storage operation, which could further reduce balancing capacity need and increase its capacity factor while also maintaining

reliable power output, even at critical time of scarcity, via implementation of forecasting and postponing stored energy use for such critical time.

Fig. 4.26 illustrates the balancing capacity required under varying storage and curtailment levels for the 50-50 PV–wind scenario, where seasonal storage is deployed alongside diurnal storage. Let's examine the different conditions by applying seasonal storage of a maximum of 10 average daily demands. At all storage levels, curtailment lowers balancing capacity. For example, with seasonal storage equal to 5 average daily demand and RE-to-load ratio of 1, a balancing capacity of 79 % is required with 2.1% curtailment. The highest balancing need occurred on May 21 at 8 PM, when demand was at its peak, solar was absent, and wind was minimal. Raising the RE-to-load ratio to 1.2 reduces balancing capacity to 74%, shifting the peak to the morning of December 6, but at the expense of increased curtailment. Increasing the generation to 1.4 RE-to-load ratio, balancing capacity drops to 28% (December 6, 7 AM), achieving 99.7% penetration.

At a RE-to-load ratio of 1.2, 100% penetration is achieved, without balancing capacity when seasonal storage of about 8 average daily demands is deployed. At this generation and storage size, no balancing is required for mixes of 0.3 to 0.8 PV ratio. However, outside this range, significant balancing capacity is required, especially in wind-only and solar-only scenarios, even with generation and storage are at their maximum values of 1.4 and 10, respectively.

In the wind-only scenario, when renewable generation is set to 1.2 times the load and storage capacity is equivalent to 8 average daily demand, the system requires approximately 77.5% balancing capacity at 10% curtailment, achieving 99.1% penetration. Under the same renewable generation and storage conditions, the solar-only scenario requires around 85% balancing capacity.

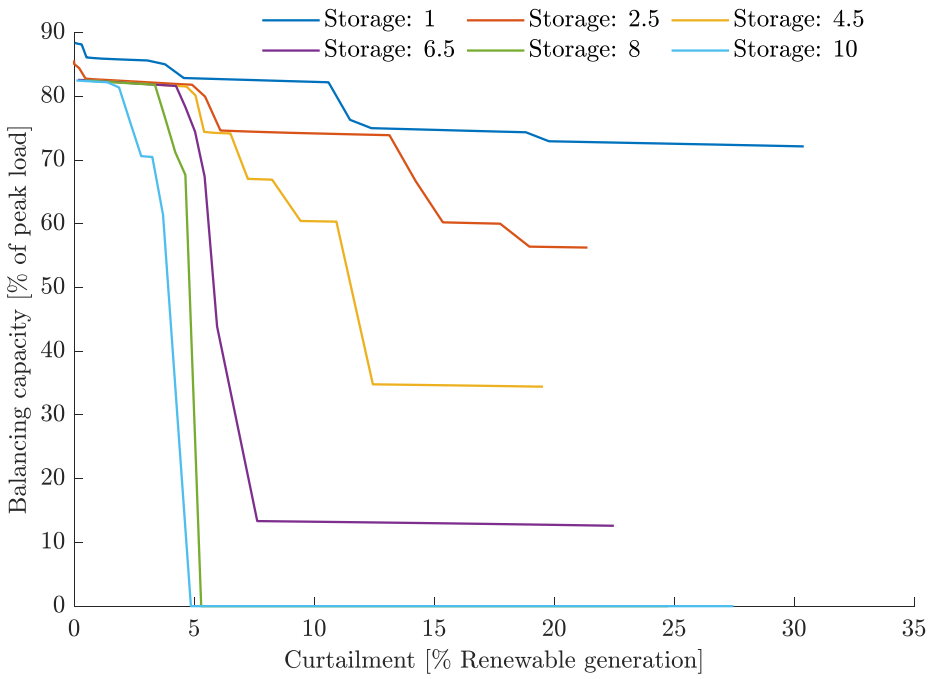

Fig. 4.26. Impact of storage and curtailment combinations on reducing balancing requirements

The unit of storage in the figures is a fraction of the average daily demand. In all evaluated scenarios, except the wind-only case with zero solar share, night-time hours present the biggest challenge for meeting demand, even with seasonal storage. In the wind-only scenario, some hours also see significant unmet demand due to the high variability of wind generation, causing mismatches with peak demand in some seasons.

The matching capability of load and generation profiles and resource diversity greatly influences the reduction in balancing requirements. Despite limited control over VRE generation, power operators can reduce balancing capacity needs by partially managing VRE output in response to demand fluctuations. Effective storage dispatch and management further enhance this capability, as a more controlled and gradual discharge strategy – rather than rapidly depleting storage – helps distribute stored energy evenly over time, reducing reliance on balancing capacity during peak periods. This approach not only improves operational efficiency and renewable penetration but also yields economic benefits by minimizing the need for large-scale balancing capacity, which is often required only on a few critical days each year. Although more detailed and flexible storage dispatch strategies and an expanded set of simulations/optimisation are required to accurately determine balancing capacity requirements, the methodological approach developed in this study provides valuable insights into how balancing needs depend on storage, curtailment, and resource mix. These findings underscore the importance of careful future system design to avoid risks to society while optimizing system reliability and cost-effectiveness.

The preceding analysis demonstrated that the synergy between PV and wind through complementarity is pivotal in achieving higher renewable penetration, reducing reliance on conventional backup resources, minimizing storage needs, and smoothing generation profiles to better match demand. Consequently, the system becomes more efficient in utilizing renewable resources and optimizing their contribution to the overall energy mix. Therefore, designing an efficient grid with large-scale renewables requires optimizing the combination of all the above-discussed parameters.

From an international outlook, the consistency of my findings with those from diverse studies, conducted using various approaches and across different geographical locations, suggests that similar underlying physical mechanisms govern the matching of supply and demand. This calls for developing a unified framework that can be applied across various contexts. For example, research on large-scale renewable energy integration in regions like Europe (Gils et al., 2017), North America (Denholm et al., 2022; Guerra et al., 2021) and Israel (Solomon et al., 2019b) has revealed comparable challenges in balancing supply and demand, further supporting the need for a common strategy to optimize storage, curtailment, and resource mix. Specifically, Solomon et al. (2019b) showed that storage capacities below the average daily electricity demand, together with roughly 20% curtailment, can enable around 90% annual renewable penetration, beyond which seasonal storage becomes necessary. Their conclusions are derived using a linear-optimization-based LUT energy system transition framework applied to the Israeli grid. Although this modelling approach differs from the custom methodology developed in the present study, both analyses share important contextual features – most notably similar climatic conditions and the characteristics of an isolated grid system. These parallels make the insights from Solomon et al. particularly relevant for supporting and strengthening the objectives and findings of the current work. In relation to this, the newly proposed system-use index offers more profound insights into the effectiveness of storage integration within the

broader energy infrastructure, enhancing the system's capacity to manage variability and optimize resource utilization. Therefore, these studies' findings are highly relevant, as they can be a foundation for a common theoretical framework to address shared challenges in energy transition studies. It is also important to note that despite the overall similarity in trends and mechanisms that govern the interaction of various parameters, there is also a location-dependent difference that can affect system efficiency in a different way. Thus, expanded efforts that produce more of such data, using improved methodology and unified/standardized parameters, could lead to a unified framework while also clarifying the effect of locational dependent system differences.

Furthermore, the approach applied in this thesis yielded relevant outcomes that align with other studies that follow different approaches, for example, the one for U.S. (Shaner et al., 2018), that utilized a reanalysis dataset at a renewable-to-load ratio of 1, reported penetration levels of 48% for solar-only and 78% for wind-only scenarios without storage, closely reflecting the outcomes observed in my analysis. A related study for Switzerland (Dujardin et al., 2017), which employed hydropower as a storage solution, found that PV-dominated mixes (with a PV ratio above 0.6) require greater storage capacity to balance the system, consistent with my findings.

The Eritrean context offers distinct advantages due to its unique resource potential and resource complementarity. Considering the available resources, this study proposes a strategic expansion plan for various levels of renewable integration. The results indicate that wind and wind-dominated mixes with small diurnal storage are more effective at penetration levels below 60% ignoring the potential cost of high uncertainty, while solar-dominated mixes become more favourable at penetration levels above 60%. However, the current national action plan prioritizes the expansion of solar farms, aiming for a short-term renewable penetration of up to 23% and beyond. In this context, Eritrea needs decision-making that is tailored to its specific conditions, ensuring that renewable energy expansion aligns with its unique resources, challenges, and development priorities.

Limitations

This study explored the intricate relationships between key system design parameters using a novel methodological approach specifically designed for this purpose. The proposed empirical relationship effectively maps multiple pathways that enhance system performance across varying penetration, storage, and curtailment levels. However, using these various (multiple) options as boundaries, further optimization using advanced optimization tools could help in estimating the optimal range of various techno-economic parameters under different conditions. Furthermore, although the preliminary economic analysis conducted aligns well with the model's recommended best results, a more detailed economic analysis is recommended to mitigate any unfavourable scenarios and determine the most cost-effective system configuration that meets the techno-economic requirements. Additionally, some parameters, such as balancing (back-up) capacity, can be further optimized if an advanced and flexible storage dispatch strategy is followed.

The idealized assumptions, such as the copper plate (no transmission constraints) and fully flexible balancing generators, were intentionally adopted to simplify the system boundaries and isolate the core technical interactions among key design parameters. While incorporating transmission constraints and generator flexibility limits would indeed enhance the robustness

and realism of the findings, such additions would also substantially increase model complexity and computational requirements. Furthermore, integrating demand-side measures could provide additional system flexibility and improve the overall efficiency of renewable integration; however, this aspect lies beyond the current study's scope. With these limitations, the methodological approach introduced in this study demonstrated its ability to identify multiple options that significantly improve the performance of future renewable-dominated grids.

4.2. Evaluating the potential of residential PV integration

In this subsection, the contribution of residential PV to overall renewable integration is quantified by evaluating its share in meeting national electricity demand under varying feed-in limits. The analysis further explores how integrating battery storage can enhance the effective utilization of residential PV by mitigating excess generation and reducing curtailment. Particular attention is given to the interaction between storage capacity, injection limits, penetration levels, curtailment, and storage utilization, highlighting the role of residential PV as a complementary component within a large-scale renewable system.

4.2.1. Effect of feed-in limit on annual PV generation

Fig. 4.27 illustrates the annual PV generation and corresponding losses as the feed-in limit varies. The annual generated power increases with the feed-in limit, peaking when all generated energy is directly injected into the grid at a limit of 0.8 kW/kWp and above.

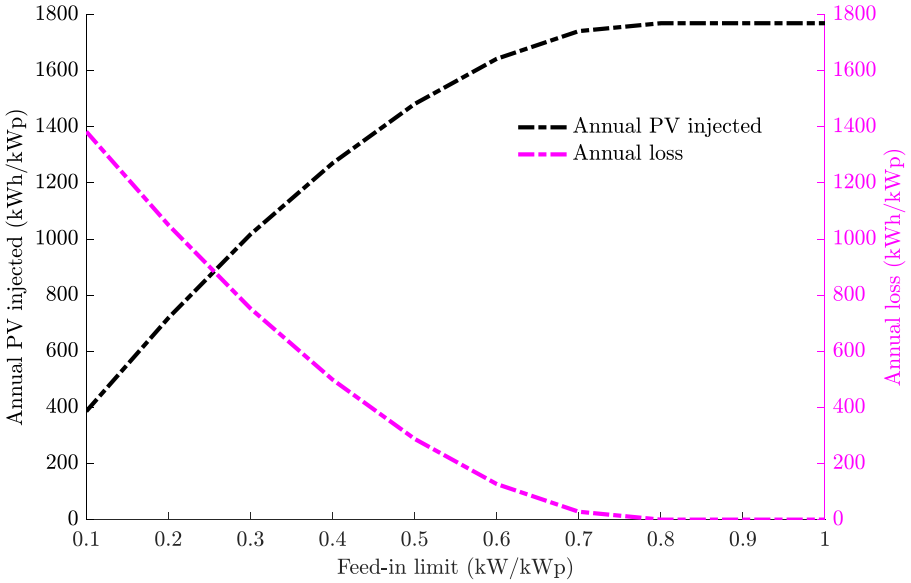

Fig. 4.27. Annual average energy generation and energy loss for varying feed-in limit for 1 kWp PV system

Allowing a high feed-in limit increases penetration and decreases losses; however, it can lead to an excess of generation over consumption in the local network, resulting in reverse power flow with severe consequences for the distribution network. To fix this issue, a feed-in limit should be imposed on the injected PV to ensure compliance with the requirements of the local network. By allowing a feed-in limit of above 0.8 kW/kWp, the system virtually experiences no energy loss. However, if we impose a feed-in limit of 0.1 kW/kWp, approximately 1400

kWh/kWp (77%) of the generated energy is lost. However, this represents the maximum loss that could occur if all residential PV systems were installed at optimal tilt and azimuth angles. In practice, this is unlikely, as the increasing adoption of residential PV will lead to panels being installed at various orientations different from the optimal angle, which could impact total generation and consequently the losses.

As shown in the figure, a feed-in limit above 0.7 kW/kWp demonstrates a negligible impact. This is because the AC output is approximately 86% even at peak generation due to assumed losses. Moreover, the solar irradiation profile rarely reaches its peak, diminishing the benefits of larger inverter capacity. Conversely, implementing a lower feed-in limit inevitably increases the curtailment of useful energy, underscoring the need for storage solutions to capture and utilize the surplus energy effectively. This highlights the trade-off between maximizing usage and adhering to grid requirements across different feed-in limits.

4.2.2. PV-battery deployment with feed-in limit constraint

Fig. 4.28 shows the penetration as a percentage of the total consumption. The penetration is computed for specific PV sizes and the corresponding feed-in limits, as a function of battery size. The base case scenario (PV capacity of 100MWp) shows a constant penetration rate regardless of the storage size, as shown in Fig. 4.28. This ensures seamless integration of all generated energy into the grid without storage or curtailment. As shown in the figure, at lower PV capacities, the increase in penetration with storage is marginal because all generated electricity is directly injected into the local network, making the battery ineffective. However, for larger PV capacities, penetration is seen to increase with increase in storage size. This is expected, as more PV is deployed, the feed-in limit is decreased to keep the LV grid safe, resulting in a significant amount of generated energy being stored for night injection that leads to higher penetration.

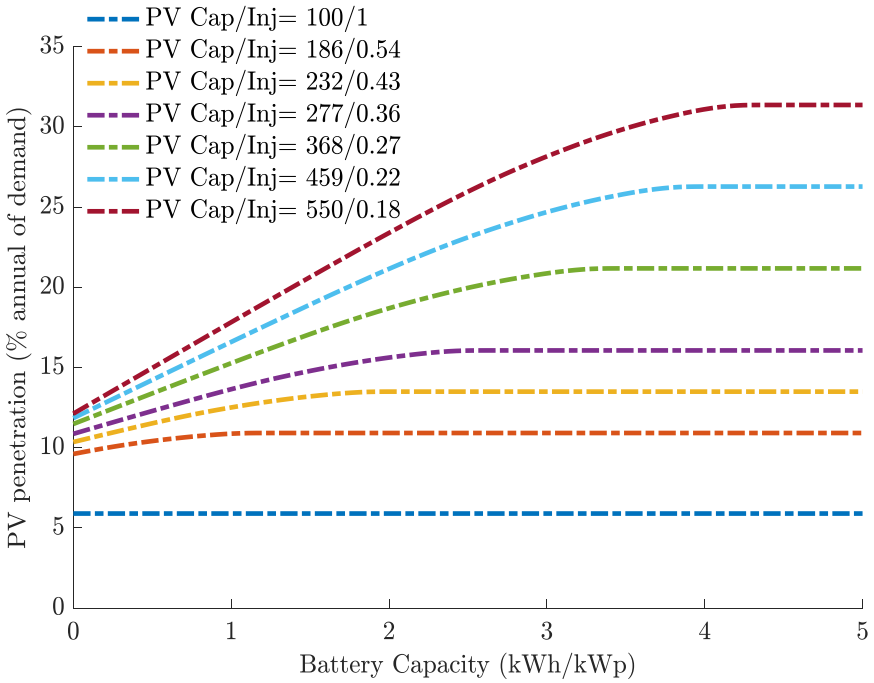

Fig. 4.28. PV penetration, as a function of battery capacity for different PV/battery feed-in limits

The increase in penetration reaches a threshold where the effect of battery storage becomes insignificant, indicating a limit beyond which storage has a diminishing effect. When PV capacity exceeds 300 MWp, adding battery storage significantly increases penetration. As the feed-in limit decreases with increase in PV capacity, storage becomes necessary to avoid wasting excess energy. For example, at 550 MWp, increasing battery capacity from 0 to 4.5 kWh/kWp boosts penetration by 20%. Thus, for larger PV capacities with small feed-in limits, larger batteries could further significantly improve penetration. However, for PV capacities below 232 MWp, increasing battery size from 0 to 4.5 kWh/kWp marginally raises penetration by less than 3.4%.

The analysis shows that residential PV can supply around 32% of annual electricity demand, a remarkable contribution achieved without competing for scarce arable land, unlike ground-mounted utility-scale PV farms. By utilizing rooftops, residential PV not only preserves valuable land for agriculture but also lays the groundwork for broader renewable energy adoption. In fact, integrating residential PV supports and enables the expansion of large-scale PV by reducing land-use conflicts, diversifying generation sites, and improving public acceptance. Moreover, when combined with approximately 120 MWp of wind capacity, the penetration level increases to about 46% of annual demand. This synergy demonstrates how distributed rooftop PV, alongside wind power, can accelerate and facilitate the integration of large-scale solar PV into the grid while ensuring sustainable land use.

Fig. 4.29 illustrates the characteristics of curtailment as a function of battery storage; curtailment decreases as battery capacity increases. However, with rising PV capacity, curtailment also increases due to the imposed feed-in limits which results in excess energy being rejected from the grid. At the maximum PV capacity of 550 MWp, curtailment reaches up to 43%, dropping to 0% when a 4 kWh/kWp battery storage is installed (with wind 120 MWp is added in the HV network as enabler). This demonstrates the significant advantage of deploying storage in large-scale PV systems. Without storage, curtailment remains below 12% for PV capacities up to 232 MWp, such a curtailment is acceptable if contributes to increased use of renewable. Incorporating 2 kWh/kWp (464 MWh) battery storage at this level reduces curtailment from 12% to 0 and increases penetration from 24.6% to 27.8%. Technically, to achieve the total penetration 27.8% or to rise the penetration by 3.2% compared to the reference penetration at 232MWp without storage, there are two options:

1) increase PV installed capacity to 277 MWp (45MWp+232MWp) along with marginal battery storage of 1 kWh/kWp (277 MWh), albeit at the cost of increased curtailment of around 10% or
2) incorporate 2 kWh/kWp (464 MWh) of battery storage for the 232MWp, to eliminate curtailment. Other options could also be possible.

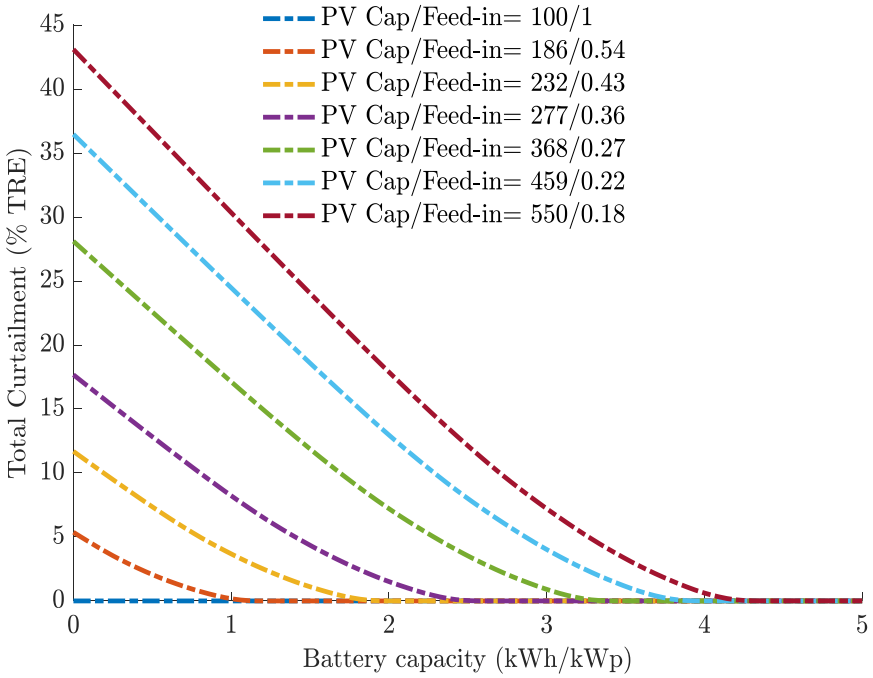

Fig. 4.29. Total curtailment as a function of battery capacity for different PV/feed-in limits

In quantitative terms, option one requires an additional 45 MWp, along with 277 MWh of battery storage, compared to option two's requirement for 187 MWh (187 MWh + 277 MWh) of battery storage. Based on current market trends (Table 5), adding 45 MWp of PV costs $39.42 million, making it more cost-effective than adding 187 MWh of battery storage, which costs $60.2 million. The increased cost of batteries in relation to the PV system is associated with a shorter battery life span. It is noted that we are comparing incremental costs, not total system costs.

The first option, though accompanied by some curtailment, is technically and economically viable. Therefore, for specific capacities of PV installations, curtailment may be preferable over storage from both economic and technical standpoints. Curtailment has recently emerged as a cost-effective tool for enhancing renewable utilization, especially when combined with optimal storage (Perez et al., 2019; Solomon et al., 2016). Additionally, demand-side management, electric vehicles, and space heating practices can help utilize a portion of the curtailed energy to enhance cost-effectiveness.

Although this thesis is designed to offer a technical perspective, the results highlight the need for a thorough economic assessment to avoid unfavourable scenarios. It has been concluded that careful technical and economic assessments are necessary, as surplus generation (curtailment) may outweigh storage benefits. The optimal design should balance storage and curtailment.

Based on the above discussion, the next section will look for the best system configuration that maximizes the overall performance.

4.2.3. Enhancing system performance through strategic parameter tuning

In this setup, an ideal feed-in limit for each PV capacity and its corresponding battery size is identified using simulation methods to maximize penetration and minimize losses. At this ideal

limit, almost all energy rejected from the grid due to feed-in constraints is stored in the battery for night-time use. Consequently, battery storage below 2 kWh/kWp is found sufficient enough to maximize the overall system performance when fitted with this ideal feed-in limit. This configuration supports up to 550 MWp of PV capacity without power curtailment during night time battery injection. In this section, the hosting capacity is slightly increased to align with the anticipated near-future grid expansion and reinforcement measures in Eritrea, and to accommodate the increased integration of residential and utility-scale PV plants over time. All simulations are based on the energy balance of aggregated solar and wind with aggregated demand

Fig. 4.30 shows penetration as a function of feed-in limits. Based on the simulation results shown in the figure, Table 9 presents the ideal combination of parameters to achieve the balance. Technically, if the network has a hosting capacity of 150 MW, installing a PV capacity below 232 MWp with marginal battery storage of less than 0.58 kWh/kWp at a feed-in limit of 0.65 kW/kWp is safe for the local network. For constant PV capacity, increasing the hosting capacity of the network may eliminate the need for storage.

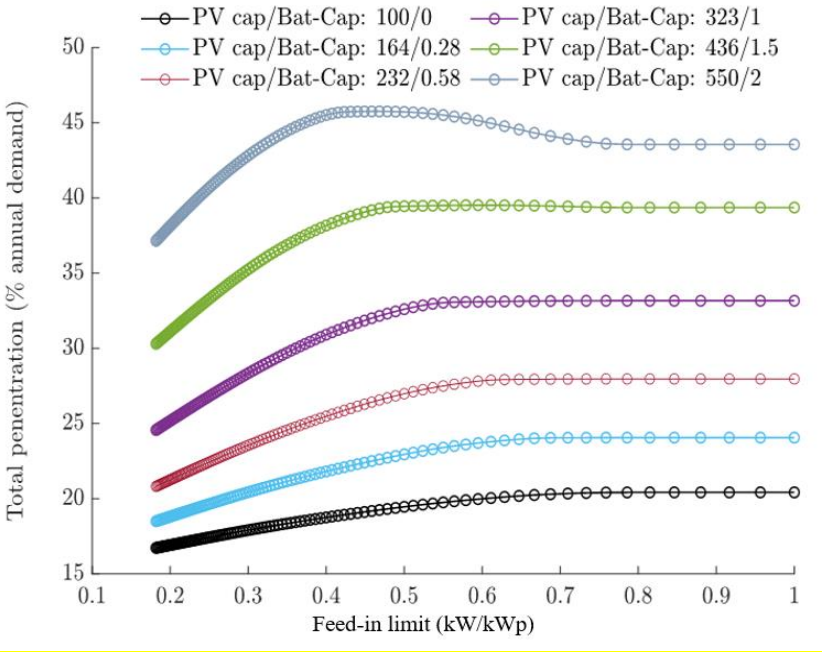

Fig. 4.30. Penetration as function of Feed-in limit for different pairs of PV capacity and battery sizes

Table 9. Ideal value of system variables that maximize the performance of the setup

System variables	PV capacity (MWp)					
	100	163	232	322	436	550
Hosting capacity (MW)	87	130	150	193	231	237
Feed-in limit (kW/kWp)	0.87	0.73	0.65	0.6	0.53	0.43
Battery (kWh/kWp)	0	0.28	0.58	1	1.5	2
Penetration (%)	20	24	28	33	40	46
Curtailment (%)	0	0	0	0	0	0.11

Additionally, Fig. 4.30 shows the impact of the feed-in limit on penetration for various PV-battery storage combinations. The figure illustrates that with larger PV capacity, there is an

initial rise in penetration as the feed-in limit increases; however, this upward trend gradually decelerates and eventually reverses with further increments in the feed-in limit. For PV capacities of above 323MWp, the penetration is shown to decrease after reaching their peak values at around 0.48-0.6 kW/kWp. The feed-in limit, which corresponds to the point of maximum penetration, is the threshold that avoids curtailment. The maximum penetration, equating approximately 46%, is achieved at a feed-in limit of 0.43 kW/kWp, with negligible curtailment. Beyond this threshold, directly injected energy increases, while energy to storage and penetration decreases. The decline in penetration is attributed to increased wind curtailment when more PV is directly injected into the local grid at higher feed-in limits during the day. This creates a scenario with excess generation during the day, where the energy intended for storage at low feed-in limits is instead directly injected into the grid, ultimately resulting in wind curtailment.

As illustrated in the Fig. 4.30, for PV capacities below 323 MWp, penetration rises until reaching a particular feed-in limit, which varies depending on PV capacity. Beyond this threshold, increasing the feed-in limit does not increase the penetration; instead, it remains constant. The threshold feed-in limit is the point at which all rejected energy is stored in the storage system without any curtailment. Further increase in the feed-in limit results in more energy being directly injected into the grid, leaving less excess energy to partially fill the storage. At higher feed-in limits, even if all the generated PV energy is directly injected into the grid, it never surpasses consumption, resulting in no curtailment and constant penetration. The key observation highlights the vital link between battery storage and PV capacity, stressing the need for proportional deployment to maximize renewable energy utilization at an ideal feed-in limit.

In the context of renewable energy integration, the paramount concern lies in efficiently optimizing resources to maximize utilization and minimize losses. Figs. 4.28 and 4.29 underscore this challenge, revealing that achieving a penetration of 37% demands a curtailment of roughly 18% of the useful generated energy, necessitating a battery storage capacity of around 2 kWh/kWp. The excessive curtailment is due to the predetermined feed-in limit that constrains the system to reach an optimum point. In contrast, Figs. 4.30 and 4.31 present a notable improvement, showcasing a significant reduction in curtailment to negligible levels. This is because the ideal feed-in limit for a specific PV/battery capacity is identified by simulating feed-in limit over a wide range of possible values. In this scenario, where PV capacity was below 232 MWp, significant curtailment is observed at lower feed-in limits, but gradually diminishes as the feed-in limit increases and eventually disappears. This curtailment is entirely linked to PV generation and is a result of the imposed feed-in limit. However, for larger PV capacities exceeding 323 MWp, the system is shown to experience a loss from both PV and wind. At specific feed-in limits, both PV and wind curtailment reached their minimum levels, and during the same interval, the share of total renewable energy consumed is also at its maximum.

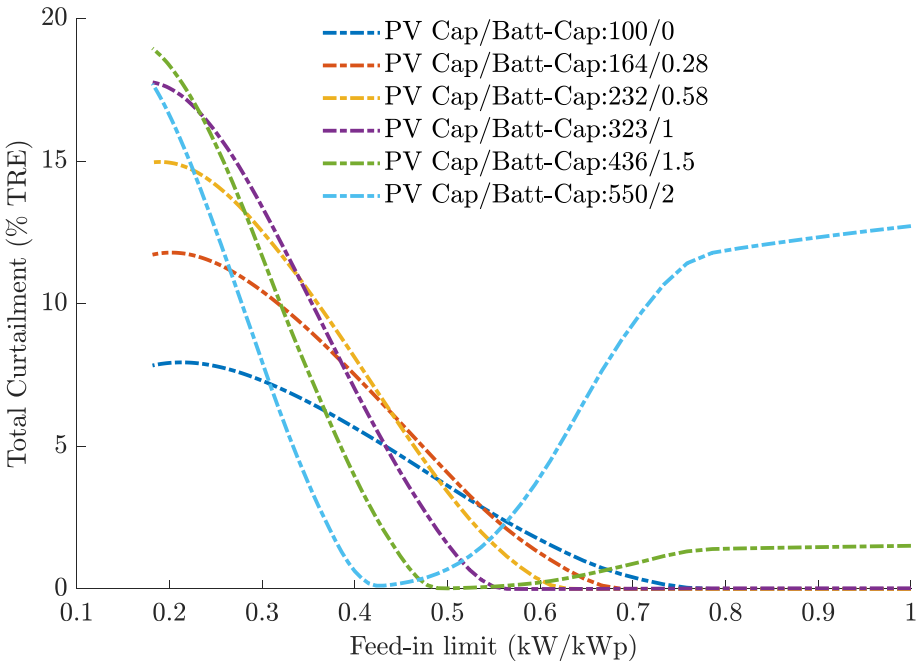

Fig. 4.31. Curtailment as a function of feed-in limit for different PV capacities and battery sizes

The system parameter curtailment as a function of feed-in limit and battery storage is shown in Fig. 4.32. This figure illustrates how total curtailment varies with both storage and feed-in limits. Curtailment is considerable at both low and high feed-in limits, as indicated by the double peak and grooved section of the 3D curve. The two peaks are related to PV and wind curtailment, respectively. However, at specific combinations of storage and feed-in limits, the energy loss suddenly decreased to its minimum point. Evidently, this minimum curtailment point aligns with the point of maximum penetration, as illustrated in Fig. 4.30.

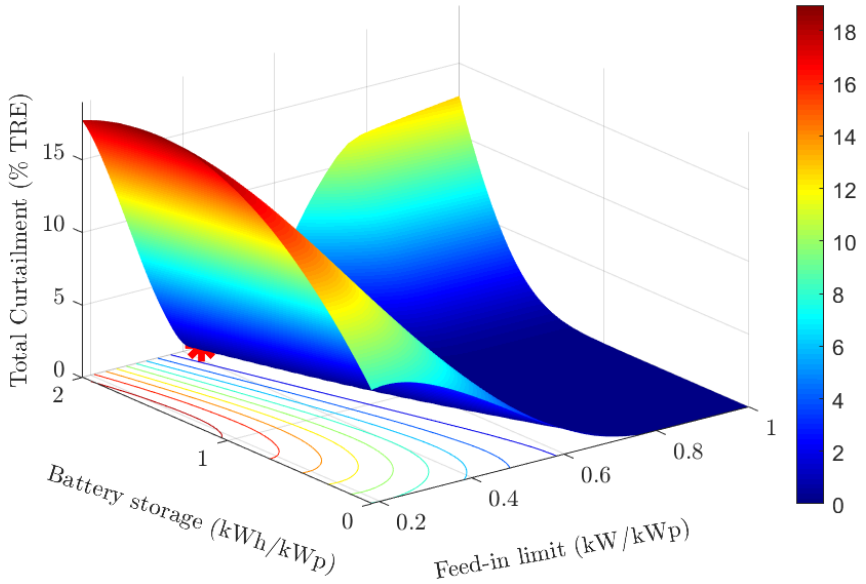

Fig. 4.32. Curtailment as a function of battery storage and feed-in limit

The best configuration of the system should maximize renewable utilization by minimizing losses. This involves ensuring that all system variables, such as PV capacity, storage capacity, wind capacity, and feed-in limit, fall within a reasonable range. Therefore, feed-in limits ranging from 0.35 to 0.55 kW/kWp, coupled with 2 kWh/kWp of battery storage, emerge as the most suitable combination for minimizing curtailment and maximizing penetration. The red asterisk in Fig. 4.32 marks the point of maximum penetration and minimum curtailment.

To place my results in a broader context, I compared them with international experiences. Studies from Belgium (Flanders) (Meuris et al., 2019). and Germany (Zeh and Witzmann, 2014) show that feed-in limits –70% and 60% of installed capacity, respectively – are used to protect low-voltage networks. These examples highlight how controlled feed-in can ease distribution-level constraints. Unlike these cases from well-developed grids, my work focuses on renewable integration in a developing-country setting and proposes grid management and expansion options suited to such conditions. This comparison helps situate my findings within the wider landscape of renewable integration challenges and solutions

To wrap up, the contribution of residential PV to the energy mix is increasing with the growing adoption of roof-mounted residential PV systems, driven by the continuous decline in the cost of home battery storage and PV components. Contributing to around 32% of the penetration, residential PV can significantly reduce households' carbon footprint, as households that were once energy consumers have recently become energy producers. The contribution of residential is expected to rise considerably with the continuous evolution of the conventional grid, allowing for the consumption of residential PV at the local network, unlike conventional ones. However, it is worth noting that with increasing distributed generation (residential PV), a proper quality is compromised if proper measures are not taken.

4.2.4. Power quality issues in grid-connected PV systems

To support and validate the theoretical framework, an experimental analysis was conducted at one of the PV installations on the Szent István Campus, whose size and capacity closely align with the system specifications recommended in this dissertation. The various power quality indicators were measured at different time scales, from the minimum 200 milliseconds (ms) to 2-hour (h) intervals. In this study, special emphasis is placed on selected parameters – active power output, current total harmonic distortion (ThdI), voltage total harmonic distortion (ThdV), and voltage deviation – measured at 3-second intervals to examine the impact of the temporal variability of weather conditions on PV power output and its quality.

Fig. 4.33 presents the active power output normalized to its peak capacity of 3.3 kW. The figure shows a gradual increase in power output from morning until noon, followed by a decline in the afternoon, and remains zero in the night hours. The maximum PV output recorded was approximately 0.72 kW/kWp, corresponding to the normalized peak capacity (P/P_{rated}). This shows that there are a few hours in the year when power generation is above 0.72 kW/kWp and this offers insignificant benefit to the system in increasing the aggregate annual generation. This aligns closely with the findings in subsection 4.2.1, which indicate that applying a feed-in limit above 0.7 kW/kWp yields negligible gains in annual energy generation.

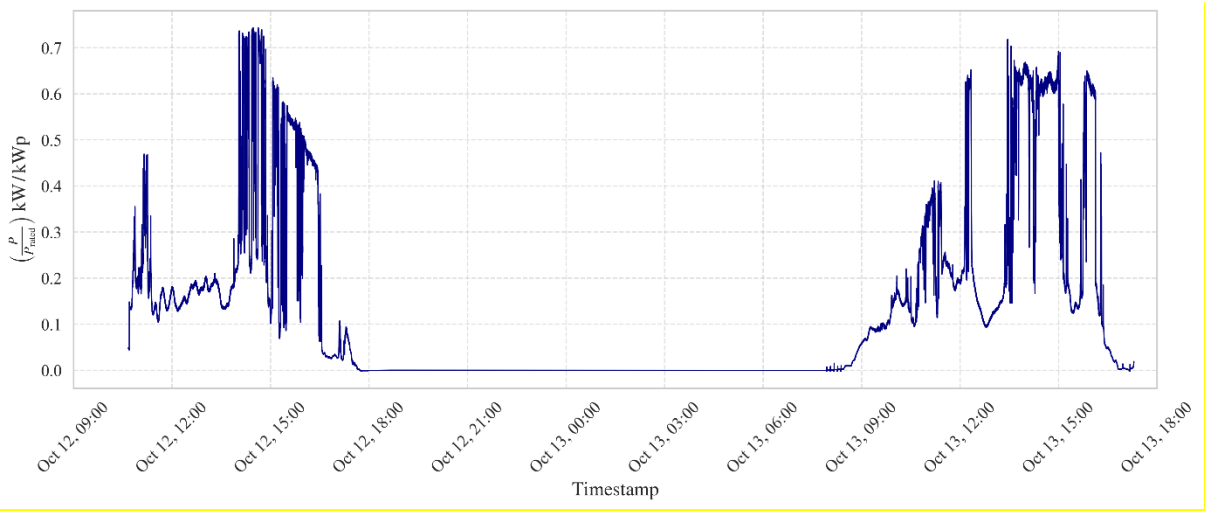

Fig. 3.33. The active PV power output as normalized to its peak capacity 3.3 kWp

The current waveform is more sensitive to irradiation than the voltage waveform. Fig. 3.34 shows the current (blue line) and voltage waveform at sunny and cloudy hours. Under sunny conditions, the phase difference is essentially zero; however, as shown in the figure, during cloudy conditions, a small phase deviation can appear due to rapid irradiance fluctuations and inverter control response (note the reference offset between V and I).

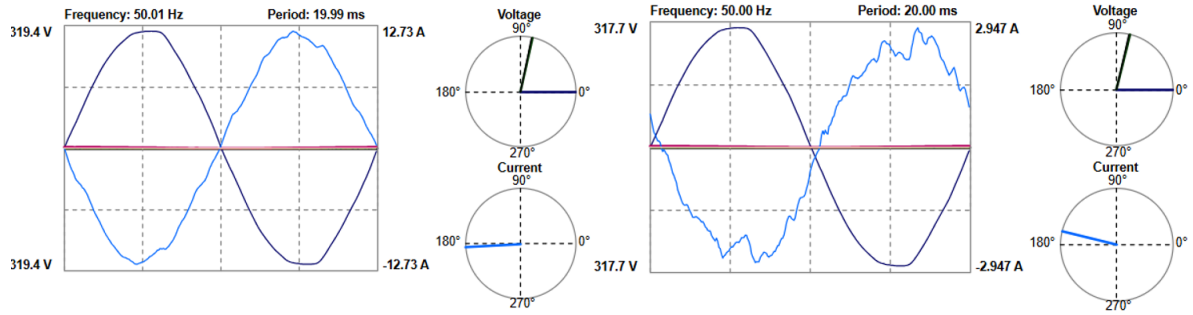

a) sunny conditions b) cloudy conditions

Fig. 3.34. Voltage and current waveform distortion at different operating conditions

To investigate the total harmonic characteristics of the PV inverter at various operating conditions of power generation, the generated power relative to its rated capacity (P/P_{rated}) is categorized into three regions: lightly loaded inverter (0-0.3), medium loaded inverter (0.31- 0.5), and heavily loaded inverter (0.51-0.74). The analysis shows that the current total harmonic distortion (ThdI) is high at low power generation conditions but decays with increasing power generation. At a low generation level, the MPPT and power factor control of the system are deactivated, but the control system is activated at higher generation conditions. At such higher operating conditions, the measurements indicate that current THD (ThdI) remains mostly within the optimum standard range of < 5%, which will be discussed further in subsequent paragraphs. The current harmonic distortion exhibits a strong correlation with inverter loading; however, the data provides limited evidence on how voltage harmonic distortion is affected by inverter loading. This is primarily because voltage total harmonic distortion is influenced not only by the inverter switching frequency but also by external factors such as grid impedance and the presence of non-linear loads. Consequently, the two major power quality indicators (ThdI and ThdV) show limited mutual correlation, as their behaviour depends on multiple underlying factors. Nevertheless, quantifying their influence on voltage

deviation (V_Dev) is crucial for understanding the origin of voltage deviation, which has significant implications for system balance and grid stability. The analysis reveals that while ThdI shows no meaningful correlation with V_Dev, there is a clear positive correlation exists between ThdV and V_Dev. Fig. 3.35 illustrates the variation of ThdV and V_Dev under different inverter operating conditions, along with their corresponding regression trends.

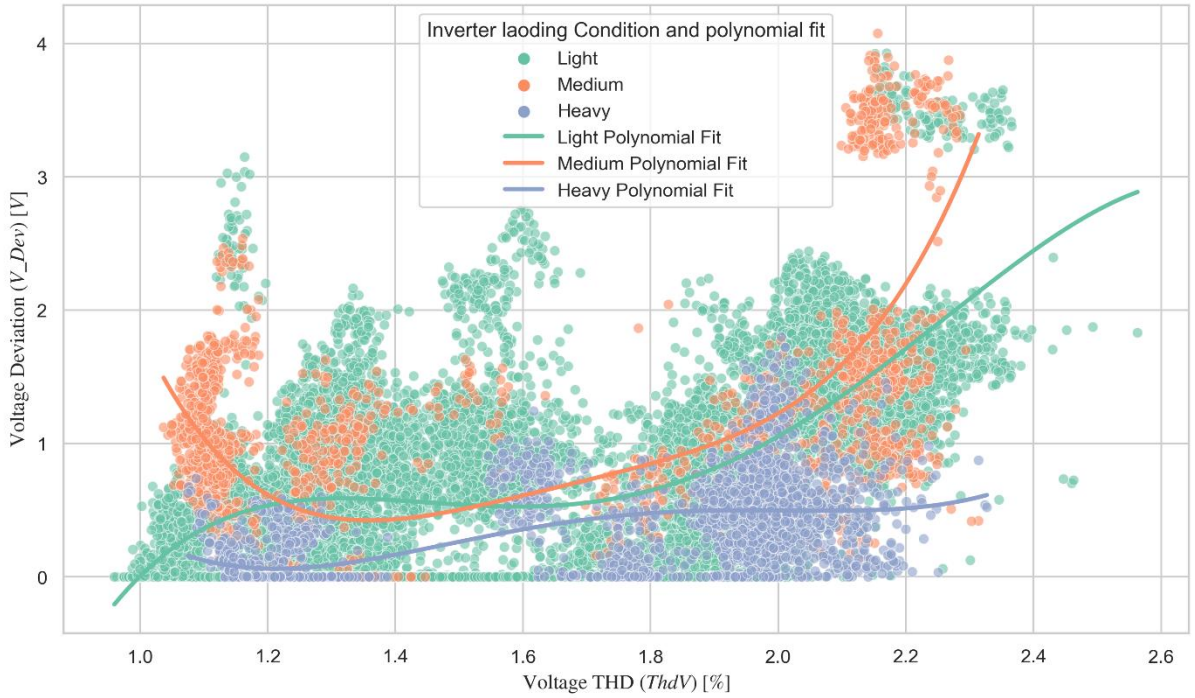

Fig. 3.35. The correlation and regression trend of ThdV and V_Dev under various loading conditions

The measurements show that the correlation between ThdV and V_Dev varies significantly with inverter loading conditions. The Pearson correlation coefficient between the two power quality indicators is 0.553 for the lightly loaded inverter, 0.495 for medium medium-loaded inverter, and 0.582 for the heavily loaded inverter.

As shown in the scatter plot and fitted polynomial curves, the relationship between ThdV and V_Dev is nonlinear. A fourth-order polynomial regression curve was identified as the most suitable model to capture the relationship between ThdV and V_Dev across the observed load conditions. These regression trends predict about 41% of the voltage deviation with some variation based on inverter loading conditions. This suggested that voltage deviation is driven more by grid-side conditions and loads than by inverter harmonics. Analysing the regression trend between ThdV and V_Dev under different loading conditions, however, helps reveal how inverter stress and grid interaction affect power quality.

Fig. 4.36 illustrates the relationship between current total harmonic distortion (ThdI) and active power. The figure shows a strong correlation between the two parameters. This indicates that inverter loading has a greater impact on ThdI than on the other power quality indicators, such as ThdV and V_Dev. Under heavily loaded inverters, ThdI remains relatively low, with only a few points exceeding the permissible limit of 5%. However, as the inverter load decreases, ThdI gradually exceeds this limit and rises further, reaching values of around 10%. The change in ThdI becomes more pronounced under lightly loaded conditions. This suggests that inverter

loading plays a decisive role in the injection of current harmonics into the grid, with a strong caution that lightly loaded (underutilized) inverters contribute significant harmonic distortion.

A cubic polynomial function fits the curve well, achieving an R^2 value of 0.926. This indicates that inverter loading exhibits a structurally measurable relationship with ThdI. At higher loading levels, inverter behaviour becomes more stable, likely because MPPT and control mechanisms operate more actively and consistently when PV generation is higher. These results highlight the importance of designing inverters that maintain robust control and predictable power-quality performance across a wide range of loading conditions.

Accordingly, the total current harmonic distortion (y) as a function of active power (x) for the three inverter loading categories (conditions) can be reliably estimated using a single cubic polynomial model:

$$y = 1.3546 + (-0.2973)\,x + (0.0239)\,x^2 + (-0.00063)\,x^3$$

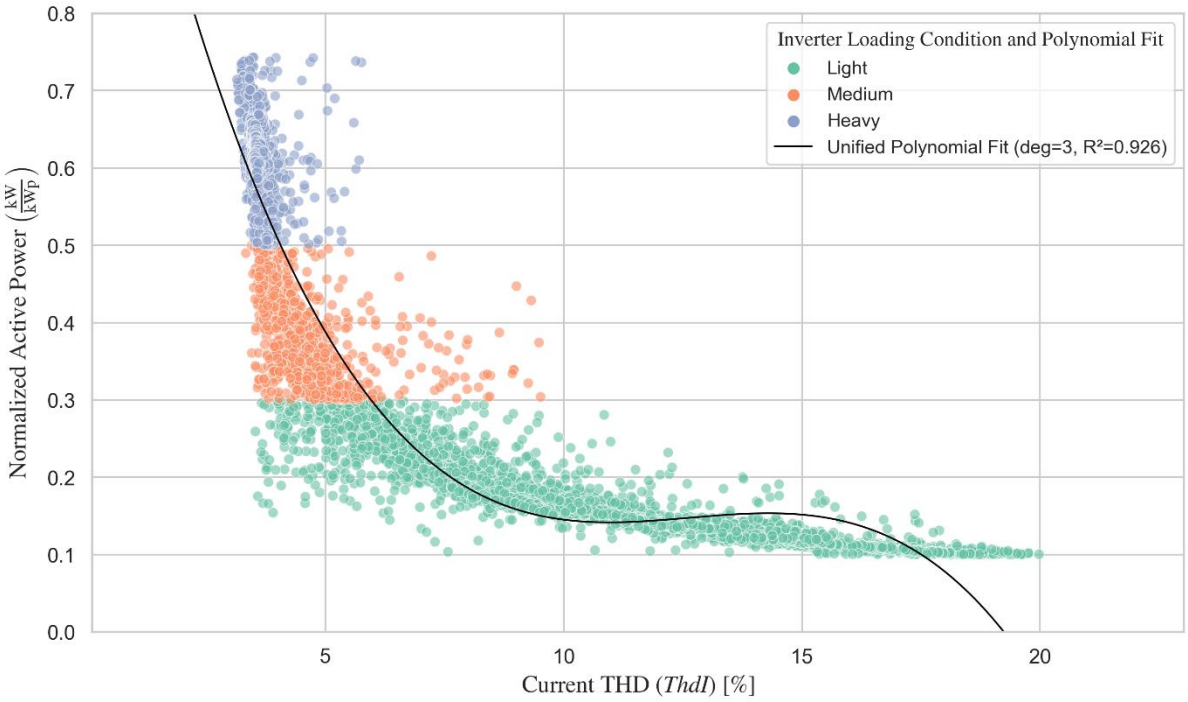

Fig. 4. 36. Active power versus total harmonic distortion under different loading conditions

The greater variation in ThdI observed in lightly loaded inverters implies that they are more sensitive to harmonic distortion when underutilized. Lightly and medium-loaded inverters exhibit higher variability per unit change in active power, whereas heavily loaded inverters show less variability. By associating these distinct regression behaviours with specific sites, utilities can tailor inverter deployment strategies and better anticipate grid stress based on localized loading profiles.

This suggests that inverter behaviour becomes more stable at higher loading levels, likely due to more effective control operation under these conditions. Consequently, oversizing an inverter for a given design can negatively impact power quality – not only cost – because an oversized inverter tends to operate predominantly under medium or light loading, where harmonic distortion is more pronounced. These findings highlight the need for inverter designs

that ensure stronger control capability and more predictable interactions among power-quality parameters across varying load conditions.

4.3. Advancing large-scale PV integration with accurate forecasting

This section presents the benefits of accurate PV generation forecasting and AI-based optimization in supporting the integration of large-scale PV systems. It underscores the importance of different forecasting horizons and addresses the persistent challenge of data scarcity in PV prediction. In addition, it discusses how integrating forecasting results across multiple horizons can significantly enhance operational performance and improve overall system reliability.

Designing and modelling a renewable-based power system is inherently complex due to the dynamic and uncertain nature of weather patterns. System design typically relies on historical weather data, yet past conditions may differ significantly from future ones. As a result, a single, static system design cannot guarantee optimal performance under all future scenarios. To address these challenges, I propose that design limitations be mitigated through advanced operational forecasting techniques. By combining robust system design with accurate, real-time forecasting, power operators can dynamically adjust system operation, reduce risks associated with variability, and enhance the reliability and efficiency of renewable energy integration. This approach ensures that the energy transition is not only technically feasible but also resilient and adaptive to the uncertainties of future climate and demand conditions. Advanced forecasting can be effectively integrated into real-time operation, providing the flexibility to optimize system performance by strategically dispatching storage and allocating balancing generators. This ensures that the system operates efficiently and reliably under all weather conditions.

More importantly, an advanced optimization tool based on a deep reinforcement learning algorithm is applied at the end of the section to optimize the system, using the same input variables presented in Section 4.1. This deep RL-based approach, a well-established and widely used method, helps validate the accuracy and reliability of the new methodology introduced in this dissertation. These advanced forecasting and optimization tools are key enablers of large-scale renewable integration, aligning closely with my core objective of applying machine learning-based forecasting to improve real-time PV system management.

4.3.1. PV generation forecasting without data limitation

Fig. 4.37 compares the accuracy of three models (LSTM, GRU, and LSTM-GRU) in predicting uni-step and multi-step PV generation. This represents scenario 1, where sufficient satellite data is available for training and testing the models. In this experiment, 17 years of satellite-based meteorological data are used for accurate PV prediction. The results are encouraging, demonstrating the potential of PV power generation forecasting in regions with adequate data for model training and testing. However, real-world measurements from operational plants are often limited to only a few years and are typically difficult to access publicly. Section 4.3.2 addresses this challenge by proposing a data-driven empirical relationship between satellite-derived and measured data.

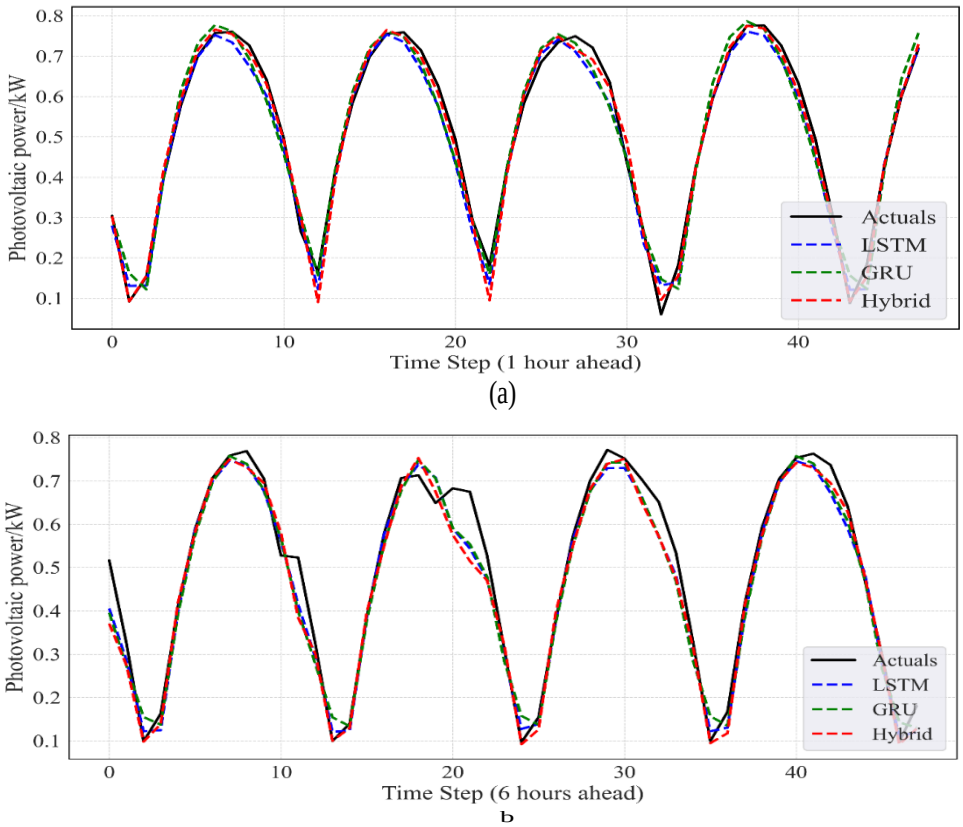

Fig. 4.37. Forecasting result on overall data sets: a) 1-step prediction, b) 6-step prediction

The forecasting experiment is conducted using several advanced, traditional, and hybrid models to identify the best architecture that effectively captures the inherent variability of PV generation. Moreover, the impact of the time distribution of solar generation has been analysed by dividing the dataset into corresponding seasons to better understand the effect of seasonal weather variability on PV forecasting.

Fig. 4.37a shows that the 1-step prediction accuracy of the hybrid model consistently outperforms that of the other models (LSTM and GRU), as also demonstrated in Table 10. 1-step denotes one hour ahead PV generation forecasting. The results show the proposed hybrid model (LSTM-GRU) predicts PV generation with high accuracy, demonstrating its capability in capturing the temporal pattern of weather variability. Such short-term forecasting is vital for enhancing PV performance by allowing the power operator to strategically dispatch units and storage facilities flexibly. An intra-hour short-term forecast can be applied to predict short-term power ramps and voltage flicker, enabling power operators to better control the real-time marketing and dispatching.

Table 10. Error metrics for different models separated into seasons (1- step forecasting)

Season	Model	RMSE (kW)	MBE (kW)	MAE (kW)	R^2
Fall	LSTM	0.0716	0.0022	0.0439	0.8999
	GRU	0.0735	0.0063	0.0467	0.8946
	LSTM-GRU	0.0813	0.0026	0.0625	0.9039
Winter	LSTM	0.0558	0.0035	0.0290	0.9448
	GRU	0.0600	0.0035	0.0329	0.9361

	LSTM-GRU	0.0548	0.0134	0.0280	0.9468
Spring	LSTM	0.0625	0.0021	0.0358	0.9194
	GRU	0.0650	0.0093	0.0404	0.8946
	LSTM-GRU	0.0617	0.0083	0.0332	0.9216
Summer	LSTM	0.1051	0.0006	0.0774	0.6668
	GRU	0.1074	0.0019	0.0776	0.6525
	LSTM-GRU	0.0702	0.0033	0.0391	0.6685
Overall	LSTM	0.0745	0.0002	0.0450	0.8729
	GRU	0.0748	0.0021	0.0455	0.8532
	LSTM-GRU	0.0737	0.0083	0.0420	0.9004

In the subsequent experiment, with multi-step (6 and 12-step) prediction, the results follow a similar pattern as one step but with only one distinct characteristic of diverging prediction error, as shown in Fig. 4.37b. This is expected and reasonable; as the number of prediction steps increases, so does error propagation. In multi-step prediction, accuracy decreases due to error propagation as the prediction horizon grows. The inherent variability in PV power generation further amplifies the challenge. The proposed hybrid model (LSTM–GRU) still exceeds the performance of individual models, providing a closer alignment between actual and predicted values. Forecasting several hours ahead of PV production allows grid operators to schedule dispatchable generators and storage more effectively for optimal dispatch and grid management. This approach reduces dependence on costly balancing generators and supports smoother, larger integration of PV.

Fig. 3.38 presents the MAE for the three models, LSTM, GRU, and LSTM-GRU, over the entire year (overall) dataset. The results show that the MAE increases with longer forecasting horizons, which can be attributed to the accumulation of prediction errors as the time step increases.

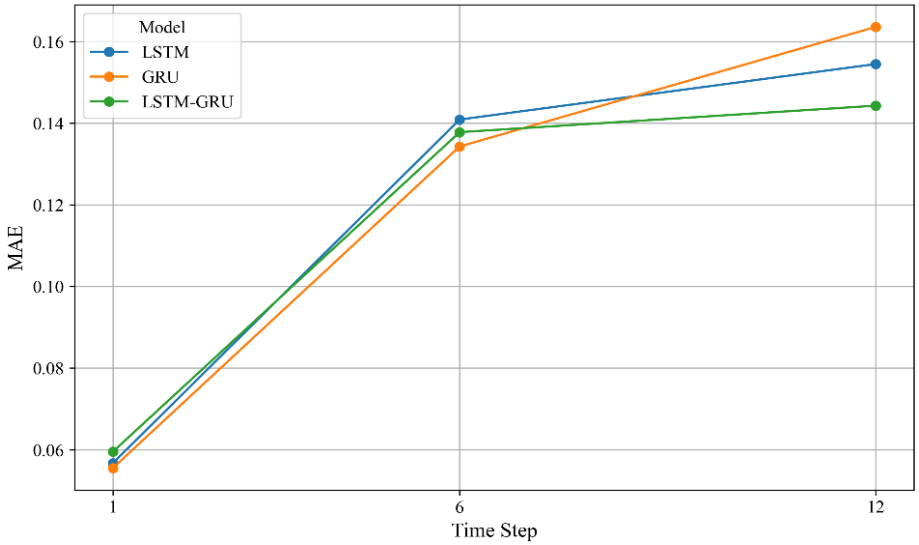

Fig. 4.38. Trendlines of MAE for 1-, 6-, and 12-step forecasts across the combined annual dataset for each model

4.3.2. Addressing data scarcity challenges in PV forecasting

The preceding discussions highlighted that accurate PV generation forecasting is vital for enabling large-scale PV to the power grid by offering flexibility to power operators to dispatch, schedule, and optimize storage, balancing generators and other grid enablers effectively. This

section presents the Z-score transformation-based results and demonstrates a significant improvement compared to those obtained without transformation.

Fig. 4.39 shows the result of one-step PV prediction. In this experiment, all three models show similar performance regardless of season, as indicated by their RMSE values. However, LSTM has very nearly outperformed the other two models in RMSE, MBE and MAE while GRU performed slightly well in R^2. Regarding prediction accuracy, the newly introduced approach achieved good results in forecasting actual PV generation, which are almost comparable to the corresponding values obtained when pure satellite-derived data was used as the training and testing dataset, as shown in Table 9.

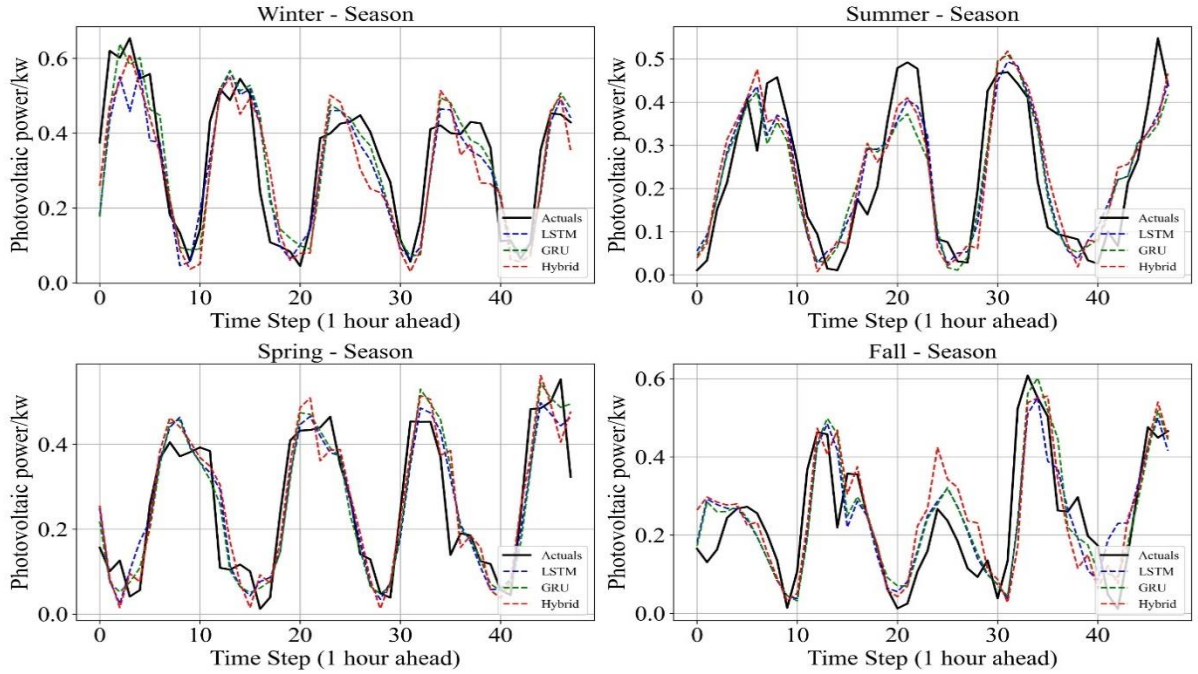

Fig. 4.39. Performance comparison of the three models' prediction of actual PV generation across four seasons in 1-step prediction

As shown in Fig. 4.39, the models satisfactorily forecast the actual PV generation with comparable performance. The proposed approach demonstrates superior performance, with accurate predictions providing power operators with 1-hour to 12-hour ahead PV generation forecasts. This enables effective scheduling and dispatching of generation units and storage facilities, enhancing grid efficiency and stability. Further improvement is needed in multistep predictions as errors become significant, particularly for 12-hour-ahead forecasts. Several hours-ahead PV power predictions is crucial in addressing intermittency-related integration challenges, offering operators more time to prepare for fluctuations and optimize grid operations. Notably, the analysis focuses exclusively on daytime hours, as night data is omitted by assuming zero PV generation. While further model enhancement and the incorporation of improved statistical tools for approximating satellite-derived data with measured data are necessary, the results of this study lay a strong foundation for predicting actual generation from satellite-derived data. The proposed methodology offers several key advantages. First, machine learning prediction models require large datasets for effective training and validation, often unavailable from measured data alone. Satellite and reanalysis datasets, with their extensive and long-term data coverage, bridge this gap by providing extensive historical data for trend analysis and model training, improving the accuracy and robustness of prediction models.

Furthermore, leveraging these datasets ensures the broader applicability of the methodology across regions lacking robust measurement infrastructure, making it a versatile solution for global energy transition efforts.

Table 11 presents a performance summary of the various investigated machine learning models, both with (✓) and without (×) transformation. These correspond to scenarios 3 and 2: in scenario 2, satellite data are used without transformation for actual PV prediction, while in scenario 3, transformed data are applied for actual PV prediction.

The proposed approach (scenario 3) is evaluated against advanced deep learning models such as CNN-LSTM, TCN-GRU, and Informer. The performance of these models was assessed for different forecasting time steps, revealing higher performance in multi-step forecasting. However, their performance was similar to that of the LSTM-GRU hybrid model in one-step prediction. This indicates that the architecture of these advanced models enabled them to capture long-term sequences and predict better for medium-duration tasks. For instance, in six-step forecasting, Informer outperforms the others, followed by TCN-LSTM in RMSE and R^2, while LSTM-GRU was shown to have good performance in terms of MBE, preceded by CNN-LSTM.

Table 11. Performance comparison of conventional and advanced deep learning (with and without data transformation-scenario

Model	Transformation	RMSE (kW)	MBE (kW)	MAE (kW)	R2
LSTM	×	0.2472	0.1900	0.2073	-0.3924
LSTM	✓	0.1731	0.0029	0.1409	0.5359
GRU	×	0.2410	0.1889	0.2032	-0.3236
GRU	✓	0.1675	0.0015	0.1343	0.5821
LSTM-GRU	×	0.2254	0.1760	0.1876	-0.1579
LSTM-GRU	✓	0.1714	0.0002	0.1378	0.6024
CNN-LSTM	×	0.2519	0.2099	0.2165	-0.4458
CNN-LSTM	✓	0.1654	0.0011	0.1339	0.6043
CNN-GRU	×	0.2545	0.2123	0.2180	-0.4758
CNN-GRU	✓	0.1786	0.0411	0.1422	0.5385
TCN-LSTM	×	0.2461	0.1989	0.2069	-0.3808
TCN-LSTM	✓	0.1589	0.0009	0.1276	0.6345
INFORMER	×	0.2245	0.1812	0.1886	-0.1482
INFORMER	✓	0.1585	0.0152	0.1273	0.6365

The performance of the other two traditional models, SARIMAX and XGBoost, is unsatisfactory (Appendix, A15). However, their performance improves significantly when the data transformation is incorporated. This suggests that traditional models are ineffective but can be substantially improved when data transformation is applied.

Within this context, deep learning algorithms with transformation are the most accurate choices for solar power forecasting; traditional models without transformation are not satisfactory. Nevertheless, traditional models such as XGBoost become viable alternatives when transformation is employed. SARIMAX has an R^2 value of -1.368, which indicates that the model performs poorly in predicting the PV generation. Even when data transformation is applied, the enhancement is marginal (0.0431).

For quantitative comparison, scenario 3, when data transformation is applied, the XGBoost and SARIMAX RMSE values are about 1.5 and 2.37 times higher than those of the hybrid (LSTM-GRU) model. This suggests that deep learning models are naturally better suited for complex forecasting tasks, such as solar energy prediction, while traditional methods show a lower performance in predicting PV generation. Similarly, when comparing the prediction accuracy of the hybrid model (LSTM-GRU) in terms of R^2, with and without transformation in 1-step prediction, the prediction accuracy increases by 43%, further demonstrating the superiority of the proposed approach. The findings further reveal that the proposed transformation improves forecasting accuracy by up to 24% in LSTM-GRU and 29.4% for Informer in six-step prediction, based on RMSE. Such improved forecasting enhances grid stability, optimizes energy dispatch, and offers a scalable solution for regions with limited measurement infrastructure, highlighting the importance of satellite-based forecasting in renewable energy policy development.

To highlight the overall system performance, Fig. 4.40 presents the RMSE values for each model (LSTM, GRU, and LSTM-GRU) across four seasons, Fall, Winter, Spring, and Summer, as well as the overall annual performance. Results are shown for forecasting horizons of 1, 6, and 12 hours, illustrating seasonal variability and the impact of longer prediction steps on model accuracy. The marked increase in error metrics with increasing horizon length (from 1 to 6 and then 12-step-ahead) reflects the error accumulation in multi-step-ahead time series forecasting. In a 1-step-ahead forecast, predictions are conditioned on the most recent observed data, minimizing input uncertainty. By contrast, in 6 and 12-step-ahead forecast using a recursive strategy, each step relies on previously forecasted values, introducing propagated errors and compounding model bias and variance over time.

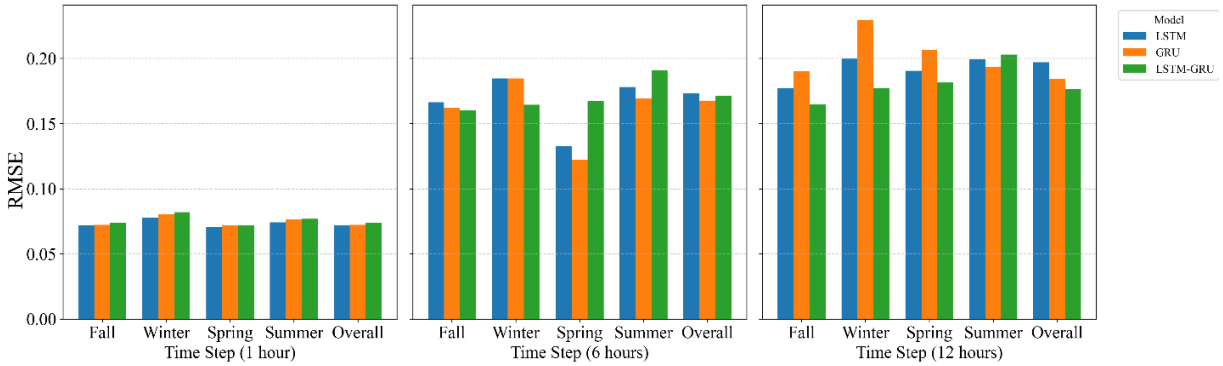

Fig. 4.40. Seasonal and overall RMSE for the models at 1, 6, and 12-hour forecasting horizons

A growing body of work has examined how different meteorological datasets – such as satellite-derived products, ground-based measurements, reanalysis data, and Numerical Weather Prediction (NWP) outputs – affect the performance of data-driven PV forecasting models. For example, Hajjaj et al. (2023) compared satellite-derived and ground-based datasets and found that forecasts built using ground-based observations consistently achieved higher accuracy, whereas satellite data led to noticeably poorer performance across all models. Likewise, Brester et al. (2023) evaluated NWP datasets, observational data, and their combined use against actual PV output, concluding that NWP inputs alone provided better generalization and achieved up to 25% lower RMSE than the combined dataset.

The findings highlight the critical role of accounting for weather variability in reliable forecasting, particularly for multi-step predictions essential to long-term renewable energy planning. These insights support grid and operational stability, optimize storage dispatch, and underscore the value of satellite-derived models for renewable integration, ensuring the energy transition remains technically feasible, resilient, and adaptable to future climate and demand uncertainties. Short-term PV forecasts are particularly important for managing intermittency, giving operators time to adjust and optimize grid operations. Furthermore, as discussed in Section 4.1, accurate forecasting allows for strategic and flexible scheduling of storage and generation units, which can substantially reduce balancing capacity requirements, improve capacity factors, and ensure reliable power output.

4.3.3. Optimizing system configuration using deep RL model

Section 4.1 introduced a novel methodological framework for integrating large-scale PV systems, centred around the 'System Use Index (SUI)', a newly developed metric designed to identify optimal and near-optimal parameter configurations that enhance overall system performance. While the results using this index demonstrated promising outcomes, establishing the credibility and robustness of the framework requires rigorous validation against widely recognized and proven modelling approaches. To this end, the current section employs a well-established machine learning technique-Deep Reinforcement Learning (DRL), to optimize system performance using one full year of PV generation and demand data. This DRL-based model serves as a benchmark, enabling direct comparison with the results obtained from the proposed rule-based methodology. Such comparative analysis not only highlights the strengths of the RL approach but also affirms the reliability and practical relevance of the newly introduced framework.

An RL-based battery dispatch model using the Proximal Policy Optimization (PPO) algorithm was implemented. The agent interacts with a custom environment simulating hourly renewable generation and load demand. The action space is continuous, representing charge/discharge decisions, and the reward function penalizes curtailment and unmet demand while incentivizing energy delivery (served load). The model was trained over a one-year horizon using PV and load data, with battery parameters reflecting realistic operational constraints.

To assess system behaviour under varying configurations, the model was evaluated across multiple values of diurnal storage. This allowed for a deeper understanding of how key system parameters interact under different design conditions. Fig. 4. 41 presents the temporal dynamics of these parameters over a representative one-week period in May, focusing on a 50-50 PV-wind scenario. The simulations were conducted using consistent input parameters as outlined in Section 4.1, with diurnal storage capacities below 0.5 times the average daily demand, a fixed storage duration of 6 hours, and a renewable-to-load ratio of 1.04. Notably, at a diurnal storage level of 0.25 times the average daily demand, the RL-based model achieved a renewable energy penetration of 89.1% with only 12.9% curtailment.

For comparison, the newly introduced rule-based framework–using the same PV–wind mix and diurnal storage size–achieved a penetration of 90% with 16% curtailment at a slightly higher RE-to-load ratio of 1.10, as measured by the SUI index. This close alignment in performance demonstrates that while the RL model exhibits marginally superior efficiency (achieving similar penetration at a lower RE-to-load ratio), the rule-based approach remains highly competitive. The dimensional consistency across both models, particularly in terms of energy flows (MWh), storage capacity (MWh), and hourly resolution (h), further reinforces the robustness of the comparison. The strong agreement between the RL model and the proposed

framework validates the reliability of the new methodology and its underlying indices, positioning it as a promising alternative for energy system optimization.

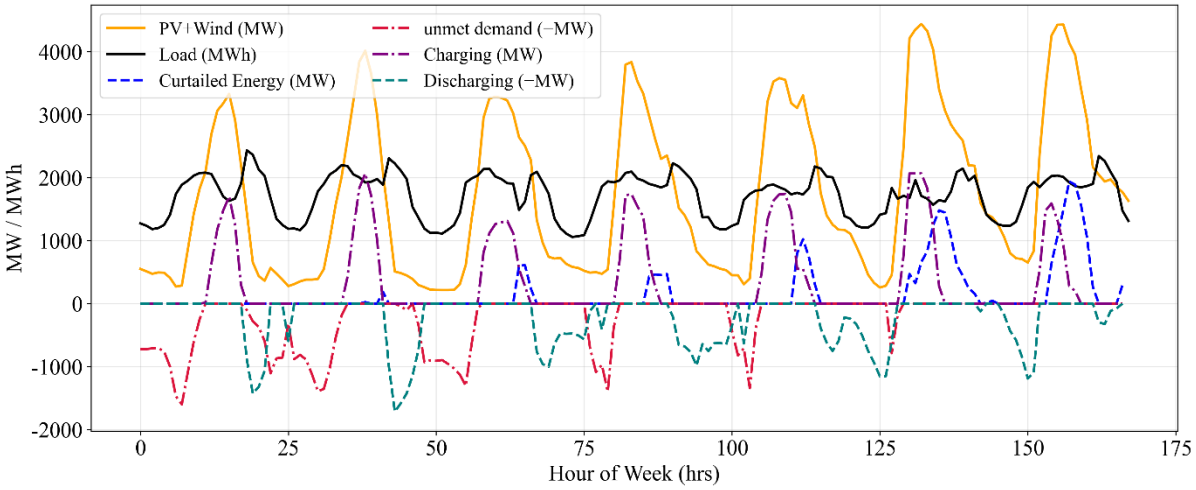

Fig. 4.41. Hourly dynamics of system performance metrics for the RL-optimized configuration over the one week of May

These advanced forecasting and optimization tools are key enablers of large-scale renewable integration, aligning closely with my core objective of applying machine learning-based forecasting to improve real-time PV system management.

An alternative approach was investigated by training the RL model using similar datasets and system parameters to those in the case above. The only difference is the testing condition. The model was trained to develop a charging /discharging policy using one year of full PV+wind data and load demand. The trained model was then evaluated against another new dataset. The testing data set was created by injecting random noise into the training dataset of about ±10% for generation and ±5% for load. This represents a measure of uncertainty introduced by variations in renewable generation and electricity demand across different years. In this scenario, the model performs based on its learned policy and achieves penetration of 91.41% and curtailment of 9.46% which is better than the previous results displayed in Fig. 4.40. This shows that models trained and evaluated on the same data sets sometimes run to overfit instead of generalizing the pattern.

5. NEW SCIENTIFIC RESULTS

This section presents the new scientific findings from this research work as follows:

1. A methodological approach for integrating large-scale PV

I have introduced a novel methodological framework aimed at maximizing PV penetration in the power grid. This approach systematically examines the interplay between key system design parameters and overall efficiency by varying these parameters to generate diverse operational scenarios and assess their sensitivities. For the first time, it explicitly incorporates the interactions among critical factors–such as PV–wind mix, storage capacity, storage duration, penetration level, curtailment, and balancing capacity needs–across a wide range of scenarios, thereby providing deeper insights into system design and performance.

The methodological framework I developed, which is the basis for designing and modelling the system with all its interacting system parameters, is presented as follows:

The different mixes of solar PV and wind-generated power can be computed by:

$$P_{\text{rew}}(t) = P_{\text{nd}}\ \alpha(r)\ (r\ p_{\text{PV}}(t) + (1-r)\ p_{\text{wind}}(t)),$$

$\alpha(r)$ is a factor that is determined from a requirement that:

$$\sum_t \alpha(r)(r\ p_{\text{PV}}(t) + (1-r)\ p_{\text{wind}}(t)) = \text{const}\,,$$

and that $\alpha(0.5) = 1$.

The no-dump capacity is, consequently, determined according to:

$$P_{\text{nd}} = \min \frac{P_{\text{load}}(t)}{(r\ p_{\text{PV}}(t) + (1-r)\ p_{\text{wind}}(t))}\,,$$

The mismatch energy between renewable generation and load can be computed as:

$$P_{\text{mix}}(t) = \beta\ P_{\text{nd}}\ \alpha(r)\ \big(r\ p_{\text{PV}}(t) + (1-r)\ p_{\text{wind}}(t)\big) - P_{\text{load}}(t),$$

where β is a multiplier that enables oversizing the generation. Based on the values extracted from these empirical relationships, the model computes the optimal range of various parameters to ensure an optimal system efficiency that ultimately maximizes PV integration.

2. Storage utilisation and system-use index

I have introduced new and novel indices that identify the optimal system design parameters, and an optimal range of these parameters yields an optimal system performance. These indices provide deeper insights into the effectiveness of curtailment and storage integration within the broader energy infrastructure, enhancing the system's capacity to manage variability and optimize resource utilization.

The empirical relationship developed for defining the system boundaries is:

$$SU = \frac{-\sum(S(t) - S(t-\Delta t))}{S_{max}}, \qquad \text{if } S(t) < S(t-\Delta t)$$

The system-use index (SUI) is computed as follows:

$$\text{SUI} = \text{SU}\ k\ m\ u$$

where k, m and u are calculated by dividing annual energy discharge by the total consumed RE, average charging power by power capacity (PC), and total consumed RE by total RE generation, respectively:

$$k = \frac{-\sum(S(t) - S(t-\Delta t)}{\sum P_{useful}}, \qquad \text{if } (S(t) < S(t-\Delta t)$$

$$m = \frac{\sum S(t) - (S(t-\Delta t)}{P.C}, \qquad \text{if } (S(t) > S(t-\Delta t)$$

where $PC = {}^{S_{max}}/_{\Delta t_{full}}$

$$u = \frac{\sum P_{useful}}{\sum P_{rew}},$$

This approach enables me to create a novel and improved 3D visualization of the intricate relationships among these various interactive factors, providing a more comprehensive understanding of their interactions to improve PV integration.

3. Storage optimisation and its link to penetration

I have established clear boundaries of renewable penetration by linking them with storage type and application, resolving longstanding ambiguities in the literature. Through systematic analysis, I structured storage use into three distinct configurations, defined by their application and degree of penetration. This optimized categorization simplifies system design and modelling and provides actionable boundaries that overcome previous inconsistencies in renewable–dominated grid studies:

i. First configuration: This represents the no-dump capacity range–the threshold below which the system operates without requiring any form of storage or curtailment. While the exact no-dump capacity varies with the PV-wind mix, the maximum penetration achievable without storage or curtailment in the solar-only (PV) scenario is about 23.6%.

ii. Second configuration: Any increase in renewable penetration beyond this level necessitates storage and/or curtailment to manage fluctuations, enabling penetration up to 80%. Within this range, diurnal storage plays the key role in balancing short-term variability.

iii. Third configuration: Beyond 80% penetration, renewable deployment rises sharply even with slight increases in penetration. Thus, meeting the final 20% of demand presents a distinct challenge, which I addressed through seasonal storage capable of resolving long-term seasonal mismatches.

4. Maximizing the direct consumption of residential PV by imposing feed-in constraints

I have explored strategies for maximizing direct consumption of PV power in the low-voltage network. I have introduced a distinctive approach that proposes tailored grid-expansion and management solutions to enhance local network PV consumption. Building on this analysis, I have identified remarkably effective strategies that maximize the direct use of generated PV. The most efficient configuration combines a feed-in limit of 0.4–0.5 kW/kWp with battery storage capacities below 2 kWh/kWp, a setup that sharply reduces curtailment and achieves the highest levels of direct PV utilization.

Using the new approach – supported and validated with laboratory experiment – I have demonstrated that feed-in limits above 0.7 kW/kWp offer only negligible improvements in annual energy output. This confirms that the common practice of sizing inverters at 80–90% of the PV array capacity is not only economically inefficient but can also degrade system operation and power quality.

5. Addressing the data scarcity challenge in PV power forecasting

I found a practical solution to the data scarcity challenge in PV generation forecasting by developing a method that bridges satellite-derived and ground-measured data. Using a modified Z-score transformation, I have approximated satellite data to measured data based on their respective means and standard deviations. This approach enables the integration of widely available satellite data with the reliability of ground-based measurements by establishing a transparent empirical relationship, using transformation formulas derived from observed correlations. The resulting adjusted dataset is used to train the forecasting model. At the same time, testing is conducted on actual measured PV output, ensuring both accuracy and applicability in regions with limited monitoring infrastructure.

For each value in satellite-derived data, I found the standard normal form using the Z-score transformation (z):

$$z = \frac{P_{sat,i} - \mu_{sat}}{\sigma_{sat}} \qquad \text{and}$$

the rescaled satellite value ($P'_{sat,i}$) is determined to match the distribution of the measured data using:

$$P'_{sat,i} = z\,\sigma_{meas} + \mu_{meas}$$

where, $P_{sat,i}$, μ_{sat} and σ_{sat} are the hourly PV generation, mean, and standard deviation of the satellite-derived data, whereas, μ_{meas} and σ_{meas} are the mean and standard deviation of the measured data.

The proposed transformation has been rigorously validated against various well-established forecasting models. It demonstrates significant improvements in forecasting accuracy, achieving up to 24% in the LSTM-GRU model and 29.4% in the Informer model for six-step forecasts, based on RMSE metrics. For one-step predictions, the hybrid LSTM-GRU model yields a 43% increase in accuracy using the R^2 coefficient, confirming the effectiveness of the transformation approach. The method offers a scalable solution for regions with limited measurement infrastructure, reinforcing the role of satellite-based forecasting in advancing PV integration and shaping renewable energy policy development. Moreover, these forecasting improvements contribute to enhanced grid stability, optimize storage dispatch, and improve load balancing by offering flexibility to system operators.

The newly introduced methodological framework was validated against a well-established RL-based machine learning algorithm, showing negligible disparities. This strong agreement confirms the reliability of the framework and its underlying indices, reinforcing its accuracy and positioning it as a promising alternative for energy system optimization.

6. Impact of inverter loading on power quality

I have investigated the total harmonic characteristics of the PV inverter at various inverter loading conditions and I identified that inverter loading has a greater impact on the current total harmonic distortion (ThdI) than on the other power quality indicators. In heavily loaded inverters, ThdI remains relatively low, with only a few points exceeding the permissible limit of 5%. However, as the inverter load decreases, ThdI gradually exceeds this limit and rises further, reaching values of around 10%. The change in ThdI becomes more pronounced under lightly loaded conditions.

Accordingly, I have shown that the total current harmonic distortion (y) as a function of active power (P/P_{rated}) (x) for the three inverter loading conditions can be reliably estimated using a cubic polynomial model, achieving an R^2 value of 0.926.

$$y = 1.3546 + (-0.2973)\, x + (0.0239)\, x^2 + (-0.00063)\, x^3$$

The greater variation in ThdI observed in lightly loaded inverters implies that they are more sensitive to harmonic distortion when underutilized. Lightly and medium-loaded inverters exhibit higher variability per unit change in active power, whereas in heavily loaded conditions, inverter behaviour becomes more stable, likely because MPPT and control mechanisms operate more actively and consistently when PV generation is higher. By associating these distinct regression behaviours with specific sites, utilities can tailor inverter deployment strategies and better anticipate grid stress based on localized loading profiles.

This suggests oversizing an inverter for a given design can negatively impact power quality – not only cost – because an oversized inverter tends to operate predominantly under medium or light loading, where harmonic distortion is more pronounced. These findings highlight the need for inverter designs that ensure stronger control capability and more predictable interactions among power-quality parameters across varying load conditions.

6. CONCLUSION AND RECOMMENDATION

In this thesis, strategies have been investigated for maximizing PV integration into the power grid through three complementary approaches: large-scale PV deployment, residential PV integration, and PV generation forecasting and optimization.

To support large - scale PV integration, a novel methodological framework has been developed that flexibly captures the interactions between key system design parameters, such as storage capacity, storage duration, penetration, curtailment, wind-solar mix, and balancing requirements, while linking these parameters to a newly developed System–use index (SUI), which serves as a proxy of system efficiency. Various scenarios have been evaluated by fixing the PV share at 0%, 50%, and 100% of total RE capacity and applying different storage durations. Results show that penetration, curtailment, and storage all increase simultaneously; however, penetration gains diminish once storage or curtailment exceeds certain thresholds. Nevertheless, reaching 80–90% penetration is feasible with diurnal storage below 0.5 average daily demand with 6 hours of storage, alongside moderate curtailment. Achieving 100% renewable penetration is, however, challenging in the last 10–20% of the transition due to seasonal mismatches. Incorporating seasonal storage, about 8 average daily demand with a RE-to-load ratio of 1.2, enables complete decarbonization without balancing (back-up) needs. These findings highlight that an optimal mix of curtailment, storage, and wind-solar mix is essential for maximizing system efficiency, forming multidimensional constraints that are difficult to implement in existing techno-economic tools but critical for guiding policy development and regulation.

The role of residential PV in large-scale PV integration has been investigated by introducing a new concept of direct PV injection into low-voltage networks, overcoming the limitations of conventional self-sufficiency models. Findings reveal that imposing a feed-in limit and integrating battery storage significantly reduce curtailment, with a feed-in limit of 0.4 to 0.5 kW/kWp and battery storage below 2 kWh/kWp. This setup maximizes photovoltaic integration and enables renewable energy penetration of up to 30%. The study further examined the impact of inverter loading on power quality and found that highly loaded inverters operate more stably, while underutilized inverters exhibit significant distortion.

Machine learning based forecasting and optimization models have been proposed to maximize PV integration. To achieve this, a modified Z-score transformation and an RL model have been applied to align satellite-derived data with measured values to improve generation forecasting and optimize the system configuration. The findings reveal that the proposed transformation improves forecasting accuracy by up to 43%, demonstrating the effectiveness of the approach in providing a scalable solution for regions in regions with limited measurement infrastructure.

These approaches collectively establish a comprehensive framework for addressing both system design and operational challenges in maximizing PV integration. By combining optimized PV–wind–storage configurations, effective residential PV deployment, and enhanced forecasting, the study provides valuable insights for achieving high levels of PV penetration in future renewable-dominated grids. Adopting, technical-first perspective, the study outlines multiple transition pathways by defining boundary conditions that can guide more detailed economic analyses and policy development. Furthermore, improved transmission planning and demand-side management will be essential for achieving more optimal system configurations and understanding parameter interactions. Incorporating more fine-tuned household data in residential PV analysis could further improve accuracy. This study emphasizes the importance of understanding the future renewable energy grid, using Eritrea as a case study; nevertheless, the methodology employed can be applied to a broader range of applications in a global perspective.

7. SUMMARY

MODELLING AND OPTIMIZATION OF LARGE-SCALE GRID-CONNECTED PHOTOVOLTAIC SYSTEMS WITH ENABLING TECHNOLOGIES

A holistic and innovative multifunctional simulation model is developed to maximize PV integration and offer a broader perspective on system design under interacting factors. Using hourly weather data from PVGIS and GWA, geographically distributed solar and wind sites in Eritrea were analysed to explore scenarios achieving 90% and beyond renewable penetration with and without storage. The results offer important insights of global importance by linking parameters in a uniquely broad way, while also addressing the context-specific requirements.

The analysis focuses on enabling large-scale PV integration through resource complementarity, energy storage, curtailment strategies, balancing capacity and improved forecasting, recognising that PV alone cannot capture full system complexity. Two new indicators, Storage Utilisation (SU) and System Use Index (SUI) are introduced to reveal the interactions between these variables. Results show that variable renewable penetration, curtailment and storage capacity increase simultaneously across all scenarios. The framework provides multiple options for combining storage and curtailment to achieve specific penetrations (including 100%), tailored to individual priorities and policy preferences, with the optimal approach lying in determining approximate optimal sizes to balance technical and economic feasibility.

Findings show that with a storage capacity below 0.5 of average daily demand, grid penetration exceeding 90% can be achieved while keeping curtailment under 20%, except in wind-only scenarios, which require higher curtailment. Diurnal storage manages short-term fluctuations and facilitates high renewable penetration of 80-90%, but its limitations become evident beyond this range. Meeting the final 10–20% of demand requires solutions beyond diurnal storage, as seasonal mismatches necessitate large storage and generation capacities. Incorporating seasonal storage of about 8 average daily demand with a RE-to-load ratio of 1.2 enables complete decarbonisation without balancing back-up needs. Overall, the study highlights that an optimal mix of curtailment, storage and wind–solar complementarity is essential for maximising system efficiency and for shaping policies and regulations that support deep decarbonisation.

Two additional approaches are introduced to maximise PV integration into the grid: expanding rooftop PV adoption (residential PV) and applying advanced PV generation forecasting. Using simulation techniques, the study examined the optimal deployment of residential PV and battery storage to boost PV penetration while minimising curtailment, applying a simple algorithm for PV injection, battery charging, and discharging. Key results show that imposing a feed-in limit and adding battery storage markedly cut curtailment, with limits of 0.4–0.5 kW/kWp and storage below 2 kWh/kWp giving the best outcomes. The study reveals that the power quality of grid-connected PV systems is strongly influenced by loading conditions, showing that highly loaded inverters maintain stable operation, while lightly loaded (underutilized) inverters exhibit increased distortion. The advantage of Effective PV forecasting for increasing renewable energy integration is studied, as it allows better management of generation and system operations. The new PV forecasting approach raises accuracy by up to 43%, enhancing generation management. When combined with resource complementarity and storage adoption, this improved forecasting strengthens grid stability, optimises scheduling, improves storage dispatch, reduces balancing needs, and boosts overall system efficiency, ultimately maximising renewable energy integration.

8. ÖSSZEFOGLALÁS (SUMMARY IN HUNGARIAN)

NAGYMÉRETŰ, HÁLÓZATRA KAPCSOLT FOTOVILLAMOS RENDSZEREK MODELLEZÉSÉT ÉS OPTIMALIZÁLÁSÁT TÁMOGATÓ TECHNOLÓGIÁK

Egy holisztikus, innovatív többfunkciós szimulációs modell került kifejlesztésre a napelemek integrációjának maximalizálására és a rendszertervezés szélesebb perspektívájának biztosítására a kölcsönhatásban lévő tényezők figyelembevételével. A PVGIS és GWA óránkénti adatait felhasználva eritreai helyszíneken készült elemzés olyan forgatókönyveket vizsgál, amelyekben a nap- és szélenergia kombinációjával – tárolással és anélkül – 90% feletti megújulóenergia elterjedés érhető el. Bár az eredmények helyspecifikusak, globális jelentőségük is van a paraméterek széles körű összekapcsolásának köszönhetően.

Az elemzés a nagy léptékű napelemes integráció megvalósíthatóságára összpontosít az erőforrások kiegészítő jellege, az energiatárolás, a betáplálási korlátozások, a kiegyenlítő kapacitás és az előrejelzés szerepének vizsgálatával. Két új mutató, a tároláskihasználás (SU) és a rendszerhasználati index (SUI) került bevezetésre. Az eredmények szerint a megújulóenergia elterjedés, a korlátozás és a tárolási kapacitás minden forgatókönyvben együtt növekszik. A keretrendszer több lehetőséget kínál a tárolás és a korlátozás kombinálására, különböző prioritásokhoz és menetrendekhez igazodva, meghatározott elterjedés (akár 100%) elérése érdekében. Az optimális megközelítés a műszaki és gazdasági megvalósíthatóság egyensúlyát biztosító paraméterek meghatározásában rejlik.

A napi energiaigény 50%-ánál kisebb tárolási kapacitás mellett 90% feletti hálózati elterjedés érhető el, miközben a betáplálási korlátozás 20% alatt marad – kivéve a kizárólag szélenergiát alkalmazó forgatókönyveket. A napi tárolás hatékonyan kezeli a rövid távú ingadozásokat és 80–90%-os megújulóenergia részarányt tesz lehetővé, de ezen szint felett korlátjai jelentkeznek. A maradék 10–20% fedezéséhez szezonális tárolás szükséges nagyobb kapacitással és termelési potenciállal. A napi átlagos kereslet körülbelül nyolcszorosának megfelelő szezonális tárolás 1,2-es megújuló energia terhelés aránnyal teljes dekarbonizációt tesz lehetővé kiegyenlítő tartalék nélkül. A dolgozat kiemeli, hogy a rendszerhatékonyság maximalizálásához – a dekarbonizációt támogató politikai és szabályozási háttér mellett – kulcsfontosságú a betáplálási korlátozás, a tárolás és a nap- és szélenergia optimális kombinációja.

További két tényező is jelentős a napelemes energia integrációjának növelésében: a tetőre szerelt (lakossági) napelemes rendszerek elterjesztése és a fejlett napenergia előrejelzés alkalmazása. Szimulációk vizsgálták a lakossági napelemek és akkumulátoros tárolók optimális telepítését a fotovillamos energiaforrások terjedésének elősegítése és a betáplálási korlátozások csökkentése érdekében, óránkénti ütemezésű algoritmust alkalmazva a betáplálás, töltés és kisütés irányítására. Az eredmények szerint a betáplálási korlát bevezetése és az akkumulátoros tárolás együttesen jelentősen mérsékli a korlátozást, a legjobb eredmények 0,4–0,5 kW/kWp betáplálási korlát és 2 kWh/kWp alatti tárolás mellett érhetők el. A hatékony napenergia előrejelzés elengedhetetlen a megújuló energia integrációjának növeléséhez, mivel javítja a termelés és a rendszerirányítás hatékonyságát. Az új előrejelzési megközelítés akár 43%-kal növeli a pontosságot, javítva a hálózat stabilitását, az akkumulátorok kihasználtságát és a rendszer általános hatékonyságát.

9. APPENDICES

A1: Bibliography

1. Abdelhady, S., Abd-Elhady, M. S., & Fouad, M. M. (2017): An understanding of the operation of silicon photovoltaic panels. *Energy Procedia*, 113, 466–475. https://doi.org/10.1016/j.egypro.2017.04.041
2. Abdel-Nasser, M., & Mahmoud, K. (2019): Accurate photovoltaic power forecasting models using deep LSTM-RNN. *Neural Computing and Applications*, 31(7), 2727–2740. https://doi.org/10.1007/s00521-017-3225-z
3. Aghaei, M., Fairbrother, A., Gok, A., Ahmad, S., Kazim, S., Lobato, K., Oreski, G., Reinders, A., Schmitz, J., Theelen, M., Yilmaz, P., & Kettle, J. (2022): Review of degradation and failure phenomena in photovoltaic modules. *Renewable and Sustainable Energy Reviews*, 159(February), 112160. https://doi.org/10.1016/j.rser.2022.112160
4. Aguiar, L. M., Pereira, B., Lauret, P., Díaz, F., & David, M. (2016): Combining solar irradiance measurements, satellite-derived data and a numerical weather prediction model to improve intra-day solar forecasting. *Renewable Energy*, 97, 599–610. https://doi.org/10.1016/j.renene.2016.06.018
5. Ali, A. O., Elgohr, A. T., El-Mahdy, M. H., Zohir, H. M., Emam, A. Z., Mostafa, M. G., ... & Elhadidy, M. S. (2025). Advancements in photovoltaic technology: A comprehensive review of recent advances and future prospects. Energy Conversion and Management: X, 100952. https://doi.org/10.1016/j.ecmx.2025.100952
6. Almutairi, A., Abo-Khalil, A. G., Sayed, K., & Albagami, N. (2020): MPPT for a PV grid-connected system to improve efficiency under partial shading conditions. *Sustainability (Switzerland)*, 12(24), 1–18. https://doi.org/10.3390/su122410310
7. Amir, M., Deshmukh, R. G., Khalid, H. M., Said, Z., Raza, A., Muyeen, S. M., Nizami, A. S., Elavarasan, R. M., Saidur, R., & Sopian, K. (2023): Energy storage technologies: An integrated survey of developments, global economical/environmental effects, optimal scheduling model, and sustainable adaption policies. *Journal of Energy Storage*, 72(PE), 108694. https://doi.org/10.1016/j.est.2023.108694
8. Andrade, C. (2021): Z scores, standard scores, and composite test scores explained. *Indian Journal of Psychological Medicine*, 43(6), 555–557. https://doi.org/10.1177/02537176211046525
9. Antonanzas, J., Osorio, N., Escobar, R., Urraca, R., Martinez-de-Pison, F. J., & Antonanzas-Torres, F. (2016): Review of photovoltaic power forecasting. *Solar Energy*, 136, 78–111. https://doi.org/10.1016/j.solener.2016.06.069
10. Ardenas, B. C., Swinfen-Styles, L., Rouse, J., Hoskin, A., Xu, W., & Garvey, S. D. (2021): Energy storage capacity vs. renewable penetration: A study for the UK. *Renewable Energy*. https://doi.org/10.1016/j.renene.2021.02.149
11. Atsu, D., Seres, I., & Farkas, I. (2021): The state of solar PV and performance analysis of different PV technologies grid-connected installations in Hungary. *Renewable and Sustainable Energy Reviews*, 141. https://doi.org/10.1016/j.rser.2021.110808
12. Badwawi, R. Al, Abusara, M., & Mallick, T. (2016): A review of hybrid solar PV and wind energy system. 0477(2015). https://doi.org/10.1080/23080477.2015.11665647

13. Bai, S., Kolter, J. Z., & Koltun, V. (2018): An empirical evaluation of generic convolutional and recurrent networks for sequence modeling. https://doi.org/10.48550/arXiv.1803.01271

14. Barasa, M., Bogdanov, D., Oyewo, A. S., & Breyer, C. (2018): A cost optimal resolution for Sub-Saharan Africa powered by 100% renewables in 2030. *Renewable and Sustainable Energy Reviews*, 92(April), 440–457. https://doi.org/10.1016/j.rser.2018.04.110

15. Barbieri, F., Rajakaruna, S., & Ghosh, A. (2017): Very short-term photovoltaic power forecasting with cloud modeling: A review. *Renewable and Sustainable Energy Reviews*, 75(October 2016), 242–263. https://doi.org/10.1016/j.rser.2016.10.068

16. Becker, S., Frew, B. A., Andresen, G. B., Zeyer, T., Schramm, S., Greiner, M., & Jacobson, M. Z. (2014): Features of a fully renewable US electricity system: Optimized mixes of wind and solar PV and transmission grid extensions. *Energy*, 72, 443–458. https://doi.org/10.1016/j.energy.2014.05.067

17. Bird, L., Lew, D., Milligan, M., Carlini, E. M., Estanqueiro, A., Flynn, D., Gomez-Lazaro, E., Holttinen, H., Menemenlis, N., Orths, A., Eriksen, P. B., Smith, J. C., Soder, L., Sorensen, P., Altiparmakis, A., Yasuda, Y., & Miller, J. (2016): Wind and solar energy curtailment: A review of international experience. *Renewable and Sustainable Energy Reviews*, 65, 577–586. https://doi.org/10.1016/j.rser.2016.06.082

18. BloombergNEF (2023): BloombergNEF's annual battery price survey finds a 14% drop from 2022 to 2023. BloombergNEF. https://about.bnef.com/blog/lithium-ion-battery-pack-prices-hit-record-low-of-139-kwh/

19. Bloomfield, H. C., Brayshaw, D. J., Shaffrey, L. C., Coker, P. J., & Thornton, H. E. (2018): The changing sensitivity of power systems to meteorological drivers: A case study of Great Britain. *Environmental Research Letters*, 13(5). https://doi.org/10.1088/1748-9326/aabff9

20. Bloomfield, H. C., Wainwright, C. M., & Mitchell, N. (2022): Characterizing the variability and meteorological drivers of wind power and solar power generation over Africa. *Meteorological Applications*, 29(5), 1–19. https://doi.org/10.1002/met.2093

21. Bogdanov, D., Ram, M., Aghahosseini, A., Gulagi, A., Oyewo, A. S., Child, M., Caldera, U., Sadovskaia, K., Farfan, J., De Souza Noel Simas Barbosa, L., Fasihi, M., Khalili, S., Traber, T., & Breyer, C. (2021): Low-cost renewable electricity as the key driver of the global energy transition towards sustainability. *Energy*, 227, 120467. https://doi.org/10.1016/j.energy.2021.120467

22. Brester, C., Kallio-Myers, V., Lindfors, A. V., Kolehmainen, M., & Niska, H. (2023): Evaluating neural network models in site-specific solar PV forecasting using numerical weather prediction data and weather observations. *Renewable Energy*, 207(August 2022), 266–274. https://doi.org/10.1016/j.renene.2023.02.130

23. Breunig, H., Rosner, F., Saqline, S., Papadias, D., Grant, E., Brooks, K., Autrey, T., Ahluwalia, R., King, J., & Hammond, S. (2024): Achieving gigawatt-scale green hydrogen production and seasonal storage at industrial locations across the U.S. *Nature Communications*, 15(1), 9049. https://doi.org/10.1038/s41467-024-53189-2

24. Budischak, C., Sewell, D., Thomson, H., MacH, L., Veron, D. E., & Kempton, W. (2013): Cost-minimized combinations of wind power, solar power and electrochemical storage,

powering the grid up to 99.9% of the time. *Journal of Power Sources*, 225, 60–74. https://doi.org/10.1016/j.jpowsour.2012.09.054

25. Bullich-Massagué, E., Cifuentes-García, F. J., Glenny-Crende, I., Cheah-Mañé, M., Aragüés-Peñalba, M., Díaz-González, F., & Gomis-Bellmunt, O. (2020): A review of energy storage technologies for large scale photovoltaic power plants. *Applied Energy*, 274(June), 115213. https://doi.org/10.1016/j.apenergy.2020.115213
26. Camilo, F. M., Castro, R., Almeida, M. E., & Pires, V. F. (2017): Economic assessment of residential PV systems with self-consumption and storage in Portugal. *Solar Energy*, 150, 353–362. https://doi.org/10.1016/j.solener.2017.04.062
27. Cañete, C., Carretero, J., & Sidrach-de-Cardona, M. (2014): Energy performance of different photovoltaic module technologies under outdoor conditions. *Energy*, 65, 295–302. https://doi.org/10.1016/j.energy.2013.12.013
28. Cardo-Miota, J., Beltran, H., Pérez, E., & et al. (2025): Deep reinforcement learning-based strategy for maximizing returns from renewable energy and energy storage systems in multi-electricity markets. Applied Energy, 388, 125561. https://doi.org/10.1016/j.apenergy.2025.125561
29. Cauley, G. W., & Cook, D. N. (2011): In response to the Federal Energy Regulatory Commission's. 3801(202).
30. Chandel, R., Chandel, S. S., Prasad, D., & Dwivedi, R. P. (2024): Sustainable passive solar and photovoltaic integrated technology interventions for climate responsive net zero energy buildings in western Himalayan mountainous terrain of India. *Next Sustainability*, 3(November 2023), 100039. https://doi.org/10.1016/j.nxsust.2024.100039
31. Chauhan, A. (2017): Time series data mining for solar active region classification. May. https://doi.org/10.13140/RG.2.2.15327.05283
32. Child, M., & Breyer, C. (2016): The role of energy storage solutions in a 100% renewable Finnish energy system. *Energy Procedia*, 99(March), 25–34. https://doi.org/10.1016/j.egypro.2016.10.094
33. Cole, W., & Frazier, A. W. (2023): Cost projections for utility-scale battery storage: 2023 update. *National Renewable Energy Laboratory*, June, 20. https://www.nrel.gov/docs/fy23osti/85332.pdf
34. Cole, W. J., Greer, D., Denholm, P., Frazier, A. W., Machen, S., Mai, T., Vincent, N., & Baldwin, S. F. (2021): Quantifying the challenge of reaching a 100% renewable energy power system for the United States. *Joule*, 5(7), 1732–1748. https://doi.org/10.1016/j.joule.2021.05.011
35. Connolly, D., Lund, H., Mathiesen, B. V., & Leahy, M. (2010): A review of computer tools for analysing the integration of renewable energy into various energy systems. Applied Energy, 87(4), 1059–1082. https://doi.org/10.1016/j.apenergy.2009.09.026
36. Couto, A., & Estanqueiro, A. (2021). Assessment of wind and solar PV local complementarity for the hybridization of the wind power plants installed in Portugal. *Journal of Cleaner Production*, 319(August). https://doi.org/10.1016/j.jclepro.2021.128728
37. Dai, Q., Huo, X., Hao, Y., & Yu, R. (2023). Spatio-temporal prediction for distributed PV generation system based on deep learning neural network model. *Frontiers in Energy Research*, 11(June), 1–11. https://doi.org/10.3389/fenrg.2023.1204032

38. Daud, M. Z., Mohamed, A., Che Wanik, M. Z., & Hannan, M. A. (2012). Performance evaluation of grid-connected photovoltaic system with battery energy storage. *PECon 2012 - 2012 IEEE International Conference on Power and Energy*, December, 337–342. https://doi.org/10.1109/PECon.2012.6450234

39. Davis, N. N., Badger, J., Hahmann, A. N., Hansen, B. O., Mortensen, N. G., Kelly, M., Larsén, X. G., Olsen, B. T., Floors, R., Lizcano, G., Casso, P., Lacave, O., Bosch, A., Bauwens, I., Knight, O. J., Loon, A. P. Van, Fox, R., Parvanyan, T., Bo, S., … Drummond, R. (2023). The Global Wind Atlas. *Bulletin of the American Meteorological Society*, 104(8), 1507–1525.

40. de Oliveira e Silva, G., & Hendrick, P. (2017a). Photovoltaic self-sufficiency of Belgian households using lithium-ion batteries, and its impact on the grid. *Applied Energy*, 195, 786–799. https://doi.org/10.1016/j.apenergy.2017.03.112

41. Denholm, P. (2011). Enabling Technologies for High Penetration of Wind and Solar Energy. *ASME 2011 5th International Conference on Energy Sustainability, ES 2011*, 1451–1458.

42. Denholm, P., Arent, D. J., Baldwin, S. F., Bilello, D. E., Brinkman, G. L., Cochran, J. M., Cole, W. J., Frew, B., Gevorgian, V., Heeter, J., Hodge, B. M. S., Kroposki, B., Mai, T., O'Malley, M. J., Palmintier, B., Steinberg, D., & Zhang, Y. (2021). The challenges of achieving a 100% renewable electricity system in the United States. *Joule*, 5(6), 1331–1352. https://doi.org/10.1016/j.joule.2021.03.028

43. Denholm, P., Brown, P., Cole, W., Mai, T., Sergi, B., Brown, M., Jadun, P., Ho, J., Mayernik, J., McMillan, C., & Sreenath, R. (2022). Examining Supply-Side Options to Achieve 100% Clean Electricity by 2035. *NREL*, 161. www.nrel.gov/publications

44. Denholm, P., Cole, W., & Blair, N. (2023). Moving Beyond 4-Hour Li-Ion Batteries: Challenges and Opportunities for Long(er)-Duration Energy Storage. *NREL Technical Report - NREL/TP-6A40-85878*, September. https://www.nrel.gov/docs/fy23osti/85878.pdf

45. Denholm, P., Cole, W., Frazier, A. W., Podkaminer, K., & Blair, N. (2021). Storage Futures Study: The Four Phases of Storage Deployment: A Framework for the Expanding Role of Storage in the U.S. Power System. https://www.osti.gov/servlets/purl/1763974/

46. Denholm, P. L., Margolis, R. M., & Eichman, J. D. (2017). Evaluating the Technical and Economic Performance of PV Plus Storage Power Plants. *National Renewable Energy Laboratory*, August. https://doi.org/10.2172/1376049

47. Denholm, P., & Mai, T. (2019). Timescales of energy storage needed for reducing renewable energy curtailment. *Renewable Energy*, 130, 388–399. https://doi.org/10.1016/j.renene.2018.06.079

48. Denholm, P., & Margolis, R. M. (2007a). Evaluating the limits of solar photovoltaics (PV) in electric power systems utilizing energy storage and other enabling technologies. *Energy Policy*, 35(9), 4424–4433. https://doi.org/10.1016/j.enpol.2007.03.004

49. Denholm, P., & Margolis, R. M. (2007b). Evaluating the limits of solar photovoltaics (PV) in traditional electric power systems. *Energy Policy*, 35(5), 2852–2861. https://doi.org/10.1016/j.enpol.2006.10.014

50. Dhankar, U., Dahiya, S., & Chawla, R. (2025). Mitigating the Solar PV Landscape: A Comprehensive Review of Challenges and Innovations. Transactions on Electrical and Electronic Materials, 26(4), 429–456. https://doi.org/10.1007/s42341-025-00616-w

51. Dierckxsens, C., Woyte, A., Bletterie, B., Zegers, A., Deprez, W., Dexters, A., Roey, K. Van, Lemmens, J., Lowette, J., Nulens, K., Fawzy, Y. T., Blazic, B., Uljanic, B., & Kolenc, M. (2015). Cost-effective integration of photovoltaics in existing distribution grids: Results and recommendations. 64.

52. Diesendorf, M., & Elliston, B. (2018). The feasibility of 100% renewable electricity systems: A response to critics. *Renewable and Sustainable Energy Reviews*, 93, 318–330. https://doi.org/10.1016/j.rser.2018.05.042

53. Dolara, A., Grimaccia, F., Leva, S., Mussetta, M., & Ogliari, E. (2018). Comparison of training approaches for photovoltaic forecasts by means of machine learning. Applied Sciences, 8(2), 228. https://doi.org/10.3390/app8020228

54. Dujardin, J., Kahl, A., Kruyt, B., Bartlett, S., & Lehning, M. (2017a). Interplay between photovoltaic, wind energy and storage hydropower in a fully renewable Switzerland. *Energy*, 135, 513–525. https://doi.org/10.1016/j.energy.2017.06.092

55. Sebastian, S., Wijewardane, S., & Srinivasan, S. (2023). Recent advances in hydrogen production, storage, and fuel cell Technologies with an emphasis on inventions, innovations, and commercialization. Solar Compass, 8, 100065. https://doi.org/10.1016/j.solcom.2023.100065

56. Elliston, B., Riesz, J., & MacGill, I. (2016). What cost for more renewables? The incremental cost of renewable generation - An Australian National Electricity Market case study. *Renewable Energy*, 95, 127–139. https://doi.org/10.1016/j.renene.2016.03.080

57. Elmousaid, R., Drioui, N., Elgouri, R., Agueny, H., & Adnani, Y. (2024). Ultra-short-term global horizontal irradiance forecasting based on a novel and hybrid GRU-TCN model. *Results in Engineering*, 23(August), 102817. https://doi.org/10.1016/j.rineng.2024.102817

58. Eltawil, M. A., & Zhao, Z. (2010). Grid-connected photovoltaic power systems: Technical and potential problems - A review. *Renewable and Sustainable Energy Reviews*, 14(1), 112–129. https://doi.org/10.1016/j.rser.2009.07.015

59. Fattahi, A., Sijm, J., & Faaij, A. (2020). A systemic approach to analyze integrated energy system modeling tools: A review of national models. *Renewable and Sustainable Energy Reviews*, 133(November 2019), 110195. https://doi.org/10.1016/j.rser.2020.110195

60. Femin, V., Petra, M. I., Mathew, S., Hazra, J., & Ismail, H. (2016). Modeling the Temporal Variations in the Output of Large Solar PV Power Plants. *Energy Procedia*, 95, 294–301. https://doi.org/10.1016/j.egypro.2016.09.005

61. Fernández, L. (2023). Global solar PV installed cost 2010-2022. *Statista*. https://www.statista.com/statistics/809796/global-solar-power-installation-cost-per-kilowatt/

62. Frazier, A. W., Cole, W., Denholm, P., Machen, S., Gates, N., & Blair, N. (2021). Storage Futures Study: Economic Potential of Diurnal Storage in the U.S. Power Sector. *NREL/TP-6A20-77449*. https://www.nrel.gov/docs/fy21osti/77449.pdf

63. Frew, B., Sergi, B., Denholm, P., Cole, W., Gates, N., Levie, D., & Margolis, R. (2021). The curtailment paradox in the transition to high solar power systems. *Joule*, 5(5), 1143–1167. https://doi.org/10.1016/j.joule.2021.03.021

64. Gabrielli, P., Poluzzi, A., Kramer, G. J., Spiers, C., Mazzotti, M., & Gazzani, M. (2020). Seasonal energy storage for zero-emissions multi-energy systems via underground

hydrogen storage. *Renewable and Sustainable Energy Reviews*, 121, 109629. https://doi.org/10.1016/j.rser.2019.109629

65. Gallo, A. B., Simões-Moreira, J. R., Costa, H. K. M., Santos, M. M., & Moutinho dos Santos, E. (2016). Energy storage in the energy transition context: A technology review. *Renewable and Sustainable Energy Reviews*, 65, 800–822. https://doi.org/10.1016/j.rser.2016.07.028

66. Ghebrezgabher, M. G., Yang, T., Yang, X., Wang, X., & Khan, M. (2016). Extracting and analyzing forest and woodland cover change in Eritrea based on landsat data using supervised classification. *Egyptian Journal of Remote Sensing and Space Science*, 19(1), 37–47. https://doi.org/10.1016/j.ejrs.2015.09.002

67. Gils, H. C., Scholz, Y., Pregger, T., Luca de Tena, D., & Heide, D. (2017). Integrated modelling of variable renewable energy-based power supply in Europe. *Energy*, 123, 173–188. https://doi.org/10.1016/j.energy.2017.01.115

68. Golden, R., & Paulos, B. (2015). Energy in California and. *The Electricity Journal*, 28(6), 36–50. http://dx.doi.org/10.1016/j.tej.2015.06.008

69. Graabak, I., & Korpås, M. (2016). Variability Characteristics of European Wind and Solar Power Resources—A Review. *Energies*, 9(6). https://doi.org/10.3390/en9060449

70. Gu, Y., & Xie, L. (2014). Fast Sensitivity Analysis Approach to Assessing Congestion Induced Wind Curtailment. *IEEE Transactions on Power Systems*, 29(101–110). https://doi,org: 10.1109/TPWRS.2013.2282286

71. Gudmunds, D., Nyholm, E., Taljegard, M., & Odenberger, M. (2020). Self-consumption and self-sufficiency for household solar producers when introducing an electric vehicle. *Renewable Energy*, 148. https://doi.org/10.1016/j.renene.2019.10.030

72. Guerra, O. J., Eichman, J., & Denholm, P. (2021). Optimal energy storage portfolio for high and ultrahigh carbon-free and renewable power systems. *Energy and Environmental Science*, 14(10), 5132–5146. https://doi.org/10.1039/d1ee01835c

73. Guerra, O. J., Zhang, J., Eichman, J., Denholm, P., Kurtz, J., & Hodge, B. M. (2020a). The value of seasonal energy storage technologies for the integration of wind and solar power. *Energy and Environmental Science*, 13(7), 1909–1922. https://doi.org/10.1039/d0ee00771d

74. Guezgouz, M., Jurasz, J., Bekkouche, B., Ma, T., Javed, M. S., and Kies, A. (2019): Optimal hybrid pumped hydro-battery storage scheme for off-grid renewable energy systems. *Energy Conversion and Management*, 199, 112046. https://doi.org/10.1016/j.enconman.2019.112046

75. Hajjaj, C., El Ydrissi, M., Azouzoute, A., Oufadel, A., El Alani, O., Boujoudar, M., Abraim, M., and Ghennioui, A. (2023): Comparing photovoltaic power prediction: Ground-based measurements vs. satellite data using an ANN model. *IEEE Journal of Photovoltaics*, 13(6), 998–1006. https://doi.org/10.1109/JPHOTOV.2023.3306827

76. Hansen, A. D., Poul Sørensen, L. H., and Bindner, H. (2000): Models for a stand-alone PV system. *Risø National Laboratory*

77. Hansen, K., Mathiesen, B. V., and Skov, I. R. (2019): Full energy system transition towards 100% renewable energy in Germany in 2050. *Renewable and Sustainable Energy Reviews*, 102, 1–13. https://doi.org/10.1016/j.rser.2018.11.038

78. Hasan, R., Mekhilef, S., Seyedmahmoudian, M., and Horan, B. (2017): Grid-connected isolated PV microinverters: A review. *Renewable and Sustainable Energy Reviews*, 67, 1065–1080. https://doi.org/10.1016/j.rser.2016.09.082

79. Hassaine, L., Olias, E., Quintero, J., and Salas, V. (2014): Overview of power inverter topologies and control structures for grid connected photovoltaic systems. *Renewable and Sustainable Energy Reviews*, 30, 796–807. https://doi.org/10.1016/j.rser.2013.11.005

80. Heide, D., Greiner, M., von Bremen, L., and Hoffmann, C. (2011): Reduced storage and balancing needs in a fully renewable European power system with excess wind and solar power generation. *Renewable Energy*, 36(9), 2515–2523. https://doi.org/10.1016/j.renene.2011.02.009

81. Heide, D., von Bremen, L., Greiner, M., Hoffmann, C., Speckmann, M., and Bofinger, S. (2010): Seasonal optimal mix of wind and solar power in a future, highly renewable Europe. *Renewable Energy*, 35(11), 2483–2489. https://doi.org/10.1016/j.renene.2010.03.012

82. Held, L., Armbruster, M., Zimmerlin, M., Suriyah, M. R., Leibfried, T., and Hoche, R. (2020): The operation of a battery storage system to avoid overvoltages in a low voltage grid. *6th IEEE International Energy Conference, ENERGYCon 2020*, 321–325. https://doi.org/10.1109/ENERGYCon48941.2020.9236533

83. Henriot, A. (2015): Economic curtailment of intermittent renewable energy sources. *Energy Economics*, 49, 370–379. https://doi.org/10.1016/j.eneco.2015.03.002

84. Heuberger, C. F., and Mac Dowell, N. (2018): Real-world challenges with a rapid transition to 100% renewable power systems. *Joule*, 2(3), 367–370. https://doi.org/10.1016/j.joule.2018.02.002

85. Hirschl, B. (2009): International renewable energy policy—between marginalization and initial approaches. *Energy Policy*, 37(11), 4407–4416. https://doi.org/10.1016/j.enpol.2009.05.059

86. Hirth, L., and Ziegenhagen, I. (2015): Balancing power and variable renewables: Three links. *Renewable and Sustainable Energy Reviews*, 50, 1035–1051. https://doi.org/10.1016/j.rser.2015.04.180

87. Hochreiter, S., and Schmidhuber, J. (1997): Long short-term memory. *Neural Computation*, 9(8), 1735–1780. https://doi.org/10.1162/neco.1997.9.8.1735

88. Hossain, M. A., Xu, Y., Peshek, T. J., Ji, L., Abramson, A. R., and French, R. H. (2015): Microinverter thermal performance in the real-world: Measurements and modeling. *PLoS ONE*, 10(7). https://doi.org/10.1371/journal.pone.0131279

89. Hossain, E., Tur, M.R., Padmanaban, S., Ay, S., Khan, I., 2018. Analysis and Mitigation of Power Quality Issues in Distributed Generation Systems Using Custom Power Devices. IEEE Access 6, 16816–16833. https://doi.org/10.1109/ACCESS.2018.2814981

90. Huang, Y., Lu, J., Liu, C., Xu, X., Wang, W., and Zhou, X. (2010): Comparative study of power forecasting methods for PV stations. *2010 International Conference on Power System Technology: Technological Innovations Making Power Grid Smarter, POWERCON2010*, 1–6. https://doi.org/10.1109/POWERCON.2010.5666688

91. Huld, T., Müller, R., and Gambardella, A. (2012): A new solar radiation database for estimating PV performance in Europe and Africa. *Solar Energy*, 86(6), 1803–1815. https://doi.org/10.1016/j.solener.2012.03.006

92. IEA (2025), Electricity 2025, IEA, Paris https://www.iea.org/reports/electricity-2025, Licence: CC BY 4.0

93. IEA (2024), Renewables 2023, IEA, Paris https://www.iea.org/reports/renewables-2023, Licence: CC BY 4.0

94. Inman, R. H., Pedro, H. T. C., and Coimbra, C. F. M. (2013): Solar forecasting methods for renewable energy integration. *Progress in Energy and Combustion Science*, 39(6), 535–576. https://doi.org/10.1016/j.pecs.2013.06.002

95. IRENA. (2019): *Enabling Technologies: Innovation Landscape*.

96. IRENA(2023): *Renewable Capacity Statistics 2023*. IRENA. www.irena.org

97. Jacobson, M. Z., Delucchi, M. A., Cameron, M. A., Coughlin, S. J., Hay, C. A., Manogaran, I. P., Shu, Y., and von Krauland, A. K. (2019): Impacts of Green New Deal energy plans on grid stability, costs, jobs, health, and climate in 143 countries. *One Earth*, 1(4), 449–463. https://doi.org/10.1016/j.oneear.2019.12.003

98. Jain, S., and Agarwal, V. (2007): New current control based MPPT technique for single stage grid-connected PV systems. *Energy Conversion and Management*, 48(2), 625–644. https://doi.org/10.1016/j.enconman.2006.05.018

99. Javed, M. S., Song, A., and Ma, T. (2019): Techno-economic assessment of a stand-alone hybrid solar-wind-battery system for a remote island using genetic algorithm. *Energy*, 176, 704–717. https://doi.org/10.1016/j.energy.2019.03.131

100. Jean-Michel, G. (2021): *Handbook on Electricity Markets*. Edward Elgar Publishing.

101. Jordehi, A. R. (2016): Parameter estimation of solar photovoltaic (PV) cells: A review. *Renewable and Sustainable Energy Reviews*, 61, 354–371. https://doi.org/10.1016/j.rser.2016.03.049

102. Jurasz, J., Canales, F. A., Kies, A., Guezgouz, M., and Beluco, A. (2020a): A review on the complementarity of renewable energy sources: Concept, metrics, application and future research directions. *Solar Energy*, 195, 703–724. https://doi.org/10.1016/j.solener.2019.11.087

103. Kabalcı, E. (2020): Review on novel single-phase grid-connected solar inverters: Circuits and control methods. *Solar Energy*, 198, 247–274. https://doi.org/10.1016/j.solener.2020.01.063

104. Kavlak, G., McNerney, J., and Trancik, J. E. (2018): Evaluating the causes of cost reduction in photovoltaic modules. *Energy Policy*, 123, 700–710. https://doi.org/10.1016/j.enpol.2018.08.015

105. Kbret Solomon. (2006): *Wind and Solar Monitoring Network Summary Report*.

106. Kebede, A.A., Kalogiannis, T., Van Mierlo, J., et al., 2022. A comprehensive review of stationary energy storage devices for large scale renewable energy sources grid integration. Renew. Sustain. Energy Rev. 159, 112213. https://doi.org/10.1016/j.rser.2022.112213

107. Kenneth, A. P., and Folly, K. (2014): Voltage rise issue with high penetration of grid-connected PV. *IFAC Proceedings Volumes (IFAC-PapersOnline)*, 19(3). https://doi.org/10.3182/20140824-6-za-1003.01989

108. Khan, M. A., Haque, A., Kurukuru, V. S. B., and Saad, M. (2022): Islanding detection techniques for grid-connected photovoltaic systems—a review. *Renewable and Sustainable Energy Reviews*, 154, 111854. https://doi.org/10.1016/j.rser.2021.111854

109. Kjaer, S. B., Pedersen, J. K., and Blaabjerg, F. (2005): A review of single-phase grid-connected inverters for photovoltaic modules. *IEEE Transactions on Industry Applications*, 41(5), 1292–1306. https://doi.org/10.1109/TIA.2005.853371

110. Kouro, S., Leon, J. I., Vinnikov, D., and Franquelo, L. G. (2015): Grid-connected photovoltaic systems: An overview of recent research and emerging PV converter technology. *IEEE Industrial Electronics Magazine*, 9(1), 47–61. https://doi.org/10.1109/MIE.2014.2376976

111. Krizhevsky, A., Sutskever, I., and Hinton, G. E. (2017): ImageNet classification with deep convolutional neural networks. *Communications of the ACM*, 60(6), 84–90. https://doi.org/10.1145/3065386

112. Kroposki, B., Johnson, B., Zhang, Y., Gevorgian, V., Denholm, P., Hodge, B. M., and Hannegan, B. (2017): Achieving a 100% renewable grid: Operating electric power systems with extremely high levels of variable renewable energy. *IEEE Power and Energy Magazine*, 15(2), 61–73. https://doi.org/10.1109/MPE.2016.2637122

113. Li, Y., Gao, W., and Ruan, Y. (2018): Performance investigation of grid-connected residential PV-battery system focusing on enhancing self-consumption and peak shaving in Kyushu, Japan. *Renewable Energy*, 127, 514–523. https://doi.org/10.1016/j.renene.2018.04.074

114. Li, Y., He, Y., Su, Y., and Shu, L. (2016): Forecasting the daily power output of a grid-connected photovoltaic system based on multivariate adaptive regression splines. *Applied Energy*, 180, 392–401. https://doi.org/10.1016/j.apenergy.2016.07.052

115. Li, Z., Liu, Y., Du, M., Cheng, Y., and Shi, L. (2023): Modeling and multi-objective optimization of a stand-alone photovoltaic-wind turbine-hydrogen-battery hybrid energy system. *International Journal of Hydrogen Energy*, 48(22), 7959–7974. https://doi.org/10.1016/j.ijhydene.2022.11.196

116. Limouni, T., Yaagoubi, R., Bouziane, K., Guissi, K., and Baali, E. H. (2022): Univariate and multivariate LSTM models for one step and multistep PV power forecasting. *International Journal of Renewable Energy Development*, 11(3), 815–828. https://doi.org/10.14710/ijred.2022.43953

117. Limouni, T., Yaagoubi, R., Bouziane, K., Guissi, K., and Baali, E. H. (2023): Accurate one step and multistep forecasting of very short-term PV power using LSTM-TCN model. *Renewable Energy*, 205, 1010–1024. https://doi.org/10.1016/j.renene.2023.01.118

118. Luceño-Sánchez, J. A., Díez-Pascual, A. M., and Capilla, R. P. (2019): Materials for photovoltaics: State of art and recent developments. *International Journal of Molecular Sciences*, 20(4). https://doi.org/10.3390/ijms20040976

119. Mai, T., Denholm, P., Brown, P., Cole, W., Hale, E., Lamers, P., Murphy, C., Ruth, M., Sergi, B., Steinberg, D., and Baldwin, S. F. (2022): Getting to 100%: Six strategies for the challenging last 10%. *Joule*, 6(9), 1981–1994. https://doi.org/10.1016/j.joule.2022.08.004

120. Mansouri, N., Lashab, A., Guerrero, J. M., and Cherif, A. (2020): Photovoltaic power plants in electrical distribution networks: A review on their impact and solutions. *IET Renewable Power Generation*, 14(12), 2114–2125. https://doi.org/10.1049/iet-rpg.2019.1172

121. Mansouri, N., Lashab, A., Sera, D., Guerrero, J. M., and Cherif, A. (2019): Large photovoltaic power plants integration: A review of challenges and solutions. *Energies*, 12(19). https://doi.org/10.3390/en12193798

122. Mateo, C., Frías, P., Cossent, R., Sonvilla, P., and Barth, B. (2017): Overcoming the barriers that hamper a large-scale integration of solar photovoltaic power generation in European distribution grids. *Solar Energy*, 153, 574–583. https://doi.org/10.1016/j.solener.2017.06.008

123. Mazorra Aguiar, L., Pereira, B., David, M., Díaz, F., and Lauret, P. (2015): Use of satellite data to improve solar radiation forecasting with Bayesian artificial neural networks. *Solar Energy*, 122, 1309–1324. https://doi.org/10.1016/j.solener.2015.10.041

124. Mellit, A., Massi Pavan, A., and Lughi, V. (2014): Short-term forecasting of power production in a large-scale photovoltaic plant. *Solar Energy*, 105, 401–413. https://doi.org/10.1016/j.solener.2014.03.018

125. Mensah, T. N. O., Oyewo, A. S., and Breyer, C. (2021): The role of biomass in sub-Saharan Africa's fully renewable power sector – The case of Ghana. *Renewable Energy*, 173, 297–317. https://doi.org/10.1016/j.renene.2021.03.098

126. Meuris, M., Lodewijks, P., Ponnette, R., Meinke-Hubeny, F., Valkering, P., Belmans, R., and Poortmans, J. (2019): Managing PV power injection and storage, enabling a larger direct consumption of renewable energy: A case study for the Belgian electricity system. *Progress in Photovoltaics: Research and Applications*, 27(11), 905–917. https://doi.org/10.1002/pip.3084

127. Miglietta, M. M., Huld, T., and Monforti-Ferrario, F. (2017): Local complementarity of wind and solar energy resources over Europe: An assessment study from a meteorological perspective. *Journal of Applied Meteorology and Climatology*, 56(1), 217–234. https://doi.org/10.1175/JAMC-D-16-0031.1

128. Miles, R. W., Hynes, K. M., and Forbes, I. (2005): Photovoltaic solar cells: An overview of state-of-the-art cell development and environmental issues. *Progress in Crystal Growth and Characterization of Materials*, 51(1–3), 1–42. https://doi.org/10.1016/j.pcrysgrow.2005.10.002

129. Ministry of Energy and Mines. (2022): *Dekemhare Solar Power Project*, 1–229.

130. Ministry of Information. (2018): Securing the future through renewable energy. https://shabait.com/2018/07/07/securing-the-future-through-renewable-energy/

131. Mirhassani, S., Ong, H. C., Chong, W. T., and Leong, K. Y. (2015): Advances and challenges in grid-tied photovoltaic systems. *Renewable and Sustainable Energy Reviews*, 49, 121–131. https://doi.org/10.1016/j.rser.2015.04.064

132. Mulder, F. M. (2014): Implications of diurnal and seasonal variations in renewable energy generation for large scale energy storage. *Journal of Renewable and Sustainable Energy*, 6(3). https://doi.org/10.1063/1.4874845

133. Naeem, A., Hassan, N. U., Yuen, C., and Muyeen, S. M. (2019): Maximizing the economic benefits of a grid-tied microgrid using solar-wind complementarity. *Energies*, 12(3). https://doi.org/10.3390/en12030395

134. Nayak, P. K., Mahesh, S., Snaith, H. J., and Cahen, D. (2019): Photovoltaic solar cell technologies: analysing the state of the art. *Nature Reviews Materials*, 4(4), 269–285. http://doi.org/10.1038/s41578-019-0097-0

135. Negash, T., Asfaw, S., Ottermo, F., Möllerström, E., Istvan, F., and Istvan, S. (2023): System design issues of high renewable energy system, the case of Eritrea. *SSRN Electronic Journal*.

136. Negash, T., Möllerström, E., and Ottermo, F. (2020): An assessment of wind energy potential for the three topographic regions of Eritrea. *Energies*, 13(7). https://doi.org/10.3390/en13071846

137. Negash, T., Weldemikael, N., & Ghebregziabiher, M. (2025). Addressing photovoltaic (PV) forecasting challenges : Satellite-driven data models for predicting actual PV generation using hybrid (LSTM-GRU) model. 14(August), 2141–2156. https://doi.org/10.1016/j.egyr.2025.08.034

138. Noyanbayev, N. K., Forsyth, A. J., and Feehally, T. (2018): Efficiency analysis for a grid-connected battery energy storage system. *Materials Today: Proceedings*, 5(11), 22811–22818. https://doi.org/10.1016/j.matpr.2018.07.095

139. NREL (2025): Interactive Best Research-Cell Efficiency Chart. National Renewable Energy Laboratory (Photovoltaic Research).

140. Obi, M., and Bass, R. (2016): Trends and challenges of grid-connected photovoltaic systems—a review. *Renewable and Sustainable Energy Reviews*, 58, 1082–1094. https://doi.org/10.1016/j.rser.2015.12.289

141. Olayiwola, T. N., Hyun, S. H., and Choi, S. J. (2024): Photovoltaic modeling: A comprehensive analysis of the I–V characteristic curve. *Sustainability (Switzerland)*, 16(1). https://doi.org/10.3390/su16010432

142. Ourya, I., Nabil, N., Abderafi, S., Boutammachte, N., and Rachidi, S. (2023): Assessment of green hydrogen production in Morocco, using hybrid renewable sources (PV and wind). *International Journal of Hydrogen Energy*, 48(96), 37428–37442. https://doi.org/10.1016/j.ijhydene.2022.12.362

143. Oyewo, A. S., Aghahosseini, A., Ram, M., and Breyer, C. (2020): Transition towards decarbonised power systems and its socio-economic impacts in West Africa. *Renewable Energy*, 154, 1092–1112. https://doi.org/10.1016/j.renene.2020.03.085

144. Oyewo, A. S., Aghahosseini, A., Ram, M., Lohrmann, A., and Breyer, C. (2019): Pathway towards achieving 100% renewable electricity by 2050 for South Africa. *Solar Energy*, 191, 549–565. https://doi.org/10.1016/j.solener.2019.09.039

145. Oyewo, A. S., Solomon, A. A., Bogdanov, D., Aghahosseini, A., Mensah, T. N. O., Ram, M., and Breyer, C. (2021): Just transition towards defossilised energy systems for developing economies: A case study of Ethiopia. *Renewable Energy*, 176, 346–365. https://doi.org/10.1016/j.renene.2021.05.029

146. Palmintier, B. S., and Webster, M. D. (2016): Impact of operational flexibility on electricity generation planning with renewable and carbon targets. *IEEE Transactions on Sustainable Energy*, 7(2), 672–684. https://doi.org/10.1109/TSTE.2015.2498640

147. Perez, M., Perez, R., Rábago, K. R., and Putnam, M. (2019): Overbuilding & curtailment: The cost-effective enablers of firm PV generation. *Solar Energy*, 180, 412–422. https://doi.org/10.1016/j.solener.2018.12.074

148. Pierro, M., Bucci, F., De Felice, M., Maggioni, E., Perotto, A., Spada, F., Moser, D., and Cornaro, C. (2017): Deterministic and stochastic approaches for day-ahead solar power

forecasting. *Journal of Solar Energy Engineering, Transactions of the ASME*, 139(2), 1–12. https://doi.org/10.1115/1.4034823

149. Procopiou, A. T., Petrou, K., Ochoa, L. F., Langstaff, T., and Theunissen, J. (2019): Adaptive decentralized control of residential storage in PV-rich MV-LV networks. *IEEE Transactions on Power Systems*, 34(3), 2378–2389. https://doi.org/10.1109/TPWRS.2018.2889843

150. Qiu, Y., Li, Q., Ai, Y., Wang, T., Chen, W., Bai, H., Benbouzid, M., Liu, S., and Gao, F. (2024): Optimal scheduling for microgrids considering long-term and short-term energy storage. *Journal of Energy Storage*, 93. https://doi.org/10.1016/j.est.2024.112137

151. Quaschning, V. (2016). Understanding Renewable Energy Systems (2nd ed.). Routledge. https://doi.org/10.4324/9781315769431

152. Quoilin, S., Kavvadias, K., Mercier, A., Pappone, I., and Zucker, A. (2016): Quantifying self-consumption linked to solar home battery systems: Statistical analysis and economic assessment. *Applied Energy*, 182, 58–67. https://doi.org/10.1016/j.apenergy.2016.08.077

153. Rahman, M. M., Oni, A. O., Gemechu, E., and Kumar, A. (2020): Assessment of energy storage technologies: A review. *Energy Conversion and Management*, 223, 113295. https://doi.org/10.1016/j.enconman.2020.113295

154. Rakhshani, E., Rouzbehi, K., Sánchez, A. J., Tobar, A. C., and Pouresmaeil, E. (2019): Integration of large scale PV-based generation into power systems: A survey. *Energies*, 12(8). https://doi.org/10.3390/en12081425

155. Rehman, F., Syed, I. H., Khanam, S., Ijaz, S., Mehmood, H., Zubair, M., Massoud, Y., and Mehmood, M. Q. (2023): Fourth-generation solar cells: A review. *Energy Advances*, 2(9), 1239–1262. https://doi.org/10.1039/d3ya00179b

156. Ren, G., Liu, J., Wan, J., Wang, W., Fang, F., Hong, F., and Yu, D. (2022): Investigating the complementarity characteristics of wind and solar power for load matching based on the typical load demand in China. *IEEE Transactions on Sustainable Energy*, 13(2), 778–790. https://doi.org/10.1109/TSTE.2021.3131560

157. Ren, G., Wan, J., Liu, J., and Yu, D. (2019): Spatial and temporal assessments of complementarity for renewable energy resources in China. *Energy*, 177, 262–275. https://doi.org/10.1016/j.energy.2019.04.023

158. Rosen, K., Van Buskirk, R., and Garbesi, K. (1999): Wind energy potential of coastal Eritrea: An analysis of sparse wind data. *Solar Energy*, 66(3), 201–213. https://doi.org/10.1016/S0038-092X(99)00026-2

159. Ruf, H. (2018): Limitations for the feed-in power of residential photovoltaic systems in Germany – An overview of the regulatory framework. *Solar Energy*, 159, 588–600. https://doi.org/10.1016/j.solener.2017.10.072

160. Sadiqa, A., Gulagi, A., and Breyer, C. (2018): Energy transition roadmap towards 100% renewable energy and role of storage technologies for Pakistan by 2050. *Energy*, 147, 518–533. https://doi.org/10.1016/j.energy.2018.01.027

161. Sangrody, H., Sarailoo, M., Zhou, N., Shokrollahi, A., and Foruzan, E. (2017): On the performance of forecasting models in the presence of input uncertainty. *2017 North American Power Symposium (NAPS)*. https://doi.org/10.1109/NAPS.2017.8107379

162. Sangster, A. J. (2014): Solar photovoltaics. *Green Energy and Technology*, 194(4), 145–172. https://doi.org/10.1007/978-3-319-08512-8_7

163. Schmela, M., Rossi, R., Lits, C., Chunduri, S. K., Shah, A., Muthyal, R., ... & Saratchandra, P. (2023). Advancements in solar technology, markets, and investments–a summary of the 2022 ISA World Solar Reports, Sol. Compass 6 (2023) 100045. https://doi.org/10.1016/j.solcom.2023.100045

164. Shaner, M. R., Davis, S. J., Lewis, N. S., and Caldeira, K. (2018): Geophysical constraints on the reliability of solar and wind power in the United States. *Energy and Environmental Science*, 11(4), 914–925. https://doi.org/10.1039/c7ee03029k

165. Shubbak, M. H. (2019): Advances in solar photovoltaics: Technology review and patent trends. *Renewable and Sustainable Energy Reviews*, 115. https://doi.org/10.1016/j.rser.2019.109383

166. Simoes, S., Zeyringer, M., Mayr, D., Huld, T., Nijs, W., and Schmidt, J. (2017): Impact of different levels of geographical disaggregation of wind and PV electricity generation in large energy system models: A case study for Austria. *Renewable Energy*, 105, 183–198. https://doi.org/10.1016/j.renene.2016.12.020

167. Soham, D., and Bhasme, N. R. (2017): A review of topologies of inverter for grid connected PV systems. *International Conference on Innovations in Power and Advanced Computing Technologies. https://doi.org/ 10.1109/IPACT.2017.8245191*

168. Solomon, A. A. (2019a): Large scale photovoltaics and the future energy system requirement. *AIMS Energy*, 7(5), 600–618. https://doi.org/10.3934/energy.2019.5.600

169. Solomon, A. A., Bogdanov, D., and Breyer, C. (2019b): Curtailment-storage-penetration nexus in the energy transition. *Applied Energy*, 235, 1351–1368. https://doi.org/10.1016/j.apenergy.2018.11.069

170. Solomon, A. A., Child, M., Caldera, U., and Breyer, C. (2017): How much energy storage is needed to incorporate very large intermittent renewables? *Energy Procedia*, 135, 283–293. https://doi.org/10.1016/j.egypro.2017.09.520

171. Solomon, A. A., Child, M., Caldera, U., and Breyer, C. (2020): Exploiting wind-solar resource complementarity to reduce energy storage need. *AIMS Energy*, 8(5), 749–770. https://doi.org/10.3934/ENERGY.2020.5.749

172. Solomon, A. A., Faiman, D., and Meron, G. (2010a): An energy-based evaluation of the matching possibilities of very large photovoltaic plants to the electricity grid: Israel as a case study. *Energy Policy*, 38(10), 5457–5468. https://doi.org/10.1016/j.enpol.2009.12.024

173. Solomon, A. A., Faiman, D., and Meron, G. (2010b): Grid matching of large-scale wind energy conversion systems, alone and in tandem with large-scale photovoltaic systems: An Israeli case study. *Energy Policy*. https://doi.org/10.1016/j.enpol.2010.07.026

174. Solomon, A. A., Faiman, D., and Meron, G. (2010c): Properties and uses of storage for enhancing the grid penetration of very large photovoltaic systems. *Energy Policy*, 38(9), 5208–5222. https://doi.org/10.1016/j.enpol.2010.05.006

175. Solomon, A. A., Faiman, D., and Meron, G. (2012a): The role of conventional power plants in a grid fed mainly by PV and storage, and the largest shadow capacity requirement. *Energy Policy*, 48, 479–486. https://doi.org/10.1016/j.enpol.2012.05.050

176. Solomon, A. A., Faiman, D., and Meron, G. (2012b): Appropriate storage for high-penetration grid-connected photovoltaic plants. *Energy Policy*, 40, 335–344. https://doi.org/10.1016/j.enpol.2011.10.019

177. Solomon, A. A., Kammen, D. M., and Callaway, D. (2014): The role of large-scale energy storage design and dispatch in the power grid: A study of very high grid penetration of variable renewable resources. *Applied Energy*, 134, 75–89. https://doi.org/10.1016/j.apenergy.2014.07.095

178. Solomon, A. A., Kammen, D. M., and Callaway, D. (2016): Investigating the impact of wind-solar complementarities on energy storage requirement and the corresponding supply reliability criteria. *Applied Energy*, 168, 130–145. https://doi.org/10.1016/j.apenergy.2016.01.070

179. Solomon, A. A., Sahin, H., and Breyer, C. (2024): The pitfall in designing future electrical power systems without considering energy return on investment in planning. *Applied Energy*, 369, 123570. https://doi.org/10.1016/j.apenergy.2024.123570

180. Subiyanto, M., Mohamed, A., and Hannan, M. A. (2009): Maximum power point tracking in grid connected PV system using a novel fuzzy logic controller. SCOReD2009 - Proceedings of 2009 IEEE Student Conference on Research and Development, 349–352. https://doi.org/10.1109/SCORED.2009.5443002

181. Tajjour, S., and Singh Chandel, S. (2023): A comprehensive review on sustainable energy management systems for optimal operation of future-generation of solar microgrids. Sustainable Energy Technologies and Assessments, 58(July). https://doi.org/10.1016/j.seta.2023.103377

182. Teklebrhan, N., Solomon, A. A., Ottermo, F., Möllerström, E., Seres, I., and Farkas, I. (2025): Strategies for integrating residential PV and wind energy in Eritrea's electricity grid by imposing feed-in constraints in low voltage network. Solar Energy, 286(September). https://doi.org/10.1016/j.solener.2024.113140

183. Teske, S. (2022): Achieving the Paris Climate Agreement Goals. https://doi.org/10.1007/978-3-030-99177-7

184. Torreglosa, J. P., García, P., Fernández, L. M., and Jurado, F. (2015): Energy dispatching based on predictive controller of an off-grid wind turbine/photovoltaic/hydrogen/battery hybrid system. Renewable Energy, 74, 326–336. https://doi.org/10.1016/j.renene.2014.08.010

185. Twitchell, J., DeSomber, K., and Bhatnagar, D. (2023): Defining long duration energy storage. Journal of Energy Storage, 60(August 2022), 105787. https://doi.org/10.1016/j.est.2022.105787

186. Udayakumar, M. D., Anushree, G., Sathyaraj, J., and Manjunathan, A. (2021): The impact of advanced technological developments on solar PV value chain. Materials Today: Proceedings, 45(March 2020), 2053–2058. https://doi.org/10.1016/j.matpr.2020.09.588

187. Vinod, Kumar, R., and Singh, S. K. (2018): Solar photovoltaic modeling and simulation: As a renewable energy solution. Energy Reports, 4, 701–712. https://doi.org/10.1016/j.egyr.2018.09.008

188. Voyant, C., Notton, G., Kalogirou, S., Nivet, M. L., Paoli, C., Motte, F., and Fouilloy, A. (2017): Machine learning methods for solar radiation forecasting: A review. Renewable Energy, 105, 569–582. https://doi.org/10.1016/j.renene.2016.12.095

189. Wang, X., Liesaputra, V., Liu, Z., Wang, Y., and Huang, Z. (2024): An in-depth survey on Deep Learning-based Motor Imagery Electroencephalogram (EEG) classification. Artificial Intelligence in Medicine, 147(November 2023), 102738. https://doi.org/10.1016/j.artmed.2023.102738

190. Yaro, A. S., Maly, F., and Prazak, P. (2023): Outlier Detection in Time-Series Receive Signal Strength Observation Using Z-Score Method with Sn Scale Estimator for Indoor Localization. Applied Sciences (Switzerland), 13(6). https://doi.org/10.3390/app13063900

191. Ye, H., Yang, B., Han, Y., and Chen, N. (2022): State-of-the-art solar energy forecasting approaches: Critical potentials and challenges. Frontiers in Energy Research, 10(March), 1–5. https://doi.org/10.3389/fenrg.2022.875790

192. Zakeri, B., and Syri, S. (2015): Electrical energy storage systems: A comparative life cycle cost analysis. Renewable and Sustainable Energy Reviews, 42, 569–596. https://doi.org/10.1016/j.rser.2014.10.011

193. Zeb, K., Uddin, W., Khan, M. A., Ali, Z., Ali, M. U., Christofides, N., and Kim, H. J. (2018): A comprehensive review on inverter topologies and control strategies for grid connected photovoltaic system. Renewable and Sustainable Energy Reviews, 94(November 2017), 1120–1141. https://doi.org/10.1016/j.rser.2018.06.053

194. Zeh, A., and Witzmann, R. (2014): Operational strategies for battery storage systems in low-voltage distribution grids to limit the feed-in power of roof-mounted solar power systems. Energy Procedia, 46, 114–123. https://doi.org/10.1016/j.egypro.2014.01.164

195. Zhang, S., Andrews-Speed, P., Zhao, X., and He, Y. (2013): Interactions between renewable energy policy and renewable energy industrial policy: A critical analysis of China's policy approach to renewable energies. Energy Policy, 62, 342–353. https://doi.org/10.1016/j.enpol.2013.07.063

196. Zhao, C., Andersen, P. B., Træholt, C., and Hashemi, S. (2023): Grid-connected battery energy storage system: a review on application and integration. Renewable and Sustainable Energy Reviews, 182(September 2022), 113400. https://doi.org/10.1016/j.rser.2023.113400

197. Zheng, Y., Zhang, E., and An, P. (2022): Peafowl optimization algorithm based PV cell models parameter identification. Frontiers in Energy Research, 10(August), 1–9. https://doi.org/10.3389/fenrg.2022.985523

198. Zhong, J., Bollen, M., and Rönnberg, S. (2021): Towards a 100% renewable energy electricity generation system in Sweden. Renewable Energy, 171, 812–824. https://doi.org/10.1016/j.renene.2021.02.153

199. Zhou, H., Zhang, S., Peng, J., Zhang, S., Li, J., Xiong, H., and Zhang, W. (2021): Informer: Beyond Efficient Transformer for Long Sequence Time-Series Forecasting. 35th AAAI Conference on Artificial Intelligence, AAAI 2021, 12B, 11106–11115. https://doi.org/10.1609/aaai.v35i12.17325

200. Zubi, G., Parag, Y., and Wald, S. (2025): Implications of large-scale PV integration on grid operation, costs, and emissions: Challenges and proposed solutions. Energies, 18(1), 1–22. https://doi.org/10.3390/en18010130

201. Zucker, A., and Hinchliffe, T. (2014): Optimum sizing of PV-attached electricity storage according to power market signals - A case study for Germany and Italy. Applied Energy, 127, 141–155. https://doi.org/10.1016/j.apenergy.2014.04.038

A2: Publications related to the dissertation

Refereed papers in foreign languages:

1. **Teklebrhan, N.**, Seres, I., Farkas, I. (2021): Matlab/Simulink-based modeling of grid-connected PV systems, *R&D in Mechanical Engineering Letters*, Vol**.** 21, pp. 5-13.
2. **Teklebrhan, N.**, Seres, I., Farkas, I. (2023): Large-scale Photovoltaic integration, *R&D in Mechanical Engineering Letters*, Vol. 24, pp. 199-222.
3. **Teklebrhan, N.**, Seres, I., Farkas, I. (2023): Energetic Complementarity of Solar PV and Wind Power Based on Satellite Data, European Energy Research Journal (2736-5506), Vol. 3, Issue 4, pp. 7-12, https://doi.org/10.24018/ejenergy.2023.3.4.97
4. **Teklebrhan, N.,** Solomon, A.A., Fredric. O., Erik. M., Seres, I., Farkas, I. (2025): Strategies for integrating residential PV and wind energy in Eritrea's electricity grid by imposing feed-in constraints in low voltage network, *Solar Energy*, vol. 286, https://doi.org/10.1016/j.solener.2024.113140 (Scopus: Q1, IF: 6.5)
5. **Teklebrhan, N.,** Nahom, W., Merhawi. G., Yemane, T., Seres, I., Farkas, I. (2025): Addressing photovoltaic (PV) forecasting challenges: Satellite-driven data models for predicting actual PV generation using hybrid (LSTM-GRU) model, *Energy Report*, Vol. 14, pp. 2141-2156, https://doi.org/10.1016/j.egyr.2025.08.034 (Scopus: Q1, IF: 5.1)
6. **Teklebrhan, N.,** Solomon, A.A., Fredric. O., Erik. M., Seres, I., Farkas, I. (2024): System design issues of high renewable energy systems, the case Eritrea, *Energy Policy*, Vol. xx(xx), pp. xxx. https://doi.org/xxxxx/xxxxxx *(*Scopus: D1: IF: 9.2) *(accepted)*
7. **Teklebrhan, N**., Solomon, A.A., Fredric. O., Erik. M., Seres, I., Farkas, I. (2025): System-level analysis of energy storage requirements for large-scale renewable integration, *Sustainable Energy Technology and Assessments* (Scopus: Q1, IF: 7) *(in progress)*

International conference abstracts

8. **Teklebrhan, N**., Seres, I., Farkas, I. (2021): Power quality analysis and possible mitigation approaches for grid-connected PV systems, 27th Workshop on Energy and Environment, Gödöllő, Hungary, December 9-10, pp 29-29, ISBN: 9789632699721
9. **Teklebrhan, N**., Seres, I., Farkas, I. (2022): Power Quality Issues in Grid-Connected PV systems (2022), 21th International Workshop for Young Scientists (BioPhys Spring 2022), Nitra, Slovakia, May 30- 3, 2022, pp. 77-78, ISBN 978-83-89969-74-3
10. **Teklebrhan, N**., Seres, I., Farkas, I. (2022): Spatial and temporal complementarity of PV and wind power, 28th Workshop on Energy and Environment, Gödöllő, Hungary, December 9–10, 2022, pp. 29–29. ISBN 978-963-623-016-6.
11. **Teklebrhan, N**., Seres, I., Farkas, I. (2023): Large-scale PV integration employing enabling technologies, 29th Workshop on Energy and Environment, December 7-8, 2023, Gödöllő, Hungary, pp. 53–54. ISBN 978-963-623-079-1.
12. **Teklebrhan, N**., Seres, I., Farkas, I. (2023): Decarbonising the electricity sector in the context of Eritrea, (2023), 22nd International Workshop for Young Scientists, Book of Abstracts: BioPhys Spring 2023, Gödöllő, Hungary, June 15–16, 2023, pp. 51-51. ISBN 978-963-623-054-8.

13. **Teklebrhan, N**., Seres, I., Farkas, I. (2024): The Role of Residential PV on Large Scale Photovoltaic Integration (2024), 23th International Workshop for Young Scientists (BioPhys Spring 2024), Lublin, Poland, May 23 – 24, 2024, pp. 106 -108, ISBN: 978-83-89969-88-0
14. **Teklebrhan, N**., Seres, I., Farkas, I. Farkas, I. (2024)), Solar PV forecasting using deep neural network, 30th Workshop on Energy and Environment, December 12-13, 2024, Gödöllő, Hungary, pp 49-50, ISBN: 9789632699721
15. **Teklebrhan, N**., Seres, I., Farkas, I. (2025): Renewable Synergy: A Holistic Approach to Power System Design in Eritrea, International Conference on Eritrean Studies (ICES2025), January 4-6, 2025, Asmara, Eritrea *(in progress)*

A3. Power curve for 3.45 MW Vestas wind Turbine

Turbine specification V117 - 3.45MW (rated speed=12.5 m/s) and V136-3.45MW (rated speed =11.5 m/s)

V117 - 3.45MW (cut-in 3 m/s, cut-out 25 m/s)			V136-3.45MW (cut-in 3 m/s, cut-out 22.5 m/s)		
Windspeed (m/s)	Power (kW)	Cp	Wind speed (m/s)	Power (kW)	Cp
3	22.00	0.124	3.00	49.00	0.204
3.5	78.00	0.276	3.50	127.00	0.333
4	150.00	0.356	4.00	224.00	0.393
4.5	237.00	0.395	4.50	339.00	0.418
5	340.00	0.413	5.00	480.00	0.432
5.5	466.00	0.425	5.50	651.00	0.440
6	617.00	0.434	6.00	857.00	0.446
6.5	796.00	0.44	6.50	1099.00	0.450
7	1 006.00	0.445	7.00	1382.00	0.453
7.5	1 247.00	0.449	7.50	1705.00	0.454
8	1 522.00	0.451	8.00	2067.00	0.454
8.5	1 831.00	0.453	8.50	2460.00	0.450
9	2 178.00	0.454	9.00	2849.00	0.439
9.5	2 544.00	0.451	9.50	3174.00	0.416
10	2 905.00	0.441	10.00	3369.00	0.379
10.5	3 201.00	0.42	10.50	3434.00	0.333
11	3 374.00	0.385	11.00	3449.00	0.291
11.5	3 435.00	0.343	11.50	3450.00	0.255
12	3 448.00	0.303	12.00	3450.00	0.224
12.5	3 450.00	0.268	12.50	3450.00	0.199
13	3 450.00	0.238	13.00	3450.00	0.176
⋮	⋮	⋮	⋮	⋮	⋮
25	3 450.00	0.034	22.5	3450.00	0.034

A4: Hourly Kandall's rank correlation matrix

Kendall's (τ) rank correlation between different hourly generation profiles.NA. wind stands for National average wind and NA. solar PV for National average solar PV

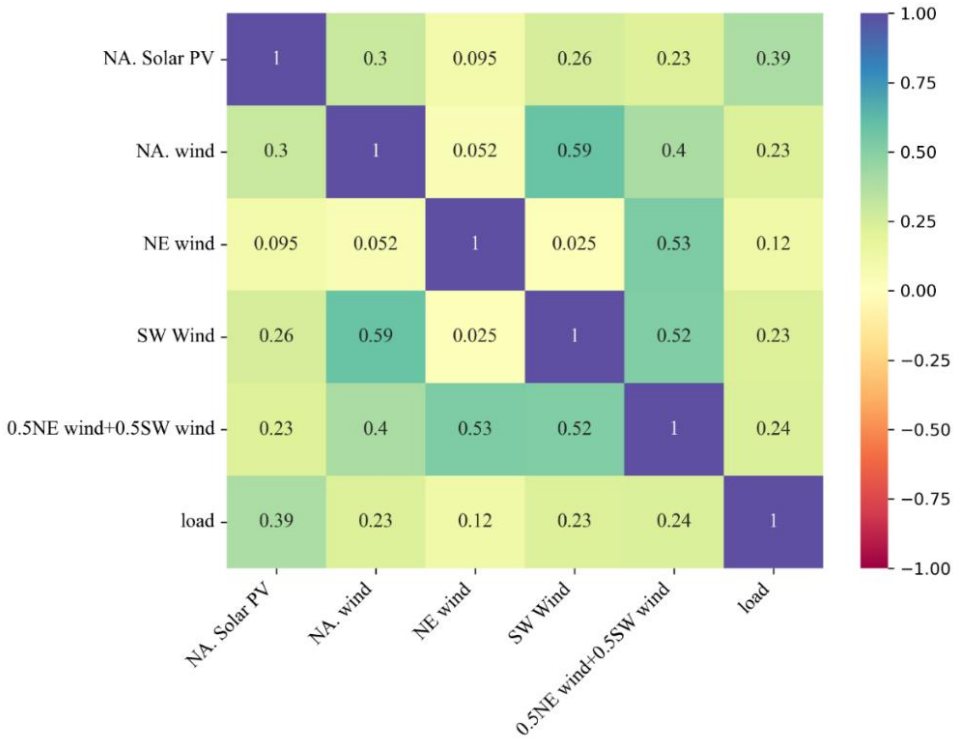

A5: Daily Kandall's rank correlation matrix

Kendall's (τ) rank correlation between different daily generation profiles.

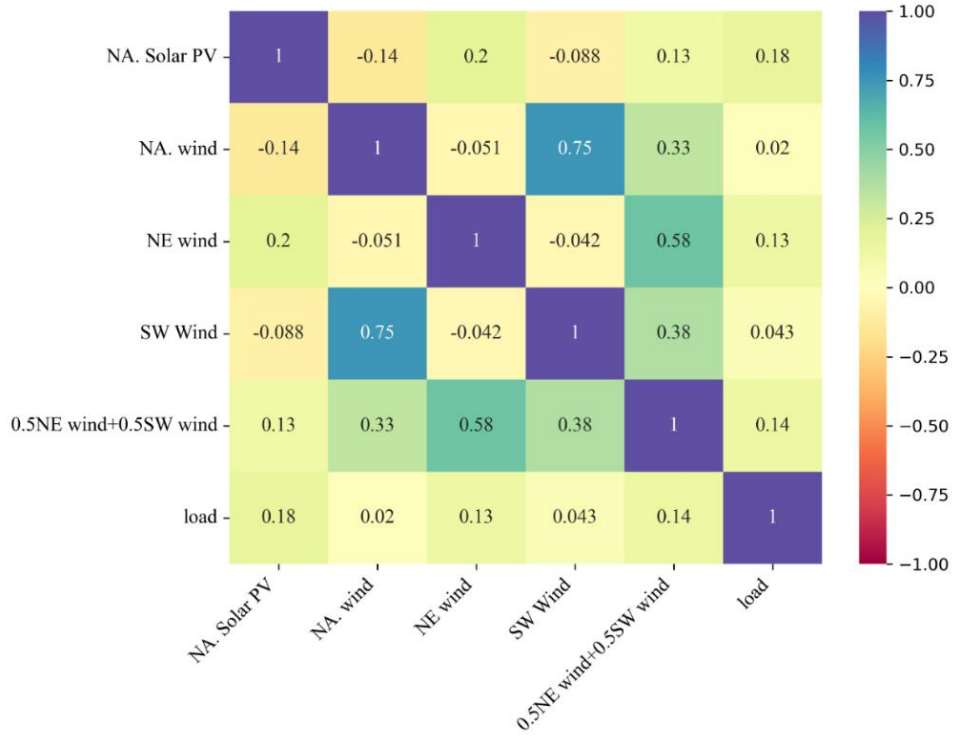

A6. Seasonal power generation mismatch

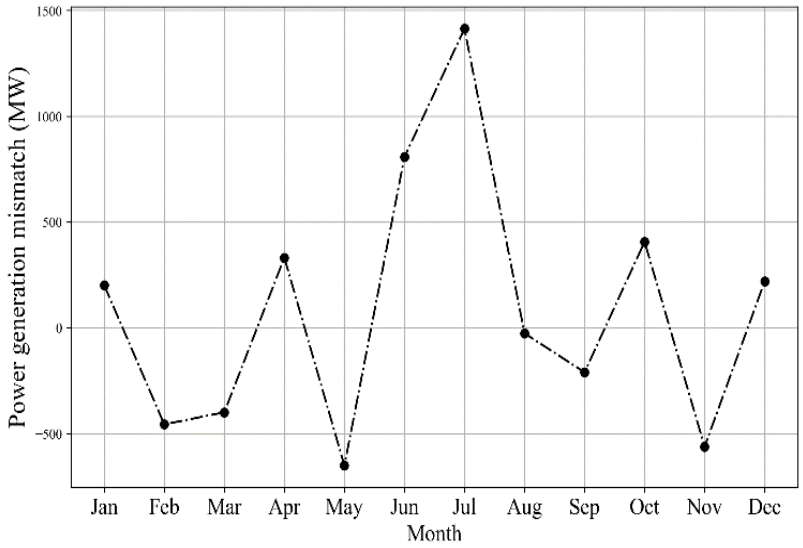

A7. Specifications of PV module and inverter

PV module			**Inverter**	
Type of the collector modules	SolarWatt Vision 36M Glass		Inverter type	SE 3500-ER-01-ITA
Technology	Monocrystalline		Phases	Single-phase
Covering material	Partly tempered high transparent float glass, 4 mm		Operating voltage range	270 – 500 Vdc
Transparency	20%		Maximum input current	13.5 Adc
Open Circuit Voltage	23.4 V		Maximum output power	3500 VAac
Short Circuit Current	9 A		Operating voltage	220/230 Vac
Nominal Voltage (under STC)	19.2 V		Maximum output current	19.5 Aac
Nominal current (under STC)	8.7 A		AC Nominal frequency	50/60 Hz
Nominal power	165 Wp		Power factor range	+/- 0.9 to 1
Total system capacity	3.3 kWp		Transformerless ungrounded	Yes
Maximal system voltage	1000 V		Maximum inverter efficiency	97.6%
			European weighted efficiency	97.5%

A8. Error metrics for the different models

Error metrics showing four seasons (1-step actual PV Generation forecasting)

Season	Model	RMSE (kW)	MBE (kW)	MAE (kW)	R^2
Fall	LSTM	0.0721	0.0033	0.05673	0.8161
	GRU	0.0722	0.0008	0.0555	0.8258
	LSTM-GRU	0.0740	0.0186	0.0595	0.8199
Winter	LSTM	0.0778	0.0102	0.05951	0.7931
	GRU	0.0803	0.0058	0.0600	0.7886
	LSTM-GRU	0.0820	0.0327	0.0664	0.7967
Spring	LSTM	0.0707	0.0031	0.0570	0.8210
	GRU	0.0718	0.0001	0.0568	0.8256
	LSTM-GRU	0.0720	0.0198	0.0595	0.8132
Summer	LSTM	0.0742	0.0005	0.0572	0.7833
	GRU	0.0764	0.0001	0.0584	0.7764
	LSTM-GRU	0.0769	0.0154	0.0599	0.7624
Overall	LSTM	0.0721	0.0033	0.0567	0.8054
	GRU	0.0722	0.0008	0.0555	0.8072
	LSTM-GRU	0.0740	0.0186	0.0595	0.7999

A9. Performance comparison of the three models

Prediction of actual PV generation across four seasons for a 12-step prediction

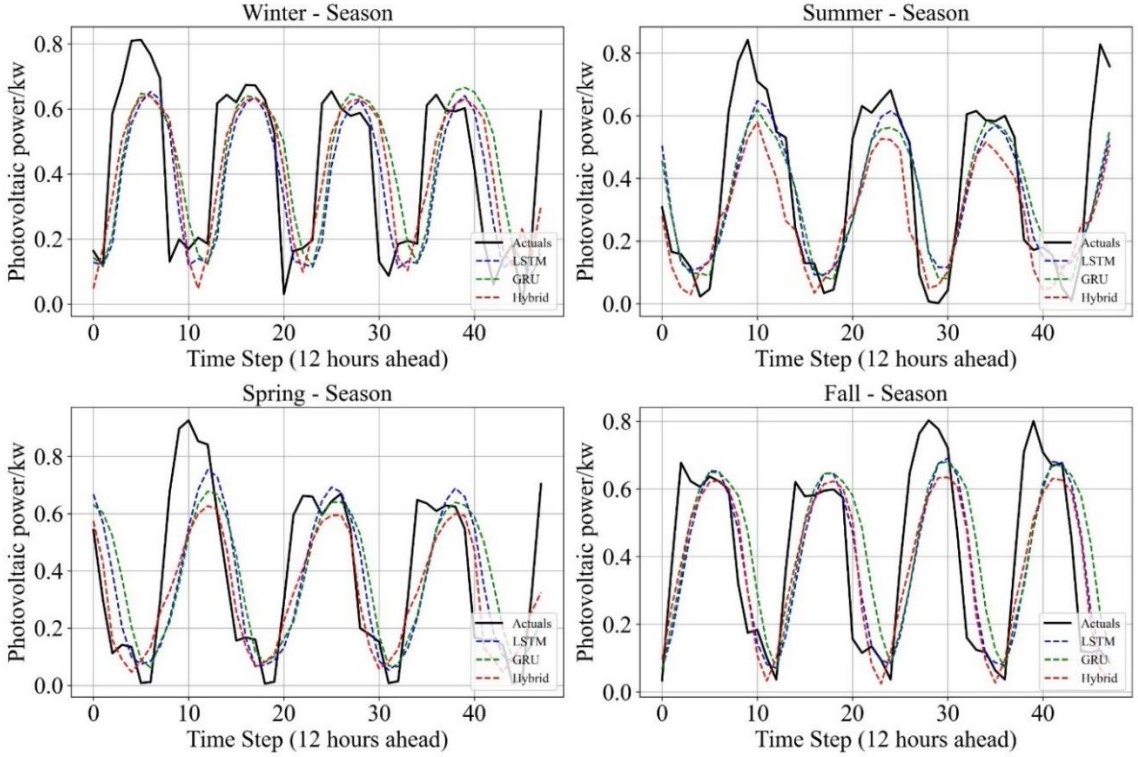

A10: Performance evaluation of RMSE error metrics across different seasons

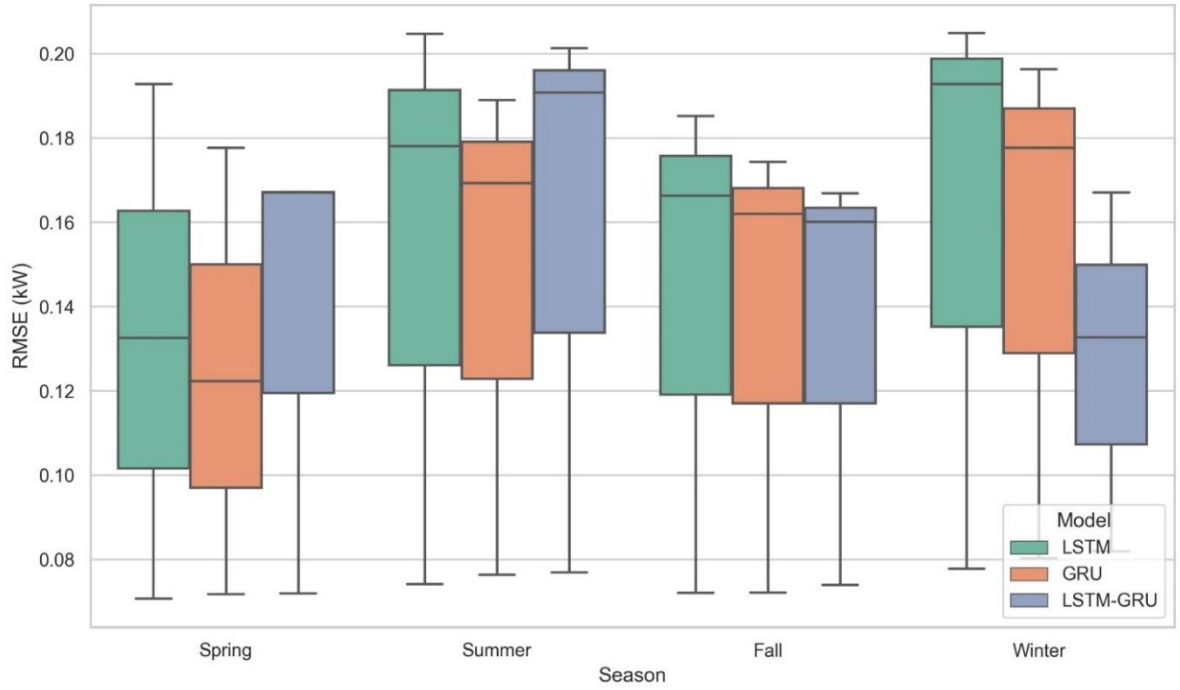

A11: LSTM learning Curve of uni-step prediction

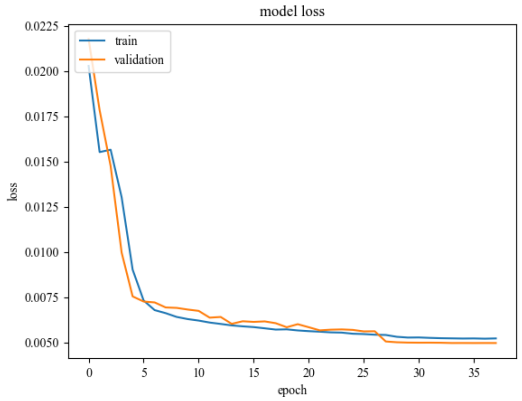

A12: GRU learning Curve of uni-step prediction

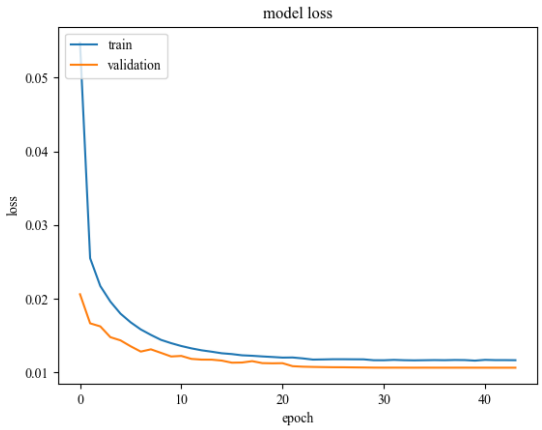

A13: Six-step forecasting error distribution

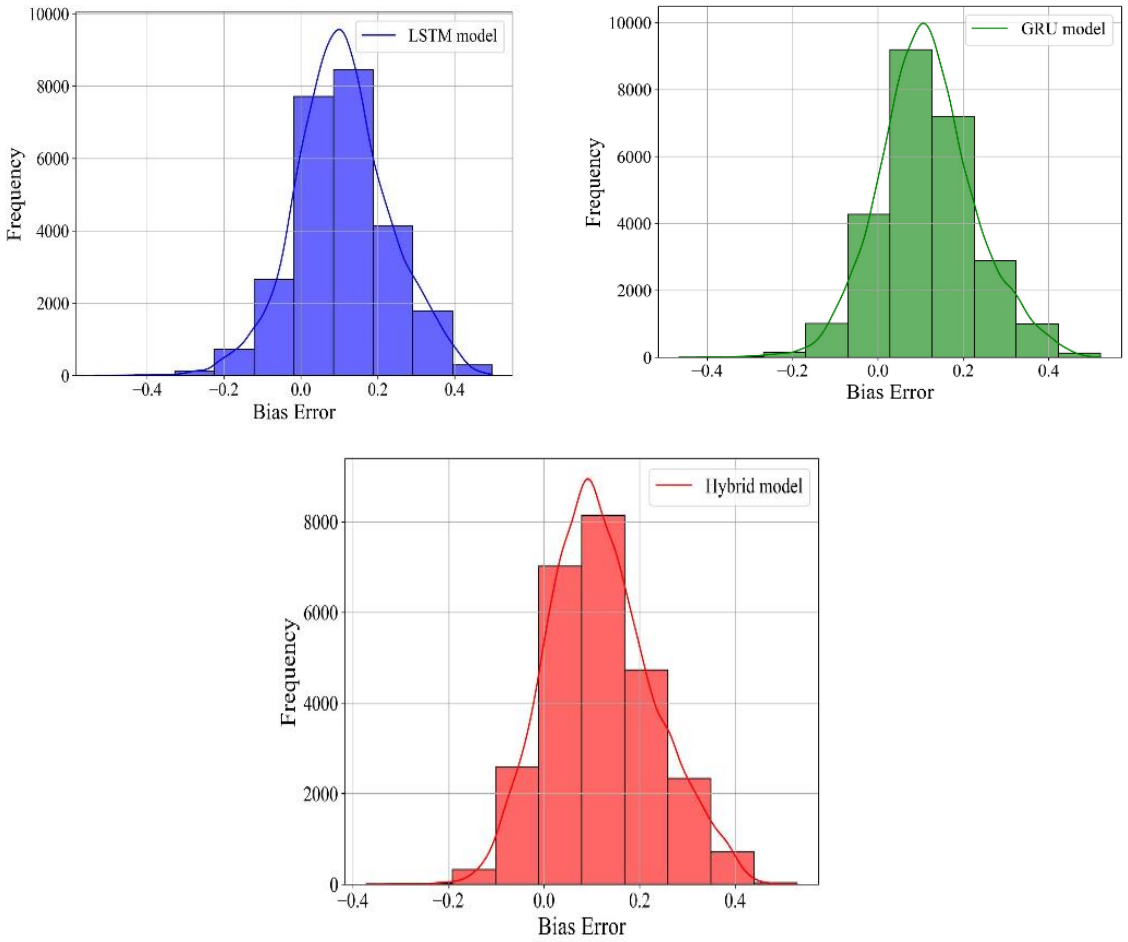

A14: Error metrics for different models separated into seasons

Deviations showing for the 6-step for actual PV generation forecasting

Season	Model	RMSE (kW)	MBE (kW)	MAE (kW)	R^2
Fall	LSTM	0.1663	0.0112	0.1351	0.5792
	GRU	0.1620	0.0054	0.1302	0.6124
	LSTM-GRU	0.1601	0.0127	0.1288	0.6410
Winter	LSTM	0.1847	0.0346	0.1464	0.4290
	GRU	0.1846	0.0294	0.1451	0.4775
	LSTM-GRU	0.1644	0.0403	0.1306	0.6194
Spring	LSTM	0.1326	0.0130	0.1638	0.5747
	GRU	0.1223	0.0210	0.1549	0.6355
	LSTM-GRU	0.1672	0.0218	0.1333	0.6245
Summer	LSTM	0.1781	0.0164	0.1500	0.5283
	GRU	0.1693	0.0156	0.1407	0.5717
	LSTM-GRU	0.1908	0.0260	0.1573	0.5103
Overall	LSTM	0.1731	0.0029	0.1409	0.5359
	GRU	0.1675	0.0015	0.1343	0.5821
	LSTM-GRU	0.1714	0.0002	0.1378	0.6024

A15. Performance of models with and without data transformation

(Performance comparison of traditional and deep learning models (with and without data transformation), for 1-step-ahead forecasting over the full-year dataset)

Model	Z-score Tran	RMSE (kW)	MBE (kW)	MAE (kW)	R2
LSTM	×	0.1964	0.1394	0.1548	0.1210
LSTM	✓	0.0721	0.0033	0.0567	0.8054
GRU	×	0.1417	0.0943	0.1115	0.5422
GRU	✓	0.0722	0.0008	0.0555	0.8072
LSTM-GRU	×	0.1553	0.1033	0.1220	0.4505
LSTM-GRU	✓	0.0740	0.0186	0.0595	0.7999
XGBOOST	×	0.1826	0.1468	0.1525	-0.0395
XGBOOST	✓	0.1120	0.0684	0.0906	0.6089
SARIMAX	×	0.2756	0.2134	0.2194	-1.3682
SARIMAX	✓	0.1752	0.1143	0.1320	0.0431

10. DECLARATION ON THE USE OF ARTIFICIAL INTELLIGENCE

I hereby declare that the research and intellectual content of this dissertation are my own original work, under the guidance of my supervisors and sometimes in collaboration with a research team, except where explicitly noted. The core intellectual contributions, including the Research questions, data collection, analysis, and interpretation, are entirely my responsibility.

Specific use of artificial intelligence (AI) software

AI software: ChatGPT was used exclusively to refine language and expression: act as an advanced language polishing and editing aid to enhance the clarity, fluency, and professional English expression of the final written text. This included correcting grammar, improving sentence structure, and suggesting precise terminology.

Exclusion of AI in content generation

I confirm that AI software **was not used** for:

- Generating any original research ideas, hypotheses, or theoretical frameworks.
- Creating or modifying the core content, including the literature review, methodology, results, or discussion sections.
- Any form of data collection, manipulation, or interpretation.
- The creation or modification of figures, tables, or graphical elements.

The substance and intellectual originality of this dissertation remain my sole responsibility, Supported by my supervisors' guidance.

Signature: 

Date: November 15, 20

11. ACKNOWLEDGEMENT

First and foremost, I glorify and thank GOD the Almighty for His boundless mercy, strength, and divine guidance through the course of my PhD journey. I am thankful to the Stipendium Hungaricum Scholarship Program and the Mechanical Engineering Doctoral School at MATE University, Hungary, for financing my PhD study.

I am deeply grateful to my esteemed supervisors, Prof. István Farkas and Dr. István Seres, for their professional guidance, unwavering support, and steadfast commitment throughout this journey. Their thoughtful guidance, insightful suggestions, constructive feedback, and intellectual mentorship played a pivotal role in shaping the direction and depth of this research. Working under their supervision has been an immensely enriching experience that has profoundly shaped both my academic growth and professional development. Without their dedication, the realization of this work would not have been possible.

My profound gratitude goes to Dr. Solomon Abebe Asfaw of Vaasa University, Finland, and Prof. Fredric Ottermo and Prof. Erik Möllerström of Halmstad University, Sweden, for their exceptional mentorship, critical insights, and constructive discussions throughout my doctoral journey. Working with these distinguished scholars has profoundly shaped my academic path and expanded my scholarly attitude. I am grateful to Halmstad University for hosting me as a visiting scholar and to the Pannonia Mobility Program for funding this invaluable research stay.

I extend my special thanks to my parents, my father Kesis Tuemzghi Negash, and my mother Bri Desta, for their love, care, prayers, and belief in me, which have carried me to this stage. I only wish my father could be here to witness this milestone.

My special gratitude to my beloved wife, Rahwa, for her constant support, encouragement, and motivation during the challenging journey. Her strength and love have been a constant source of inspiration. To my lovely and wonderful children –Naomi, Dimiana, and Siem – thanks for your affection, which has filled my heart and kept me motivated. Thanks to my sister Hiwet and brother Zeremariam for their unwavering support and encouragement. For my relatives and friends who stood by me with constant support and encouragement, I am grateful for your presence in my life.

I am thankful to the university staff and coordinators, Mrs. Judit Czingli, Ms. Zsuzsanna Tassy, Mrs. Edit Dolányi Sima, and Mrs. Katalin Fekete Sivatagi, for their unwavering support and guidance.

Finally, I would like to extend my gratitude to the government of Eritrea and Mai-nefhi College of Engineering and Technology for their valuable support during my studies.

Gödöllő, November 2025

Teklebrhan Tuemzghi Negash